VOLUME 80 JANUARY 29, 1976 / NUMBER 3

JPCHAx

THE JOURNAL OF PHYSICAL CHEMISTRY

PUBLISHED BIWEEKLY BY THE AMERICAN CHEMICAL SOCIETY

THE JOURNAL OF

PHYSICAL CHEMISTRY

Published by the
AMERICAN CHEMICAL SOCIETY
BOOKS AND JOURNALS DIVISION
D. H. Michael Bowen, Director

Editorial Department: Charles R. Bertsch, Head; Marianne C. Brogan, Associate Head; Celia B. McFarland, Joseph E. Yurvati, Assistant Editors
Graphics and Production Department: Bacil Guiley, Head
Research and Development Department: Seldon W. Terrant, Head

Advertising Office: Centcom, Ltd., 50 W. State St., Westport, Conn. 06880.

Published biweekly by the American Chemical Society at 20th and Northampton Sts., Easton, Pennsylvania 18042. Second class postage paid at Washington, D.C. and at additional mailing offices.

Editorial Information

Instructions for authors are printed in the first issue of each volume. Please conform to these instructions when submitting manuscripts.

Manuscripts for publication should be submitted to *The Journal of Physical Chemistry*, Department of Chemistry, University of Minnesota, Minneapolis, Minn. 55455. Correspondence regarding accepted papers and proofs should be directed to the Editorial Department at the ACS Easton address.

Page charges of $60.00 per page are assessed for papers published in this journal. Ability to pay does not affect acceptance or scheduling of papers.

Bulk reprints or photocopies of individual articles are available. For information write to Business Operations, Books and Journals Division at the ACS Washington address.

Requests for **permission to reprint** should be directed to Permissions, Books and Journals Division at the ACS Washington address. The American Chemical Society and its Editors assume no responsibility for the statements and opinions advanced by contributors.

Subscription and Business Information

1976 Subscription rates—including surface postage

	U.S.	PUAS	Canada, Foreign
Member	$24.00	$29.75	$30.25
Nonmember	96.00	101.75	102.25
Supplementary material	15.00	19.00	20.00

Air mail and air freight rates are available from Membership & Subscription Services, at the ACS Columbus address.

New and renewal subscriptions should be sent with payment to the Office of the Controller at the ACS Washington address. **Changes of address** must include both old and new addresses with ZIP code and a recent mailing label. Send all address changes to the ACS Columbus address. Please allow six weeks for change to become effective. **Claims** for missing numbers will not be allowed if loss was due to failure of notice of change of address to be received in the time specified; if claim is dated (a) North America—more than 90 days beyond issue date, (b) all other foreign—more than 1 year beyond issue date; or if the reason given is "missing from files". Hard copy claims are handled at the ACS Columbus address.

Microfiche subscriptions are available at the same rates but are mailed first class to U.S. subscribers, air mail to the rest of the world. Direct all inquiries to Business Operations, Books and Journals Division, at the ACS Washington address or call (202) 872-4444. **Single issues** in hard copy and/or microfiche are available from Special Issues Sales at the ACS Washington address. Current year $4.75. Back issue rates available from Special Issues Sales. **Back volumes** are available in hard copy and/or microform. Write to Special Issues Sales at the ACS Washington address for further information. **Microfilm** editions of ACS periodical publications are available from volume 1 to the present. For further information, contact Special Issues Sales at the ACS Washington address. **Supplementary material** must be ordered directly from Business Operations, Books and Journals Division, at the ACS Washington address.

	U.S.	PUAS, Canada	Other Foreign
Microfiche	$2.50	$3.00	$3.50
Photocopy			
1–7 pages	4.00	5.50	7.00
8–20 pages	5.00	6.50	8.00

Orders over 20 pages are available only on microfiche, 4 × 6 in., 24X, negative, silver halide. Orders must state photocopy or microfiche if both are available. Full bibliographic citation including names of all authors and prepayment are required. Prices are subject to change.

American Chemical Society
1155 16th Street, N.W.
Washington, D.C. 20036
(202) 872-4600

Member & Subscription Services
American Chemical Society
P.O. Box 3337
Columbus, Ohio 43210
(614) 421-7230

Editorial Department
American Chemical Society
20th and Northampton Sts.
Easton, Pennsylvania 18042
(215) 258-9111

Notice to Authors last printed in the issue of January 1, 1976

THE JOURNAL OF
PHYSICAL CHEMISTRY

Volume 80, Number 3 January 29, 1976

JPCHAx 80(3) 217–340 (1976)

ISSN 0022-3654

COMMUNICATIONS TO THE EDITOR

■ Supplementary material for this paper is available separately (consult the masthead page for ordering information); it will also appear following the paper in the microfilm edition of this journal.

* In papers with more than one author, the asterisk indicates the name of the author to whom inquiries about the paper should be addressed.

AUTHOR INDEX

ANNOUNCEMENT

On the last two pages of this issue you will find reproduced the table of contents of the January 1976 issue of the Journal of Chemical and Engineering Data.

THE JOURNAL OF
PHYSICAL CHEMISTRY

VOLUME 80, NUMBER 3 JANUARY 29, 1976

Collisional Quenching of Electronically Excited Bismuth Atoms, Bi($6p^3\ ^2D_{3/2}$) and Bi($6p^3\ ^2D_{5/2}$), by Time-Resolved Attenuation of Atomic Resonance Radiation

M. J. Bevan and D. Husain*

Department of Physical Chemistry, The University of Cambridge, Cambridge CB2 1EP, England *(Received July 23, 1975)*

A kinetic study is presented of electronically excited bismuth atoms, Bi($6p^3\ ^2D_{3/2}$) and Bi($6p^3\ ^2D_{5/2}$), respectively 1.416 and 1.914 eV above the $6p^3\ ^4S_{3/2}$ ground state. These optically metastable atoms were generated by pulsed irradiation and monitored photoelectrically in absorption by time-resolved attenuation of atomic resonance radiation. Rate constants for the collisional quenching of these two states by the gases He, Xe, H_2, D_2, O_2, N_2, CO, CO_2, N_2O, and C_2H_4 are reported. The resulting data are compared, where possible, with previous analogous data for Sb($5p^3\ ^2D_{3/2}$) and Sb($5p^3\ ^2D_{5/2}$), and the results discussed within the context of symmetry arguments based on correlation diagrams employing (J,Ω) coupling.

Introduction

There have been extensive developments in recent years in the direct kinetic study of relatively highly energized spin–orbit states arising from the gross overall electronic structure of the ground-state configuration, for example, I($5p^5\ ^2P_{1/2}$) (0.943 eV),[1-4] Tl($6p\ ^2P_{3/2}$) (0.966 eV),[5-7] Te($5p^4\ ^3P_{0,1}$) (0.584 and 0.589 eV, respectively),[8] and Br($4p^5\ ^2P_{1/2}$) (0.457 eV).[1,9,10] These studies constitute part of a wider program aimed at an understanding of the relationship between electronic structure and atomic reactivity.[1,11-14] Consideration of the rate data derived from such measurements has normally been on an individual basis rather than within the context of a general framework, because the principal structure for considering the reactivity of electronically excited atoms has hitherto been that of correlating initial and final states using the weak spin–orbit coupling approximation.[14,15] Clearly, the constraints of such an approach omit the effects of spin–orbit coupling. Very recently, the chemistry of some electronically excited states of heavy atoms have been considered within the context of (J,Ω) coupling which has been discussed generally by Husain.[13] These include the collisional behavior of Sn($5p^2\ ^1S_0$)[16,17] together with that of Sn($5p^2\ ^1D_2$)[18,19] and the analogous pair of states of the lead atom.[20-23] Brown and Husain[17] have also discussed the limitations of (J,Ω) coupling in heavy atom–molecule collisions. Further, this approach has also been used by Foo et al.[24,25] for considering spin–orbit quenching of Sn($5p^2\ ^3P_{1,2}$) (0.210 and 0.425 eV, respectively)[24,25] and Pb($6p^2\ ^3P_{1,2}$) (0.969 and 1.320 eV, respectively).[26,27] This method has also been found to be of some use when considering rate data for the much less energized states, Ge($4p^2\ ^3P_{1,2}$) (557 and 1410 cm^{-1}, respectively).[28]

A major experimental objective for the present general development is to obtain absolute rate data for all of the low-lying states of the overall ground-state configuration within a given group of the periodic table, considering light atom–molecule collisions using weak spin–orbit coupling and those for heavy atoms using (J,Ω) coupling. While this has not been completely achieved for any group, group 5 represents a particularly developed area in this respect, as, with the present work, we now have absolute rate data for various electronic states of atoms in the np^3 configuration for N → Bi. The rate data for N(2^2D_J 2^2P_J)[29-32] and P(3^2D_J, 3^2P_J)[33-35] have been found to be in accord with correlations based on the weak spin–orbit coupling approximation. Correlations on this basis have, however, been found[36] to be of limited use for considering the collisional behavior of As(4^2D_J, 4^2P_J).[36-38] For the heavier Sb($5^2D_{3/2,5/2}$) (1.055 and 1.222 eV, respectively) (J,Ω) coupling provided the more satisfactory framework for interpreting the collisional behavior of these atomic states.[39] The bismuth atom clearly represents the strongest case within the group where (J,Ω) coupling should apply and hence it is in this context and against the foregoing general background that the specific body of work presented here may be viewed.

We present here a kinetic study leading to the first detailed, quantitative rate data for the bismuth atom in the $^2D_{3/2}$ (1.416 eV)[40] and $^2D_{5/2}$ (1.914 eV)[40] states. Hitherto, detailed rate data for the bismuth atom has been confined to those derived from quenching of emission from the higher lying 7s $^4P_{1/2}$ state.[41] The data obtained here are compared with those for Sb($5^2D_{3/2,5/2}$), where available, and considered within the framework of (J,Ω) coupling on collision.

Experimental Section

It may be emphasized from the outset that, by the standards of this type of investigation, this experimental system for the bismuth atom presented particular practical difficulties. We have already indicated difficulties encountered previously, when studying Sb($5^2D_{3/2,5/2}$),[39] compared to the more straightforward measurements involved for As($4^2D_{3/2,5/2}$) and As($4^2P_{1/2,3/2}$)[36,37] by similar techniques. These problems[39] were even more intensified in the present investigation and included difficulties encountered in developing a suitably intense, stable, and long-running spectroscopic source and generating Bi($6^2D_{3/2}$) and Bi($6^2D_{5/2}$) in transient concentrations of a magnitude suitable for "single-shot" measurements[36,37] without using signal-averaging techniques.[32] The present method yielded a body of absolute collisional quenching data for the two atomic states significant for discussion within the basis of the general framework laid down in the Introduction.

Bi($6^2D_{3/2}$) and Bi($6^2D_{5/2}$) were produced by the pulsed irradiation respectively of bismuth trimethyl and of bismuth triethyl (E = 845 J). The yields of the $J = \frac{5}{2}$ state from $BiMe_3$ were very small; this, at least, enjoys the advantage of permitting kinetic study on the $J = \frac{3}{2}$ level without accompanying significant effects of collisional relaxation from $J = \frac{5}{2}$. The atoms were monitored photoelectrically in absorption by time-resolved attenuation of atomic resonance radiation. Excess helium buffer gas (p_{He}: p_{BiMe_3} or p_{BiEt_3} = ca. 10 000:1) was always employed in order to ensure no significant temperature rise above that of the ambient condition on photolysis. These two molecules constituted the only suitably stable, convenient gaseous sources of the electronically excited atomic bismuth. Further, while various reactor–photolysis vessel arrangements of the types discussed previously were tried,[36] that employed for the study of As($4^2D_{3/2,5/2}$) and As($4^2P_{1/2,3/2}$) gave the highest and most consistent atomic yields. Convenient photolysis lamp fillings in the reactor assembly[42] were found to be krypton for generating Bi($6^2D_{3/2}$) and nitrogen for generating Bi($6^2D_{5/2}$).

Resonance lines connecting with Bi(6^2D_J) and Bi(6^2P_J) were derived from a microwave-powered discharge through a flow system containing $BiMe_3$ in He (p_{BiMe_3} = 1.3 N m^{-2}, $p_{total\ with\ He}$ = 133 N m^{-2}; incident intensity 100 W). This yielded an intense, relatively stable discharge and had an effective running time of ca. 20 min, after which deposits, principally of bismuth metal, in the quartz flow tube caused quenching of the discharge, following which the tube was replaced and easily cleaned. Sealed sources (EMI electrodeless discharge lamp (Bi), Type 9776B; EMI cavity, Type C111), similar to that used for studies of As(4^2D_J) and As(4^2P_J),[36,37] were not found to yield spectral intensities sufficiently high for the present measurements, and the discharges were found to self-extinguish rapidly. Further details of this bismuth flow lamp including a sample of the spectrum and actinometric measurements leading to absolute line intensities are being published in a general article on atomic emission flow sources elsewhere.[43] The atomic lines were separated with a Seya-Namioka grating monochromator,[44,45] which was constructed in this laboratory and which has been described previously.[37] Following irradiation, time-resolved resonance absorption by the transient atoms was detected by means of a photomultiplier tube (EMI 9783B) mounted on the exit slit of the monochromator.

Garstang[46] has calculated the Einstein coefficients for emission from the spin–orbit states of Bi(6^2D) and Bi(6^2P), the sum for each state, ΣA (A_m and A_q),[46] indicating the optical metastability of these transient species.

Atomic state	E,[40] eV	ΣA,[46] s^{-1}
$6p^3\ ^2D_{3/2}$	1.416	31.2
$6p^3\ ^2D_{5/2}$	1.914	12.4
$6p^3\ ^2P_{1/2}$	2.686	63.0
$6p^3\ ^2P_{3/2}$	4.112	173.9

Thus, they may be monitored readily by absorption spectroscopy using the appropriate resonance lines (see Results and Discussion). The relatively high overall Einstein coefficient for the $6^2P_{3/2}$ state presumably arises from mixing with the lower, close-lying (4.040 eV) $7^4P_{1/2}$ Rydberg state. The detection system was similar to that employed for the study of Sb($5^2D_{3/2,5/2}$).[39] Thus, in essence, the photoelectric pulses representing time-variable light absorption by the transient atomic species were fed into a current-to-voltage converter.[47] The resulting signals were then digitized and stored in a transient recorder (Datalab D 1905) and the contents of the 1024-word memory were then punched onto paper tape in ASCII code (Datadynamics punch 1133) for direct input into a computer (IBM 370). Unlike our experiments on As(4^2P_J),[36] we did not employ a precision logarithmic circuit[32] on account of the low absorption signals and the magnitude of the decay rates in relation to the sweep time of this particular transient recorder.

Materials. He, Kr (for the photoflash lamp), Xe, H_2, D_2, O_2, N_2, CO, CO_2, N_2O, and C_2H_4 were prepared as described previously.[36,37] $BiMe_3$ was prepared by the action of bismuth trichloride ($BiCl_3$) with lithium methyl, LiMe, in ether. The product was separated by destroying the excess LiMe with water and then the ethereal solution was dried with magnesium sulfate, followed by fractionation under reduced pressure. The product was then purified by repeated fractional condensation at 210 K (Chloroform–liquid nitrogen slush) in a high-vacuum apparatus (vapor pressure data from Bamford et al.[48]). Any remaining traces of water were removed by distillation in the presence of phosphorus peroxide. $BiEt_3$ was prepared by using the appropriate Grignard reagent. The condensation of the product was carried out once with no further purification procedure.

Results and Discussion

The following atomic transitions were employed in this investigation.

Transition	λ,[49] nm	$10^{-8}gA$,[49] s^{-1}
$7s\ ^2P_{1/2} \rightarrow 6p^3\ ^2D^0_{3/2}$	289.80	32
$7s\ ^4P_{5/2} \rightarrow 6p^3\ ^2D^0_{5/2}$	302.46	38
$7s\ ^2P_{3/2} \rightarrow 6p^3\ ^2P^0_{1/2}$	359.61	8.8

We were unable to detect even the lower spin–orbit level of the ^2P state, Bi($6^2P_{1/2}$), in these experiments. It is thus clear that any transient concentration in the 6^2P state is

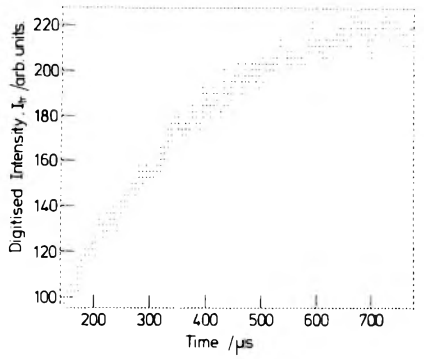

Figure 1. Digitized time variation of the transmitted light intensity at λ 289.8 nm ($Bi(7^2P_{1/2}) \rightarrow Bi(6^2D^0_{3/2})$) indicating the decay of resonance absorption by $Bi(6^2D_{3/2})$; p_{BiMe_3} = 0.40 N m^{-2}, $p_{total\ with\ He}$ = 6.66 kN m^{-2}, $p_{Kr(flash\ lamp)}$ = 1.33 kN m^{-2}; E = 845 J; recording delayed by 140 μs.

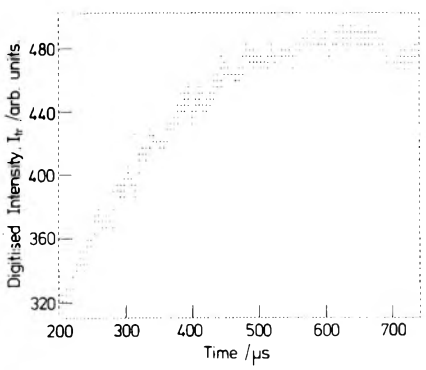

Figure 2. Digitized time variation of the transmitted light intensity at λ 302.5 nm ($Bi(7^4P_{5/2}) \rightarrow Bi(6^2D^0_{5/2})$) indicating the decay of resonance absorption by $Bi(6^2D_{5/2})$; p_{BiEt_3} = 1.5 N m^{-2}, $p_{total\ with\ He}$ = 6.66 kN m^{-2}, $p_{N_2(flash\ lamp)}$ = 1.33 kN m^{-2}; E = 845 J; recording delayed by 200 μs.

very small. Hence, the present studies are restricted to the $6^2D_{3/2}$ and $6^2D_{5/2}$ states.

Figures 1 and 2 show, respectively, the digitized time variation of the transmittent light intensity at λ 289.8 and 302.5 nm following respectively the photolysis of $BiMe_3$ and $BiEt_3$ in the presence of excess helium. Figures 3 and 4 show examples of first-order kinetic plots derived from the data of Figures 1 and 2, respectively. Unfortunately, γ values for the modified Beer–Lambert law[50]

$$I_{tr} = I_0 \exp(-\epsilon(cl)^\gamma) \quad (1)$$

(where the symbols have their usual significance[50]) could not be determined for the two atomic transitions employed in Figures 1–4. As we emphasized in the investigation on $Sb(5^2D_{3/2,5/2})$,[39] this would require an accuracy and reproducibility in the intercepts of plots such as those given in Figures 3 and 4 considerably better than those of the slopes. We consider that the most suitable approximation that we may make in the present circumstances is to employ γ values of unity for both transitions at λ 289.8 and 302.5 nm. In our investigations of $As(4^2D_J)$ and $As(4^2P_J)$,[36,37] γ values for the transitions and conditions employed then were found to be of the order of ca. 0.8.[36,37] As quenching constants depend upon using the reciprocal of γ, this would yield (*if* γ = ca. 0.8 in these experiments) absolute rate constants which are low by ca. 20% but the relative values would still be correct. As an extreme exam-

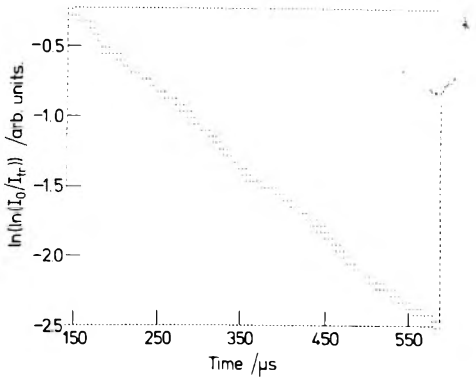

Figure 3. Typical pseudo-first-order plots for the decay of $Bi(6^2D_{3/2})$ obtained by monitoring the absorption of light at λ 289.8 nm ($Bi(7^2P_{1/2}) \leftarrow Bi(6^2D^0_{3/2})$); p_{BiMe_3} = 0.40 N m^{-2}, $p_{total\ with\ He}$ = 6.66 kN m^{-2}; E = 845 J.

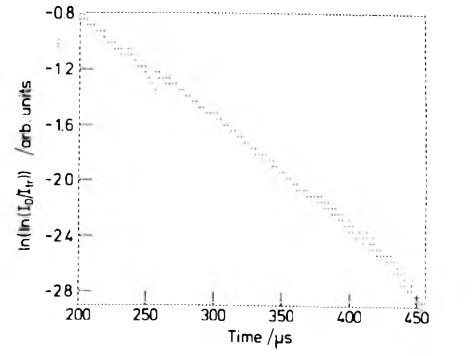

Figure 4. Typical pseudo-first-order plots for the decay of $Bi(6^2D_{5/2})$ obtained by monitoring the absorption of light at λ 302.5 nm ($Bi(7^4P_{5/2}) \leftarrow Bi(6^2D^0_{5/2})$); p_{BiEt_3} = 1.5 N m^{-2}, $p_{total\ with\ He}$ = 6.66 kN m^{-2}; E = 845 J.

ple, a γ value of ca. 0.4 has been reported for experiments employing the $7s(^3P^0_1)$–$6p^2(^3P_0)$ transition of ground-state atomic lead at λ 283.3 nm,[51] and clearly a value as low as this in the present context would thus mean that the reported rate data *could* be as low as a factor of ca. 2.5. In the absence here of measured γ values, we simply draw attention to the possibility of the absolute data being low overall by a constant factor, with preference clearly given to values for the heaviest atom in the group in analogous electronic states, namely, $As(4^2D_{3/2,5/2})$,[37] for which measurements have been made. Further, we are concerned, in fundamental terms, with the difference between the collisional behaviors of the two J states being considerably greater than that arising from the γ values.

The slopes of the plots of the type shown in Figures 3 and 4 are given by $-\gamma k'$ where k' is the overall first-order coefficient for the decay of the particular spin–orbit state under the given experimental conditions. Experimentally, k' (or $\gamma k'$) is investigated for each spin–orbit state in the presence of added quenching gas, Q. This variation is taken to follow the form

$$k' = K + k_Q[Q] \quad (2)$$

where k_Q is the absolute second-order rate constant for collisional removal by the added quenching gas. K is taken to be constant in a series of kinetic runs in which [Q] is varied. It comprises first-order contributions from diffusion, weak spontaneous emission,[46] and collisional quenching by impurities, products of photolysis, and, principally, the undis-

sociated parent molecule. It is no trivial point to mention that experiments with a given quenching gas were carried out in batches of six. Small variations in the low pressures of $BiMe_3$ or $BiEt_3$ from batch to batch were eliminated by taking a blank (i.e., $p_Q = 0$, $k' = K$) in each set and hence presenting all the data for a given gas, Q, in the form $(k' - K)$ (or $\gamma(k' - K)$) vs. p_Q.

Examples of quenching data for $Bi(6^2D_{3/2})$ and $Bi(6^2D_{5/2})$ for different quenching gases in the form of eq 2 are presented graphically in Figures 5–8. The plots for H_2 and D_2 (Figures 6 and 8) are presented separately on account of current interest in the effect of the isotopes on electronic quenching (see later). The accuracy of the present experiments is not significantly affected by relaxation from higher states. Clearly, in the case of $Bi(6^2D_{5/2})$, the higher lying 6^2P_J state could not be detected in these experiments. On the other hand, while some small collisional relaxation may take place with some gases for $Bi(6^2D_{5/2}) \rightarrow Bi(6^2D_{3/2})$ even using $BiMe_3$, treatment of each J state as being governed principally by kinetics which are overall first order is seen to be a reasonable approximation by the sensible linearity observed in plots of the type given in Figure 3 for the added gas. Further, relaxation of the $J = 3/2$ state was generally found to be so much slower than that of $J = 5/2$ that it would not appear principally to be the result of $J = 5/2 \rightarrow 3/2$ conversion. The slopes of plots of the type shown in Figures 5–8 are given by k_Q. All of the results of the present investigation are given in Table I.

In our previous investigation on $As(4^2D_J)$ and $As(4^2P_J)$,[36,37] we had shown experimentally that the relaxation of the J levels in each state was the same. This arose on account of the relatively small J splittings ($\Delta E(As(4^2D_{5/2})-As(4^2D_{3/2})) = 322$ cm^{-1}; $\Delta E(As(4^2P_{3/2})-As(4^2P_{1/2})) = 461$ cm^{-1})[37] which resulted in the maintenance of a Boltzmann equilibrium arising from the small electronic energies to be transferred, even if only to translation.[52] Hence it was meaningful to compare the data for $As(4^2D_J)$ and $As(4^2P_J)$ with those of $P(3^2D_J, 3^2P_J)$ and $N(2^2D_J, 2P_J)$, discussing all of the data within the context of correlation diagrams based on the weak spin–orbit coupling approximation.[36] Although the present study clearly falls within the general framework of the analogous data for N → Bi, it is obvious that we are concerned here with heavy atoms, showing different kinetics for the different spin–orbit states and where (J,Ω) coupling only can be considered. Hence, we restrict the comparison of our data for $Bi(6^2D_{3/2,5/2})$ with those of the other relatively heavy atom in group 5, Sb, showing differing collisional behavior for the J states, and these, where available, are given in Table I.

Noble Gases. There is no major effect by the noble gases He and Xe on the quenching of either spin–orbit state (Table I). We presume that the standard mechanism employed by Ewing et al.[27] for $Pb(6^3P_{1,2})$ will apply here, namely, a Hund's coupling case (c) molecular description at large atomic separation, converging, presumably via repulsive states, to a common electronic state at close internuclear distance in Hund's case (a) or (b).

Hydrogen and Deuterium. Experimentally, the data for $Bi(6^2D_{3/2})$ showed some anomalous behavior in that the plot of $\gamma(k' - K)$ vs. p_{H_2} began to flatten out at p_{H_2} = ca. 200 N m^{-2}. Investigation of this effect was considered too complex for the present system and we have therefore simply taken the initial slope of the plot in order to calculate

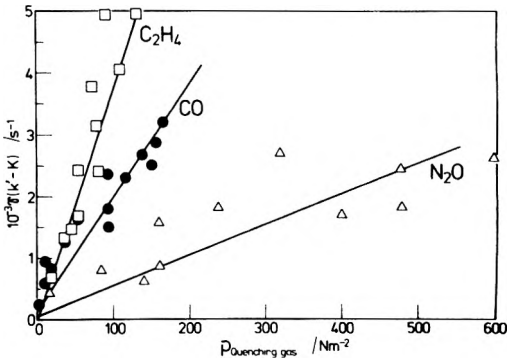

Figure 5. Pseudo-first-order rate coefficients ($\gamma(k' - K)$) for the decay of $Bi(6^2D_{3/2})$ in the presence of carbon monoxide, nitrous oxide, and ethylene; p_{BiMe_3} = 0.40 N m^{-2}, $p_{total\ with\ He}$ = 6.66 kN m^{-2}; E = 845 J.

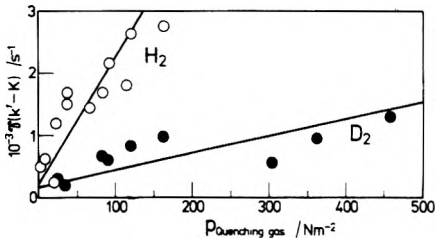

Figure 6. Pseudo-first-order rate coefficients ($\gamma(k' - K)$) for the decay of $Bi(6^2D_{3/2})$ in the presence of hydrogen and deuterium; p_{BiMe_3} = 0.40 N m^{-2}, $p_{total\ with\ He}$ = 6.66 kN m^{-2}; E = 845 J.

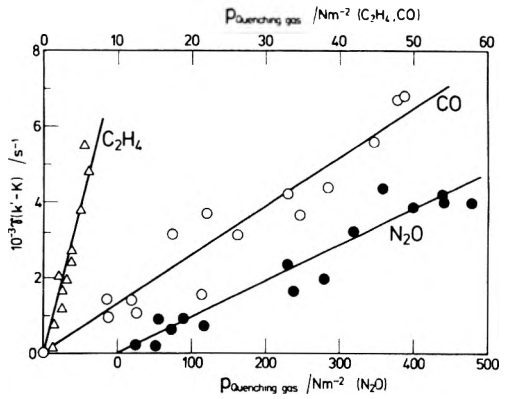

Figure 7. Pseudo-first-order rate coefficients ($\gamma(k' - K)$) for the decay of $Bi(6^2D_{5/2})$ in the presence of carbon monoxide, nitrous oxide, and ethylene; p_{BiEt_3} = 1.5 N m^{-2}, $p_{total\ with\ He}$ = 6.66 kN m^{-2}; E = 845 J.

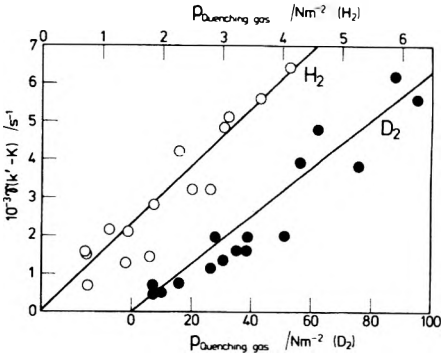

Figure 8. Pseudo-first-order rate coefficients ($\gamma(k' - K)$) for the decay of $Bi(6^2D_{5/2})$ in the presence of hydrogen and deuterium; p_{BiEt_3} = 1.5 N m^{-2}, $p_{total\ with\ He}$ = 6.66 kN m^{-2}; E = 845 J.

TABLE I: Rate Constants (k_Q, cm^3 molecule^{-1} s^{-1}, 300 K) for the Collisional Removal of Bi($6^2D_{3/2,5/2}$) and Sb($5^2D_{3/2,5/2}$) by Various Gases

Gas	Bi($6^2D_{3/2}$)(1.416 eV)	Bi($6^2D_{5/2}$)(1.914 eV)	Sb($5^2D_{3/2}$)(1.055 eV)[39]	Sb($5^2D_{5/2}$)(1.222 eV)[39]
He	$(4.8 \pm 1.1) \times 10^{-16}$	$(4.2 \pm 2.5) \times 10^{-16}$	$< 10^{-16}$	$\leq 6 \times 10^{-15}$
Xe	$\leq (2.4 \pm 1.0) \times 10^{-15}$	$< 5 \times 10^{-15}$		
H_2	$(7.9 \pm 0.8) \times 10^{-14}$	$(5.6 \pm 0.5) \times 10^{-12}$	$(6.6 \pm 0.2) \times 10^{-12}$	$(2.5 \pm 0.3) \times 10^{-12}$
D_2	$(1.1 \pm 0.3) \times 10^{-14}$	$(2.4 \pm 0.2) \times 10^{-13}$		
O_2		$(8.1 \pm 0.6) \times 10^{-12}$	$(1.7 \pm 0.1) \times 10^{-11}$	$(1.8 \pm 0.2) \times 10^{-11}$
N_2	$< 2 \times 10^{-15}$	$< 5 \times 10^{-15}$		
CO	$(7.6 \pm 0.6) \times 10^{-14}$	$(5.4 \pm 0.3) \times 10^{-13}$	$(1.3 \pm 0.1) \times 10^{-11}$	$(7.5 \pm 1.1) \times 10^{-12}$
CO_2	$< 4 \times 10^{-15}$	$(2.1 \pm 0.1) \times 10^{-13}$	$(2.1 \pm 0.5) \times 10^{-13}$	$< 1 \times 10^{-13}$
N_2O	$(1.9 \pm 0.2) \times 10^{-14}$	$(3.8 \pm 0.2) \times 10^{-14}$		
C_2H_4	$(1.6 \pm 0.1) \times 10^{-13}$	$(3.3 \pm 0.3) \times 10^{-12}$		

k_Q as a basis for discussion. No anomalous behavior was observed with the remainder of the relevant data appropriate to this section.

Separate consideration in some detail of the quenching of the two spin–orbit states by H_2 and D_2 is merited here, particularly in view of recent strong current interest in such isotope effects.[7,53-56] First, in view of the relative novelty of discussing heavy atom–molecule collisions in terms of correlation diagrams based on (J,Ω) coupling and also in view of the difference from the appropriate diagram given hitherto for Sb + H_2,[39] that correlating the relevant states of Bi + H_2 and BiH + H is given here (Figure 9). This diagram is constructed using Gaydon's[57] recommended value for the bond dissociation energy of BiH of 2.5 ± 0.3 eV, based on a linear Birge–Sponer extrapolation of Heimer's data.[58] Further, and particularly relevant to our discussion, is that Herzberg[59] and Rosen[60] have designated the relevant low-lying states in Hund's coupling case (c). Hence, in purely electronic terms, either reaction (possibly for Bi($6^2D_{5/2}$)) or physical quenching for both states must involve nonadiabatic transitions (NAT) in the absence of suitable correlations (Figure 9). The quenching processes may further be facilitated by a chemical interaction involving a BiH_2 species analogous to AsH_2.[61]

As to the effect of the hydrogen isotopes in determining the magnitudes of the probabilities of the NAT's, while the effect is not as dramatic as that observed hitherto for I($5^2P_{1/2}$),[3,4,53] large differences are observed. Quenching of the $^2D_{3/2}$ state by H_2 is 7 times faster than that by D_2 (Table I). No simple reason for this is offered. Near-resonance processes would involve multiquantum vibrational jumps. On the other hand, the faster quenching rate of the $^2D_{5/2}$ state by H_2 may arise from the near-resonance process Bi($6^2D_{5/2}$) + $H_2(v'' = 0)$ → Bi($6^2D_{3/2}$) + $H_2(v'' = 1)$; ΔE = +140 cm^{-1}. Further, the recent calculation by Ewing[55] on the quenching of Pb($6^3P_{1,2}$) and Sn($5^3P_{1,2}$) by H_2 and D_2, employing a modified form of the theory of Sharma and Brau[53,54] and involving long-range multipole interactions for near-resonance E (electronic) → V (vibration), R (rotation) transfer, clearly shows that electronic selection rules as well as nuclear dynamic factors are critical in considering such processes. It can only be hoped that this type of calculation in the future may include consideration of the data presented here, in particular, the faster rates for the $^2D_{5/2}$ state (assuming, of course, that this is not due to chemical reaction). Furthermore, arguments based on the Sharma–Brau theory have been employed by Butcher et al.[53] to account for the temperature dependence of the quenching of I($5^2P_{1/2}$) by H_2, D_2, and HD.[4,53] One conclusion of this work[53] is the emergence of "propensity" or selection rules for rotation for long-range interactions as

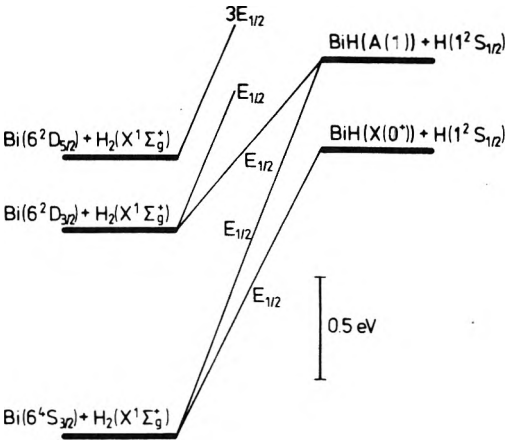

Figure 9. Correlation diagram connecting the states of Bi + H_2 and BiH + H using (J,Ω) coupling for reactants and products.

observed through such temperature effects. This is clearly one direction for future work in the present case.

Diatomic Molecules. While Bi($6^2D_{3/2}$) exhibited good first-order plots in the presence of molecular oxygen, the plot of $\gamma(k' - K)$ vs. p_{O_2} showed a large initial *decrease* with *increasing* pressure of the quenching molecule. This presumably arises from pumping of the $^4S_{3/2}$ ground state by the low-lying $b^1\Sigma_g^+$ state of molecular oxygen,[60,61] which, in turn, has resulted from energy-transfer processes. Although the system is complex, one can certainly say that, in general, relatively slow rates were observed for the decay of the $^2D_{3/2}$ state with O_2. By contrast, the $^2D_{5/2}$ state, generated only in small concentrations in this particular system, showed a relatively more rapid systematic decay with no anomalous behavior, presumably because population into the state by energy transfer from the low-lying states of O_2 could not take place. The decay rates for Bi($6^2D_{3/2}$) and Bi($6^2D_{5/2}$) were *slower* than those for their antimony analogues, and this is consistent with the relevant correlation diagrams. That connecting the states of Sb + O_2 and SbO + O has been given previously[39] and the diagram for the bismuth system is presented here (Figure 10). In the case of antimony, there are either thermoneutral or exothermic adiabatic pathways leading directly to chemical products for both atomic states; in the case of Bi($6^2D_{3/2,5/2}$) + O_2, all processes, whether of reaction or relaxation, must involve NAT's, as readily seen in Figure 10.

No detailed discussion is presented for quenching by molecular nitrogen or carbon monoxide. Chemical reaction of either spin–orbit state with either molecule would be highly endothermic and relaxation must occur in both cases by NAT's with the appropriate $E_{1/2}$ surfaces. In the case of

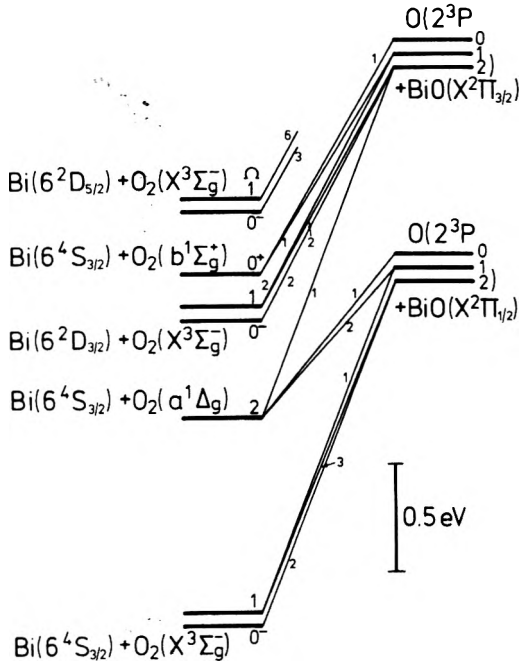

Figure 10. Correlation diagram connecting the states of Bi + O_2 and BiO + O using (J,Ω) coupling for reactants and products. (All surfaces are of the type $E_{-/2}$. Correlations are indicated by the number of $E_{1/2}$ surfaces.)

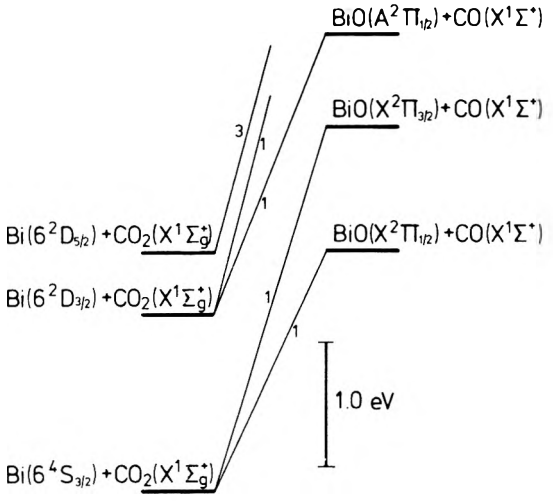

Figure 11. Correlation diagram connecting the states of Bi + CO_2 and BiO + CO using (J,Ω) coupling for reactants and products and assuming C_s symmetry in the collision complex. (All surfaces are of the type $E_{1/2}$. Correlations are indicated by the number of $E_{1/2}$ surfaces.)

CO (where the data for Bi($6^2D_{3/2}$) + CO were derived from the initial-slope method as described for this spin–orbit state with H_2), relaxation is clearly seen to be slower than that indicated by the analogous data for Sb($5^2D_{3/2,5/2}$)[39] (Table I).

In the cases of both antimony and bismuth, we presume that quenching is to some degree facilitated by chemical interaction.

Carbon Dioxide and Nitrous Oxide. The relatively slow rates (Table I) for the quenching of Bi($6^2D_{3/2}$) and Bi($6^2D_{5/2}$) by carbon dioxide are consistent with the appropriate correlation diagram (Figure 11) where there are clearly no direct adiabatic pathways to products. On the other hand, the low probabilities for deactivation and/or reaction for both states with nitrous oxide (Table I) are

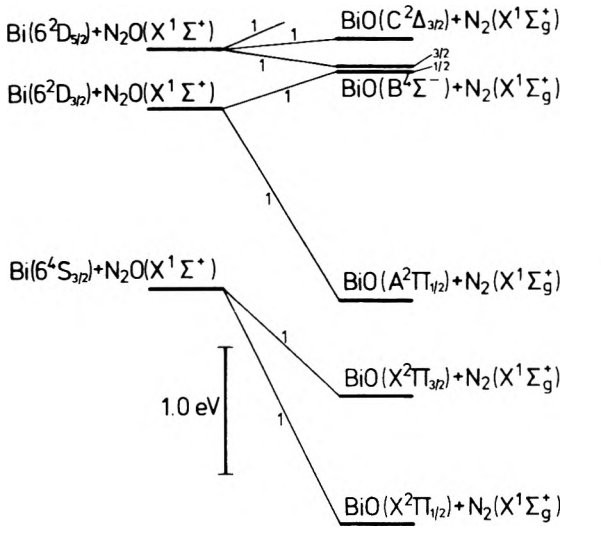

Figure 12. Correlation diagram connecting the states of Bi + N_2O and BiO + N_2 using (J,Ω) coupling for reactants and products and assuming C_s symmetry in the collision complex. (All surfaces are of the type $E_{1/2}$. Correlations are indicated by the number of $E_{1/2}$ surfaces.)

surprising in view of there clearly being direct channels leading exothermically to products (Figure 12). However, we may at least note that, especially in the case of N_2O, there are a large number of different atomic states for which there are often many surfaces leading directly and exothermically to products; these states, however, involve collisional removal rates of low probability.[11,12] This is particularly the case for a range of light atomic species where the weak spin–orbit coupling approximation has been employed.[11,12] Appropriate examples are too numerous to discuss and the reader is referred to the relevant papers cited in reviews.[11,12] The traditional explanation and one which we would put forward here is that the N_2O molecule is characterized by a linear, closed-shell electronic structure, and hence any collisional interaction with an atom, particularly involving any degree of electron promotion for the quenching molecule, will be characterized by a significant potential energy barrier.

Ethylene. Relaxation by ethylene is presumed to arise from chemical interaction with the π-bond system of the quenching molecule.

Acknowledgment. We thank the Science Research Council of Great Britain for a research studentship held by M.J.B., during the tenure of which this work was carried out, and for a grant for equipment.

References and Notes

(1) D. Husain and R. J. Donovan, *Adv. Photochem.*, **8**, 1 (1970).
(2) D. Husain and J. R. Wiesenfeld, *Trans. Faraday Soc.*, **63**, 1349 (1967).
(3) J. J. Deakin and D. Husain, *J. Chem. Soc., Faraday Trans. 2*, **68**, 41 (1972).
(4) J. J. Deakin and D. Husain, *J. Chem. Soc., Faraday Trans. 2*, **68**, 1603 (1972).
(5) J. A. Bellisio and P. Davidovits, *J. Chem. Phys.*, **53**, 3474 (1970).
(6) J. R. Wiesenfeld, *Chem. Phys. Lett.*, **21**, 517 (1973).
(7) P. D. Foo, T. Lohman, J. Podolske, and J. R. Wiesenfeld, *J. Phys. Chem.*, **79**, 414 (1975).
(8) R. J. Donovan and D. J. Little, *J. Chem. Soc., Faraday Trans. 2*, **69**, 952 (1973).
(9) R. J. Donovan and D. Husain, *Trans. Faraday Soc.*, **62**, 2643 (1966).
(10) R. J. Donovan and D. Husain, *Trans. Faraday Soc.*, **62**, 2987 (1966).
(11) R. J. Donovan and D. Husain, *Annu. Rep. Prog. Chem., Sect. A*, **68**, 124 (1972).
(12) R. J. Donovan, D. Husain, and L. J. Kirsch, *Annu. Rep. Prog. Chem.*,

Sect. A, **69**, 19 (1973).
(13) D. Husain, submitted for publication in *Acc. Chem. Res.*
(14) R. J. Donovan and D. Husain, *Chem. Rev.*, **70**, 489 (1970).
(15) K. E. Shuler, *J. Chem. Phys.*, **21**, 624 (1953).
(16) A. Brown and D. Husain, *J. Photochem.*, **3**, 305 (1974).
(17) A. Brown and D. Husain, *J. Chem. Soc., Faraday Trans. 2*, **71**, 699 (1975).
(18) A. Brown and D. Husain, *J. Photochem.*, **3**, 37 (1974).
(19) A. Brown and D. Husain, *Int. J. Chem. Kinet.*, **7**, 77 (1975).
(20) D. Husain and J. G. F. Littler, *J. Photochem.*, **1**, 327 (1972).
(21) D. Husain and J. G. F. Littler, *J. Chem. Soc., Faraday Trans. 2*, **69**, 842 (1973).
(22) D. Husain and J. G. F. Littler, *Chem. Phys. Lett.*, **16**, 145 (1972).
(23) D. Husain and J. G. F. Littler, *J. Chem. Soc., Faraday Trans. 2*, **68**, 2110 (1972).
(24) P. D. Foo, J. R. Wiesenfeld, and D. Husain, *Chem. Phys. Lett.*, **32**, 443 (1975).
(25) P. D. Foo, J. R. Wiesenfeld, and D. Husain, *J. Phys. Chem.*, in press.
(26) D. Husain and J. G. F. Littler, *Int. J. Chem. Kinet.*, **6**, 61 (1974).
(27) J. J. Ewing, D. W. Trainor, and S. Yatsiv, *J. Chem. Phys.*, **61**, 4433 (1974).
(28) A. Brown and D. Husain, *Can. J. Chem.*, in press.
(29) C.-L. Lin and F. Kaufman, *J. Chem. Phys.*, **55**, 3760 (1971).
(30) D. Husain, L. J. Kirsch, and J. R. Wiesenfeld, *Faraday Discuss. Chem. Soc.*, **53**, 201 (1972).
(31) G. Black, T. G. Slanger, G. A. St. John, and R. A. Young, *J. Chem. Phys.*, **51**, 116 (1965).
(32) D. Husain, S. K. Mitra, and A. N. Young, *J. Chem. Soc., Faraday Trans. 2*, **70**, 1721 (1974).
(33) A. U. Acuna, D. Husain, and J. R. Wiesenfeld, *J. Chem. Phys.*, **58**, 494 (1973).
(34) A. U. Acuna, D. Husain, and J. R. Wiesenfeld, *J. Chem. Phys.*, **58**, 5272 (1973).
(35) A. U. Acuna and D. Husain, *J. Chem. Soc., Faraday Trans. 2*, **69**, 585 (1973).
(36) M. J. Bevan and D. Husain, *Int. J. Chem. Kinet.*, **7**, 63 (1975).
(37) M. J. Bevan and D. Husain, *J. Photochem.*, **3**, 1 (1974).
(38) A. B. Callear and R. J. Oldman, *Trans. Faraday Soc.*, **64**, 840 (1968).
(39) M. J. Bevan and D. Husain, *J. Photochem.*, **4**, 51 (1975).
(40) C. E. Moore, Ed., *Natl. Bur. Stand. (U.S.), Circ.*, No. 467 (1958).
(41) J. Connor, P. J. Young, and O. P. Strausz, *J. Am. Chem. Soc.*, **93**, 822 (1971).
(42) P. P. Sorokin, J. R. Lankard, V. L. Moruzzi, and E. C. Hammond, *J. Chem. Phys.*, **48**, 4726 (1968).
(43) M. J. Bevan, A. Brown, and D. Husain, *Analyst (London)*, in press.
(44) M. Seya, *Sci. Light (Tokyo)*, **2**, 8 (1952).
(45) T. Namioka, *Sci. Light (Tokyo)*, **3**, 15 (1954).
(46) R. H. Garstang, *J. Res. Natl. Bur. Stand., Sect. A*, **68**, 61 (1964).
(47) W. H. Wing and T. M. Sanders, *Rev. Sci. Instrum.*, **38**, 1341 (1967).
(48) C. H. Bamford, D. L. Levi, and D. M. Newitt, *J. Chem. Soc.*, 468 (1946).
(49) C. H. Corliss and W. R. Bozman, *Nat. Bur. Stand. (U.S.), Monogr.*, **No. 53** (1962).
(50) R. J. Donovan, D. Husain, and L. J. Kirsch, *Trans. Faraday Soc.*, **66**, 2551 (1970).
(51) D. Husain and J. G. F. Littler, *J. Photochem.*, **2**, 247 (1973).
(52) A. B. Callear, *Appl. Opt., Suppl.*, No. 2, 145 (1965).
(53) R. J. Butcher, R. J. Donovan, and R. H. Strain, *J. Chem. Soc., Faraday Trans. 2*, **70**, 1837 (1974).
(54) R. D. Sharma and C. A. Brau, *Phys. Rev. Lett.*, **19**, 1273 (1967).
(55) R. D. Sharma and C. A. Brau, *J. Chem. Phys.*, **50**, 924 (1969).
(56) J. J. Ewing, *Chem. Phys. Lett.*, **29**, 50 (1974).
(57) A. G. Gaydon, "Dissociation Energies and Spectra of Diatomic Molecules", Chapman and Hall, London, 1968.
(58) A. Heimer, *Z. Phys.*, **95**, 328 (1935).
(59) G. Herzberg, "Spectra of Diatomic Molecules", Van Nostrand, New York, N.Y., 1961.
(60) B. Rosen, "Spectroscopic Data Relative to Diatomic Molecules", Pergamon Press, Oxford, 1970.
(61) R. N. Dixon, G. Duxburg, and H. M. Lamberton, *Proc. R. Soc. London, Ser. A*, **305**, 271 (1968).

Photoreduction of Hydrogen Peroxide by Hydrogen

Richard J. Field,*[1a,b,d] Richard M. Noyes,[1b] and Dennis Postlethwaite[1b,c]

Radiation Research Laboratories and Department of Chemistry, Mellon Institute of Science, Carnegie-Mellon University, Pittsburgh, Pennsylvania 15213 and Department of Chemistry, University of Oregon, Eugene, Oregon 97403 *(Received June 16, 1975)*

Publication costs assisted by the U.S. Energy Research and Development Administration

The photoreduction of hydrogen peroxide in water under hydrogen of up to 100 atm pressure has been investigated. The reaction involves a chain mechanism with the quantum efficiency for the disappearance of hydrogen peroxide being strongly dependent upon the concentration of hydrogen peroxide. A maximum quantum efficiency of about 35 mol/einstein occurs at a hydrogen peroxide concentration of about 5×10^{-4} M. At higher hydrogen peroxide concentrations the reaction ($HO\cdot + H_2O_2 \rightarrow H_2O + HO_2\cdot$), which leads to chain termination by subsequent $HO_2\cdot$ reactions, is competitive with the chain-propagating reaction ($HO\cdot + H_2 \rightarrow H_2O + H\cdot$) so that the quantum efficiency decreases with increasing $[H_2O_2]$. At lower hydrogen peroxide concentrations the chain-propagating step ($H\cdot + H_2O_2 \rightarrow H_2O + HO\cdot$) cannot compete with chain termination by ($H\cdot + O_2 \rightarrow HO_2\cdot$) so the yield again decreases. Scavenging of hydrogen atoms at lower hydrogen peroxide concentrations is not well understood. The participation of $HO_2\cdot$ radical is inferred from the observation of a strong pH effect which shows an inflection point at a pH near the pK_a of $HO_2\cdot$ (4.88). A complex mechanism for the reaction is proposed and analyzed by numerical integration of the resulting rate expressions. This part of the work is an example of the usefulness of recently developed numerical integration techniques in the analysis of complex nonlinear reaction mechanisms.

Introduction

Because the reactions of radicals in solution are often so rapid that rates are controlled by diffusion times, the diffusion coefficients of such species are of considerable practical interest. Furthermore, precise values of these diffusion coefficients contribute to a more detailed theory of molecular behavior in liquids. However, exactly because of the reactivity of these radicals, it is virtually impossible to measure their diffusion coefficients using conventional techniques.[2] Noyes has developed[3] and applied[4] a technique based upon the fact that if photochemically produced radicals are destroyed by a second-order process and if a cell is

illuminated with a pattern of light and dark areas, then the average radical concentration in space depends upon the intensity of the light, the sizes of individual light areas, and the diffusive properties of the radical. This average radical concentration can be conveniently measured if the radical takes part in a chain process whose quantum efficiency can be measured. The technique is called photochemical space intermittency (PSI). The hydrogen atom is a very reactive radical whose diffusive properties are interesting both in their own right and as part of the radiation chemistry of aqueous systems.[5] It was proposed to use PSI to determine its diffusion coefficient in water. The photoreduction of hydrogen peroxide by hydrogen in water seemed a likely system in which to establish the required long chain mechanism with termination only by hydrogen atom recombination. However, it was not possible to establish these conditions and we report here only the results of a kinetic investigation of the system.

The elementary processes originally expected to participate in the reaction are

$$H_2O_2 + h\nu \rightarrow 2HO\cdot$$

$$HO\cdot + H_2 \rightarrow H_2O + H\cdot \quad (1)$$

$$H\cdot + H_2O_2 \rightarrow H_2O + HO\cdot \quad (2)$$

$$H\cdot + H_2O_2 \rightarrow H_2 + HO_2\cdot \quad (3)$$

$$HO\cdot + H_2O_2 \rightarrow H_2O + HO_2\cdot \quad (4)$$

$$H\cdot + O_2 \rightarrow HO_2\cdot \quad (5)$$

$$HO_2\cdot + HO_2\cdot \rightarrow H_2O_2 + O_2 \quad (8)$$

$$H\cdot + H\cdot \rightarrow H_2 \quad (14)$$

Because of the similarity in magnitude[6] of the rate constants of reactions 1, 2, and 4 the ratio $[H_2]/[H_2O_2]$ must be much greater than one to suppress formation of the chain-terminating $HO_2\cdot$ radical and to keep $[H\cdot]/[HO\cdot]$ sufficiently large that only hydrogen atoms participate significantly in chain termination. Calculations using available rate constants[6] and neglecting reaction 3 indicate that in order to establish these conditions experiments must be done using solutions under at least 100 atm of hydrogen. Even at this hydrogen concentration (0.078 *M*) reaction 4 totally dominates chain termination at hydrogen peroxide concentrations near 0.01 *M* and the quantum efficiencies for hydrogen peroxide reduction are of the order of 1–2 mol/einstein. According to the above mechanism, only at hydrogen peroxide concentrations less than 10^{-5} *M* and in the absence of O_2 can termination by hydrogen atom combination become dominant. The calculated quantum efficiency under these conditions is about 1000 mol/einstein.

Experimental Section

Materials. The hydrogen used was Matheson Ultra-High Purity grade and the manufacturer's analysis found it to be 99.999% pure. In some experiments the hydrogen was passed through a liquid N_2 trap before use. Baker Analyzed reagent grade 30% H_2O_2 and 70% $HClO_4$ were used without further purification. All water was triply distilled with the second and third distillations being from acidic dichromate and basic permanganate, respectively. In some cases the water was subjected to ^{60}Co (γ) irradiation before use and the H_2O_2 thus generated was used directly in the photolysis experiments.[7] All glassware was cleaned in hot dilute HNO_3–H_2O_2 solutions and baked in an oven before use.

Photolysis Cells and the Pressure Chamber. The photolyses were carried out using an all quartz vessel with three compartments (Figure 1) contained in a stainless steel chamber (Figure 1) capable of sustaining pressures of over 100 atm. The system was designed so that the photolyte could be prephotolyzed to deactivate impurities. Prephotolysis leads to a net consumption of oxygen in experiments having hydrogen peroxide concentrations of less than 10^{-5} *M*. The three compartment vessel had two cells which were actually used for photolysis. These cells were 1 cm deep, had a diameter of 2 cm and were attached to a central reservoir by 1-mm capillary tubing. This cylindrical central reservoir was 10 cm long and had a diameter of 2 cm. The pressure chamber had three windows (Figure 1) of which two were situated so that the two cells could be positioned in a light beam. The third window was positioned so that by using a mirror the entire length of the central reservoir could be photolyzed. The windows were made of quartz disks that were $\frac{5}{8}$ in. thick and had a diameter of 2 in. They were seated on 1.25-in. rubber "O" rings. The windows withstood pressures of up to 100 atm. Access to the interior of the pressure chamber was by the removal of a 1 in. thick 7 in. diameter plate held in place by 36, $\frac{5}{16}$-in. bolts. The pressure chamber had wheels and ran on a track so that either cell could be positioned in the highly collimated photolysis beam or all three windows could be positioned in a diffuse prephotolysis beam.

Photolysis Lamp. Since the eventual goal of this work was the use of photochemical space intermittency, the photolysis beam was highly collimated so that the patterns could be accurately projected. This was done using a 100-W, low-pressure, point source mercury lamp obtained from PEK, Sunnyvale, Calif. The light from this lamp was passed through a diffraction filter with a maximum transmission near 2537 Å and then focused using a quartz lens. Actinometry was done using potassium ferrioxalate according to Calvert and Pitts.[8] The rate of absorption of light by H_2O_2, *R*, was found to be

$$R\left(\frac{\text{einstein}}{\text{liter sec}}\right) = I_0(1 - e^{-\epsilon l[H_2O_2]})\frac{A}{V} =$$

$$1.1 \times 10^{-7}(1 - e^{-20[H_2O_2]})$$

where ϵ is molar absorptivity of H_2O_2 at 2537 Å (20 M^{-1} sec^{-1}), l is the light path in the cell (1 cm), A is the area of the light beam passing through the cell, and V is the volume of the cell.

Procedure. The chamber was pressurized by hydrogen led in through the photolysis cells as shown in Figure 1. During pressurization the photolyte was pushed out of the cells into the central reservoir and all of the entering gas bubbled through it. This was done to ensure (as much as possible) that the photolyte was purged of foreign gasses and saturated with H_2. In each experiment the system was degassed by five cycles of pressurization to 5 atm with H_2 followed by evacuation to about 50 Torr. The H_2 pressure was then slowly raised to that desired for the photolysis. When the final pressure was attained, pressures among the three compartments were equalized so that the photolyte reached the same level in each. The system was then prephotolyzed for several hours using a low-pressure mercury lamp. Generally near 10% of the photolyte was consumed in prephotolysis. After prephotolysis a small pressure differential was applied to the leads of the cells and all of the photolyte pushed into the central reservoir and mixed. After reequalization of pressures the two cells were photo-

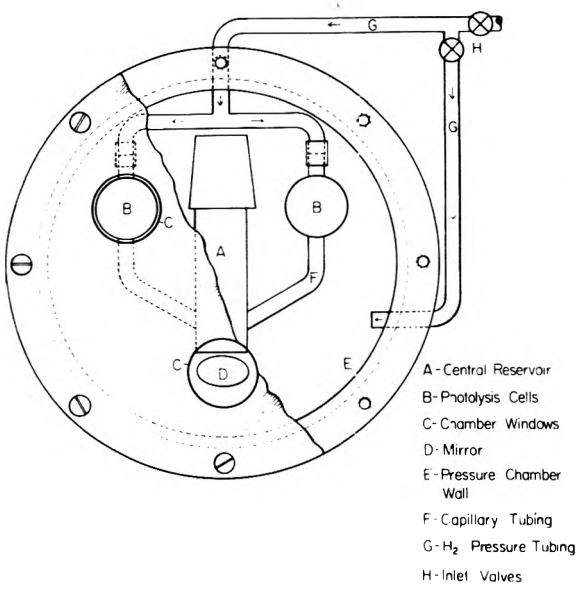

Figure 1. Diagram of the pressure chamber and the photolysis cell used in this work.

lyzed with the sample in the central reservoir used to establish the initial H_2O_2 concentration in the cells. Depressurization had to be done very carefully to avoid mixing of the contents of the three compartments.

Analysis for the concentration of H_2O_2 was done using the method of Ghormley.[9] The H_2O_2 was allowed to oxidize iodide ion to triiodide ion using molybdate as a catalyst and the triiodide ion determined spectrophotometrically at 3540 Å. This analysis was accurate to 5% in the 10^{-6} to 10^{-5} M H_2O_2 range.

Results and Discussion

Experiments were initially performed using a hydrogen pressure of 100 atm and hydrogen peroxide concentrations in the range 10^{-6} to 10^{-5} M since these were the conditions expected to be useful for PSI. However, the observed quantum efficiencies for hydrogen peroxide reduction were found to be only 1 or 2 mol/einstein rather than the larger values expected from the calculations. The discrepancy was laid to chain inhibition probably by an adventitious impurity and every effort was made to find and exclude the source of the inhibition. The hydrogen used was the purest available commercially but attempts were made to purify it further using various traps. All water was triply distilled and in some cases it was irradiated in a ^{60}Co γ source before use. In these cases the hydrogen peroxide generated by the irradiation was used directly in the experiments thus eliminating the added hydrogen peroxide as a source of contamination.[7] After the system was degassed and hydrogen introduced to the desired pressure the solution was strongly prephotolyzed before each experiment. At these lower hydrogen peroxide concentrations, the system is reducing, and it is expected that prephotolysis led to a net consumption of reducible impurities. These include oxygen even though it is in fact produced in experiments at higher hydrogen peroxide concentrations. However these efforts had no effect and the quantum efficiency stubbornly remained in the 1 to 2 mol/einstein range.

Finally, in order to establish the general validity of the mechanism of eq 1–5, 8, and 14, experiments were carried out over much wider ranges of hydrogen and hydrogen peroxide concentrations. Figures 2 and 3 show the results obtained at pH 2 and at hydrogen pressures of 10 and 100 atm, respectively, as the hydrogen peroxide concentration is varied. The dashed line in Figure 3 shows the results expected on the basis of a mechanism including reactions 1, 2, 4, 5, 8, and 14 and with no O_2 present initially. The behavior at higher hydrogen peroxide concentrations is as expected. The quantum efficiency starts out near 1 mol/einstein at $[H_2O_2]$ = 0.1 M and rises as $[H_2O_2]$ decreases toward 10^{-3} M, but between 10^{-3} and 10^{-4} M hydrogen peroxide the quantum efficiency passes through a maximum and then falls back to 1–2 mol/einstein as $[H_2O_2]$ falls below 10^{-5} M. Figures 2 and 3 indicate that there is a chain-inhibiting process that becomes important at hydrogen peroxide concentrations lower than 5×10^{-4} M. Since H_2O_2 participates in chain propagation only through its reaction with hydrogen atoms to produce hydroxyl radicals (reaction 2), it seems that the inhibiting process must act by removing hydrogen atoms. Reaction 5 is a good candidate for the inhibitory process since $HO_2\cdot$ is a chain-terminating species and it is very difficult to exclude oxygen from aqueous solutions.

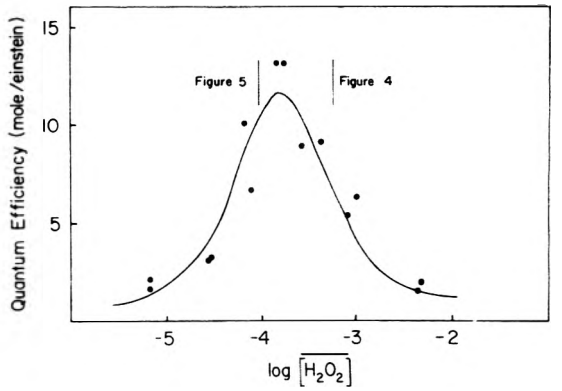

Figure 2. Experimental (●) and calculated (——) values of the quantum efficiency of photoreduction of H_2O_2 over a broad range of H_2O_2 concentrations and at a pH of 2. The H_2 concentration is assumed to be 0.0078 M which is the equilibrium value for a solution under 10 atm of H_2 gas. The vertical lines on either side of the maximum quantum efficiency indicate the H_2O_2 concentrations used in Figures 4 and 5.

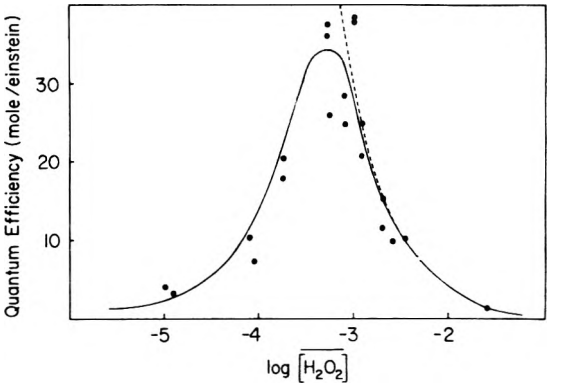

Figure 3. Experimental (●) and calculated (——) values of the quantum efficiency of photoreduction of H_2O_2 over a broad range of H_2O_2 concentrations and at a pH of 2. The H_2 concentration is assumed to be 0.078 M which is the equilibrium value for a solution under 100 atm of H_2 gas. The dashed line indicates the behavior calculated by considering only reactions 1, 2, 4, 5, 8, and 14.

Numerical Integration. Even in a system as simple as this one which contains in principle only the two elements

hydrogen and oxygen, a rather large number of formally possible chemical reactions can be written. Some can be immediately eliminated as thermodynamically unfavorable or as having rate constants too small to be competitive, but 21 reactions remain which might become important at some point in the wide range of experimental conditions investigated here. They are listed in Table I.

Comparison of a model composed of a large number of elementary reactions with data obtained over a wide range of experimental conditions is most conveniently done by numerical integration of the rate expressions resulting from the model. This was done here using a HP-9830A programmable desk calculator and a BASIC version[10] of the algorithm due to Gear[11] for numerical integration of "stiff" differential equations. This method allows the calculation to be done without recourse to the steady-state approximation.[12] Numerical integration is most useful for treating chemical kinetics data when the values of the rate constants for most or all of the reactions are known initially. Table I lists the literature values available for the model used here. The values of some other rate constants were estimated or treated as parameters to be varied until a good fit to the experimental data was achieved. The rate constants for the acidic dissociation of the hydroperoxy radical ($pK_a = 4.88$)[13] were assumed to be comparable to those determined for acetic acid[14] which has a very similar pK_a. The estimated rate constants are by far large enough so that equilibrium between $HO_2\cdot$ and O_2^- was always maintained during the integrations. Reaction 19 represents the removal of hydrogen atoms by an unknown process. The pseudo-first-order rate constant for this reaction, k_{19}, may be the product of the concentration of an inhibitor and the second-order rate constant for its reaction with hydrogen atoms. This step only becomes important at lower hydrogen peroxide concentrations. The value of k_{20} is apparently strongly dependent upon experimental conditions (Table II) and it was treated as an expendable parameter in the present work. The value obtained by Davies, Kirschenbaum, and Kustin (Table II, ref e) at pH 0 probably corresponds to reaction 20a rather than reaction 20.

$$H_2O_2^+ + H_2O_2 \rightarrow HO\cdot + H_3O^+ + O_2 \qquad (20a)$$

The model composed of the reactions in Table I leads to a set of five simultaneous differential equations in the concentrations of the species: H·, HO·, $HO_2\cdot$, O_2^-, and O_2. The concentration of hydrogen peroxide was held constant to save calculation time. The photolysis times were adjusted so that less than 20% of the H_2O_2 would have been consumed. The times used in the calculations were very similar to the experimental photolysis times and were in the range of 1 500–40 000 sec. The initial concentrations of the radical intermediates H·, HO·, $HO_2\cdot$, and O_2^- were set at 10^{-15} M and the calculations indicated that they reached pseudo-steady-state[12] concentrations after a few seconds of photolysis. It was found at lower hydrogen peroxide concentrations that the value chosen for the initial concentration of oxygen was very critical and so it is clear that the experimental results will depend very strongly on the purity of the hydrogen used. The manufacturer of the hydrogen used in the experiments reported that it contained less than 1 ppm oxygen. A thoroughly degassed solution under 100 atm of this gas will be in equilibrium with 0.076 mmHg of O_2 and have an O_2 concentration of about 10^{-7} M. Calculations were carried out using initial O_2 concentrations in the range of 10^{-8} to 10^{-6} M. The lower values may be justified at lower hydrogen peroxide concentrations because of the effect of the prephotolysis.

It was immediately apparent over the entire range of reactant concentrations and initial conditions of experimental interest here that reactions 1 and 4 are fast enough to be the only significant fates of the hydroxyl radical. The diffusion-controlled radical–radical reactions 15–18 were not included in later calculations.

Higher Hydrogen Peroxide Concentrations. The solid lines in Figures 2 and 3 show quantum efficiencies calculated using the model and rate constants listed in Table I. The agreement between experimental and calculated values of the quantum efficiency is good over a range of H_2 concentrations of a factor of ten and a range of H_2O_2 concentrations of a factor of several thousand. However the results obtained at concentrations of H_2O_2 higher than that at which the maximum quantum efficiency occurs are more satisfying than those at lower concentrations of H_2O_2 since these calculated values of the quantum efficiency depend only upon already established rate constants. At these higher concentrations of H_2O_2 the removal of hydrogen atoms by reaction 19 is too slow to compete with reactions 2, 3, and 5. Furthermore, even in this strongly reducing solution, net production of O_2 by the sequence of reaction 4 followed by reactions 8 or 9 quickly leads to concentrations of O_2 much greater than any amount that could reasonably be expected to be present initially. Final concentrations of O_2 approach 10^{-4} M at the higher hydrogen peroxide concentrations. The already good agreement between calculated and experimental values of the quantum efficiency in this higher H_2O_2 concentration region could be improved to any arbitrary precision by the adjustment of the rate constants, but there is no guarantee that the final set of rate constants would be either unique or any better than the literature set.

The reaction of hydrogen atoms with hydrogen peroxide can in principle lead to either H_2O and HO· (reaction 2) or H_2 and $HO_2\cdot$ (reaction 3). In discussion of earlier work in solution[15] it has been assumed that reaction 2 is completely dominant, but results from gas phase work at the same temperature of Gorse and Volman[16] and by Meagher and Heicklen[17] indicate that k_2 and k_3 are of the same order. The overall rate constant for the reaction of hydrogen atoms with H_2O_2 was found to be about the same in all cases. Our results agree with those in solution. The value of k_3 must be less than 5×10^4 M^{-1} sec^{-1} since for higher values of this rate constant the calculated values of the *maximum* quantum efficiency begins to drop significantly below that observed experimentally. It is not apparent why there should be such a difference between the solution and gas phase values of k_2 and k_3.

The calculated value of the concentration of $HO_2\cdot$ approaches 10^{-7} M at the highest H_2O_2 concentrations used. Even at the highest concentration of $HO_2\cdot$ encountered it is not necessary to include reactions 20 and 21 in the calculations. The value of k_{20} must be less than 5 M^{-1} sec^{-1} and the value of k_{21} less than 1 M^{-1} sec^{-1} since higher values of either rate constant immediately lead to much higher calculated quantum efficiencies at *higher* concentrations of H_2O_2 than are actually observed. Reaction 3 is the reverse of reaction 21. A value of ΔG°_{21} can be estimated on the basis of available values of ΔG_f° for the pertinent species. Thus $\Delta G^\circ_{21} \sim 8$ kcal/mol and $K_{21} \sim 10^{-6}$. Combining K_{21} with our value of k_3 indicates that k_{21} is actually $\leq 5 \times 10^{-2}$ M^{-1} sec^{-1}.

TABLE I:

No.	Reaction	Rate constant, M^{-1} sec^{-1}	Ref
	$H_2O_2 + h\nu \rightarrow 2HO\cdot$	$\psi R = 0.5R$	*a*
1	$HO\cdot + H_2 \rightarrow H_2O + H\cdot$	4×10^7	*b*
2	$H\cdot + H_2O_2 \rightarrow H_2O + HO\cdot$	9×10^7	*c*
3	$H\cdot + H_2O_2 \rightarrow H_2 + HO_2\cdot$	$\leq 5 \times 10^4$	This work
4	$HO\cdot + H_2O_2 \rightarrow H_2O + HO_2\cdot$	4.5×10^7	*d*
5	$H\cdot + O_2 \rightarrow HO_2\cdot$	2×10^{10}	*e*
6	$HO_2\cdot \rightarrow H^+ + O_2^-$	1.3×10^6	This work
7	$O_2^- + H^+ \rightarrow HO_2\cdot$	7.2×10^{10}	This work
8	$HO_2\cdot + HO_2\cdot \rightarrow H_2O_2 + O_2$	7.5×10^5	*f*
9	$HO_2\cdot + O_2^- \xrightarrow{H^+} H_2O_2 + O_2$	8.5×10^8	*f*
10	$H\cdot + HO_2\cdot \rightarrow H_2O_2$	2×10^{10}	*g*
11	$O_2^- + H\cdot \xrightarrow{H^+} H_2O_2$	2×10^{10}	*h*
12	$H\cdot + HO_2^* \rightarrow H_2 + O_2$	?	*h*
13	$H\cdot + H^+ + O_2^- \rightarrow H_2 + O_2$	?	*h*
14	$H\cdot + H\cdot \rightarrow H_2$	1×10^{10}	*i*
15	$HO\cdot + H\cdot \rightarrow H_2O$	2×10^{10}	*j*
16	$HO\cdot + HO\cdot \rightarrow H_2O_2$	5×10^9	*k*
17	$HO\cdot + HO_2\cdot \rightarrow H_2O + O_2$	7×10^9	*l*
18	$HO\cdot + O_2^- \xrightarrow{H^+} H_2O + O_2$	1×10^{10}	*l*
19	$H\cdot + X \rightarrow ?$	$k_{1,2}X = 600$ sec^{-1}	This work
20	$HO_2\cdot + H_2O_2 \rightarrow H_2O + O_2 + HO\cdot$	<5	This work
21	$HO_2\cdot + H_2 \rightarrow H_2O_2 + H\cdot$	<1	This work

[a] J. L. Weeks and M. S. Matheson, *J. Am. Chem. Soc.*, 78, 1273 (1956). [b] H. A. Schwarz, *J. Phys. Chem*, 66, 225 (1962). M. S. Matheson, *Adv. Chem. Ser.*, No. 50, 45 (1965). [c] J. P. Sweet and J. K. Thomas, *J. Phys. Chem.*, 68, 1363 (1964). [d] H. A. Schwarz, *J. Phys. Chem.*, 66, 225 (1962). [e] R. L. Willson, *Trans. Faraday Soc.*, 67, 3008 (1971). [f] D. Behar, G. Czapski, L. M. Dorfman, and H. A. Schwarz, *J. Phys. Chem.*, 74, 3209 (1970). [g] P. Y. Feng, A. Brynjolfsson, J. W. Halliday, and R. D. Jarrett, *J. Phys. Chem.*, 74, 1221 (1970). [h] Assumed. [i] J. K. Thomas, *Int. J. Appl. Radiat. Isotopes*, 16, 451 (1965). [j] J. K. Thomas, *Trans. Faraday Soc.*, 61, 702 (1965). [k] J. Rabani and M. S. Matheson, *J. Phys. Chem.*, 70, 761 (1966). [l] K. Sehested, O. L. Rasmussen, and H. J. Fricke, *J. Phys. Chem.*, 72, 626 (1968).

TABLE II

Ref	System	$[H_2O_2]$, M	pH	k_{20}, M^{-1} sec^{-1}
a	γ ray and uv irradiation of H_2O_2	8×10^{-5} to 0.2	Natural	530
b	γ ray irradiation of H_2O_2	1–20	Natural	3.7
c	γ ray irradiation of H_2O_2	0.1–5	1–1.5	0.2
d	γ ray and uv irradiation of H_2O_2	1–40	Natural and 1	10^{-2}
e	Mn(III) + H_2O_2	10^{-3} to 10^{-4}	0	600

[a] E. J. Hart and M. S. Matheson, *Discuss. Faraday Soc.*, 12, 169 (1952). [b] F. Dainton and J. Rowbottom, *Trans. Faraday Soc.*, 49, 1160 (1953). [c] C. Ferradini and C. Seide, *Int. J. Radiat. Phys. Chem.*, 1, 219 (1969). [d] D. Currie and F. Dainton, *Trans. Faraday Soc.*, 61, 1156 (1965). [e] G. Davies, L. Kirschenbaum, and K. Kustin, *Inorg. Chem.*, 7, 146 (1968).

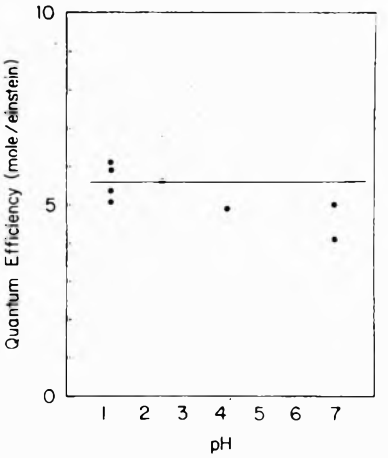

Figure 4. Experimental (●) and calculated (——) values of the quantum efficiency of photoreduction of H_2O_2 as a function of pH in solutions under 10 atm of H_2 (equivalent to 0.0078 *M*) and having an average H_2O_2 concentration of 3×10^{-4} *M*. These results are at the higher H_2O_2 concentration indicated in Figure 2.

At an average concentration of H_2O_2 of 3×10^{-4} *M* (Figure 2 shows this H_2O_2 concentration relative to that at which the maximum quantum efficiency occurs) and a H_2 concentration of 7.8×10^{-3} *M* there is little effect on either the calculated or experimental quantum efficiency as the pH is varied from 1 to 7. Figure 4 shows these results. Even though $pK_a(HO_2\cdot) = 4.88$, it is not expected that there should be a strong pH effect because under these conditions since there is no fate of $HO_2\cdot$ or O_2^- competitive with disproportionation (reaction 8 and 9) and reactions 4 and 5 become rate determining for chain termination.

Lower Hydrogen Peroxide Concentrations. The situation becomes much more complex as the concentration of H_2O_2 falls below that at which the maximum quantum efficiency occurs (10^{-4} *M*). The most obvious cause of these lower quantum efficiencies is adventitious oxygen that is not removed by degassing or prephotolysis. Calculated quantum efficiencies are greatly affected by variations in initial oxygen concentration over a range similar to that probably present in the experiments, i.e., 10^{-8} to 10^{-6} *M*. However, no single initial oxygen concentration seems to

lead to agreement between observed and calculated quantum efficiencies over the entire range of H_2 and H_2O_2 concentrations investigated. At these lower concentrations of H_2O_2 there is a net loss of O_2 during photolysis. The rate of O_2 consumption depends upon the rate of photon absorption which in turn is directly proportional to the H_2O_2 concentration. An initial concentration of O_2 that is sufficient not to be completely reduced during a typical photolysis at H_2O_2 concentrations close to 10^{-4} M is so high that the quantum efficiency falls nearly to zero for H_2O_2 concentrations near 10^{-5} M. Even so, the difficulties of quantitatively assessing the effects of adventitious oxygen in this system are so great that we are not totally convinced that these considerations unequivocally demonstrate that it is not the cause of the low quantum efficiencies observed. This is especially so as it may be that at the long photolysis times used in these experiments small but important quantities of oxygen are produced by the thermal decomposition of hydrogen peroxide.

It is likely that $HO_2\cdot$ (pK = 4.88)[13] is involved in chain termination here in a process other than simple disproportionation. The results in Figure 5 show that there is a much stronger pH effect on the quantum efficiency at this lower hydrogen peroxide concentration than in the experiments at the higher hydrogen peroxide concentration (Figure 4), and that there seems to be an inflection point in the vicinity of pH 5. Since the $HO_2\cdot$ radical is easily derived from O_2 this is taken as further evidence of the possible importance of adventitious O_2 under these conditions.

Calculations indicate that at these lower concentrations of H_2O_2 the reaction of H· with $HO_2\cdot$ can become important. In the gas phase[18] this reaction leads mainly to H_2 and O_2 (reaction 12) rather than H_2O_2 (reaction 10) because of the exothermicity of the combination reaction. While it does not seem likely that this could be true in solution, the replacement of reaction 10 by reaction 12 with k_{12} = 10^{10} M^{-1} sec^{-1} does lead to a fall-off of the calculated quantum efficiencies at lower hydrogen peroxide concentrations. However, the agreement between calculated and experimental quantum efficiencies cannot be made quantitative and the suggestion that reaction 12 is the sole cause of the low quantum efficiencies observed is not supportable.

The assumption which led to the agreement between calculated and experimental quantum efficiencies shown in Figures 2 and 3 is embodied in reaction 19; there is a H· scavenging process that acts with a pseudo-first-order rate constant that seems to retain a nearly constant value of 600 sec^{-1} during photolysis. This corresponds to an oxygen concentration of 6×10^{-8} M if the inhibition results from reaction 5. We can think of no reaction of H· with water or any intermediate species possible in this system that is not too thermodynamically unfavored to be important under our conditions. If the inhibition arises from H· scavenging by an adventitious impurity other than O_2, then it is not likely that this impurity is introduced with the H_2 since the same value of k_{19} satisfies the data from experiments under both 10 and 100 atm of H_2. Similarly, it is not likely that the scavenger was introduced with the hydrogen peroxide since the same results were obtained when the hydrogen peroxide was generated in situ by ^{60}Co γ irradiation of the water. It is possible that an organic impurity was introduced either with the water or from the pressure apparatus. One can imagine schemes in which the concentration of a scavenger remains constant because of its regeneration either by disproportionation or reoxidation of its H· adduct by $HO_2\cdot$.

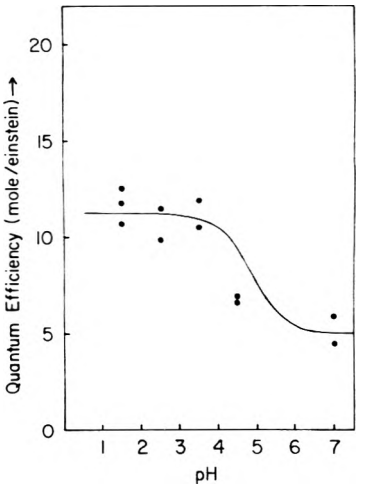

Figure 5. Experimental (●) values of the quantum efficiency of photoreduction of H_2O_2 as a function of pH in solutions under 10 atm of H_2 (equivalent to 0.0078 M) and having an average H_2O_2 concentration of 6×10^{-5} M. These results are at the lower H_2O_2 concentration indicated in Figure 2. The solid line indicates the sort of dependence of ϕ on pH that would be expected if $HO_2\cdot$ and $O_2\cdot^-$ participated in chain propogation with different rate constants.

Conclusion

It has been demonstrated that the kinetic behavior of the photoreduction of H_2O_2 by H_2 can be quantitatively rationalized by a mechanism composed of the 21 reactions listed in Table I. Numerical integration of the rate expressions resulting from this mechanism using literature values of the rate constants reproduces the data. Reactions 3, 15–18, 20, and 21 are found to be too slow to participate significantly in the reaction under the conditions of the experiments. This allows upper limits to be set on the values of the rate constants of reactions 3, 20, and 21. Reaction 19 represents the removal of hydrogen atoms by an unknown process probably related to adventious oxygen. This process suppresses chain termination by the combination of hydrogen atoms and makes this system useless for the measurement of the diffusion coefficient of the hydrogen atom by means of photochemical space intermittency. Reaction 19 does not participate significantly at hydrogen peroxide concentrations greater than 10^{-3} M. This makes the agreement of calculated with experimental quantum efficiencies more satisfying at H_2O_2 concentrations above this value. The upper limits placed upon the values of the rate constants for reactions 3, 20, and 21 are based upon results at H_2O_2 concentrations above 10^{-3} M.

Acknowledgment. This work was supported in part by the U.S. Energy Research and Development Administration.

References and Notes

(1) (a) Carnegie-Mellon University. (b) University of Oregon. (c) Unilever Research, Port Sunlight, United Kingdom. (d) Address correspondence to this author at the Department of Chemistry, University of Montana, Missoula, Mont. 59801.

(2) A. L. Geddis and R. B. Pontius in "Technique of Organic Chemistry", 3rd ed, Vol. I, Part II, A. Weissburger, Ed., Interscience, New York, N.Y., 1960, Chapter XVI.

(3) R. M. Noyes, *J. Am. Chem. Soc.*, **81**, 556 (1959).
(4) S. Levinson and R. M. Noyes, *J. Am. Chem. Soc.*, **86**, 4525 (1964).
(5) P. Neta, *Adv. Phys. Org. Chem.*, submitted for publication.
(6) M. Anbar and P. Neta, *Int. J. Appl. Radiat. Isotopes*, **18**, 493 (1967).
(7) A. O. Allen and R. A. Holroyd, *J. Am. Chem. Soc.*, **77**, 5852 (1955).
(8) J. G. Calvert and J. N. Pitts, "Photochemistry", Wiley, New York, N.Y., 1966, p 783.
(9) A. O. Allen, T. W. Davis, G. Elmore, J. A. Ghormley, B. M. Haines, and C. J. Hochanadel, Oak Ridge National Laboratory Publication, ORNL 130, 1949. See also C. J. Hochanadel, *J. Phys. Chem.*, **56**, 587 (1952).
(10) Request Special Report No. SR-21 from Mr. Gerald Buzzard, Carnegie-Mellon University, 4400 Fifth Avenue, Pittsburgh, Pa. 15213.
(11) C. W. Gear, "Numerical Initial Value Problems in Ordinary Differential Equations", Prentice-Hall, Englewood Cliffs, N.J., 1971, Chapter 11, pp 209–229.
(12) L. A. Farrow and D. Edelson, *Int. J. Chem. Kinet.*, **6**, 787 (1974).
(13) D. Behar, G. Czapski, L. Dorfman, and H. A. Schwarz, *J. Phys. Chem.*, **74**, 3209 (1970).
(14) E. M. Eyring, J. J. Auborn, and P. Warrick, *J. Phys. Chem.*, **75**, 2498 (1971).
(15) J. P. Sweet and J. K. Thomas, *J. Phys. Chem.*, **68**, 1363 (1964).
(16) R. A. Gorse and D. H. Volman, *J. Photochem.*, **1**, 1 (1972).
(17) J. F. Meagher and J. Heicklen, *J. Photochem.*, **3**, 455 (1974–1975).
(18) R. R. Baldwin, D. Jackson, R. W. Walker, and S. J. Webster, *Trans. Faraday Soc.*, **68**, 1676 (1967); L. Vordonyen, G. A. Jochyan, and Nalbandyon, *Int. J. Chem. Kin.*, **1**, 23 (1975).

Kinetics of Oxygen-18 Exchange between Carboxylic Acids and Water

Richard L. Redington

Department of Chemistry, Texas Tech University, Lubbock, Texas 79409 *(Received August 18, 1975)*

Using the example of trifluoroacetic acid, infrared matrix-isolation spectroscopy is shown to provide an analytical method for monitoring the oxygen exchange kinetics that occur in solutions of carboxylic acids and water. The method should prove valuable in cases where locating specific ^{18}O labels is important. The spectra demonstrate that the singly ^{18}O-labeled acid molecules are generated at equal rates on a macroscopic time scale. The rate equation is followed over large changes of the ^{18}O label for both acid and water molecules. The samples, highly concentrated in CF_3COOH, possess approximately equimolar amounts of ^{16}O and ^{18}O. Deuteration (50%) reduces the specific rate constant by approximately 30%. Literature data for the oxygen exchange kinetics of CF_3COOH, CCl_3COOH, CH_3COOH, and $C(CH_3)_3COOH$ are reexamined and the rate constants and exchange pathways are discussed. In acidic solutions it appears that the primary exchange pathway is by direct attack of hydronium ion on the neutral acid molecule. The rate constants determined using matrix-isolation spectroscopy are similar to those obtained using mass spectrometric analysis.

I. Introduction

Highly enriched ^{18}O water has been used to hydrolyze carboxylic acid chlorides or to undergo direct acid-catalyzed oxygen exchange with the acids in order to obtain samples for infrared matrix isolation study.[1] During the course of the research it appeared that matrix-isolation spectroscopy might be useful as an analytical tool for studying the kinetics of ^{18}O exchange. The present results confirm that it is a practical alternative to the usual mass spectrometric examination of CO_2 generated from samples slightly enriched in ^{18}O. In addition to its relative experimental simplicity, infrared spectroscopy enjoys a particular advantage over mass spectrometry in that it can identify the exact position of ^{18}O labels.

The kinetics of oxygen exchange between slightly enriched ^{18}O trifluoroacetic acid (TFA) and water have been studied previously in dilute aqueous[2] and mixed[3] solvent systems. The present experiments use very concentrated TFA solutions with high acidities and approximately equimolar amounts of ^{16}O and ^{18}O. Thus, in addition to testing the feasibility of a different analytical tool for the study of isotope exchange reactions on a previously studied system, the present research extends the scope of the kinetics data and tests the rate equation of the TFA–water exchange reaction in a new concentration region. It demonstrates the explicit behavior of the individual isotopic acids.

The kinetics of oxygen exchange has been studied mass spectrometrically for other carboxylic acids[2,4-7] and literature results for the series CX_3COOH, with X = F, Cl, H and CH_3, are discussed. One reason is that the exchange pathways are ambiguous in the published rate equations: a direct H_3O^+ attack on the neutral acid molecule is kinetically indistinguishable from attack by molecular H_2O on $RCO_2H_2^+$ cation formed in a protonation preequilibrium. The latter two step mechanism is assumed in the original papers; however, a recent publication[8] presents Raman data as evidence to favor the direct H_3O^+ attack on the acid molecule. In addition to the mechanistic question, values for the literature rate constants are determined assuming unit activity coefficient ratios in the acid dissociation constants under conditions that are distinctly nonideal.

In an attempt to clarify details of the exchange pathways and rate constant values the general exchange rate constant is expressed in terms of nine different elementary exchange pathways. The literature data are analyzed using this equation and all rate constants are placed on the same comparative basis.

II. Experimental Technique and Data Processing

The rate constants reported in this work are for ^{18}O exchange in the liquid phase at 22°C. The oxygen exchange kinetics are followed by quickly vaporizing the sample at

known reaction times and then isolating a portion of the vapor in a neon matrix. The relative populations of the four isotopic acid molecules are then found by measuring the intensities of their nominal COH angle bending vibration. Composition data for the three samples, each of milligram quantity in TFA, water, and HCl, are given in Table I. Sample A consists of nearly equimolar quantities of ^{16}O and ^{18}O initially distributed in ^{16}O TFA and 96.5% enriched[9] ^{18}O water. Sample B has a similar composition but it was allowed to exchange for 15 hr prior to use in order to prepare nearly equimolar amounts of the four TFA isotopic acids (CF_3COOH = a_1; $CF_3(C^{18}O)OH$ = a_2; $CF_3CO(^{18}OH)$ = a_3; $CF_3C^{18}O^{18}OH$ = a_4). This sample is used to calibrate the relative absorption coefficients of the four species as discussed below and, with the addition of $D_2{}^{16}O$, provides kinetics run B. Sample C is similar to sample A except that it contains HCl at a higher mole fraction. The distribution of HCl between the liquid and vapor phases in the small exchange vessel is necessarily approximated using the volume of the exchange vessel and the vapor pressure data of Haase et al.[10] for hydrochloric acid solutions.

Each of the exchange reaction vessels, 3.5–5.0 ml in volume, consists of the sealed-off stem of a 4 mm stopcock. The stopcock is sealed to a 1- or a 2-l. storage bulb that is used for metering the reagents, for stopping the exchange reaction (by vaporization of the sample into this large volume) and, originally, for preparing the matrix-isolation samples.

The liquid samples were prepared by successively condensing into the small reaction vessel (with liquid nitrogen) the gaseous TFA, $H_2{}^{18}O$, and HCl using an oil manometer to measure gas pressures of approximately 1 Torr. The kinetics of oxygen exchange were followed by rapidly warming the frozen reaction mixture to 22°C and then maintaining this temperature in a water bath for the desired time interval (15 min to 1 hr). The isotopic exchange reaction was stopped by vaporizing the sample into the large 1- or 2-l. bulb. An aliquot (200 ml) was removed for spectral analysis and the bulk of the sample was then trapped back into the small reaction vessel for additional reaction.

Neon matrices were used with matrix to sample ratios near 700. The samples were deposited using a cryostat of classical design and the spectra were recorded at 5 cm^{-1}/in. chart dispersion using a Beckman IR-9 spectrophotometer. Both single beam and double beam modes were recorded, sometimes using the scale expansion.

Neon was chosen as the matrix material since experience with TFA has shown that data with a neon matrix are better than data with argon or nitrogen matrices. In addition, the neon samples could be volatilized from the sample holder by warming the cryostat tip, rather than the entire cryostat, thus making the experiments considerably more economical.

The ^{18}O isotope effect is large for the nominal COH bending mode of the carboxylic acids.[1] This is the only vibrational mode for TFA (and other acids observed in this laboratory) or for water molecules that shows a wide frequency separation among the four isotopic molecules, is very intense, and shows no matrix-induced multiplet structure when isolated in solid Ar or Ne. The absorption of this strong band is therefore used to monitor the relative concentrations of the four monomeric acid species. Little or no acid dimer occurs under the matrix-isolation conditions used. Spectra are presented in Figure 1 for sample A isolated in neon near 5 K.

TABLE I: Sample Compositions, μmol

Sample	CF_3COOH[a]	H_2O*[b]	D_2O[a]	HCl
A	30	68	0	0.6
B (calibration)	59	125	0	1.3
B (kinetics)	53	113	125	1.2
C	36	72	0	36[c]

[a] Normal O isotope: ^{16}O = 99.759%, ^{17}O = 0.037%, ^{18}O = 0.204%. [b] Enriched: ^{16}O = 2.7%, ^{17}O = 0.8%, ^{18}O = 96.5%. [c] Estimated partition during exchange reaction: 19 μmol in liquid phase, 17 μmol in vapor phase. The presence of the HCl in samples A and B is not very significant; however, HCl is needed to catalyze oxygen exchange in similar experiments using acetic acid.

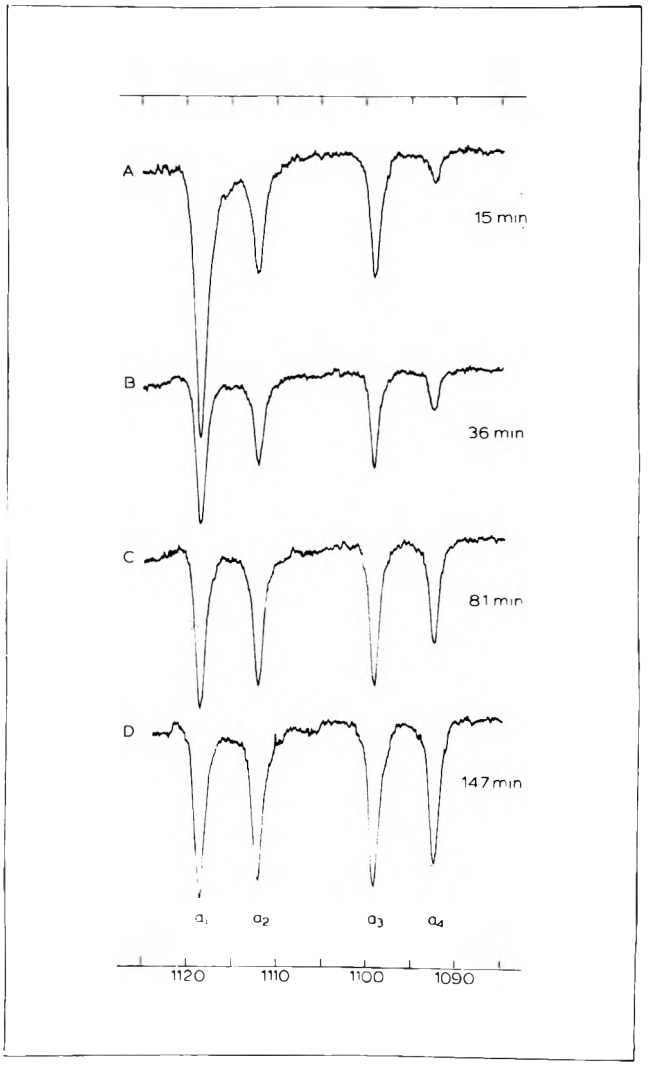

Figure 1. Nominal δ COH angle deformation band of monomeric trifluoroacetic acid matrix-isolated in neon at M/S ~ 700. Data for sample A with liquid phase samples held at 22°C for the indicated (total) time intervals. The band frequencies are 1118.8 for CF_3COOH, 1112.3 for $CF_3(C^{18}O)OH$, 1099.5 for $CF_3(CO)^{18}OH$, and 1092.9 for $CF_3C^{18}O^{18}OH$.

The absorption coefficients, B_i, for the nominal COH bending mode vary for the four acid species and Figure 1d clearly shows that B_4 is smaller than the others. The relative B_i values are calibrated using spectra from two deposits (one on top of the other) of the initial sample B.

The population of each acid is directly proportional to

TABLE II: Kinetic Data

Sample	Time, min	Relative band areas[a]				Relative populations			
		a_1	a_2	a_3	a_4	a_1	a_2	a_3	a_4
A	0					1.00	0.00	0.00	0.00
	15	1.48	0.46	0.47	0.15	0.58	0.18	0.19	0.06
	36	0.65	0.39	0.39	0.22	0.39	0.24	0.24	0.13
	81	0.65	0.59	0.57	0.22	0.27	0.25	0.24	0.24
	147	0.70	0.69	0.68	0.83	0.24	0.24	0.23	0.29
B	0	0.48	0.44	0.41	0.28	(0.248	0.250		0.252)[b]
	0	0.70	0.67	0.60	0.44				
	15	0.15	0.14	0.12	0.07	0.27	0.26	0.26	0.21
	47	0.36	0.24	0.22	0.10	0.35	0.24	0.25	0.16
	108	0.41	0.25	0.21	0.09	0.38	0.25	0.23	0.14
C	0					1.00	0.00	0.00	0.00
	15	0.48	0.19	0.14	0.03	0.53	0.23	0.19	0.06
	31	0.43	0.28	0.22	0.09	0.38	0.26	0.23	0.13
	59	1.02	0.74	0.57	0.31	0.34	0.27	0.22	0.17

[a] "Area" = $\Delta\nu_{1/2} \log I_0/I$, cf. eq 1. [b] Calibration sample taken with statistical equilibrium isotope distribution.

B_i, which should be obtained by integrating the area under each absorption band. However, planimeter measurements for several of the band areas in the presently limited body of data were too subjective (in view of noise and background) and the approximate equation[11]

$$B_i = K_i\left[\Delta\nu_{1/2} \ln \frac{I_0}{I}\right]_i \quad (1)$$

for the integrated absorption coefficient was used instead. Here $\Delta\nu_{1/2}$ is the band half-width, I and I_0 are measured at the band maximum, and K_i is a constant. A single straight line was sufficient to define a uniform background level for the four bands in nearly every recording. An average value of $\Delta\nu_{1/2}$ (based on at least eight of the best recordings) was established for each acid. Values of $\Delta\nu_{1/2}$ were 1.33, 1.37, 1.16, and 1.21 cm^{-1} for a_1, a_2, a_3, and a_4, respectively. Relative K_i values obtained using the calibration bands (ignoring nonclassical isotope effects on the populations) are $K_1 = 1.000$, $K_2 = 1.068$, $K_3 = 1.175$, and $K_4 = 1.682$. The relative populations reported in Table II are obtained using these $\Delta\nu_{1/2}$ and K_i values with the I and I_0 measurements taken from the single best (double beam) record for each time point.

III. Kinetics Equations

The four isotopically different TFA molecules (a_1, a_2, a_3, a_4) can each react with $H_2{}^{16}O$ (s) or $H_2{}^{18}O$ (e). In addition, ions derived from the acid ($CF_3CO_2H_2^+$, CF_3COO^-) and the water molecules (H_3O^+, OH^-) can enter into exchange reactions. The kinetics equations presented in this section and used to analyze the rate data are written for reactions between neutral molecules alone since all of the ionic reactions are incorporated into these equations through acid and base equilibrium constants present in the rate constant k_x. It seems sufficient on experimental grounds to consider only the elementary bimolecular reactions between acid species and water species as done by previous investigators.

Of the eight possible bimolecular reactions between a_1, a_2, a_3, a_4 and e, s, all except a_1 + s and a_4 + e lead to isotopic exchange products. Each elemental rate equation is assumed to be of the form

$$-d[a_1]/dt = k_x[a_1][e] \quad (2)$$

which is written explicitly for the single reaction a_1 + e → a_2 + s. Of course, an identical equation exists for the reaction a_1 + e → a_3 + s. The rate constant k_x is assumed to be independent of oxygen isotope but, as seen in the next section, it clearly depends upon pH, temperature, and solution conditions such as ionic strength. In addition, it is dependent on deuteration.

To analyze the data the set of elementary rate equations must be combined over all reaction possibilities. This yields the overall rate expressions:

$$d[a_1]/dt = k_x(-2[a_1][e] + ([a_2] + [a_3])[s]) \quad (3a)$$

$$d[a_2]/dt = k_x(([a_1] - 2[a_2] + [a_3])[e] + ([a_4] - 2[a_2] + [a_3])[s]) \quad (3b)$$

$$d[a_3]/dt = k_x(([a_1] + [a_2] - 2[a_3])[e] - ([a_4] + [a_2] - 2[a_3])[s]) = d[a_2]/dt \quad (3c)$$

$$d[a_4]/dt = k_x(([a_2] + [a_3])[e] - 2[a_4][s]) \quad (3d)$$

$$d[s]/dt = k_x(2[a_1][e] + ([a_2] + [a_3])([e] - [s]) - 2[a_4][s]) \quad (3e)$$

$$d[e]/dt = -d[s]/dt \quad (3f)$$

These six equations were solved numerically as a function of k_x using time increments of 0.005 min. The initial amounts of acid and water were obtained from the data of Table I. The optimum calculated curves for runs A and B are shown in Figures 2 and 3. The rate constants, which are listed in the first column of Table III, are determined from an unweighted least-squares fit of points on the calculated curves to the 12 or 16 data points. The calculated rates $d[a_2]/dt$ and $d[a_3]/dt$ are equated (cf. eq 3c) because the expected rapid interconversion of these two species seems to be borne out by the experimental observations.

Equations 3b and 3c, with negligible values for [e] and $[a_4]$, are valid for the mass spectrometric experiments described in the literature. Then

$$\text{rate} = -d([a_2] + [a_3])/dt = (k_x[s])([a_2] + [a_3]) = (2k_x[s])[a_3] \quad (4)$$

since a_2 and a_3 are not distinguished by mass spectrometric

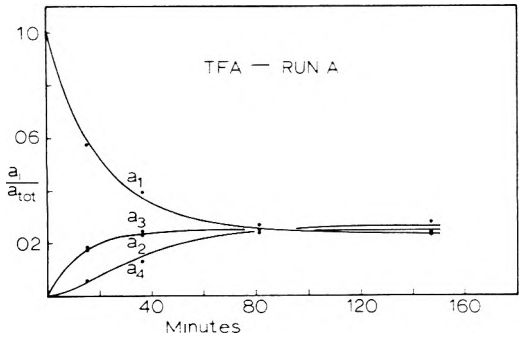

Figure 2. Plot of kinetic data for run A with the best-fit least-squares solutions to eq 3.

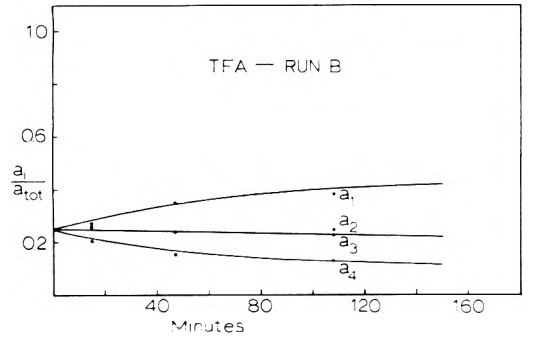

Figure 3. Plot of kinetic cata for run B (53% deuterium content) with the best-fit least-squares solutions to eq 3.

analysis. Dividing by the initial total isotopic acid concentration $([a_2] + [a_3])^0$, with the definition $F = ([a_2] + [a_3])/([a_2] + [a_3])^0$, leads to the usual pseudo-first-order rate equation

$$-dF/dt = (k_x[s])F = k_x'F \qquad (5)$$

The observed rate constant k_x' is given as $(k_x[s])$ when it is expressed relative to the total isotopic acid concentration $([a_2] + [a_3])$ but it is given as $(2k_x[s])$ when expressed relative to a single acid, i.e., to a_2 or to a_3 alone.

To allow literature comparisons, the present rate constants are expressed relative to a single acid isotope, e.g., a_1 in eq 3a (cf. run A) so that $k_x' = (2k_xW)$. Here W is the *total* quantity of water present in the given experiment; all the water is effectively present as $H_2{}^{16}O$ in the literature experiments. The proper comparisons are clear in eq 3a–c. Each elementary exchange reaction proceeds with a rate constant k_x' given by k_x times the appropriate water concentration. The two elementary reactions occurring in the literature experiments have net result $a_2 \rightarrow a_1$ and $a_3 \rightarrow a_1$, whereas the initial rate of experiment A is described by exactly the opposite of these two reactions. Under other experimental conditions, e.g., those of run B, the same two reactions are of interest but only as they would occur if all the water were present as $H_2{}^{18}O$.

The various k_x' values and half-lives are compared in Table III. Values for the mole ratios (h/W) are also given there, where h refers to moles of hydronium ion and W to total moles of water. In order to more directly compare the data, a plot of $-\log k_x$ vs. $-\log (h/W)$ is shown in Figure 4. (The use of log (h/W) instead of pH will be discussed.) It is seen that the exchange rates for the concentrated acid solutions and the two mixed solvent systems are about half those from the dilute acids at an ionic strength of 4. It is also noted that the rate for experiment B, with about 50% deuteration, is slower than the rates of experiments A and C.

IV. The Exchange Rate Constant

Nine elementary exchange rate constants arise when the acid species $RCOOH_2^+$, RCOOH, and $RCOO^-$ (indicated by subscripts 1, 2, and 3 in the rate constants of eq 6) can each react with H_3O^+, H_2O, or OH^- (indicated by superscripts h, w, and b in the rate constants). Three of the nine pathways for oxygen exchange between water and TFA species are illustrated in eq 6 (cf. ref 2 and 3). The other six pathways are obtained by replacing the water molecules in eq 6 with hydronium or hydroxide ions. The set of nine exchange reactions, interconnected by equilibrium constants K_1, K_2, and K_w, are represented by the single equations $s + a_2 \rightarrow e + a_1$ in the previous section.

$$\begin{array}{ccc} H_2O + RC^{18}OOH_2^+ & \xrightarrow{k_1{}^w} & H_2{}^{18}O + RCOOH_2^+ \\ \uparrow\downarrow K_1 & & \uparrow\downarrow K_1 \\ H_2O + RC^{18}OOH & \xrightarrow{k_2{}^w} & H_2{}^{18}O + RCOOH \\ \uparrow\downarrow K_2 & & \uparrow\downarrow K_2 \\ H_2O + RC^{18}OO^- & \xrightarrow{k_3{}^w} & H_2{}^{18}O + RCOO^- \end{array} \qquad (6)$$

The exchange rate constant that is straightforwardly found on including all nine pathways, expressed relative to (RCOOH), and incorporating the concentrations of the oxygen-exchanging H_2O, H_3O^+, and OH^-, is

$$k_x' = [k_1{}^h h^3 + (k_2{}^h K_1 + k_1{}^w W)h^2 + (k_3{}^h K_1K_2 + K_1k_2{}^w W + k_1{}^b K_w)h + (k_3{}^w K_1K_2W + k_2{}^b K_1K_w) + (k_3{}^b K_1K_2)(OH^-)][h^2 + K_1h + K_1K_2]^{-1} \qquad (7)$$

As written, this expression for k_x' is appropriate for the mass spectrometric experiments since all the water species have the same isotopic label (i.e., ^{16}O). More generally, k_x for each bimolecular reaction (cf. eq 2) is given by

$$k_x = [k_1{}^h r^3 + (k_2{}^h K_1' + k_1{}^w)r^2 + (k_3{}^h K_1'K_2' + k_2{}^w K_1' + k_1{}^b K_w')r + (k_3{}^w K_1'K_2' + k_2{}^b K_1'K_w') + (k_3{}^b K_1'K_2'K_w'r^{-1})](r^2 + K_1'r + K_1'K_2')^{-1} \qquad (8)$$

The K_1', K_2', and K_w' equilibrium constants are obtained from K_1, K_2, and K_w by dividing out the water concentration terms. The parameter $r = (H_3O^+)/(H_2O) = (H_3{}^{18}O^+)/(H_2{}^{18}O) = ((H_3O^+) + (H_3{}^{18}O^+))/((H_2O) + (H_2{}^{18}O))$ is a dimensionless, pH dependent constant (that depends on having a fast proton equilibrium). These equalities disregard any nonclassical isotope effects on the ^{16}O–^{18}O isotope distribution. It is seen that k_x is pH dependent even in the absence of direct attack by hydronium or hydroxide ions in the exchange reactions. Equations 7 or 8 show that the exchange constant is a polynomial in (H_3O^+) and demonstrate the kinetic indistinguishability of pathways that are grouped into the coefficient of each power of (H_3O^+). However, on assuming that a fair degree of uniformity exists be-

TABLE III: Rate Constants for Trifluoroacetic Acid Solutions

Sample	$10^5 k_x$, μmol^{-1} sec^{-1}	$10^4 k_x'$, sec^{-1}	Half-life, min	$10^3(h/W)$	Comment
A	1.0	6.8	17	81	22° C (TFA) very conctd
B	0.15	3.5	33	54	22° C, (TFA) very conctd, 53% deuteration
C	1.2	8.3	14	290	22° C, (TFA) very conctd,
Aqueous[a]		15.7	7.4	21	25° C, (TFA) = 0.3 *M*, *I* = 4 *M*
Aqueous[a]		0.36	321	0.55	25° C, (TFA) = 0.3 *M*, *I* = 4 *M*
25% acetonitrile[b]		0.17	676	0.79	25° C, *I* = 0.065 *M*
40% tetrahydrofuran[b]		0.087	1330	0.91	25° C, *I* = 0.065 *M*

[a] Reference 2. [b] Reference 3.

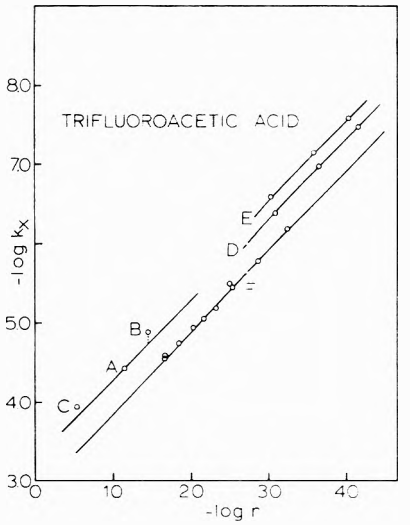

Figure 4. Correlation of observed exchange rate constants ($k_x = k_x'/W$) with hydronium ion presence. Here r is the dimensionless ratio (h/W). The nearly linear curves are obtained from eq 11 using rate constants from Table V. Points A, B, and C are for runs A, B, and C of the present work using very concentrated TFA at 22°C. Point B occurs above the line drawn through A because of its kinetic deuterium effect. Lines D and E are for TFA in 25% v:v acetonitrile and 40% v:v tetrahydrofuran at ionic strength 0.065 *M* and 25°C, respectively.[3] Line F is for 0.3 *M* TFA at ionic strength 4.0 *M* and 25°C.[2]

tween corresponding *oxygen exchange* rate constants for the carboxyl groups of different acids, it is possible to propose tentative rate constant values for the various pathways. This is examined in the following section.

V. Exchange Pathways

It is reasonable to expect that the similarities between various carboxyl groups that are expressed in their structural and spectroscopic properties should also be reflected by a pattern of similar oxygen exchange rate constants. These rate constants should be much less sensitive to parent acid than the rate constants involving simple proton transfers. In the present section a uniform set of oxygen exchange rate constants are proposed. The set is not proved but alternative interpretations of the kinetic data lead to elementary rate constants that are intuitively less satisfactory, that form erratic correlations, and which sometimes seem to be contradicted by data on other acids.

In sulfuric acid solvent, pK_1 values for TFA,[12] TCA,[12] and acetic acid[13] are −13.5, −13.1, and −6.6, respectively. If similarly large K_1 values hold under other conditions, and they are assumed to dominate their terms in eq 7, it then reduces to

$$k_x' = [k_2^h h^2 + (k_3^h K_2 + k_2^w W)h + (k_3^w K_2 W + k_2^b K_w) + k_3^b K_2(OH^-)]/(h + K_2) \quad (9)$$

In empirical form, to define rate constants k_2, k_1, k_0, and k_{-1}, this is

$$k_x' = (k_2 h^2 + k_1 h + k_0 + k_{-1}(OH^-))/(h + K_2) = 55.5R^* \quad (10)$$

The relation $k_x' = 55.5R^*$ connects the literature data for exchange in dilute aqueous solutions[2,5,6] (i.e., experimental rate values R^*) with the present k_x' expression. The empirical rate constants k_2, k_1, k_0, and k_{-1} for TFA,[2] TCA,[2] acetic,[5] and pivalic[5] acids are determined as a function of K_2 (the acid dissociation or K_a equilibrium constant) by a least-squares fitting of the literature rate data. The expression $Y = 55.5R^*(h + K_2)$ is fit with Y^{-2} weighting of the residuals in order to obtain similar percentage accuracies for the large and small Y values. The results are listed in Table IV, where all rate constants are expressed in units of M^{-1} sec^{-1}. The kinetically determined K_2 values imply activity coefficient ratios near unity for TFA and TCA at 25°C but a ratio near 3 for acetic acid. Large molar activity coefficients are reported for acetic acid in experiments at high ionic strength.[7] The temperature dependence of the suggested K_2 values for TFA with ionic strength $I = 4$ resembles that observed for the aqueous acid:[14] $K_2 = 0.588$ at 25°C and $K_2 = 0.533$ at 35°C.

The k_2 rate constants are not sensitive to K_2 but the k_1 and k_0 rate constants decrease about 50% on using $K_a/3$ in the calculations and they increase by 100–150% on using $3K_a$.

The four k_i rate constants are reduced to rate constants for specific pathways in Table V by using their definitions as given in eq 9 and 10. It is immediately seen that k_2^h (which stands alone as k_2 and is the path involving direct H_3O^+ attack on the neutral acid molecule) is large and of relatively uniform magnitude when the acids are compared at the same temperature. If k_1 is taken as $k_3^h K_2$, i.e. that $k_3^h K_2 \gg k_2^w W$ is assumed, it is found that k_3^h is comparable in magnitude to k_2^h for each acid (column 3). The marked decrease of k_1 that occurs on passing from TFA and TCA to acetic and pivalic acids is fully explained. In contrast, assuming that $k_2^w W \gg k_3^h K_2$ leads to the less plausible listing of k_2^w values given in the last column of Table V.

It is suggested that k_2^h and k_3^h are of similar magnitude ($1–15 \times 10^{-4}$ M^{-1} sec^{-1} at 25°C) and that k_3^w is smaller than this pair by a factor of approximately 10^{-4}. While k_2^w could not be determined here, a value near k_3^w is not contradicted by the data. From Table V it also seems reasonable to suggest that the k_2^h–k_3^h rate constant range may serve as an upper limit to the k_2^b and k_3^b values.

TABLE IV: Rate Constants (Eq 10)[a]

Sample	$10^4 k_2$	$10^4 k_1$	$10^4 k_0$	$10^4 k_{-1}$	K_2
Trifluoroacetic acid					
aq, 0°C	1.93	0.98	<0.001	2.17	1.038[b]
aq, 25°C	14.4	9.26	<0.01	10.3	0.788[b]
aq, 45°C	116	26.9	<0.1	28.5	0.638[b]
25% AN, 25°C	10.2	1.83	—	—	0.388[c]
40% THF, 25°C	4.65	1.06	—	—	0.388[c]
Trichloroacetic acid					
aq, 25°C	1.13	0.67	<0.01	0.77	0.25
aq, 55°C	9.62	6.02	<0.01	5.49	0.19[b]
Acetic acid					
aq, 25°C	5.34	—	—	—	
aq, 53°C	46.2	0.00071	—	—	6×10^{-6}
aq, 101°C	1050	0.0022	2.40×10^{-8}	—	(6×10^{-6})[b]
aq, 123°C	3010	0.0281	2.11×10^{-7}	—	6×10^{-6}
Pivalic acid					
aq, 101°C	117	0.0010	3.02×10^{-9}	—	3×10^{-6}
aq, 123°C	322	0.0098	3.09×10^{-8}	—	3×10^{-6}

[a] Units for all rate constants are M^{-1} sec^{-1}, data from ref 2, 3, and 5. [b] K_2 values yielding minimum least-squares error in kinetic data. Standard K_a values are 0.588, 0.25, 1.76×10^{-5}, and 8.91×10^{-6} for the four acids at 25°C. [c] Assumed value, cf. 0.588 in water[14] and 0.208 in 40% v:v dioxane.[15]

TABLE V: Rate Constants (Eq 9)[a]

Sample	$10^4 k_2^h$	$10^4 k_3^h$	$10^4 k_3^w$	$10^4 k_3^b$	$10^4 k_2^w$ if $(k_2^w W \gg k_3^h K_2)$
Trifluoroacetic acid[b]					
aq, 25°C	14.4	11.8	$<2 \times 10^{-4}$	13.1	(0.17)
25% AN, 25°C	10.2	4.7	—	—	(0.03)
40% THF, 25°C	4.7	2.7	—	—	(0.02)
Trichloroacetic acid					
aq, 25°C	1.13	2.7	$<7 \times 10^{-4}$	3.1	(0.01)
Acetic acid					
aq, 25°C	5.3	—	—	—	
aq, 101°C	1050	370	7.2×10^{-5}	—	(4.0×10^{-5})
Pivalic acid					
aq, 101°C	117	330	1.5×10^{-5}	—	(1.8×10^{-5})

[a] Units for all rate constants are M^{-1} sec^{-1}. [b] Approximate k_2^h values for samples A, B, and C are 5.4, 3.7, and 4×10^{-4} M^{-1} sec^{-1}, respectively.

The k_1^h rate constant could conceivably compare with the k_2^h in magnitude but there is no concrete evidence to support this idea; a similar remark is appropriate concerning an association of k_1^w with k_2^w and k_3^w.

In this interpretation the practical exchange pathways are seen to be dominated by the H_3O^+ or OH^- reactions. In acidic solution H_3O^+ + RCOOH occurs in all cases and H_3O^+ + $RCOO^-$ is important when there is sufficient anion present in the acidic solution. In basic solutions the slow exchange for acetic and pivalic acids is due to H_2O + $RCOO^-$. For TFA and TCA the practical contribution from this reaction is superseded by OH^- + $RCOO^-$. The $RCOOH_2^+$ concentration is too small to effectively participate in oxygen exchange unless k_1^w is many orders of magnitude larger than the various rate constants listed in Table V.

There are too few matrix-isolation experiments to determine accurate elementary rate constants; however, the new data can be compared with the literature results for acidic media. To do this, eq 8 is written as

$$k_x = \frac{k_2^h r^2 + (k_3^h K_2')r}{r + K_2'} = k_x'/W \qquad (11)$$

Estimates for W can be given for the concentrated TFA samples used for the matrix-isolation studies. Densities for solutions A, B, and C are approximately 1.25, 1.20, and 1.18 g/ml, respectively, obtained from pure component densities weighted by their solution mole fractions (for the liquid of sample C it is estimated that $X_{HCl} = 0.21$). Using these densities, W = 18, 26, and 7 M for solutions A, B, and C. Figure 4 is a plot of the available data expressed as $-\log (k_x'/W)$ vs. $-\log (h/W)$ along with eq 10 and rate constants from Table V ($K_2' = K_2/55.5$). The $r = h/W$ values for points A and C were calculated using $K_2' = 0.588/55.5$. The value of r for point C is the least reliable since the HCl solution component was not analytically determined but estimated from data for hydrochloric acid.[10] The line with unit slope is therefore drawn through point A alone.

The value calculated for r of point B is based on an estimated K_2 value of 0.288 for the mixed H_2O–D_2O system. The value 0.288 (~0.588/2) was chosen on the basis of the Gross-Butler[16] equation for H_2O–D_2O mixtures and the knowledge that K_2^h/K_2^d = 3 to 6 for carboxylic acids.[16] This ratio is unknown for TFA. The quadratic term in eq 11 is the most important for points A, B, and C and therefore allows an estimate to be made for k_2^h and k_2^m (m refers to the mixed H_2O–D_2O system). Using $k_x = k_2^h r$, where the units are now M^{-1} sec^{-1}, $k_2^h = 5.4 \times 10^{-4}$ for A, 4×10^{-4} for C, and $k_2^m = 3.7 \times 10^{-4}$ for B (cf. Table V comparisons). The kinetic isotope effect is then $k_2^m = 0.7 k_2^h$, determined using points A and B only.

It is seen in Figure 4 that the rate constants are similar

for the set of TFA samples and that the exchange rate for the concentrated aqueous solutions and for the mixed solvents is about one-half that of the dilute aqueous samples with corresponding values of h/W. It is also apparent that near linearity, with unit slope, of log-log plots is a poor diagnostic tool.

The observation that acids a_2 and a_3 are generated at equal rates does not impart new information concerning the oxygen exchange mechanism because fast proton transfers occur between the acids and water.[17,18] A likely mechanism proposed to explain the proton exchange equally well explains rapid interconversion of acids a_2 and a_3.

Proton transfers must play a very important role in the oxygen exchange process. This is clear on interpreting simple equations such as $H_3O^+ + RCOOH \rightarrow RC(OH)_2OH_2^+$ or on considering more detailed mechanisms for oxygen exchange or mechanistically similar hydrolysis reactions.[19,20]

Knowledge of the kinetic deuterium effect is therefore essential to an understanding of the detailed exchange mechanism. Generally, it is classified into primary (or zero point) effects that are strongly mass dependent and into more subtle secondary effects that involve in some manner the nearby hydrogen bonded solvent cluster or the bulk solution.

Equilibrium constants for the self-ionization of water and the ionization of carboxylic acids show large kinetic deuterium effects[16] (K^h/K^d = 9 and 3-6, respectively) while hydrolysis reactions show smaller kinetic deuterium effects. Detailed interpretations are still controversial but it appears that the above large overall kinetic deuterium effects rest with the predominantly primary character of the initial ionization step as compared to more secondary effects associated with ion recombination.

Concerning the present problem, it has been found that $k_2(H) = 0.89k_2(D)$ (which reduces to $k_2^h = 0.7k_2^d$) for acetic acid.[5] For $CClH_2COOH$ the result is $k_2^h = 0.6k_2^d$ under similar conditions of dilute acid concentration.[7] The present experiment on TFA suggests that $k_2^m = 0.7k_2^h$ (deuteration yielding the slower rate constant) in contrast to the inverse result for dilute acetic acid. It is expected that the TFA result reflects a much larger primary contribution to the isotope effect. The kinetic deuterium effect should be directly related to the water structure that surrounds the TFA molecule and there are, on the average, only two water molecules per TFA molecule in the concentrated solutions that were used. The magnitude of the changes observed, assuming that TFA is comparable to acetic acid in behavior as suggested by the results of Table V, suggests that a systematic study of the kinetic deuterium effect over a wide range of acid concentrations might provide a sensitive, fruitful means to help elucidate the role of solvent in these general hydrolysis reactions.

VI. Conclusions

1. Infrared matrix-isolation spectroscopy is shown to provide a feasible analytical method for following the oxygen exchange reactions in solutions of carboxylic acids. Trifluoroacetic acid is studied here, however, the nominal COH angle bending vibration used to monitor the isotopic acid concentrations shows similar behavior in formic, acetic, propionic, and haloacetic acids observed in this laboratory and, presumably, in other acids as well. It is hoped that the sampling technique can be used to study oxygen exchange in more complex acids, such as pyruvic acid ($CH_3(C{=}O)COOH$), which contain several exchangeable oxygen atoms and which are not amenable to mass spectrometric investigation.

2. The rate law and rate constants obtained for very concentrated trifluoroacetic acid solutions are similar to those found in dilute solutions.

3. The kinetic deuterium effect for very concentrated trifluoroacetic acid solution is much more nearly "primary" than that for dilute acetic or chloroacetic acids, which are more nearly "secondary" in nature. The study of oxygen exchange rate laws and kinetic deuterium effects in very concentrated solutions may be of wider interest, serving, for example, as a model system for studying the behavior of water in hydrated systems.

4. An expression for the general exchange rate constant is written that includes nine possible elementary exchange pathways. Exchange rate constants for several dilute carboxylic acids are evaluated using this general expression and the literature data. Upon considering comparative kinetic and equilibrium constant data for these acids, it is possible to suggest tentative rate constants for pathways that are kinetically indistinguishable on the basis of data for a single acid. Thus, it appears that the dominant exchange pathway for the four carboxylic acids investigated is via hydronium ion attack on the neutral acid molecule rather than via water molecule attack on the acid cation formed in a protonation preequilibrium.

Acknowledgments. The author gratefully acknowledges financial support of this work by the Texas Tech University Institute of University Research and the Robert A. Welch Foundation of Texas.

References and Notes

(1) R. L. Redington, *Spectrochim. Acta, Part A*, **31**, 1699 (1975).
(2) D. R. Llewellyn and C. O'Connor, *J. Chem. Soc.*, 4400 (1964).
(3) M. L. Bender and H. d'A. Heck, *J. Am. Chem. Soc.*, **89**, 1211 (1967).
(4) D. Samuel and B. L. Silver, *Adv. Phys. Org. Chem.*, **3**, 123 (1965).
(5) D. R. Llewellyn and C. O'Connor, *J. Chem. Soc.*, 545 (1964).
(6) C. O'Connor and T. A. Turney, *J. Chem. Soc. B*, 1211 (1966).
(7) P. T. McTigue, P. V. Renowden, and A. R. Watkins, *Aust. J. Chem.*, **23**, 381 (1970).
(8) C. J. O'Connor, T. A. Turney, M. E. Bridson, and A. B. Hardie, *Nature (London), Phys. Sci.*, **237**, 128 (1972).
(9) Water O-18 obtained from Koch Isotopes, Inc., 72 Rogers Street, Cambridge, Mass. 02142, with stated composition: O-18, 96.5%; O-17, 0.8%; O-16, 2.7%.
(10) R. Haase, H. Naas, and H. Thum, *Z. Phys. Chem. (Frankfurt am Main)*, **37**, 210 (1963).
(11) D. A. Ramsey, *J. Am. Chem. Soc.*, **74**, 72 (1952).
(12) References 7 and 8, based on data of M. Liler, *J. Chem. Soc.*, 4300 (1965).
(13) J. T. Edward and I. C. Wang, *Can. J. Chem.*, **40**, 966 (1962).
(14) A. L. Henne and C. J. Fox, *J. Am. Chem. Soc.*, **73**, 2323 (1951).
(15) C. A. Bunton and T. Hadwick, *J. Chem. Soc.*, 3248 (1958).
(16) P. M. Laughton and R. E. Robertson in "Solute-Solvent Interactions", J. F. Coetzee and C. D. Ritchie, Ed., Marcel Dekker, New York, N.Y., 1969, Chapter 7.
(17) E. Grunwald, C. F. Jumper, and S. Meiboom, *J. Am. Chem. Soc.*, **85**, 522 (1963).
(18) C. S. Highsmith and E. Grunwald, *J. Phys. Chem.*, **78**, 2339 (1974).
(19) E. H. Cordes and H. G. Bull, *Chem. Rev.*, **74**, 581 (1974).
(20) R. L. Schowen, *Prog. Phys. Org. Chem.*, **9**, 275 (1972).

Effect of Lithium Content on the Kinetics of Pyrophosphate Degradation in Molten Nitrates

James L. Copeland,* Arthur S. Metcalf, and Billy R. Hubble

Department of Chemistry, Kansas State University, Manhattan, Kansas 66506 *(Received August 18, 1975)*

Publication costs assisted by Kansas State University

The pyrophosphate anion is stable in molten $NaNO_3$ and nitrates of the heavier alkali metals. However, if Li^+ ion is present in the melt, $P_2O_7^{4-}$ is degraded according to the reaction: $P_2O_7^{4-} + 2NO_3^- \rightarrow 2PO_4^{3-} + 2NO_2(g) + 0.5O_2(g)$. Kinetics of this reaction, with respect to $P_2O_7^{4-}$ in excess molten nitrate (1:55 mole ratio of $P_2O_7^{4-}$ to NO_3^-), were studied by allowing $Na_4P_2O_7$ to react with molten mixtures of $LiNO_3$ and $NaNO_3$, and with pure $LiNO_3$, over the temperature range from 610 to 625 K. When account was taken of the four Na^+ ions from each $Na_4P_2O_7$ unit, the effective cation mole fractions of Li^+, X_{Li}, in the various reacting systems were 0.9323, 0.8377, 0.7431, and 0.6530, with the ratio of $P_2O_7^{4-}$ to NO_3^- being 1:55 in each case. First-order kinetics with respect to $P_2O_7^{4-}$ was observed with the rate constant, k_1, varying from $(3.31 \pm 0.19) \times 10^{-2}$ min^{-1} at 610 K and $X_{Li} = 0.6530$, to $(30.2 \pm 0.7) \times 10^{-2}$ min^{-1} at 625 K and $X_{Li} = 0.9323$. Constant temperature plots of k_1 vs. X_{Li} indicated in each case an almost tripling in value of k_1 from $X_{Li} = 0.7431$ to 0.9323, and a tendency to level off in the vicinity of $X_{Li} = 0.75$. This leveling off effect manifested itself at the lower temperatures as an inflection plateau near $X_{Li} = 0.75$. An interpretation is provided in terms of which $P_2O_7^{4-}$ experiences a change in its average coordination with Li^+ ions with changing Li^+ concentration, resulting in the P–O–P bridge being made more susceptible to rupture by NO_3^- at the higher Li^+ levels.

Introduction

Earlier work in this laboratory involved investigations of the stoichiometries and kinetics of acid–base reactions of various cyclic and chain phosphates with molten $NaNO_3$ solvent.[1] In every case the *net* reaction with respect to the NO_3^- ion was

$$2NO_3^- \rightarrow 2NO_2(g) + 0.5O_2(g) + [O^{2-}] \quad (1)$$

in which $[O^{2-}]$ denotes the *effective donation* of an oxide ion to a phosphate acid, and does *not* imply the existence of any appreciable O^{2-} concentration in a nitrate melt.[1,2] In all cases studied degradation of any phosphate species did not yield a product simpler than the $P_2O_7^{4-}$ ion, whose double end-group structure apparently represented a stable form in molten $NaNO_3$ and nitrates of the heavier alkali metals. However, it was observed that if molten $LiNO_3$ was used as the reaction medium, degradation to PO_4^{3-} occurred, indicating a distinct cation effect.[1] This is not unexpected in view of work by Markowitz et al.,[3] and by other workers cited in extenso in the work of ref 1.

The present work constitutes a study of the kinetics of the reaction

$$P_2O_7^{4-} + 2NO_3^- \xrightarrow[Li^+]{} 2PO_4^{3-} + 2NO_2(g) + 0.5O_2(g) \quad (2)$$

with respect to $P_2O_7^{4-}$ in excess molten alkali nitrate solvents (55:1 mole ratio of NO_3^- to $P_2O_7^{4-}$) as functions of Li^+ concentration from 0.6530 to 0.9323 cation mole fraction, and of temperature over a fairly small range from 610 to 625 K. Lithium content in the molten nitrates was controlled by mixing appropriate quantities of $LiNO_3$ and $NaNO_3$.

Experimental Section

Materials. Reagent grade $LiNO_3$ was obtained from Fisher Scientific Co., and reagent grade $NaNO_3$ was from Mallinckrodt Co. The $LiNO_3$ was vacuum dried at 125° for ca. 48 h, and was finely ground by mortar and pestle in a drybox. The $NaNO_3$ was oven dried at 125° for at least 24 h prior to being finely ground in the drybox. Reagent grade $Na_4P_2O_7 \cdot 10H_2O$ was from the Baker and Adamson Co. This salt was thermally and quantitatively dehydrated, as in earlier work,[4] and was also finely ground in the drybox. All handlings of these compounds were performed in the drybox, with the exception of the kinetic runs themselves to be described later. Argon, used as the reaction system purge and ambient blanket gas, was from the National Cylinder Gas Co. and had a stated purity in excess of 99.9%. It was passed through a drying tower packed with $Mg(ClO_4)_2$ before entering the system.

Apparatus and Instrumentation. NMR analyses of dissolved reaction residues were performed using a Varian Associates Model XL-100 NMR spectrometer equipped with a ^{31}P probe and proton lock. Spectra were accumulated with a Varian Associates Model C-1024 time average computer, and were integrated using a K. and E. compensating polar planimeter, Model 62 0005. Samples were contained in Wilmad Glass Co. 12-mm o.d. NMR sample tubes with plastic caps.

A constant high-temperature bath (±0.5°) was employed in the form of a thermostated, stirred bath of molten $NaNO_3$–KNO_3 eutectic, and is described in detail elsewhere.[5]

All temperature measurements were performed using a Leeds and Northrup No. 8691 millivolt potentiometer with chromel–alumel thermocouples and an ice–water reference junction bath.

Vycor reaction vessels and assemblies were identical with those described earlier for quenched reaction rate studies.[1,5,6]

Procedure. The mechanics of this procedure was basically the same as employed earlier.[1,6] Four types of alkali ni-

TABLE I: Summary of Composition Data for Molten Alkali Nitrate Solvents Allowed to React with 0.1000 g of $Na_4P_2O_7$[a]

Solvent no.	Mass of $LiNO_3$, g	Mass of $NaNO_3$, g	Cation mol fraction Li^+, X'_{Li}	Effective cation mol fraction Li^+, X_{Li}
1	1.4247	0.0000	1.0000	0.9323
2	1.2834	0.1785	0.9000	0.8377
3	1.1385	0.3570	0.8000	0.7431
4	1.0005	0.5270	0.7000	0.6530

[a] In each case the total mass of alkali nitrate solvent represents a 55:1 anion mole ratio of NO_3^- to $P_2O_7^{4-}$.

trate solvents were prepared differing in Li^+ to Na^+ ratios for a fixed amount of NO_3^- ion. Table I summarizes these composition data. Cation mole fractions of Li^+ in the four solvents, X'_{Li}, were 1 (pure $LiNO_3$), 0.9, 0.8, and 0.7. When each of the indicated quantities of the various solvents was allowed to react with 0.1000 g of $Na_4P_2O_7$, contribution of the four Na^+ ions per $P_2O_7^{4-}$ ion resulted in the actual, *effective* cation mole fraction of Li^+ having the values X_{Li}, given in the last column of Table I. In each case the amount of a solvent reacted with 0.1000 g of $Na_4P_2O_7$ represented a 55:1 molar ratio of NO_3^- to $P_2O_7^{4-}$. In this way, as earlier,[1,6] NO_3^- was in sufficient excess to permit its concentration to be approximated as constant while kinetics were observed with respect to $P_2O_7^{4-}$.

In a typical run the appropriate quantity of a nitrate solvent was prepared by weighing and mixing $LiNO_3$ and $NaNO_3$ solids in a drybox. The resulting crystalline mixture and 0.1000 g of $Na_4P_2O_7$ were loaded into the separate compartments of a Vycor reactor assembly.[1,5,6] This assembly was thermostated for several hours in the constant high-temperature bath, during which time the reactor was purged with a flow of dry Ar at a rate of ca. 20–25 cm^3 min^{-1}. Upon attainment of thermal equilibrium by the reagents the Ar flow was terminated, and the $Na_4P_2O_7$ charge was dropped into the molten nitrate reservoir as timing commenced. The assembly was manually agitated during the first minute to ensure rapid dissolution of $Na_4P_2O_7$. At an appropriate time the reaction was stopped by plunging the hot zone of the reaction vessel into ice–water (less than 10 s required for this action). The vessel was then stoppered and stored for residue analysis. This procedure was repeated for each of the four solvent compositions for several reaction times at temperatures of 610, 615, 620, and 625 K.

Dissolution of reaction residues in deionized H_2O, for ^{31}P NMR analyses, presented more of a problem than in earlier work. With the NMR instrument employed, ca. 10 cm^3 of solution represented a practical upper limit where quantitative accuracy could be expected. At longer reaction times more PO_4^{3-} ions were formed, and presumably the low solubility of Li_3PO_4 (0.03 g/100 g of solution at 25°)[7] complicated the dissolution problem. As a result, the initial masses of reagents chosen constituted the maximum quantities which could be dissolved after reasonable reaction times. Dissolution could only be effected by slight acidification of the solution. Each residue sample was dissolved at room temperature with agitation in 10 cm^3 of deionized H_2O acidified with 3 drops of concentrated HCl. The resulting solutions had pH ~3. The question arose as to whether or not hydrolytic scission of $P_2O_7^{4-}$ to PO_4^{3-} in these acid solutions would invalidate the analyses. To answer this a blank solution of 0.1000 g of $Na_4P_2O_7$ and 1.4247 g of $LiNO_3$ in 10 cm^3 of H_2O acidified with 3 drops of concentrated HCl was prepared and allowed to stand at room temperature for over 1 month. ^{31}P NMR spectra were obtained for this blank at 0, 6, 11, 19, 26, and 34 days. Peaks were found only for PO_4^{3-} and $P_2O_7^{4-}$ (except no PO_4^{3-} on day zero). A plot of the natural logarithm of fraction of $P_2O_7^{4-}$ remaining vs. time was reasonably linear and indicated a first-order hydrolysis half-life of ca. 194 days, or 6 months. It appeared, therefore, that data obtained from NMR spectra of solutions prepared no earlier than 3–7 h before should be free of any significant errors due to hydrolysis of $P_2O_7^{4-}$.

Since NMR peaks arose only for PO_4^{3-} and $P_2O_7^{4-}$, it was not necessary to include a capillary of 85% H_3PO_4 for a standard, as was required in the earlier work.[1] Total integrated peak area of a spectrum represented total (constant) atomic phosphorus content, and the mole fraction of total phosphate as unreacted $P_2O_7^{4-}$, X_{pp}, was calculated for each sample as

$$X_{pp} = \frac{0.5(\text{area } P_2O_7^{4-} \text{ peak})}{(\text{area } PO_4^{3-} \text{ peak}) + 0.5(\text{area } P_2O_7^{4-} \text{ peak})} \quad (3)$$

Limitations of the Method. As mentioned before, the quantities of $Na_4P_2O_7$ and the appropriate nitrate solvent were the optimum amounts necessary for adequate quantitative determinations of phosphate contents by the NMR method, while maintaining sufficient excess of nitrate relative to phosphate.

Conditions in the present work which caused the most rapid rates for reaction 2 were higher temperatures and greater Li^+ concentrations. At temperatures in excess of 625 K the reaction using higher Li^+ concentrations proceeded so rapidly that reliable data could not be obtained by the present method. This was presumably due to the times required for manipulations becoming more significant relative to actual reaction time (e.g., times for dissolution of $Na_4P_2O_7$ in the nitrate and for reaction quenching). At temperatures less than ca. 610 K either the $Na_4P_2O_7$ would not dissolve completely in the molten nitrate, or partial crystallization would occur shortly after onset of reaction. Thus, 610 K represented the practical lower limit of temperature.

At Li^+ solvent fraction less than $X'_{Li} \sim 0.7$ ($X_{Li} \sim 0.65$) and the lower temperatures, the reaction proceeded quite slowly and scatter of data became too great, possibly because of cumulative errors introduced by such factors as the difficulty or prolonged accurate temperature control.

Thus, combined factors of temperature and Li^+ content caused unsatisfactory reaction conditions to exist above 625 K for higher Li^+ concentrations, and below 610 K for all Li^+ concentrations. The probable errors of the rate constant data summarized in Table II tend to reflect these trends. Also shown in Table II are the half-lives spanned in collecting data for the various reaction conditions. These half-lives range from 3.1 for the fastest reaction at 625 K and X_{Li} = 0.9323 to 1.0 for the slowest reaction at 610 K and X_{Li} = 0.6520. This trend illustrates the aforementioned difficulties encountered in following slower reactions ever prolonged periods of time, since after sufficiently long times data scatter became too great.

Results and Discussion

First-order kinetics was observed for reaction 2 with respect to $P_2O_7^{4-}$ in excess molten nitrate. Plots of ln X_{pp}

TABLE II: Summary of First-Order Rate Constants at Various Temperatures and Li^+ Concentrations

Effective cation mol fraction Li^+, X_{Li}	No. of data points	No. of half-lives spanned in reaction	Rate constant, k_1, min^{-1}, × 10^2
		610 K	
0.9323	6	2.5	14.2 ± 0.4
0.8377	6	1.5	5.91 ± 0.11
0.7431	7	1.6	5.20 ± 0.08[a]
0.6530	7	1.0	3.31 ± 0.19
		615 K	
0.9323	7	2.8	16.3 ± 0.3
0.8377	6	1.9	7.23 ± 0.26
0.7431	7	1.8	6.05 ± 0.09
0.6530	7	1.3	4.30 ± 0.20
		620 K	
0.9323	6	2.9	22.6 ± 0.3
0.8377	6	2.5	9.64 ± 0.13
0.7431	6	2.0	7.53 ± 0.16
0.6530	6	1.6	6.15 ± 0.25
		625 K	
0.9323	10	3.1	30.2 ± 0.7
0.8377	6	2.5	12.5 ± 0.4
0.7431	6	2.4	9.31 ± 0.17
0.6530	6	2.0	7.77 ± 0.20

[a] See comment in text.

(calculated by eq 3) vs. time, t, were linear and yielded the rate constants, k_1, tabulated in Table II, in which the errors are least-squares probable errors. Since a definite point in each such plot was ln $X_{pp} = 0$ at $t = 0$, it seemed appropriate to perform least-squares analyses of the data while forcing each line through the origin.[8,9] Application of the statistical F test,[3] using 5% critical values for F, subsequently confirmed that in no case except one was there sufficient evidence to warrant the assertion that an intercept differed from the origin more than could be accounted for by experimental errors. The single exception was the run using $X_{Li} = 0.7431$ at 610 K, as annotated in Table II. This single case cannot be explained other than by commenting that the difference in F values was not large.

Arrhenius plots of ln k_1 vs. $1/T$ for each concentration of Li^+ gave reasonably straight lines which yielded the least-squares intercepts, slopes, preexponential factors, A, and activation energies, E_a, tabulated in Table III, in which the errors are least-squares probable errors. Analyses for the $X_{Li} = 0.7431$ series were performed both with and without the point for 610 K, as noted in the table. Admittedly one cannot attach too much significance to activation energy and preexponential factors calculated from an Arrhenius plot of only four points over a small temperature range, except to remark on the typical orders of magnitude expected.

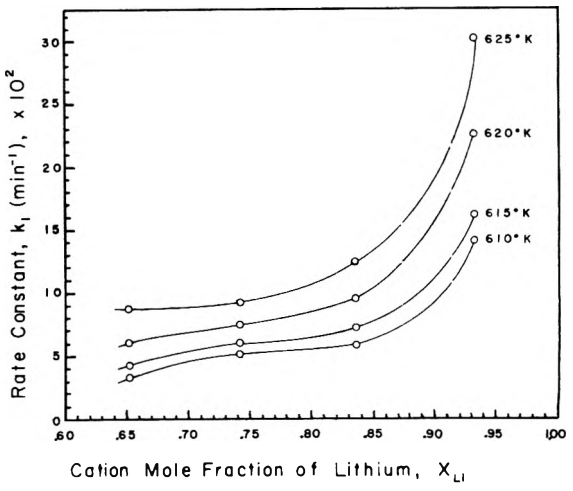

Figure 1. Plots of first-order rate constants, k_1, vs. effective cation mole fraction of Li^+, X_{Li}, at 610, 615, 620, and 625 K for the degradation of $P_2O_7^{4-}$ in excess molten alkali nitrates.

The major point of interest in the present work is the dependence of k_1 on Li^+ content, as exemplified by the plots of k_1 vs. X_{Li} shown in Figure 1 for the four temperatures. The plots are obviously nonlinear, and each indicates a rapid rise in reaction rate with increasing X_{Li} above ca. 0.75. No inflection is apparent in the highest isotherm at 625 K, but an inflection begins to be manifested at $X_{Li} \sim 0.75$ for the 620 K curve, and becomes more and more pronounced at the lower temperatures, yielding an apparently horizontal plateau in the vicinity of $X_{Li} = 0.75$. In these lower temperature curves there is also the appearance of fairly rapid falloff of reaction rate at values of X_{Li} less than ca. 0.7.

At $X_{Li} = 0.75$, on the average three of every four cations in the vicinity of a $P_2O_7^{4-}$ ion are Li^+ type. Thus, an average $P_2O_7^{4-}$ anion, before decomposition, might be conceived of as being coordinated in some way with three Li^+ ions and one Na^+ ion. The Li^+ ions, with their high ionic potential, could conceivably weaken the P–O–P bridge via strong electron-withdrawing effects, leading to easier rupture of $P_2O_7^{4-}$ by NO_3^- and subsequent production of PO_4^{3-}. For $X_{Li} > 0.75$, the average Li^+ coordination by a $P_2O_7^{4-}$ ion would be between 3 and 4, and a significant fraction of $P_2O_7^{4-}$ ions might be expected to be coordinated with *four* Li^+ ions, leading to further intensification of the bridge weakening and more rapid reaction, as seen in Figure 1. At $0.5 < X_{Li} < 0.75$, the average $P_2O_7^{4-}$ would experience between two and three Li^+ ions, the average bridge weakening would not be as great, and reaction rate

TABLE III: Summary of Least-Squares Intercepts and Slopes of Arrhenius Plots of ln k_1 (k_1 in min^{-1}) vs. $1/T$, Preexponential Factors, and Activation Energies

Effective cation mol fraction Li^+, X_{Li}	Intercept	−Slope × 10^{-4}	Preexponential factor A, min^{-1}	Activation energy, E_a, kcal mol^{-1}
0.9323	30.371 ± 3.097	1.975 ± 0.191	1.55 × 10^{13}	39 ± 4
0.8377	28.704 ± 1.308	1.925 ± 0.081	2.92 × 10^{12}	38.2 ± 1.6
0.7431[a]	21.587 ± 1.193	1.498 ± 0.074	2.37 × 10^{9}	29.8 ± 1.5
	[24.135 ± 0.113	1.657 ± 0.007	3.03 × 10^{10}	32.9 ± 0.1]
0.6530	33.062 ± 1.597	2.225 ± 0.099	2.28 × 10^{14}	44.2 ± 2.0

[a] Values in brackets are calculated for $X_{Li} = 0.7431$ neglecting point at 610 K; values not in brackets are calculated for $X_{Li} = 0.7431$ using all points.

would be expected to be slower. These effects could provide an interpretation of the apparent inflections at $X_{Li} = 0.75$ in the k_1 vs. X_{Li} curves for lower temperatures. At higher temperatures, although the rapid increase in k_1 with increasing X_{Li} is just as pronounced, presumably the enhanced thermal effect tends to "wash out" the appearance of an inflection plateau. The quite rapid increase in k_1 with increasing X_{Li} above 0.75 (k_1 approximately tripling in value from $X_{Li} \sim 0.75$ to ~ 0.93) would seem to indicate an extremely fast reaction at $X_{Li} = 1.0$, where each $P_2O_7^{4-}$ would be coordinated with four Li^+ ions (i.e., corresponding to pure $Li_4P_2O_7$ in excess pure $LiNO_3$). This latter reaction would be an interesting one to perform; however, this is not possible in view of the apparent lack of availability of $Li_4P_2O_7$ from chemical suppliers, and the lack of any effective preparation for this salt in the literature. The ionic potential of Li^+ is 1.47, and that of Na^+ is 1.03. If the hypothesis of the higher ionic potential of Li^+ causing weakening of the P–O–P bridge and subsequent reaction has merit, then cations of still higher ionic potentials should similarly catalyze degradation of $P_2O_7^{4-}$ by NO_3^-. The alkaline earth cations are of this type ($Be^{2+} = 5.71$, $Mg^{2+} = 3.03$, $Ca^{2+} = 2.02$, $Sr^{2+} = 1.79$). A brief test experiment in which $Na_4P_2O_7$ was placed in molten $Ca(NO_3)_2$ (mp = 561°) did indeed show an extremely rapid degradation of the pyrophosphate.

From the appearances of the lower temperature plots in Figure 1, and on the basis of the foregoing discussion, one might anticipate the appearance of a second inflection at $X_{Li} \sim 0.5$. Unfortunately, for reasons explained earlier, the slower reactions at these low Li^+ concentrations (especially at the lower temperatures) could not be investigated adequately by the present method.

Acknowledgments. This work was supported by the National Science Foundation, Grant No. GP-12002, A1. The major portion of this work is based on the thesis of Arthur S. Metcalf, which was submitted to the Graduate School of Kansas State University in May 1975 in partial fulfillment of the requirements for the Master of Science degree in chemistry.

References and Notes

(1) J. L. Copeland and L. Gutierrez, *J. Phys. Chem.*, **77**, 20 (1973).
(2) (a) P. G. Zambonin and J. Jordan, *Anal. Lett.*, **1**, 1 (1967); (b) *J. Am. Chem. Soc.*, **89**, 6365 (1967); (c) **91**, 2225 (1969).
(3) M. M. Markowitz, H. Stewart, Jr., and D. A. Boryta, *Inorg. Chem.*, **2**, 768 (1963).
(4) B. R. Hubble and J. L. Copeland, *J. Chem. Eng. Data*, **15**, 441 (1970).
(5) A. S. Metcalf, M.S. Thesis, Kansas State University, 1975.
(6) L. Gutierrez, Ph.D. Thesis, Kansas State University, 1972.
(7) A. D. F. Toy in "Comprehensive Inorganic Chemistry", Vol. 2, J. C. Bailar, H. J. Emeleus, R. Nyholm, and A. F. Trotman-Dickenson, Ed., Pergamon Press, Oxford, England, 1973, p 490.
(8) H. D. Young, "Statistical Treatment of Data", McGraw-Hill, New York, N.Y., 1962, pp 111–115.
(9) W. J. Youden, "Statistical Methods for Chemists", Wiley, New York, N.Y., 1951, pp 45–49.

Nickel(II) Chelation Kinetics Involving Dialkylmalonate Ligands

Giuseppe Calvaruso, F. Paolo Cavasino,* and Emanuele Di Dio

Istituto di Chimica Fisica, Università, 90123 Palermo, Italy *(Received August 4, 1975)*

Kinetic data for the aquonickel(II) ion reacting with the unprotonated and monoprotonated species of the dimethyl- and di-*n*-butylmalonic acids have been obtained at 25°C and ionic strength 0.10 *M* by the temperature-jump method. The results concerning the dimethyl derivative are similar to those previously found for some monosubstituted malonic acids, except that the chelate-ring opening rate is enhanced as a consequence of the increase of the steric hindrance of the two methyl groups. Ring opening however is faster with dimethylmalonate ion than with the di-*n*-butyl derivative despite the bulkier groups present in the latter ligand. This finding is explained on the basis of the greater basicity of the di-*n*-butylmalonate ion, which outweighs the accelerating substituent steric effect. Moreover kinetic data for the reaction involving the monoprotonated species of di-*n*-butylmalonic acid indicate that deprotonation of the intermediate monodentate complex $(H_2O)_5Ni(O_2C{\cdot}CR_2{\cdot}CO_2H)^+$ (R = Bu^n) is a slow process.

Earlier investigations[1,2] on the kinetics of the complexation reactions of the nickel(II) ion with some monosubstituted malonic acids in aqueous solution have shown that the chelate-ring closure rate is 12–16 times larger than the dissociation rate of the monodentate complex $(H_2O)_5Ni(O_2C{\cdot}CHR{\cdot}CO_2)$ (R = Me, Et, Bu^n, $PhCH_2$), and does not contribute, therefore, significantly to the limiting rate in the overall chelate-formation process ("normal substitution").[1-3] Moreover it has been observed that there is some dependence of the chelate-ring opening rate on the chain length and the size of the substituent group and that the seven-membered ring formed by the phthalate anion[4] is easier to open than the six-membered rings formed by the monosubstituted malonate anions.

In the present work we have studied, by the temperature-jump method, the kinetics of reaction of the nickel(II) ion with dimethyl- and di-*n*-butylmalonic acids in aqueous acidic solution at 25°C and $I = 0.10$ *M* in order to obtain information about the steric influence of two alkyl groups present in the molecule of malonic acid upon the opening and closure rate of the chelate ring, and to ascertain consequently the existence of a kinetic chelate effect[3,5] ("steri-

TABLE I: Experimental Conditions and Relaxation Times for the Reaction of Nickel(II) Ion with Dimethyl- and Di-*n*-butylmalonic Acids (t = 25°C; I = 0.10 M)

$10^4[Ni]_T$,[a] M	$10^4[ligand]_T$,[b] M	$10^4[H^+]$, M	HIn[c]	10^4A, M	$10^4\tau_{obsd}$, sec	$10^4\tau_{calcd}$, sec
			Dimethylmalonic Acid			
50.0	40.0	0.0341	*d*	169	4.6	4.6
60.0	40.0	0.0528	*d*	176	4.5	4.2
60.0	40.0	0.0781	*d*	173	4.5	4.1
40.0	30.0	0.152	*e*	149	4.1	4.2
50.0	40.0	0.228	*e*	152	3.6	3.6
60.0	60.0	0.271	*e*	157	3.1	3.3
70.0	60.0	0.325	*e*	159	3.3	3.1
60.0	40.0	0.356	*e*	148	3.5	3.2
70.0	65.4	0.400	*e*	153	2.7	2.9
70.0	60.0	0.476	*e*	147	2.7	2.8
60.0	50.0	0.528	*e*	138	3.0	2.9
70.0	70.0	0.606	*e*	140	2.7	2.7
70.0	70.0	0.712	*e*	135	2.6	2.5
70.0	81.8	0.799	*e*	133	2.5	2.4
80.0	70.0	0.896	*e*	132	2.5	2.3
90.0	90.0	1.07	*f*	130	2.3	2.1
90.0	80.0	1.18	*e*	127	2.4	2.1
90.0	115	1.24	*f*	127	1.8	2.0
100	100	1.44	*f*	126	2.0	1.9
100	100	1.59	*f*	124	1.9	1.8
110	90.0	1.75	*f*	123	1.7	1.7
100	131	1.87	*f*	122	1.6	1.7
120	100	2.05	*f*	122	1.6	1.6
120	100	2.10	*f*	121	1.4	1.6
120	110	2.15	*f*	121	1.5	1.6
120	110	2.30	*f*	120	1.5	1.5
120	132	2.41	*f*	120	1.6	1.5
120	164	2.47	*f*	120	1.7	1.5
140	130	2.53	*f*	121	1.6	1.5
140	130	2.65	*f*	120	1.4	1.4
140	140	2.83	*f*	120	1.4	1.4
150	150	3.07	*f*	119	1.4	1.4
150	150	3.18	*f*	119	1.3	1.3
160	160	3.33	*f*	119	1.4	1.3
150	150	3.41	*f*	118	1.2	1.3
180	180	3.57	*f*	119	1.3	1.3
			Di-*n*-butylmalonic Acid			
30.0	15.0	0.0400	*d*	62.2	12.5	12
40.0	34.8	0.0585	*d*	75.7	11.5	9.9
40.0	18.0	0.0808	*d*	62.6	11.5	12
40.0	31.5	0.0994	*d*	67.4	10.5	10
50.0	43.3	0.130	*e*	66.8	9.4	10
50.0	43.0	0.253	*e*	54.4	10.5	11
50.0	36.9	0.341	*e*	50.1	9.8	10
50.0	40.1	0.460	*e*	48.2	10.5	9.8
50.0	44.1	0.481	*e*	48.1	8.8	9.7
60.0	43.4	0.559	*e*	47.8	8.3	9.2
60.0	32.7	0.649	*e*	46.7	9.5	8.9
60.0	37.5	0.712	*e*	46.5	8.7	8.6
80.0	41.4	0.808	*e*	46.8	8.3	8.1
80.0	38.5	0.907	*e*	46.3	6.8	7.7
90.0	44.3	0.983	*e*	46.4	8.9	7.5
90.0	41.1	1.15	*e*	45.9	7.1	7.0
90.0	46.8	1.15	*f*	46.0	6.9	7.0
90.0	42.9	1.27	*e*	45.7	7.2	6.8
100	44.9	1.28	*e*	45.8	6.8	6.7
100	44.6	1.36	*e*	45.7	7.8	6.6
100	44.8	1.37	*f*	45.7	6.3	6.5
100	45.9	1.42	*e*	45.7	6.0	6.4
100	46.4	1.45	*e*	45.6	7.0	6.4
100	49.5	1.52	*f*	45.5	6.6	6.3
100	45.4	1.54	*e*	45.5	5.5	6.2
100	47.2	1.59	*e*	45.5	7.5	6.2
100	51.5	1.69	*f*	45.4	5.5	6.0
100	50.0	1.79	*f*	45.3	5.9	5.9
100	48.4	1.87	*f*	45.2	5.3	5.8
110	52.1	2.03	*f*	45.2	5.6	5.6
110	47.5	2.20	*f*	45.1	4.9	5.4
110	50.2	2.23	*f*	45.1	5.4	5.4
110	50.9	2.41	*f*	45.1	5.7	5.2
110	46.8	2.53	*f*	45.0	5.4	5.1

[a] Total molar concentration of nickel (II) perchlorate. [b] Total molar concentration of dicarboxylic acid. [c] Indicator. [d] Chlorophenol red. [e] Bromocresol green. [f] Bromochlorophenol blue.

cally controlled substitution"). In addition, for the homologous series of the malonic acids so far considered, the di-*n*-butylmalonate anion is the strongest basic ligand (pK_2^H = 7.21: see Table II) and its basicity is about two orders of magnitude higher than those of the other substituted malonate anions. This work allowed us therefore to study also the effect of the ligand basicity on the kinetics of formation and dissociation of these nickel(II) monochelate complexes.

Experimental Section

Commercial (Fluka) dimethylmalonic acid and di-*n*-butylmalonic acid, obtained by basic hydrolysis[1] of the diethyl ester (Fluka), were purified by recrystallization and the melting points were found to be in good agreement with those reported[6] in literature. Nickel perchlorate, sodium perchlorate, and the indicators (chlorophenol red, bromocresol green, and bromochlorophenol blue) were the same compounds previously utilized.[1,2,4]

The present study was made at 25°C and ionic strength 0.10 *M* (supporting electrolyte $NaClO_4$). For dimethylmalonic acid the solutions for kinetic measurements were prepared by using stock solutions of the pertinent substances as described before.[1,2,4] For di-*n*-butylmalonic acid, on the contrary, owing to its low solubility, a different procedure was followed. A weighed quantity of acid ligand, distilled water, and a given volume of dilute NaOH were mixed into a 100-ml volumetric flask and the mixture was shaken by an automatic shaker until the ligand dissolved (the quantity of added NaOH was such that the pH of the final solution was approximately the desired value). After addition of the appropriate small amounts of stock solutions of $Ni(ClO_4)_2$, $NaClO_4$, and indicator, the solution was then diluted to the mark with distilled water.

The other experimental details and the apparatus employed have been described elsewhere.[1] In the case of dimethylmalonic acid the temperature-jump experiments were carried out using a 30-kV discharge (temperature rise = 3.7°C), whereas for di-*n*-butylmalonic acid a 36-kV discharge (temperature rise = 5.4°C) was used in order to increase the amplitude of the relaxation effect. However, kinetic measurements at acidities higher than those reported in Table I were precluded by the diminution of the relaxation effect magnitude with increasing acidity. It should be pointed out that for di-*n*-butylmalonic acid preliminary measurements[7] performed using a 30-kV discharge seemed to indicate, owing to the large uncertainty in the estimated relaxation times, a kinetic behavior different from that finally observed in the present work.

Each solution examined exhibited a single relaxation effect associated with the complexation reaction. The observed relaxation times are affected by a maximum uncertainty of ca. ±10%.

Results and Discussion

The experimental conditions used and the observed relaxation times, τ_{obsd}, are assembled in Table I, whereas the equilibrium constants relevant to this study are given in Table II, where HIn indicates the indicator.

The kinetic data are found to conform to the reaction scheme previously proposed[1,2,4,8] for other dicarboxylic acids, in which only the dianionic and monoanionic ligand species react with the nickel(II) ion at a significant rate over the acidity range covered. In this reaction scheme (reactions 1–4) $(H_2O)_6Ni, O_2C{\cdot}CR_2{\cdot}CO_2$ and $(H_2O)_6Ni, O_2C{\cdot}CR_2{\cdot}CO_2H^+$ represent outer-sphere complexes, $(H_2O)_5Ni(O_2C{\cdot}CR_2{\cdot}CO_2)$ and $(H_2O)_5Ni(O_2C{\cdot}CR_2{\cdot}CO_2H)^+$ monodentate complexes (R = Me or Bu^n); reaction 3 is considered a proton-transfer process with the solvent probably acting as the proton acceptor.

TABLE II: Equilibrium Constants[a] Used in This Work (t = 25°C; I = 0.10 *M*)

	Log K_C	pK_1^H	pK_2^H	pK_i
Dimethylmalonic acid[b,c]	1.95	3.01	5.68	
Di-*n*-butylmalonic acid[c]	2.35	2.01	7.21	
Chlorophenol red[d]				5.96
Bromocresol green[d]				4.70
Bromochlorophenol blue[d]				4.00

[a] $K_C = [(H_2O)_4Ni(O_2C)_2CR_2]/[Ni(H_2O)_6^{2+}][O_2C{\cdot}CR_2{\cdot}CO_2^{2-}]$; $K_1^H = [HO_2C{\cdot}CR_2{\cdot}CO_2^-][H^+]/[HO_2C{\cdot}CR_2{\cdot}CO_2H]$; $K_2^H = [O_2C{\cdot}CR_2{\cdot}CO_2^{2-}][H^+]/[HO_2C{\cdot}CR_2{\cdot}CO_2^-]$ (R = Me or Bu^n); $K_i = [In^-][H^+]/[HIn]$. [b] G. Ostacoli, E. Campi, A. Vanni, and E. Roletto, *Atti Accad. Sci. Torino*, **100**, 723 (1966); G. Ostacoli, A. Vanni, and E. Roletto, *Ric. Sci.*, **38**, 318 (1968). [c] G. Ostacoli, A. Vanni, and E. Roletto, *Gazz. Chim. Ital.*, **100**, 350 (1970). [d] References 1, 2, and 4.

$$Ni(H_2O)_6^{2+} + -H^+ \rightleftarrows +H^+$$

$$O_2C{\cdot}CR_2{\cdot}CO_2^{2-} \overset{\text{very fast}}{\rightleftharpoons} (H_2O)_6Ni, O_2C{\cdot}CR_2{\cdot}CO_2 \qquad K_0 \qquad (1a)$$

$$HO_2C{\cdot}CR_2{\cdot}CO_2^- \overset{\text{very fast}}{\rightleftharpoons} (H_2O)_6Ni, O_2C{\cdot}CR_2{\cdot}CO_2H^+ \qquad K_0' \qquad (1b)$$

$$(H_2O)_6Ni, O_2C{\cdot}CR_2{\cdot}CO_2 \underset{k_{-1}}{\overset{k_1}{\rightleftharpoons}} H_2O + (H_2O)_5Ni(O_2C{\cdot}CR_2{\cdot}CO_2)$$

$$K_1 = k_1/k_{-1} \qquad (2a)$$

$$(H_2O)_6Ni, O_2C{\cdot}CR_2{\cdot}CO_2H^+ \underset{k_{-1}'}{\overset{k_1'}{\rightleftharpoons}} H_2O + (H_2O)_5Ni(O_2C{\cdot}CR_2{\cdot}CO_2H)^+$$

$$K_1' = k_1'/k_{-1}' \qquad (2b)$$

$$(H_2O)_5Ni(O_2C{\cdot}CR_2{\cdot}CO_2H)^+ \underset{k_H}{\overset{k_H}{\rightleftharpoons}} H^+ + (H_2O)_5Ni(O_2C{\cdot}CR_2{\cdot}CO_2)$$

$$K_H = k_H/k_{-H} \qquad (3)$$

$$(H_2O)_5Ni(O_2C{\cdot}CR_2{\cdot}CO_2) \underset{k_{-2}}{\overset{k_2}{\rightleftharpoons}} H_2O + (H_2O)_4Ni\begin{array}{l}O_2C\\ \diagdown\\ \diagup\\ O_2C\end{array}CR_2$$

$$K_2 = k_2/k_{-2} \qquad (4)$$

Under the experimental conditions of the present investigation, the previously derived[1] equation for the relaxation time τ valid for the above reaction scheme is given by expression 5, where A is a quantity depending on the equilib-

$$1/\tau A = (a + b[H^+])/(1 + c[H^+]) \qquad (5)$$

$$a = k_1k_2K_0/(k_{-1} + k_2) \qquad (6)$$

$$b = k_1'k_Hk_2K_0'/K_2^H(k_{-1}' + k_H)(k_{-1} + k_2) \qquad (7)$$

$$c = k_{-1}'k_{-H}/(k_{-1}' + k_H)(k_{-1} + k_2) \qquad (8)$$

rium concentrations of the predominant species present in solution and a, b, and c are related to the rate constants by the relationships 6–8. Note that the constant a represents the usually observed overall second-order rate constant for the reactions between the nickel(II) ion and bidentate ligands. The A values, calculated by the expression given elsewhere,[1] are also reported in Table I.

TABLE III: Kinetic Data for Formation and Dissociation of Nickel(II) Monochelate Complexes with Dimethyl- and Di-*n*-butylmalonic Acids (t = 25° C; I = 0.10 M)

	Dimethylmalonic acid	Di-*n*-butylmalonic acid
$10^{-5}\,a$, M^{-1} sec^{-1}	1.2	1.2
$10^{-9}\,b$, M^{-2} sec^{-1}	3.1	2.7
$10^{-3}\,c$, M^{-1}	2.4	3.4
k_2/k_{-1}	10	5.5
$k_2/(k_{-1} + k_2)$	0.93	0.85
$10^{-5}\,k_1K_0$, M^{-1} sec^{-1}	1.3	1.4
$10^{-3}\,k_1'k_HK_0'/(k_{-1}' + k_H)$, M^{-1} sec^{-1}	7.0[a]	0.20[b]
$10^{-3}\,k_1'K_0'$,[a] M^{-1} sec^{-1}		
$10^{-3}\,k_HK_1'K_0'$,[b] M^{-1} sec^{-1}		
$10^{-3}\,k_{-2}$, sec^{-1}	15	3.5
$10^{-2}\,k_{-1}/K_2$, sec^{-1}	15	6.3
$10^{-7}\,k_{-1}'k_{-H}/K_2(k_{-1}' + k_H)$, M^{-1} sec^{-1}	3.7[a]	1.4[b]
$10^{-7}\,k_{-1}'/K_2K_H$,[a] M^{-1} sec^{-1}		
$10^{-7}\,k_{-H}/K_2$,[b] M^{-1} sec^{-1}		

[a] $k_H > k_{-1}'$, see text. [b] $k_H < k_{-1}'$, see text.

The observed curved trend of the plot of $1/\tau A$ against the hydrogen-ion concentration for each ligand examined (cf. Figure 1) is that predicted from eq 5 and permits the estimate of the three constants a, b, and c (see Table III). The values of these constants have been obtained by analyzing the experimental data by use of a properly adapted non-linear least-squares program (OR GLS) on an IBM 370/145 computer. It should be pointed out that the procedure previously[1,2,4] followed for the evaluation of the constants a, b, and c leads to the same results. The uncertainty in the a values is ca. ±10%, whereas that in b and c is ca. ±15%.

The relaxation times τ_{calcd}, calculated by using eq 5 and the given a, b, and c values are in good agreement with those observed τ_{obsd} (cf. Table I). In addition, using the estimated c values, the plots of $(1 + c[H^+])/\tau A$ against $[H^+]$ (see Figure 1) show linear features over the whole acidity range covered (the correlation coefficients are 0.992 and 0.981 for dimethyl- and di-*n*-butylmalonic acids, respectively), yielding the same a and b values reported in accordance with expression 5. These results provide support to the reliability of the estimated values of the constants a, b, and c, and to the validity of the proposed reaction mechanism for the two ligands examined under the experimental acidity conditions of the present work.

The kinetic quantities obtainable by the appropriate combination[1,2,4] of eq 6–8 are also given in Table III, whereas some kinetic data for the homologous series of the malonic acids so far studied are reported in Table IV.

From a comparison of the k_2/k_{-1} values it is apparent that the contribution of the chelate-ring closure rate to the limiting rate in the overall chelate-formation process is more significant for di-*n*-butylmalonic acid than for the dimethyl derivative. However, the similarity of the values of k_1K_0 and a [the steric factors $k_2/(k_{-1} + k_2)$ are close to unity; cf. Table III] allows us to conclude that the reactions of the nickel(II) ion with the two dianions examined can be considered to occur mainly by a normal substitution mechanism.

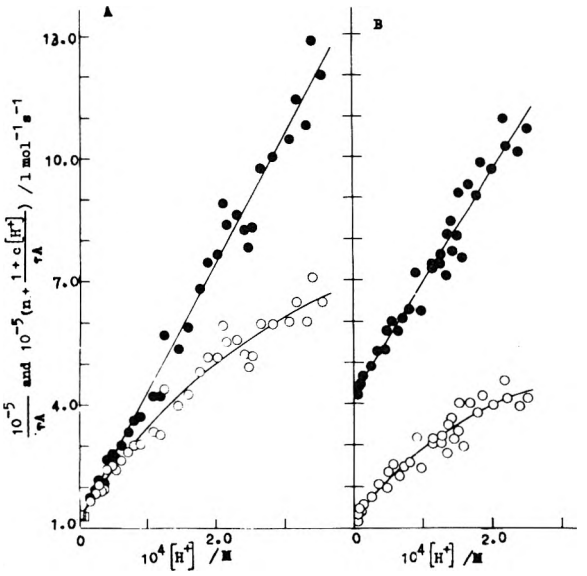

Figure 1. Plots of $1/\tau A$ (O) and $(1 + c[H^+])/\tau A$ (●) against $[H^+]$ for dimethylmalonic acid (A, n = 0) and di-*n*-butylmalonic acid (B, n = 3); (□) common points.

The identical k_1K_0 values of the present work (Table III) indicate that the different basicity and steric hindrance of the two disubstituted malonate anions have no effect on the kinetics of formation of the monodentate complexes $(H_2O)_5Ni(O_2C{\cdot}CR_2{\cdot}CO_2)$ (reactions 1a and 2a) and thus provide support to the occurrence of a dissociative mechanism, as suggested also previously[1,2] for the other malonic acids studied. It is noted that the k_1K_0 values for both disubstituted malonic acids are somewhat greater than those for monosubstituted derivatives (cf. Table IV). These different values should be ascribed to differences in the outer-sphere association constants.

According to Hoffmann's findings[1,9] concerning the dissociation rate of a series of nickel(II) mono complexes with carboxylic acids, the rate constant k_{-1} is expected to decrease to some extent with increasing the basicity of the coordinated carboxylate group. Therefore, since the rate constants k_{-1} must be larger for monosubstituted malonate anions and the dimethyl derivative (pK_2^H = 5.40–5.68; cf. Table IV) than for the di-*n*-butylmalonate ion (pK_2^H = 7.21), the lower k_2/k_{-1} value found for the latter ligand (cf. Table IV) suggests that in this case the chelate-ring closure rate (k_2) is decreased, in comparison to the related dianions, by a factor not less than 2–3. The deduced difficulty of closing the chelate ring for the di-*n*-butylmalonate ion may be reasonably ascribed to the two bulkier butyl substituents which hinder the attack of the second carboxylate group on the nickel.

The ring opening rate constant k_{-2} for the dimethylmalonate ligand is significantly larger than those for monosubstituted malonate ions having similar basicity (cf. Table IV). Hence these kinetic data substantiate our previous suggestion[1,2] that an increase in the steric hindrance of the substituted malonic acids so far considered speeds the opening of the six-membered ring. A fourfold decrease in the k_{-2} value however is observed in passing from dimethylmalonate to the di-*n*-butyl derivative despite the bulkier groups present in the latter ligand. Bearing in mind that the basicity of the two dianions differs by a factor of about 2 orders of magnitude (cf. Table IV), there is no doubt that the lower reaction rate observed for the di-*n*-butylmalon-

TABLE IV: Some Kinetic Data for Formation and Dissociation of Nickel(II) Monochelates with Substituted Malonic Acids (t = 25° C; I = 0.10 M)

Acid	k_2/k_{-1}	$10^{-3}k_1'k_HK_0'/(k_{-1}' + k_H)$, M^{-1} sec^{-1} $10^{-3}k_1'K_0'$,[d] M^{-1} sec^{-1} $10^{-3}k_HK_1'K_0'$,[e] M^{-1} sec^{-1}	$10^{-4}k_1K_0$, M^{-1} sec^{-1}	$10^{-3}k_{-2}$, sec^{-1}	pK_2H
Methylmalonic[a]	13	5.1[d]	7.3	2.2	5.40
Ethylmalonic[b]	12	4.9[d]	7.6	2.7	5.46
n-Butylmalonic[a]	16	4.0[d]	7.5	3.9	5.50
Benzylmalonic[b]	14	4.5[d]	9.4	3.4	5.42
Dimethylmalonic[c]	10	7.0[d]	13	15	5.68
Di-n-butylmalonic[c]	5.5	0.20[e]	14	3.5	7.21

[a] Reference 1. [b] Reference 2. [c] This work. [d] $k_H > k_{-1}'$, see text. [e] $k_H < k_{-1}'$, see text.

ate ion is due to its stronger base strength. Therefore it is evident that in this case the basicity plays the main role in determining the ring opening rate, the accelerating substituent steric effect being outweighed by the depressing effect of the ligand basicity.

As to the reaction of the aquonickel ion with the monoanionic ligand species, Table IV shows the values of the quantity $k_1'k_HK_0'/(k_{-1}' + k_H)$ for all the malonic acids so far studied. Two limiting cases[1,2,4] are expected to be observed, depending upon the relative magnitude of the rate constants k_{-1}' and k_H. First, if $k_H < k_{-1}'$, the quantity $k_1'k_HK_0'/(k_{-1}' + k_H)$ reduces to $k_HK_1'K_0'$ and the proton transfer process (3) is the rate-determining step. Second, if $k_H > k_{-1}'$, it follows that $k_1'k_HK_0'/(k_{-1}' + k_H) = k_1'K_0'$ and the slow step is the formation of the acid monodentate complex $(H_2O)_5Ni(O_2C{\cdot}CR_2{\cdot}CO_2H)^+$ (reaction 2b). It has been shown before[1,2] that the second case applies to the monosubstituted malonic acids. Considerations analogous to those made previously[1,2,4] lead to the same conclusion for the dimethyl derivative of the present work (i.e., $k_H > k_{-1}'$). Support for this is also given by the close values of $k_1'K_0'$ for these ligands (cf. Table IV) and, consequently, a dissociative mechanism is operative. In the case of di-n-butylmalonic acid, on the contrary, the calculated value for $k_1'k_HK_0'/(k_{-1}' + k_H)$ is anomalously low relative to those for other ligands and differs from the corresponding k_1K_0 value by a factor of 700. Large differences in the rates of reactions involving both unprotonated and monoprotonated ligand species have been found[1,2,4,10] when proton release is a relatively slow process. As a result, for the aquonickel ion reacting with the monoanionic form of di-n-butylmalonic acid the situation is $k_H < k_{-1}'$ [$k_1'k_HK_0'/(k_{-1}' + k_H) = k_HK_1'K_0'$; cf. Tables III and IV] and the rate-determining step is the proton transfer process (3).

Bearing in mind that the k_1K_0 values are identical for the two ligands used in this work (cf. Table III), it is reasonable to think that the rate constant $k_1'K_0'$ for dimethylmalonic acid is similar to that for the di-n-butyl derivative. This conclusion can also be inferred by taking into account the similarity of both the k_1K_0 and $k_1'K_0'$ values for the related monosubstituted ligands (cf. Table IV) and by considering that the formation of nickel(II) monocomplexes with unidentate ligands is generally accepted to occur[1-4] by a dissociative mechanism. Therefore, if the $k_1'K_0'$ value of 7.0×10^3 M^{-1} sec^{-1} is used for the di-n-butyl derivative, it is possible to estimate from the expression $k_1'k_HK_0'/(k_{-1}' + k_H) = 0.20 \times 10^3$ M^{-1} sec^{-1} that $k_{-1}'/k_H = 34$. That is, the dissociation rate of the protonated monodentate complex $(H_2O)_5Ni(O_2C{\cdot}CR_2{\cdot}CO_2H)^+$ (R = Bu^n) is 34 times larger than the rate of deprotonation of this intermediate.

Acknowledgment. We are grateful to the Consiglio Nazionale delle Ricerche for partial support of this work. We thank Professor R. Triolo for having adapted the program OR GLS for our purposes and Dr. G. Locanto for some preliminary kinetic measurements.

References and Notes

(1) G. Calvaruso, F. P. Cavasino, and E. Di Dio, *J. Chem. Soc., Dalton Trans.*, 2632 (1972).
(2) G. Calvaruso, F. P. Cavasino, and E. Di Dio, *J. Inorg. Nucl. Chem.*, **36**, 2061 (1974).
(3) D. J. Hewkin and R. H. Prince, *Coord. Chem. Rev.*, **5**, 45 (1970); R. G. Wilkins, *Acc. Chem. Res.*, **3**, 408 (1970); K. Kustin and J. Swinehart, *Prog. Inorg. Chem.*, **13**, 107 (1970); J. Burgess, D. N. Hague, R. D. W. Kemmitt, and A. McAuley, "Inorganic Reaction Mechanisms", Vol. 1, Chemical Society Specialist Periodical Report, London, 1971, p 210.
(4) F. P. Cavasino, E. Di Dio, and G. Locanto, *J. Chem. Soc., Dalton Trans.*, 2419 (1973).
(5) K. Kustin, R. F. Pasternack, and E. M. Weinstock, *J. Am. Chem. Soc.*, **88**, 4610 (1966); A. Kowalak, K. Kustin, R. F. Pasternack, and S. Petrucci, *ibid.*, **89**, 3126 (1967); W. B. Makinen, A. F. Pearlmutter, and J. E. Stueher, *ibid.*, **91**, 4083 (1969).
(6) J. E. Powell, J. L. Farrell, W. F. S. Neillie, and R. Russell, *J. Inorg. Nucl. Chem.*, **30**, 2223 (1968); A. I. Vogel, *J. Chem. Soc.*, 1476 (1929).
(7) F. P. Cavasino, E. Di Dio, and G. Locanto, Proceecing of the 15th International Conference on Coordination Chem., Moscow, 1973, p 436.
(8) F. P. Cavasino, *J. Phys. Chem.*, **69**, 4380 (1965); *Ric. Sci. A*, **35**, 1120 (1965).
(9) H. Hoffmann, *Ber. Bunsenges. Phys. Chem.*, **73**, 432 (1969).
(10) J. C. Cassatt and R. G. Wilkins, *J. Am. Chem. Soc.*, **90**, 6045 (1968); D. L. Rabenstein and R. J. Kula, *ibid.*, **91**, 2492 (1969); S. Funahashi and M. Tanaka, *Inorg. Chem.*, **8**, 2159 (1969); H. Diebler, *Ber. Bunsenges. Phys. Chem.*, **74**, 268 (1970); T. S. Roche and R. G. Wilkins, *Chem. Commun.*, 1681 (1970); L. J. Kirschenbaum and K. Kustin, *J. Chem. Soc. A*, 684 (1970).

Vibrational Relaxation and Photochemistry Studied by Photoluminescence Excitation Spectroscopy in Low Temperature Matrices. I. Cyclic Ketones[1]

Luisa T. Molina and Edward K. C. Lee*

Department of Chemistry, University of California, Irvine, California 92664 *(Received July 28, 1975)*

Publication costs assisted by the National Science Foundation

An experimental technique has been developed to measure photoluminescence excitation spectra and emission lifetime in inert low temperature matrices. Competition between molecular predissociation and vibrational relaxation in a low temperature matrix has been studied by phase-sensitive detection of photoluminescence (fluorescence or phosphorescence) from the first excited electronic states (n, π^*) of cyclopentanone (CP), cyclobutanone (CB), and perfluorocyclobutanone (PFCB). Strong phosphorescence emission is observed from CP and PFCB, indicating efficient vibrational relaxation and $S_1 \rightsquigarrow T_1$ intersystem crossing. No phosphorescence emission is observed from CB, and relatively weak fluorescence emission is observed only when CB is excited to low vibrational levels of the ^{1}(n, π^*) state. These observations imply that molecular predissociation in the matrix is very rapid from the high vibrational levels of CB(S_1) and that CB(T_1) is relatively unstable in contrast to PFCB(T_1) with a 2.1-msec lifetime and CP(T_1) with a 1.2-msec lifetime.

Introduction

A mechanism of photochemical transformation of cyclobutanone in the gas phase has been elucidated in some detail.[2] The unusual aspect of its photochemistry stems from the fact that the first excited singlet state, ^{1}(n, π^*), *predissociates* at excitation wavelengths shorter than 318 nm which correspond to ~4 kcal/mol above the 0–0 band of the $S_1 \leftarrow S_0$ transition. Below this level $S_1 \rightsquigarrow T_1$ intersystem crossing predominates over all other intramolecular relaxation processes, as in most of other ketones, aliphatic and cyclic. Above this level, unlike in other ketones, the predissociation which leads to the $S_1 \rightsquigarrow S_0$ internal conversion process and molecular fragmentation processes predominates over the $S_1 \rightsquigarrow T_1$ process. This mechanistic information was obtained from the pressure dependence and the excitation energy dependence of photoproducts.[2a,d] Furthermore, it has been well demonstrated through fluorescence excitation studies that the vibrational relaxation by collisional processes under atmospheric pressures of bath molecules of moderate complexity such as C_3H_8 cannot restore a complete fluorescence stabilization[2d] and also that the predissociation cannot be arrested even in cyclohexane solution at room temperature.[2b] This extreme instability of the ^{1}(n, π^*) state of cyclobutanone has been attributed to ring strain of the four-membered ring.[2b,3] Of course, the reason for this rapid predissociation lies in that the upper vibronic levels in the S_1 state may be strongly coupled to the dissociative continuum of the S_0 state. If vibrational relaxation in the low temperature matrix is very efficient as one usually supposes then a complete fluorescence stabilization indicated by enhanced fluorescence emission efficiency from the high vibronic levels of the S_1 state should be observed. If the vibrationally hot T_1 state was easily relaxed and the relaxed T_1 state was relatively stable, then one should also observe a characteristic phosphorescence emission which has not yet been observed in gas or solution phase studies.

Recent photochemical studies of perfluorocyclobutanone in the gas phase indicate that the first excited singlet state, ^{1}(n, π^*), *does not predissociate* as rapidly as cyclobutanone;[4] a moderate degree of fluorescence stabilization has been observed. Therefore, it appears that ring strain in the ^{1}(n, π^*) state of perfluorocyclobutanone either has a relatively unimportant role in the predissociation mechanism or is not as great as in cyclobutanone. In order to examine the effectiveness of the low temperature matrix for vibrational relaxation and thus for arresting extremely rapid molecular predissociation, we have measured photoluminescence excitation spectra of cyclobutanone (CB), perfluorocyclobutanone (PFCB), and cyclopentanone (CP) in a solid N_2 matrix at 20 K using a phase-sensitive detector which can also provide lifetime data on the transcient species under observation. The general applicability of photoluminescence excitation spectroscopy in a matrix as well as the specific results obtained with the above mentioned three ketones shall be presented below.

Experimental Section

Samples of cyclobutanone, cyclopentanone, and perfluorocyclobutanone used in the present experiments were satisfactory in terms of chemical purity. The ketones were premixed with research grade nitrogen (Matheson Gas Co.) in the molar ratio range of 1:50 to 1:800, using a grease-free and mercury-free vacuum line. The gas mixture was allowed to flow through a capillary inlet tube into the vacuum chamber of the cryostat with four side windows, and it was spray deposited on the cold, rotatable sapphire window (20 K) as a transparent solid film. The deposition rate was ~1 mmol hr^{-1} for a period of 3~4 hr. Faster deposition rates often resulted in an unsatisfactory film with a high light scattering property. The target temperature was controlled with a closed-cycle cryogenic cooler (Cryogenic Technology, Inc., Model 21 Cryocooler). Temperatures were measured with a calibrated chromel vs. gold, 0.07 atom % iron thermocouple wire. The temperature could be regulated at any time using a digital temperature indicator–controller (CTI Model 237A).

The optical and electronic set up used for the study of

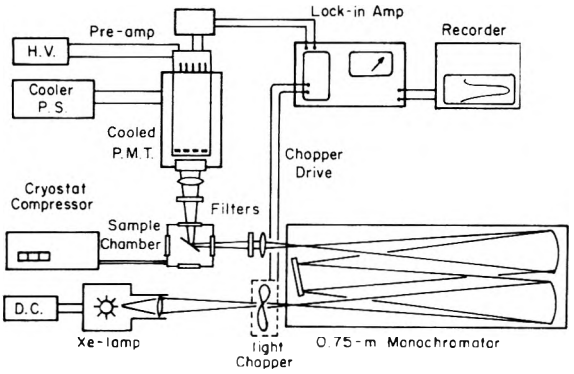

Figure 1. Schematic diagram of the experimental setup.

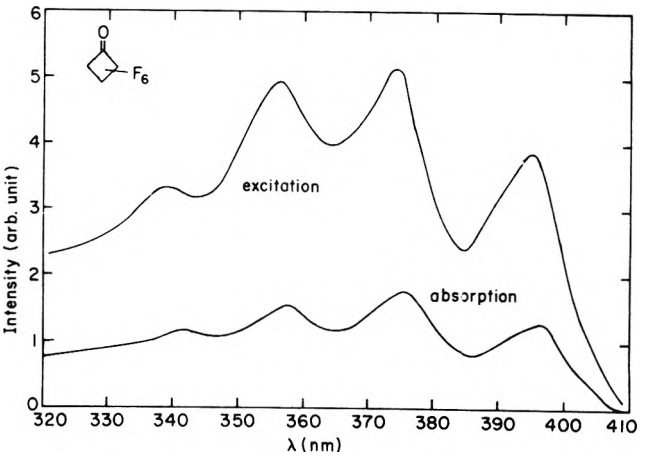

Figure 2. Absorption and photoluminescence excitation spectra (corrected for variation in excitation intensity) taken with N_2/PFCB = 100 at 20 K.

photoluminescence excitation spectra is shown in Figure 1. Light from a 150-W high-pressure xenon arc (Osram XBO/1) is focused onto the entrance slit of 0.75-m grating monochromator (Spex Industries Model 1702, f = 6.8, 1200 lines/mm, 5000-Å blaze), and it is modulated by a variable speed chopper (Princeton Applied Research Corp., Model 222). The chopping speed can be continuously varied from 5 to 4800 Hz, and the wavelength of the output radiation can be continuously varied with the scanning monochromator. For experiments with cyclobutanone and cyclopentanone, an uv envelop filter (Corning CS-7-54) was inserted to purify the light output from the monchromator, since the grating was used in the second order. The exciting light was focused onto the cold sample window mounted at approximately 30° from the incident beam.

The luminescent image was collected by a thermoelectrically cooled photomultiplier tube (EMI 9558 QB, S-20 photocathode). The range of emission wavelengths observed was varied by using the proper Corning glass filters placed between the sample cell window and the photomultiplier tube. The signal from the photomultiplier tube was passed through a preamplifier (Princeton Applied Research, Type C Preamp) and then fed into a lock-in amplifier (PAR, Model HR-8) which provided a reference input signal for driving the light chopper. The output voltage was recorded on a strip chart recorder. When it was desireable to measure the lifetime (τ) of the emitting species, the phase shift angle (ϕ) was measured. The value of τ was then calculated from the observed value of ϕ from the relationship, $\tau = \tan \phi/2\pi f$, where f is the modulation frequency.[5] Of course, it was possible to differentiate the longer-lived phosphorescence emission signal from the shorter-lived fluorescence signal by varying the chopping frequency.

Results and Discussion

A. *Perfluorocyclobutanone (PFCB).* The electronic absorption spectrum (1-nm bandpass) and the luminescence excitation spectrum (f = 500 Hz and 0.05-nm bandpass of λ_{ex}) recorded with the matrix/reagent ratio, M/R = 100, at 20 K are shown in Figure 2. The low temperature matrix absorption spectrum shows larger ratios of peak-to-valleys than the room temperature gas absorption spectrum (see Figure 1 of ref 4a), presumably due to the disappearance of hot bands in the former. The energy interval of vibronic bands at 396.5, 376.0, 357.5, and 340.7 nm can be calculated as ~1380 cm^{-1} from Figure 1. It is most likely due to one quantum of the C=O stretch vibration in the $^1(n, \pi^*)$ state of PFCB. It should also be noted that the first peak at 396.5 nm in the matrix is ~150-cm^{-1} blue shifted from the gas spectrum.[4a]

The shape of the above luminescence excitation spectrum (viewing most of the blue green emission) is very similar to the shape of the absorption spectrum as expected. The relative emission quantum yields were evaluated at 5-nm interval between 325 and 405 nm from the observed values of absorption coefficient, "excitation" intensity due to emission, and intensity of the exciting light at each wavelength. For the sample shown in Figure 2, it was found to be constant within ±10% which is the precision of the measurement. Therefore, we conclude that the observed emission quantum yields are *constant* over the entire first electronic absorption band. As will be shown below, the emission is greatly dominated by phosphorescence and therefore we can be certain that the vibrational relaxation on the S_1 manifold is very complete before the relatively slow $S_1 \rightsquigarrow T_1$ intersystem crossing (the gas phase value of k_{ISC} is ~0.9×10^7 sec^{-1})[4a] takes place.

The lifetime of PFCB emission was determined by the phase-sensitive detection method, and it was found to increase from 0.072 msec at the modulation frequency (f) of 2.0 kHz to 2.0 msec at f = 260 Hz. Below 250 Hz, the lifetime is essentially independent of the modulation frequency as shown in Figure 3. This shows that the PFCB emissions originate from two excited states; at low values of f, the observed phase shift is mainly due to the long-lived component with $\tau_2 \simeq 2.1$ msec, but at high values of f, the short-lived component becomes more apparent. We believe the long-lived emission to be phosphorescence from the triplet state of PFCB. Since it was not possible to modulate at sufficiently high frequencies, the short-lived fluorescence lifetime (τ_1) which is expected to be ~0.1 μsec on the basis of the gas phase measurement[4a] was not determined in the present experiment. The emission intensity steadily increased as the modulation frequency decreased, but the photoluminescence excitation spectrum did not change its profile. In the gas phase, the quantum yield of fluorescence was found to be 0.02,[6] and no phosphorescence emission was observed;[6] however, from the low-lying vibrational states, $S_1 \rightsquigarrow T_1$ was found to be the chief relaxation channel available. Therefore, it is quite reasonable to think that the phosphorescence in the low temperature matrix could be at least an order of magnitude greater than the fluores-

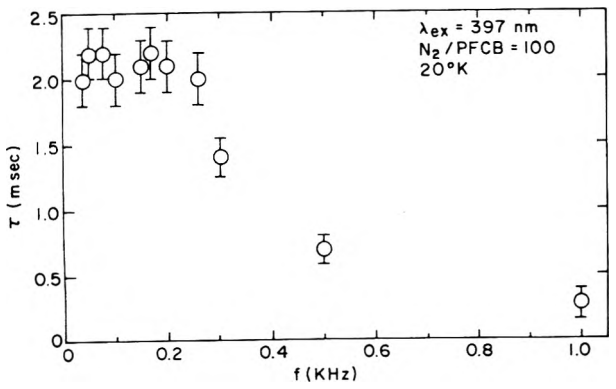

Figure 3. Variation of observed lifetime with modulation frequency.

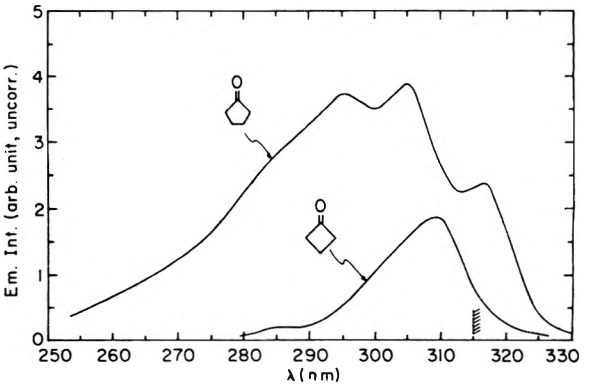

Figure 4. Photoluminescence excitation spectra (uncorrected for variation in spectral sensitivity) taken with N_2/CP = 50 and N_2/CB = 50 at 20 K; CP with Corning 3-73 and 5-60 and CB with Corning 3-72 and 5-60. The hatched line indicates the cutoff wavelength of fluorescence emission due to predissociation in the gas phase (ref 2c).

cence, although it was not possible to determine the ratio of phosphorescence to fluorescence in the present experiment.

The electronic relaxation behavior of PFCB(S_1) in the gas phase has been found to be very similar to that of hexafluoroacetone (HFA, S_1) in the gas phase;[4a,7] the values of k_F are 1.9×10^5 and 2.2×10^5 sec^{-1}, and the values of k_{ISC} are 9×10^6 and 12×10^6 sec^{-1}, respectively. The phosphorescence lifetime (τ_P) of HFA(T_1) in the gas phase has been found to be 6.7 msec at −78°C and 3.4 msec at 25°C, showing little temperature dependence below 0°C;[8] the phosphorescence quantum yield (Φ_P) at 25°C is 0.113, 6.1 times greater than the fluorescence quantum yield (Φ_F) of 0.0185.[8] Therefore, one can assign a value of $k_P = \Phi_P/\tau_P \simeq 33$ sec^{-1} for HFA(T_1). The value of k_P for acetone is $0.04/6 \times 10^{-4} \simeq 70$ sec^{-1}.[9] Therefore, the τ_P for PFCB(T_1) of 2.1 msec at 20 K is certainly reasonable in comparison; if we adopt a value of $k_P \simeq 33$ sec^{-1}, Φ_P can be estimated as $33 \times 0.0021 \approx 0.07$. In any case, if chemical decomposition takes place on the triplet manifold at all in the low temperature matrix, the rate is very slow, less than 5×10^2 sec^{-1}.

B. *Cyclopentanone (CP).* The photoluminescence excitation spectrum for cyclopentanone was taken mainly for calibration purposes in connection with the cyclobutanone experiment. The N_2/CP ratio of 50 was used at 20 K. A spectral bandpass of 0.03 nm was used for excitation, and the emission between 400 and 520 nm was observed through the combination of two filters, Corning 3-73 and 5-60. This set of filters eliminated the emission originating from the "matrix" alone (between 330 and 400 nm) as well as the near-uv part of the CP emission, and thus they eliminated the matrix excitation peaks around 314, 316, 326, and 330 nm. The spectrum taken at the modulation frequency of 100 Hz is shown in Figure 4 with no correction for the variation in spectral sensitivity. Relative quantum yields of emission between 310 and 260 nm are constant within ~20%, the accuracy of measurements. The absorption peaks at 316, 305, 295, and 285 nm give an interval of ~1150 cm^{-1}, corresponding to one quantum of the C=O stretching vibration in the $^1(n, \pi^*)$ excited state, which compares well with 1173 cm^{-1} for the C=O stretching vibration in the $^1(n, \pi^*)$ state of H_2CO.

The emission lifetime from CP was measured at λ_{ex} 305 nm with the phase shift technique as in the case of PFCB. Again, the observed lifetime increased with the decreasing value of the modulation frequency: 1.2 msec at f = 0.05, 0.08, or 0.10 kHz, 0.25 msec at 0.50 kHz, 0.17 msec at 1.0 kHz, and 0.03 msec at 2.0 kHz. Thus the lifetime of the long-lived state (τ_2) in the N_2 matrix at 20 K is ~1.2 msec due to phosphorescence. This value is in agreement with the phosphorescence lifetime of 1.1 msec observed in dilute EPA glass at 77 K.[10] All of the above results are consistent with a mechanism involving rapid vibrational relaxation (in the matrix) of the S_1 state over the entire singlet absorption band as compared to the gas phase results,[2c] subsequent electronic relaxation by efficient $S_1 \rightsquigarrow T_1$ intersystem crossing process, and production of a relatively unreactive triplet state of cyclopentanone. Presumably, the fluorescence decay time (τ_F) of CP in the N_2 matrix is similar to the value found in the gas phase, ~2.4 nsec, which is determined largely by the rate of the $S_1 \rightsquigarrow T_1$ process.[11] Although the absolute fluorescence emission quantum yield was not measured here, the fluorescence yield is very weak compared to the phosphorescence yield. The present result is quite consistent with the efficient vibrational deactivation observed with the $^1(n, \pi^*)$ state of cyclopentanone in cyclohexane solution at room temperature.[2b]

C. *Cyclobutanone (CB).* Measurement of the photoexcitation spectrum of cyclobutanone in solid N_2 or Ar was complicated by its weak emission intensity and the appearance of relatively intense matrix emission in the 320-nm region as described previously. The interference by this matrix emission was circumvented by using a set of Corning glass filters 3-73 with 5-60 as used for cyclopentanone or by using a set of Corning 3-72 with 5-60 which limited the emission detection region to 430~520 nm. The photoluminescence excitation spectrum taken with a N_2/CB ratio of 50 at 20 K, a spectral bandpass of 0.03 nm, and the modulation frequency of 2.0 kHz is shown in Figure 4 with that of CP. There was little change in the intensity and the phase angle with change in the modulation frequency down to 100 Hz, unlike in the cases of CP and PFCB. There was practically no phase shift indicating the absence of the long-lived emission component and the presence of weak fluorescence emission. The excitation spectrum is considerably narrow as has been observed in cyclohexane solution at room temperature,[2b] and it peaks near 309 nm. There is no vibrational structures in contrast to the gas phase.[2d] The quantum yield of emission in the matrix smoothly drops tenfold from 305 to 280 nm.

This result simply suggests that below 285 nm ($>5 \times 10^3$ cm^{-1} of excess vibrational energy) the vibrational relaxation on the $^1(n, \pi^*)$ manifold of CB in the N_2 matrix at 20 K is too slow to compete with the molecular predissociation process which could involve ring opening[2,12] as well as ring

expansion.[3] Since the fluorescence decay time (τ_F) of $CB(S_1)$ at low vibrational excitation energies is ~4.9 nsec in the gas phase,[2d] and since the molecular predissociation rate is faster than $1/\tau_F$ by ~2 orders of magnitude,[2d] the vibrational relaxation time in the N_2 matrix cannot be shorter than $\sim 10^{-11}$ sec. Furthermore, the absence of the phosphorescence component in the photoluminescence excitation spectrum near 310 nm suggests that *either* the vibrationally hot (guessed at ~3000 cm^{-1} for the energy gap between S_1 and T_1) triplet state which could be populated through the $S_1 \rightsquigarrow T_1$ intersystem crossing cannot be vibrationally relaxed rapidly enough or $CB(T_1)$ is very unstable. It is conceivable that $CB(T_1)$ has no minimum or very shallow minimum on the potential energy surface. Whether this is due to the matrix or not cannot be answered with the present data alone. Again, the rapid disappearance of $CB(T_1)$ may involve ring opening or ring expansion. In any case, it is clear that ring strain on cyclobutanone drastically modifies its excited state chemistry unlike in the case of perfluorocyclobutanone.

Chandler and Goodman[13] have reported the observation of polarized phosphorescence emission of CB in EPA glass at 77 K in the excitation wavelength range 250–320 nm. O'Sullivan and Testa[14] have recently reported the phosphorescence emission quantum yield of $\Phi_P = 0.003$ for CB in EPA glass at 77 K and λ_{ex} 285 nm, and also they observed $\Phi_P = 0.17$ for CP under the same condition. If we assume the latter value to be applicable to our phosphorescence lifetime data in the N_2 matrix at 10 K, we obtain $k_P = \Phi_P/\tau_P = 0.17/1.2 \times 10^{-3}$ sec $= 1.4 \times 10^2$ sec^{-1} for CP, which is comparable to the value of $k_P = 70$ sec^{-1} for acetone.[9] If we can further assume this value of k_P for CP to be valid for CB in the N_2 matrix, then the estimate of τ_P of CB can be obtained as $\Phi_P/k_P = 0.003/1.4 \times 10^2$ $sec^{-1} \simeq 2 \times 10^{-5}$ sec. The upper limit of the observed photoluminescence decay time of CB in the N_2 matrix can be set at 5×10^{-6} sec, on the basis of the observation that there was no phase angle shift in the modulation frequency range 5–4000 Hz. We believe that the fluorescence emission quantum yield for CB in the N_2 matrix should be close to 2×10^{-3} for near 310-nm excitation, and therefore we could have readily detected the phosphorescence emission with our phase-sensitive detector if it were present with a minimum value of $\Phi_P \simeq 0.001$. Therefore, we must conclude that the phosphorescence quantum yield of CB in solid N_2 at 20 K is less than 1×10^{-3}. Either the vibrational relaxation in the N_2 matrix must be considerably more inefficient than in EPA glass or the phosphorescence decay time and the excitation spectrum should be measured in EPA glass to verify the previously observed phosphorescence emission.[13,14]

Thomas and Guillory observed no photochemical products upon irradiating CB in the solid Ar, N_2, and CO matrices at 8–10 K with light above ~310 nm, but they observed CO and $c\text{-}C_3H_6$ with 302.2-nm light.[15] The observed lack of photoproduct at $\lambda_{ex} > 310$ nm[15] and the absence of phosphorescence in our work suggest that $CB(T_1)$ in the solid matrix at low temperature may isomerize but not dissociate at low photoexcitation energies to give CO and $c\text{-}C_3H_6$. Only at higher energies, it dissociate rapidly to give these products, due to inefficient vibrational relaxation in the solid matrix. Since the threshold for the formation of CH_2CO is ~290 nm[15] and it approximately coincides with the extinction of the fluorescence in the N_2 matrix in our experiment, the predissociation on the S_1 manifold should be responsible for ketene formation.

The experiments described above illustrate the failure of the low temperature matrix technique in arresting the very rapid molecular predissociation of $CB(S_1)$. However, the vibrational relaxation is in general fast enough, and therefore this technique could provide a means to extend the stability of electronically excited transient species and to study their behavior with regard to radiative and radiationless processes. The use of permanent gases as matrices simplifies the problem of avoiding reactive "solvent" impurities in general and probably circumvents exciplex formation in many cases. Replacement of the mechanical chopper with an electrooptical modulator should greatly extend the range of lifetimes one can study.

References and Notes

(1) This research has been supported by the National Science Foundation Grant No. GP 41407X.
(2) (a) N. E. Lee and E. K. C. Lee, *J. Chem. Phys.*, **50**, 2094 (1969); (b) J. C. Hemminger, C. F. Rusbult, and E. K. C. Lee, *J. Am. Chem. Soc.*, **93**, 1867 (1971); (c) R. G. Shortridge, Jr., C. F. Rusbult and E. K. C. Lee, *J. Am. Chem. Soc.*, **93**, 1863 (1971); (d) J. C. Hemminger and E. K. C. Lee, *J. Chem. Phys.*, **56**, 5284 (1972).
(3) (a) D. R. Morton, E. Lee-Ruff, R. M. Southam, and N. J. Turro, *J. Am. Chem. Soc.*, **92**, 4349 (1970); (b) G. Quinkert, P. Jacobs, and W.-D. Stohrer, *Angew. Chem., Int. Ed. Engl.*, **13**, 197 (1974); (c) G. Quinkert, K. H. Kaiser, and W.-D. Stohrer, *ibid.*, **13**, 198 (1974).
(4) (a) R. S. Lewis and E. K. C. Lee, *J. Chem. Phys.*, **61**, 3436 (1974); (b) *J. Phys. Chem.*, **79**, 179 (1975).
(5) (a) E. A. Bailey, Jr., and G. K. Rollefson, *J. Chem. Phys.*, **21**, 1315 (1953); (b) L. Brewer, C. G. James, R. G. Brewer, F. E. Stafford, R. A. Berg, and G. M. Rosenblatt, *Rev. Sci. Instrum.*, **33**, 1450 (1963).
(6) D. Phillips, *J. Phys. Chem.*, 70, 1235 (1966).
(7) A. M. Halpern and W. R. Ware, *J. Chem. Phys.*, **53**, 1969 (1970).
(8) A. Gandini and K. O. Kutschke, *Proc. R. Soc. London, Ser. A*, **306**, 511 (1968).
(9) E. H. Gilmore, G. E. Gibson, and D. S. McClure, *J. Chem. Phys.*, **20**, 829 (1952); **23**, 399 (1955).
(10) S. R. LaPaglia and B. C. Roquitte, *J. Phys. Chem.*, **66**, 1739 (1962).
(11) G. M. Breuer and E. K. C. Lee, *J. Phys. Chem.*, **75**, 389 (1971).
(12) (a) H. A. J. Carless and E. K. C. Lee, *J. Am. Chem. Soc.*, **94**, 1 (1972); (b) H. A. J. Carless, J. Metcalfe, and E. K. C. Lee, *ibid.*, **94**, 7221 (1972).
(13) W. D. Chandler and L. Goodman, *J. Mol. Spectrosc.*, **35**, 232 (1970).
(14) M. O'Sullivan and A. C. Testa, *J. Lumin.*, **10**, 123 (1975). Professor A. C. Testa has informed us subsequently in a private communication that the lower limit of phosphorescence detection in their experiment was Φ_P 0.003 and this value was reported.
(15) S. G. Thomas, Jr., and W. A. Guillory, *J. Phys. Chem.*, **78**, 1461 (1974).

Triboluminescence of Sugars

Jeffrey I. Zink,*[1a] Gordon E. Hardy, and James E. Sutton

Department of Chemistry,[1b] University of California, Los Angeles, California 90024 *(Received July 14, 1975)*

The triboluminescence of a variety of mono- and disaccharides including sucrose is luminescence from molecular nitrogen. The absence of triboluminescence from some saccharides is not a function of crystal size. The diminished intensity of triboluminescence excited in crystals under denitrogenated liquids in which they are insoluble is discussed.

The earliest record of triboluminescences (TL), the luminescence caused by the application of mechanical stress to crystals, is contained in the writings of Bacon[2] who observed that lumps of sugar emitted light when scraped. The triboluminescence of sugar was known to many other early writers including Boyle who observed that "hard sugar being nimbly scraped with a knife would afford a sparkling light".[2] He also observed that the luminescence still occurred when the sugar was scraped under vacuum.

In spite of the long history of the TL of sugar, the origin of the luminescence has never been determined. For organic crystals and some inorganic salts, the most common origins are crystal fluorescence[3] or phosphorescence.[4-7] The previously postulated[2] gas discharge origin is rarer. In some cases, room temperature TL can occur from crystals which are not photoluminescent at that temperature.[5] We have spectroscopically investigated the TL of mono- and oligosaccharides. We report here spectroscopic proof that the TL of saccharides originates from gas discharge and note general observations regarding the phenomenon.

Samples of D-glucose, lactose, maltose, L-rhamnose, and sucrose are triboluminescent while samples of cellobiose, fructose, fucose, galactose, and mannose are not. The TL spectrum of sucrose, a typical member of the triboluminescent sugars, is shown in Figure 1. All TL was excited by grinding the sample in a Pyrex vial with a stainless steel rod. The TL could also be excited by grinding the sample between any hard objects including glass, wood, plastic, and other metals. The spectra were obtained using the method previously reported.[6]

The spectrum shown in Figure 1 is that of the second positive group of molecular nitrogen.[9] As we have previously remarked,[8] an excitation energy of over 11 eV is necessary to excite N_2 from the ground state to the emitting $^3\pi_u$ state. The vibrational progression shown arises from the vibrational levels of the $^3\pi_g$ state of N_2.

In order to gain insight into the location of the emitting molecular nitrogen, we have measured the relative intensities of the TL of sucrose crystals in a variety of argon stripped solvents in which the sugar is insoluble. In all cases, the intensity of the TL excited under the liquid decreased compared to that excited in air. Typical decreases ranged from a minimum of 38% in benzene through 68% in chloroform to 100% in nujol. No correlation between the intensity and any bulk property of the liquid was found. The absence of a correlation may occur because the intensity is a sensitive function of the mechanical energy applied to the crystal. The lubrication properties of the solvent and/or the softening of the crystals due to solvent penetration could account for the decreased intensity. A sample of sucrose was vacuum degassed at 80° to remove nitrogen adsorbed in the crystals. No TL was observed when this sample was excited under argon stripped benzene. However, TL was observed when the degassed sample was excited in the atmosphere. From these observations, it is reasonable to conclude that ambient nitrogen gas is not necessary for the phenomenon to occur but that adsorbed or absorbed nitrogen is sufficient. The above experiments, combined with the insensitivity of the TL to the nature of the grinding implement, argue against the TL being caused by an electrical discharge between the crystal and the grinding implement. However, the detailed mechanism by which the high energy $^3\pi_u$ state of N_2 is populated is not yet known.

The TL spectra of all the triboluminescent saccharides studied are similar and are assigned to N_2 emission. The relative intensities of the TL from the various saccharides cannot be meaningfully compared because of the differences in the crystal sizes and the possible differences in their mechanical properties. In order to determine whether or not the apparent absence of TL from a given saccharide is caused by crystal size, we have examined both crystals and finely ground powders of representative samples of triboluminescent and nontriboluminescent saccharides. Weak TL could be visually observed in a dark room even from finely ground powders of the triboluminescent sugars,

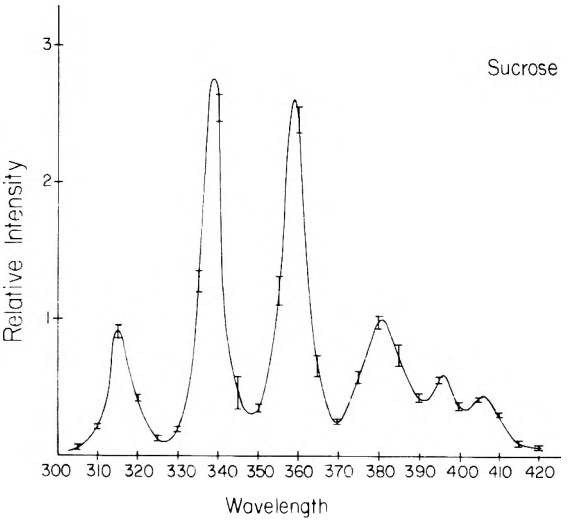

Figure 1. The triboluminescence spectrum of sucrose. The emission is from the second positive group of molecular nitrogen. The error bars represent the standard deviation of at least five separate measurements.

while no TL was observed from fructose, mannose, galactose, fucose, or cellobiose. Thus, the presence or absence of TL is probably a function of the crystal structure or the packing of molecules in a crystal and not solely a function of the size of a crystal.

We have observed similar behavior of the TL of *N*-acetylanthranilic acid and its derivatives. Minor changes of the substituents which barely affect the luminescence properties of the molecule prohibit the TL.[10] Work is in progress to determine the structural factors necessary for a crystal to be triboluminescent.

Acknowledgment. The Army Research Office, Durham, is gratefully acknowledged for support of this work.

References and Notes

(1) (a) Camille and Henry Dreyfus Teacher-Scholar, 1974–1979. (b) Contribution No. 3494.
(2) (a) F. Bacon, "Of the Advancement of Learning", 1605, G. W. Kitchin, Ed., J. M. Dent and Sons, London, 1915. (b) E. N. Harvey, "A History of Luminescence", American Philosophical Society, Philadelphia, Pa., 1957, Chapter 10.
(3) J. I. Zink and W. Klimt, *J. Am. Chem. Soc.*, **96**, 4690 (1974).
(4) J. I. Zink and W. C. Kaska, *J. Am. Chem. Soc.*, **95**, 7510 (1973).
(5) J. I. Zink, *J. Am. Chem. Soc.*, **96**, 6775 (1974).
(6) J. I. Zink, *Inorg. Chem.*, **14**, 555 (1975).
(7) C. R. Hurt, N. Mcavoy, S. Bjorklund, and N. Fillipescu, *Nature (London)*, **212**, 179 (1966).
(8) J. I. Zink, *Chem. Phys., Lett.*, **32**, 236 (1975).
(9) G. Herzberg, "Molecular Spectra and Molecular Structure. I Spectra of Diatomic Molecules", 2nd ed., Van Nostrand, New York, N.Y., 1950, p 32.
(10) W. C. Kaska, G. Hardy, and J. I. Zink, unpublished observations.

Effects of Sugar Solutions on the Activity Coefficients of Aromatic Amino Acids and Their *N*-Acetyl Ethyl Esters

T. S. Lakshmi and P. K. Nandi*

Protein Technology Discipline, Central Food Technological Research Institute, Mysore 570013, India *(Received May 14, 1975)*

Activity coefficients of *N*-acetyl ethyl esters of phenylalanine, tyrosine, and tryptophan have been determined in aqueous sucrose and glucose solutions. Similar measurements have been carried out with phenylalanine, tyrosine, and tryptophan in sucrose solution. The compounds show increased activity coefficients (decrease in solubility or *"sugaring out"*) in the solutions studied. The molar free energy of transfer, ΔF_{tr}, of these compounds from water to sugar solutions has positive values and indicates increased hydrophobicity in sugar solutions. The ΔF_{tr} value is found to remain unaltered over a considerable range of temperature. These observations have been utilized to explain the thermal stability of protein in aqueous sugar solutions.

Prevention of heat coagulation of ovalbumin in sucrose solution was recorded a long time back.[1] Similar observations of the stability of ovalbumin and serum proteins in sugar solutions have been reported.[2-4] Simpson and Kauzmann observed that the extent of ovalbumin denaturation in urea was reduced in presence of sucrose.[5] Gerlsma and Stuur observed that the melting temperature of both ribonuclease and lysozyme increases in sorbitol solution indicating their increased thermal stabilities in the solution.[6] Recently we have observed that the heat coagulation of α-globulin, the major protein component of sesame seed (*Sesamum indicum L.*) proteins, is prevented in sucrose and glucose solutions (unpublished work).

The manner in which sugar induces the increased heat stability of proteins or reduces the extent of denaturation by other reagents is not known. Studies during past few years have indicated how the groups which are mainly involved in the denaturation process of a protein molecule would behave in different solvent systems, e.g., simple electrolytes, urea, guanidine hydrochloride, and tetralkylammonium salt solutions.[7-10] This information was obtained from a study of the activity coefficients of model compounds which are representative of different groups in a protein molecule. In our previous studies we chose blocked amino acid ethyl esters, e.g., $CH_3CONHCH(R)COOC_2H_5$, R being a nonpolar side chain. Here we report measurements of the activity coefficient of the above compounds where R is phenylalanyl, tyrosyl, and tryptophanyl side groups in sucrose and glucose and also aromatic amino acids in sucrose solutions. The phenylalanyl derivative has also been studied in aqueous glycerol, ethylene glycol, and 1-butanol solutions. Temperature effect on the activity coefficient of the compounds has also been determined to obtain a better insight into the mechanism of sugar effects on model compounds and hence protein.

Experimental Section

Materials and Methods. *N*-Acetyl-L-phenylalanine ethyl ester (Sigma Chemical Co.), *N*-acetyl-L-tyrosine ethyl ester (Grade I, Cyclo Chemical Corp.), *N*-acetyl-L-tryptophan ethyl ester (Grade I, Cyclo Chemical Corp.), L-phenylalanine (BDH), L-tyrosine (E. Merck), and L-tryptophan (E. Merck) were used. Solubility phase curves for these compounds showed the absence of impurities. Sucrose and glucose were reagent grade chemicals. Fractions of ethylene glycol (E. Merck) and 1-butanol (E. Merck) distilling respectively at 115–117 and 194–196° were used; BDH glycerol was used. Glass distilled water was used.

The solutes were equilibrated with the solvents in 10-ml capacity tubes sealed with Teflon-lined screw caps. For the measurements at 28 ± 0.1 and 5 ± 1° the tubes were submerged in a water bath in a rotating rack, and mixing was accomplished by rotating tubes end-over-end at 35–40 rpm. The solubility measurements at 40 (±0.2°) and 55° (±0.3°) were carried out in an incubator shaker (New Brunswick Scientific Co., N.J.) at 180 oscillation/min. In general the period of equilibration was 5 days at 5°, 60 h at 28°, and 48 h at both 40 and 55°. The measurement at 65° with APE was carried out by shaking the solutions intermittently for 8 h. Equilibrated solutions were filtered at the temperatures of equilibration. Sampling of aliquots was also carried out near the equilibration temperature.

The concentration of the solutes was determined by measuring the absorbance of the solution, after proper dilution, at 257 nm for Phe and APE, 275 nm for Tyr and ATYE, and 278 nm for Try and ATRE in a Carl-Zeiss VSU-2 spectrophotometer.[31] Molar extinction values are APE 186 (lit. 188[9]), ATYE 1335, ATRE 5445, Phe 170 (lit. 190[11]), Tyr 1250 (lit. 1370[8]), and Try 5610 (lit. 5500[12]). The solubility values of APE in water at 5, 28, 40, 55 and 65° are 2.55, 4.13, 6.62, 8.04, and 17.1 g/l., respectively. The solubilities of ATYE at 5 and 28° are 1.40 and 3.48 g/l., respectively, values for ATRE at 5 and 28° are 0.52 and 1.47 g/l., respectively. At 28°, the solubilities of Phe, Tyr, and Try are 30.3, 0.579, and 11.0 g/l., respectively. Solubility values are reproducible within ~5%. We have assumed that this range of experimental error applies also to determinations in other solvents studied here.

Results

Activity coefficients of the solutes have been obtained from

$$f_i^s = C_i^0/C_i^s \quad (1)$$

where f_i^s is the activity coefficient of the solutes, i, in sugar or other solutions; C_i^0 and C_i^s are the molar concentrations of i in water and the sugar solutions, respectively. Activity coefficients of the solutes have been assumed to be unity in water.[13] The solubility values of the compounds in different solvents have been shown in Tables I and II.

Figure 1 shows a semilogarithmic plot of activity coefficient of APE as a function of sugar or alcohol concentration. The plots are nonlinear. In sugar solutions, the increase in the activity coefficient is observed. The increase becomes more pronounced at higher concentrations of sugars. Glycerol and glycol also increase the activity coefficients, but to a smaller extent compared to sugars. In contrast in 1-butanol the activity coefficient decreases. Figure 2 shows similar plots of activity coefficients of the compounds studied here in sucrose solution. At a constant sucrose concentration (>1 M particularly), the increase in the activity coefficient follows the order: ATYE > APE > ATRE, Try > Tyr, Phe. The same trend is observed for the esters in glucose solution. Analogous to salting out phenomenon, where the solubility decreases and correspondingly activity coefficient increases, the present observation of increased activity coefficient of the amino acids and esters can be considered as "sugaring out" phenomenon.

The relative effects of different solvents on the activity coefficient of the solutes can be obtained from an equation similar to Setchnow equation in electrolyte solution, viz., $\log f_i = K_s C_s$ where K_s is the value of f_i at 1 M sugar or alcohol concentration (C_s = 1). The plots are curved and there are not many data at lower concentrations (<1 M), through which the best straight line can be extrapolated to 1 M to give K_s value for its meaningful comparison in different solvents.

TABLE I: Values of the Solubility in g/l. of the *N*-Acetyl Aromatic Amino Acid Esters and Aromatic Amino Acids in Sucrose and Glucose Solutions at (28° C)

	Compound					
Concn, M	APE	ATYE	ATRE	Phenyl-alanine	Tyro-sine	Trypto-phan
Water	4.13	3.48	1.47	30.3	0.58	11.0
Sucrose						
0.25	3.88	3.20	1.43	28.78	0.56	10.20
0.5	3.59	2.96	1.35	27.87	0.54	9.68
1.0	2.89	2.33	1.17	25.45	0.50	8.36
1.5	2.31	1.74	0.99	23.33	0.46	7.15
2.0	1.57	1.15	0.83	21.21	0.42	6.05
Glucose						
0.25	3.82	3.27	1.43			
0.5	3.60	3.06	1.35			
1.0	3.22	2.64	1.25			
1.5	2.89	2.22	1.11			
2.0	2.56	1.93	0.99			

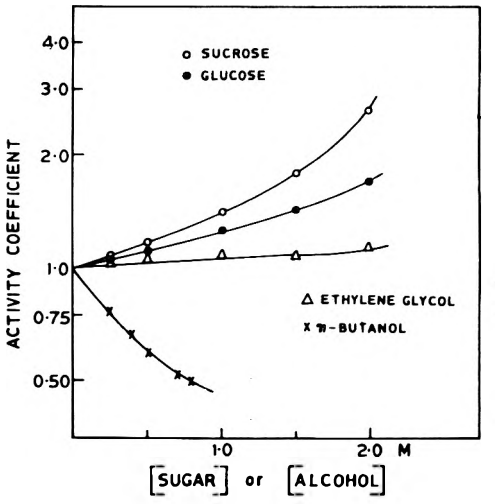

Figure 1. Effects of different solvents on the activity coefficients of acetyl phenylalanine ethyl ester at 28°.

Another method of comparison of the effect of solvents would be to compare the free energy of transfer, ΔF_{tr}, which can be calculated from the equation $\Delta F_{tr} = RT \ln f_i$ and represents the free energy of transfer of 1 mol of a given component, i, from water into the other solvents. The values of ΔF_{tr} from water to 1 and 2 M solvents have been reported in Table III. It can be seen from Table IV that for APE, which has been studied relatively thoroughly, a variation of 60° does not effect the value of positive ΔF_{tr} from water to glucose solution significantly. Similar constancy of ΔF_{tr} values for ATYE and ATRE are also observed, although the temperature range was less. Glucose solution was preferred for the study of temperature effects, as the viscosity of sucrose solution particularly at lower temperature was considerable.

Discussion

In native protein molecules the majority of the peptide groups (-(R)CH-CONH-) remains buried in its interior.[14] Under a denaturing condition, these groups from the inte-

TABLE II: Solubility Values in g/l. of *N*-Acetyl-L-phenyl Ethyl Ester in Glycerol, Ethylene Glycol, and 1-Butanol at 28°C

Glycerol, M					Ethylene glycol, M					1-Butanol, M				
0.25	0.5	1.0	1.5	2.0	0.25	0.5	1.0	1.5	2.0	0.25	0.4	0.5	0.7	0.8
4.05	3.92	3.84	3.76	3.68	4.06	3.92	3.84	3.72	3.63	5.37	6.60	7.02	7.85	8.26

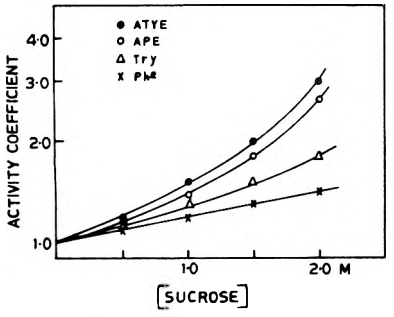

Figure 2. Effect of sucrose on the activity coefficients of acetyl tyrosine, acetyl phenylalanine ethyl esters, tryptophan, and phenylalanine at 28°.

rior of the protein would be exposed to the surrounding solvent with consequent increase in their concentrations (decrease in their activity coefficients). In a solvent system where the activity coefficient of these groups increases (decrease in their concentration), the protein would become more stable against denaturation in this solvent compared to the same process in water (or dilute aqueous buffer). This model of the stability of a protein molecule in solvents has been used previously.[7,9,10] In the present investigation the behavior of the compounds which can be considered to be as models for groups present in proteins has been studied in solvents which are known to increase the stability of protein against denaturation.

Considerable amount of information is available on the behavior of model compounds for different groups in protein in urea, guanidine hydrochloride, and electrolyte solutions to understand the mechanism of denaturation of proteins in these solutions.[7-10] The probable mechanism by which denaturation or its extent is prevented in sugar or polyhydroxy solutions is not known and no information at present is available about the behavior of peptide groups in these solutions. We have chosen the compounds $CH_3CONHCH(R)COOC_2H_5$ for this purpose. The combination of hydrocarbon side chain R and polar groups in these compounds might be considered to provide a model for the portion of the polypeptide chain present in protein. The compound where R is phenylalanine has been studied in detail. In addition, the amino acids phenylalanine, tyrosine, and tryptophan have been studied in sucrose solution.

The increase in the activity coefficient (Figures 1 and 2) and the corresponding positive ΔF_{tr} (Table III) show that esters find sugar solutions unfavorable compared to water. Similarly sucrose solution is unfavorable for the amino acids. The decreased solubility of the esters and amino acids in sugar solutions indicates that the presence of sugar induces more hydrophobicity. It is known that the tryptophanyl group is the most hydrophobic group of proteins followed by the tyrosyl and phenylalanine group.[5] In sucrose solution, tryptophan is most hydrophobic whereas the hydrophobicity of Tyr and Phe are similar. However, the positive ΔF_{tr} in the ester series is maximum for ATYE followed by APE and ATRE (see the Mechanism section). The critical micelle concentration (cmc) value of a nonionic detergent Triton X-100, the micelle of which is formed by

TABLE III: Values of Free Energy of Transfer, ΔF_{tr} cal/mol, for the Transfer of the Solutes from Water to Different Solvents at 28°C[a]

Compound	Sucrose		Glucose	
	1 M	2 M	1 M	2 M
APE[b]	205	580	140	290
ATYE	250	660	150	370
ATRE	125	305	110	260
Phenylalanine	110	200		
Tyrosine	95	190		
Tryptophan	150	360		

[a] ΔF_{tr} has been defined in the text. [b] Values of ΔF_{tr} in 2 M glycerol and ethylene glycol are 70 and 85 cal/mol, respectively; the ΔF_{tr} value is −415 cal/mol in 0.8 M 1-butanol. Values have been rounded to the nearest 5.

TABLE IV: Effect of Temperature on the ΔF_{tr} Values for the Transfer of Different Esters from Water to 1 M Glucose Solution[a]

Compd	Temp, °C				
	5	28	40	55	65
APE	130	140	185	150	185
ATYE	165	150			
ATRE	150	110			

[a] Values are in cal/mol.

the aggregation of its nonpolar moieties in water, can be found to reduce from 0.2 mg/ml in water to ~0.14 and 0.1 mg/ml in 1 and 2 M sucrose solution, respectively.[16] This can be considered as increase in the hydrophobic interaction between nonpolar moieties in sucrose solution. Prakash and Nandi from the increased retention of the above esters and amino acids in electrolyte solution compared to water in Sephadex LH-20 gel concluded that the hydrophobicity increases in electrolyte solution.[17] Lakshmi and Nandi (*J. Chromatogr.*, in press) also observed increased retention of the esters in the Sephadex LH-20 gel in sugar solutions which indicated the increased hydrophobicity in these solutions.

Mechanism of the Sugar Effect. The increase in the activity coefficient of the solutes studied here cannot be explained as arising from the change in the dielectric constant of the sugar solutions since (~2 M) glucose and sucrose decrease the dielectric constant of the solvent to the same extent[18] (42 and 40, respectively, from 80 of pure water) although the activity coefficients of the esters are observed to be considerably larger in sucrose solutions. Further, though 1-butanol, ethylene glycol, and glycerol reduce the dielectric constant of the medium, considerable decrease in the activity coefficient of APE is observed in 1-butanol in contrast to increase, albeit to a small extent, of the activity coefficient in the other two solvents. Nozaki and Tanford[19] observed that the solubility of tryptophan increases in aqueous ethylene glycol which also indicates that the dielectric constant does not play an important role on the observed activity coefficient behavior.

The decrease in the solubility of the solutes in sugar solution is not caused by the reduced water activity in the

system due to the presence of sugar, since the solubilities of amino acids which depend upon solvation by water should have reduced by a larger extent than the ester molecules. In addition the increase in the solubility of adenine and no change in the solubility of thymine in sucrose and glucose solutions (unpublished work) cannot be explained as arising from the reduced water activity in sugar solution. Walrafen[20] from Raman spectral measurements observed that sucrose induces structure in aqueous solution a conclusion which has been questioned recently by James and Frost[21] who from the study of the librational band of water in sucrose concluded that intermolecular water–water interactions appear to be similar to intermolecular water–sucrose interaction. Taylor and Rowlinson[22] from the calorimetric measurements of aqueous glucose and sucrose solutions concluded that strong hydrogen bonding exists between sugars and surrounding water molecules, which is stronger than the hydrogen bonding between water molecule themselves. Calorimetric results being more reliable will be utilized to explain the present observation. Since sugar–water hydrogen bonds are stronger than water–water hydrogen bonds, placement of the same molecule would require more work in sugar solution than in water which explains the positive ΔF_{tr} values for the transfer of the solutes from water to sugar solutions. The placement of the ester molecules would require breaking up of stronger sugar–water combination which can probably explain the small positive ΔF_{tr} observed here (see Results). The corresponding positive entropy change due to the freeing of water and sugar molecules would probably be neutralized by the decrease in the entropy of the system caused by the restriction of the solvent, particularly water molecules, around the nonpolar groups. The above explanation based on cavity formation theory of Sinanoglu and Abdulnur[23] however, depends on the surface tension of the solvent. Glucose and sucrose do not appreciably change the surface tension of water (the change is within 1–2 dyn cm^{-1} for 1 M solutions[18,24]). Instances are, however, known where hydrophobic effects arising from the ordering of solvent molecules around the solutes dominate the surface tension effect.[25]

The reduced unfavorable ΔF_{tr} for ATRE compared to ATYE and APE may arise from some favorable interaction between (by hydrogen bond) heterocyclic moiety and sugar molecules which is not possible with Try due to the presence of charge groups.

The foregoing discussion of sugar effect, albeit to a reduced extent, would be applicable to the polyhydric alcohols, e.g., glycol and glycerol.

Application of the Observed Effects to Protein. The present result with model compound shows that sugar molecules and probably polyalcohols also would introduce more hydrophobicity in aqueous solution. This would result in a solvent system where the already exposed peptide attached with nonpolar groups in the native protein molecule would have a tendency to enter into the protein interior due to unfavorable environment produced by sugar molecules. Similar groups in the interior of the protein would find an even more unfavorable environment in sugar solution than water on their exposure. This would result in more stability of a protein molecule in these solvents and would reduce the extent of denaturation of protein molecule induced thermally or by other denaturing agents. Clement-Metral and Yon concluded that the conformational change resulting in increased stabilization of β-lactoglobulin A is responsible for their observed inhibition of tryptic hydrolysis of the protein in sucrose solution.[26]

The CH groups in the sugar or polyalcohols may have some favorable interaction with the nonpolar groups in the protein, but this would be suppressed by the unfavorable effect described above.[27] Alcohols, in which the proportion of nonpolar groups are more than OH groups, e.g., in 1-butanol, by favorable hydrophobic interaction with the nonpolar groups would destabilize the protein leading to its denaturation.

The foregoing discussions may have some consequences on the perturbation spectrum of proteins in sugar and polyalcohol solutions. It is generally considered that these solutions perturb the spectrum of protein by effects other than any conformational changes in them although a few instances to the contrary are known.[28–30] The present result of the unfavorable interaction between sugar solution and aromatic chromophores indicates that the groups which are fully or partially exposed to water, may get partially or completely buried in the protein interior. The change of the environment of the chromophores from the high dielectric constant of water to the protein interior of low dielectric constant (that of ethanol) may induce spectral red shift which is generally attributed as arising from the change of the polarizability of the chromophores in the presence of perturbing molecules. The above possibility is only suggestive and by no means a conclusive one.

References and Notes

(1) A. Beilinsson, *Biochem. Z.*, **213**, 399 (1929).
(2) C. D. Ball, D. T. Hardt, and W. J. Duddles, *J. Biol. Chem.*, **151**, 163 (1943).
(3) C. R. Hardt, I. F. Huddelson, and C. D. Ball, *J. Biol. Chem.*, **163**, 211 (1946).
(4) M. Kerues, *Biochim (Rumania)*, **6**, 245 (1963).
(5) R. B. Simpson and W. Kauzmann, *J. Am. Chem. Soc.*, **75**, 5139 (1953).
(6) S. Y. Gerlsma and E. R. Stuur, *Int. J. Peptide Protein Res.*, **4**, 377 (1972).
(7) D. R. Robinson and W. P. Jencks, *J. Am. Chem. Soc.*, **87**, 2462, 2470, (1965).
(8) Y. Nozaki and C. Tanford, *J. Biol. Chem.*, **238**, 4075, (1963); **245**, **1648** (1970).
(9) P. K. Nandi and D. R. Robinson, *Fed. Proc.*, **30**, 1107 (1971); *J. Am. Chem. Soc.*, **94**, 1299, 1308 (1972).
(10) P. K. Nandi, *J. Phys. Chem.*, **78**, 1197 (1974).
(11) J. A. Schellman and C. Schellman in "The Proteins", Vol. II, H. Neurath, Ed., Academic Press, New York, N.Y., 1964, p 54.
(12) P. Elodi and S. Lakatos, *Eur. J. Biochem.*, **36**, 45 (1973).
(13) F. A. Long and W. F. McDevit, *Chem. Rev.*, **51**, 119 (1952).
(14) C. Tanford, *Adv. Protein Chem.*, **23**, 121 (1968).
(15) C. Tanford, *Adv. Protein Chem.*, **24**, 1 (1970).
(16) W. B. Gratzer and G. H. Bevan, *J. Phys. Chem.*, **73**, 2270 (1969).
(17) V. Prakash and P. K. Nandi, *J. Chromatog.*, **106**, 23 (1975).
(18) "International Critical Tables", McGraw-Hill, New York, N.Y.: Vol. 6, p 101, 1929; Vol. 4, p 470, 1928.
(19) Y. Nozaki and C. Tanford, *J. Biol. Chem.*, **246**, 2211 (1971).
(20) G. E. Walrafen, *J. Chem. Phys.*, **44**, 3726 (1966).
(21) D. W. James and R. L. Frost, *J. Phys. Chem.*, **78**, 1754 (1974).
(22) J. B. Taylor and J. S. Rowlinson, *Trans. Faraday Soc.*, **51**, 1183 (1955).
(23) O. Sinanoğlu and S. Abdulnur, *Fed. Proc.*, **24**, 5 (1965).
(24) S. Lewin, "Displacement of Water and Its Control of Biochemical Reactions", Academic Press, New York, N.Y., 1974, p 207.
(25) D. M. Crothers and D. I. Ratner, *Biochemistry*, **7**, 1823 (1968).
(26) J. Clement-Metral and J. Yon, *Biochim. Biophys Acta*, **160**, 340 (1968).
(27) B. S. Harrap, *Int. J. Peptide Protein Res.*, **1**, 245 (1969).
(28) M. Laskowski, Jr., *Fed. Proc.*, **25**, 20 (1966).
(29) M. J. Cronan and F. M. Robins in "Fine Structure of Proteins and Nucleic Acids", G. D. Fasman and S. N. Timasheff, Ed., Marcel Dekker, New York, N.Y., 1970, p 271.
(30) J. S. Meyer and W. B. Jakoby, *J. Biol. Chem.*, **250**, 3785 (1975).
(31) Abbreviations used are *N*-acetyl-L-phenylalanine ethyl ester (APE), *N*-acetyl-L-tyrosine ethyl ester (ATYE), *N*-acetyl-L-tryptophan ethyl ester (ATRE), L-phenylalanine (Phe), L-tyrosine, (Tyr), and L-tryptophan (Try).

A Method for Rapid Measurement of Particle Size and Relative Number Density of Particles in Suspension. I[1]

N. Ben-Yosef, O. Ginio, D. Mahlab, A. Weitz,

Division of Applied Physics, The School of Applied Science and Technology, The Hebrew University of Jerusalem, Jerusalem, Israel

and S. Sarig*

Casali Institute of Applied Chemistry, The School of Applied Science and Technology, The Hebrew University of Jerusalem, Jerusalem, Israel *(Received March 20, 1975; Revised Manuscript Received October 8, 1975)*

Publication costs assisted by the Casali Institute of Applied Chemistry

It is shown that by using a multifilter spectrum analyzer one can obtain, by means of light beating spectroscopy techniques, the time evolution of average size and number density of the scatterers. The time evolution is obtained at a rate of 1 min^{-1}. By numerical calculation it is shown that even when the scatterers are not monodisperse the spectrum can be used to calculate the average size with satisfactory accuracy.

Introduction

In order to test the nucleation process of strontium sulfate in a saturated solution in the presence of a small amount of a polymer which retards the precipitation, there was a need to measure the time evolution of the size distribution of the microcrystals.[1]

Size measurement of microscopic particles in solution can be measured by light beating spectroscopy. This powerful tool was employed in the present case after certain modifications, due to the experimental requirements, were introduced. The aim of the present communication is to show the experimental system and the data interpretation process by which the time evolution of the average size and number density of the microcrystals was measured at a rate of 1 min^{-1}.

Measurement of the size of microscopic particles in solution by the measurement of the scattered light spectrum is an accepted and well tried method.[2] Briefly, the optical spectrum of coherent light scattered by spherical particles of size r is given by

$$I(\omega) = \pi^{-1} N |A(r)|^2 \frac{Dq^2}{(\omega - \omega_0)^2 + (Dq^2)^2} \qquad (1)$$

Where N is the number density of the scatterers, $A(r)$ is the scattering amplitude, D the diffusion coefficient, and q the scattering vector

$$q = \frac{4\pi n_0}{\lambda} \sin(\tfrac{1}{2}\theta)$$

where n_0 is the refractive index of the solvent, λ the wavelength, θ the scattering angle, and ω_0 the light frequency. The measured quantity in light beating spectroscopy is the power spectrum obtained from the optical spectrum by convoluting $I(\omega)$ with itself. Particle size is derived from measurement of the diffusion coefficient which is size dependent. In the present case, the aim is to measure the time evolution of the size distribution of microcrystals growing in the solution. This requirement imposes two difficulties: (a) fast measurement, since the sample evolves with time the spectrum has to be measured faster than any time constant related to the time evolution; (b) data interpretation, as the microcrystals are not necessarily monodisperse, the spectrum obtained may not be a simple Lorentzian so that the size is not simply related to the spectral shape.

Experimental Section

These problems were partially solved in the system to be described. The optical part of the spectrometer used is similar to those already reported in the literature.[3] The laser used was a Spectra-physics Model 124A He–Ne laser, while the photomultiplier used was the RCA 7265 model.

For a stationary sample the easiest way of measuring the photomultiplier current power spectra is to use a spectrum analyzer, as reported in ref 4. For a time-evolving sample this approach is unacceptable because the time of measurement needed is too long. The time of measurement has to be taken into account due to the signal-to-noise ratio of the final signal. As has been shown,[2] this ratio depends on the square root of the time of measurement at a fixed frequency. In the case of swept frequency, the sweep rate has to be slow enough; in practical cases, the total time of measurement is about 20 min.

In the present case, the rate of the time evolution of the sample was such that the spectrum had to be obtained in a time of 1 min. For this purpose a multifilter spectrum analyzer (MFSA) was designed and built. The MFSA is composed of eleven parallel channels, one of them monitors the d.c. component of the photomultiplier output, whereas the other ten are composed of active band pass filters having different central frequency but equal transmission curves. The output of each filter is rectified and integrated, so that the output is composed of eleven capacitors whose potential is proportional to the rms value at the band passed by the respective filters. Each a.c. channel has a width of 10 Hz, and the time constant of each integrating circuit is such that for 1 min integration the capacitor potential is more than 95% of its maximum value. At the end of the measuring time (1 min) the voltage of the capacitors is relayed through a multiplexer to a recorder; after the recording, each memory is shortened and a new measuring sequence starts. In the present system, the frequency range covered starts at 15 Hz with a 30-Hz step to 285 Hz. Using this system, the power spectra of a time-evolving sample can be obtained, provided the rate of change of the sample is not faster than 1 min.

The output of the MFSA includes the power spectra as well as the shot noise level using the d.c. channel data. For single size scatterers, the data interpretation is straight forward; the signal is processed as a Lorentzian, its half-width found, and the particle size calculated. The system was checked and calibrated using commercially available polystryrene latex spheres of known size; the size and their monodispersivity were checked and measured using a scanning electron microscope. The results show 5% accuracy (in particle size).

Data Interpretation

When the scatterers are size distributed the relation between the power spectrum and size distribution is more complex. If the size distribution is given by $dN = G(r)\,dr$, i.e., at size $r + dr$ there are dN particles, the optical spectrum is:

$$I(\omega) = \frac{1}{\pi}\int_0^\infty \frac{G(r)\,|A(r)|^2 D(r)q^2}{(\omega-\omega_0)^2 + [D(r)q^2]^2}\,dr \qquad (2)$$

the power spectrum is the convulution of $I(\omega)$ with itself, and the zero frequency centered result is

$$P(\omega) = \frac{1}{\pi^2}\int\int_0^\infty \frac{G(r)\,G(x)\,|A(r)|^2|A(x)|^2 D(r)D(x)q^4}{\omega^2 + q^4[D(r)+D(x)]^2}\,dr\,dx \qquad (3)$$

In the integral q is given as before, $D(r)$ is the diffusion coefficient given by $kT/6\pi\eta r$, where T is the solution temperature, η the solvent viscosity, and r the particle radius. $A(r)$ is the scattering amplitude which depends on size, refractive index of particle and solvent, wavelength, and scattering angle.[5] The integral equation relating between the size distribution function $G(r)$ and the power spectra $P(\omega)$ is not easily inverted and it seems that no unique solution exists. Nevertheless, some approximation of the average size of the scatterers can be obtained from numerical calculations of eq 2 starting with an assumed size distribution.

To check the accuracy of a monodisperse approximation for size distributed scatterers, numerical calculations of eq 2 and 3 were performed. Assuming that the scatterers are size distributed according to the log-normal distribution, i.e.

$$G(r) = \frac{1}{2r}\exp\left\{-\frac{1}{\beta}\ln\left(\frac{2r}{\alpha}\right)^2\right\} \qquad (4)$$

Using the calculated values of $A(r)$ one calculates the optical spectra using eq 2, and by numerical convolution the power spectra are obtained.

The best single Lorentzian is fitted to that function, i.e., data of size distributed particles are analyzed as if due to monodisperse particles. From the best fit obtained one calculates the particle size, which can be compared to the average size with which the calculation was started.

In Table I the results of such a comparison are shown. The first column represents the average diameter used in eq 4, the second column is the size distribution width (30% of the average size in all cases), whereas the third column gives the diameter calculated from the power spectra which were analyzed as if it is due to monosize particles, as previously described. One observes that the original average size and the calculated size do not differ by more than 15% in the size range of (0.2–1.0) μm for a distribution of appreciable width. As shown in Figure 1, the scatterers in the present case do not possess a wide distribution so that one can calculate that the measured spectra can be analyzed as

TABLE I:[a]

Av diameter, μ	Half-width, μ	Calcd diameter, μ	Rel. error, %
0.200	0.060	0.228	14
0.400	0.120	0.446	11
0.600	0.180	0.631	5
0.800	0.240	0.825	3
1.000	0.300	1.067	0.7

[a] The calculation was performed on ideal spherical particles, size distributed according to eq 4, with parameters as stated in the table. The refractive index used in the calculation of the scattering amplitude was $n = 1.5983$, the refractive index of bulk strontium sulfate. The particles were assumed to be suspended in water, $n = 1.333$.

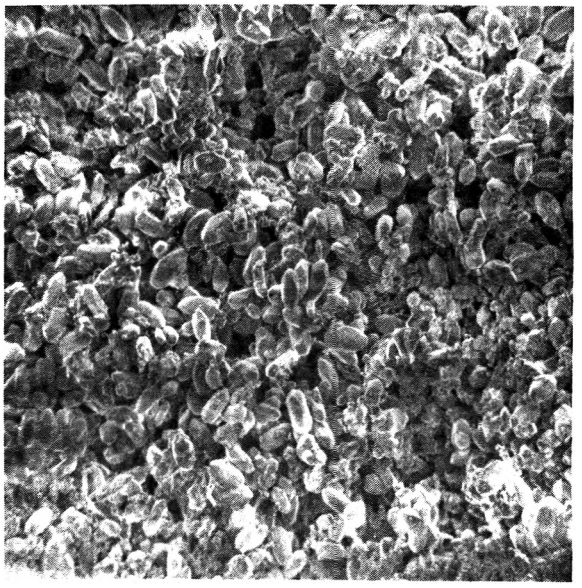

Figure 1. Scanning electron microscope photograph of the final strontium sulfate microcrystals. Note that the size distribution is narrow.

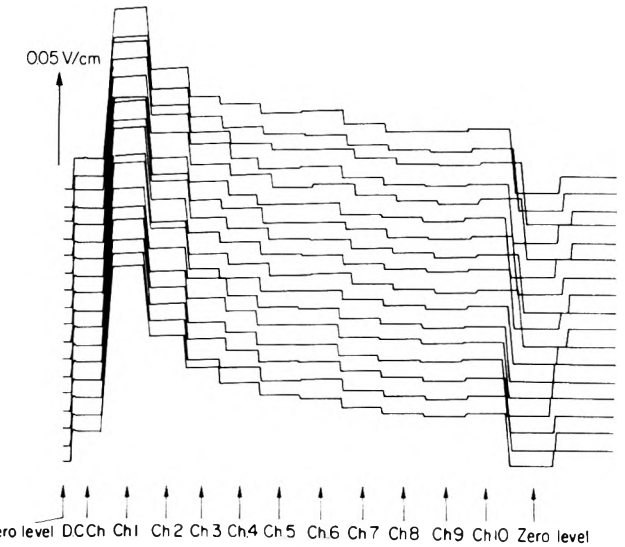

Figure 2. Recording of the MFSA output at intervals of 1 min. Each recording is shifted upward by a fixed amount.

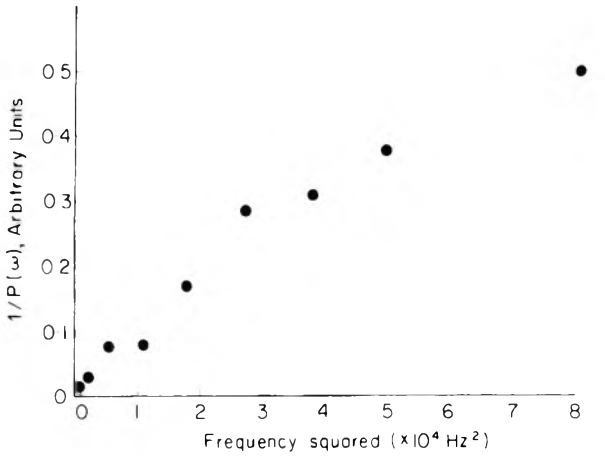

Figure 3. Graphical representation of the reciprocal of the power spectrum vs. the square of frequency. Note the near linearity.

if due to monodisperse scatterers and the calculated size represents the average size within the limits of 20%.

Data Analysis

As described, the scattered light spectrum was obtained from the MFSA on a recorder. A set of consecutive measurements recorded in this way is shown in Figure 2. each recording is further analyzed as a Lorentzian. The recorded data are the square root of the power spectra and the shot noise. The level of the shot noise is known from the d.c. level.

Using these data, one writes the power spectra $P(\omega)$ as follows:

$$P(\omega) = S(\omega)^2 - N(\omega)^2 \tag{5}$$

where $S(\omega)$ is the recorded signal and $N(\omega)$ the shot noise (slightly dependent on frequency due to the system transfer characteristics). Since $P(\omega)$ is a Lorentzian, one designs Δ as its half-width and obtains

$$\frac{1}{P(\omega)} = \frac{1}{B}\omega^2 + \frac{\Delta^2}{B} \tag{6}$$

where B is a constant. By graphical analysis of $1/P(\omega)$ (measured quantity, eq 5) as a function of ω^2 one obtains Δ. Since $\Delta = 2Dq^2$ (eq 3) and q is known, one calculates D and from it the size r. Furthermore, the nonlinearity of the data is an indicator of the distribution width of the scatterers.

Relative Number Density Measurement

By integrating eq 1 over all the frequencies one obtains the total light intensity scattered. It is observed that this intensity is proportional to $N|A(r)|^2$. To obtain the absolute light intensity one has to consider the geometry of the experiment as well. For an experiment, such as discussed previously, where the number density and average size change with time, the relative number density of the scatterers can be calculated from this relation.

The total light scattered into the photomultiplier is proportional to the d.c. current. Using the previous proportionality one can write

$$I(t) = KN|A(r)|^2$$

where $I(t)$ is the measured current, K an unknown constant, N the number density of the scatterers, and $A(r)$ the scattering amplitude. As described previously, r is obtained experimentally, and $A(r)$ can be calculated. $I(t)$ is measured directly, so that KN can be calculated as a function of time, to obtain the relative number density of the scatterers.

Conclusion

It has been shown that by using the MFSA one can obtain the time evolution of the scattered light. For the case under discussion, where the size distribution width does not exceed 30% of the average size, one can analyze the data as if it is due to monodisperse particles. Using this approximation one obtains the average size and the relative number density of the scatterers as a function of time.

The time evolution of the average size and number density of the evolving microcrystals in a retarded precipitation of saturated strontium sulfate solution are summerized and discussed in the second part of this article.[1]

References and Notes

(1) The second part of this article is entitled A Mechanism for Retarded Precipitation Based on the Time Evolution of Particle Size and Relative Number Density, S. Sarig and O. Ginio, *J. Phys. Chem.*, following article in this issue.
(2) H. Z. Cummins and H. L. Swinney, "Progress in Optics", Vol. VIII, E. Wolf, Ed., North Holland Publishing Co., Amsterdam, 1970.
(3) S. B. Dubin, J. M. Lunaceck, and G. B. Benedeck, *Proc. Natl. Acad. Sci., USA*, **57**, 1164 (1967).
(4) N. Ben-Yosef, S. Zweigenbaum, and A. Weitz, *Appl Phys. Lett.*, **21**, 436 (1972).
(5) M. Kerker, "The Scattering of Light", Academic Press, New York, N.Y., 1969.

A Mechanism for Retarded Precipitation Based on the Time Evolution of Particle Size and Relative Number Density. II[1]

Sara Sarig* and Ofra Ginio

Casali Institute of Applied Chemistry, The Hebrew University of Jerusalem, Jerusalem, Israel *(Received March 20, 1975; Revised Manuscript Received October 8, 1975)*

Publication costs assisted by the Casali Institute of Applied Chemistry

The time evolution of the diameters of strontium sulfate particles, during the process of precipitation, was determined by light scattering technique. A multifilter spectrum analyzer for use on the usual apparatus for light beating spectroscopy was designed which reduced the time required for a single measurement to 1 min. The solutions employed contained admixtures of poly(vinyl sulfonate) at low concentrations. The results are explained by a mechanism of strontium sulfate heterogeneous nucleation on the poly(vinyl sulfonate) macromolecules, which act as microsubstrates.

Introduction

The precipitation of sparingly soluble salts at high supersaturation may be significantly retarded by an admixture of polyelectrolytes at extremely low concentrations. Although this phenomenon is important in industrial and biological systems, the mechanisms of retardation are not well understood. For instance, desalination plants of sea water are designed for operation in economically non-optimal scale-free conditions, because the commercial scale retardants are not effective enough for scale prevention at the technologically sound concentration–temperature regions. The screening for the most suitable additives is mostly carried out by an empirical approach because investigators are unable to predict the effectiveness of a substance on the basis of first principles. The mechanisms of retardation of kidney and gall stones formation and the overly effective inhibition of crystal growth as in certain bone diseases also belong to the class of phenomena, the mechanisms of which should be elucidated.

In this study, we present new experimental data about the time evolution of the size and relative number density of particles in a system of sparingly soluble salt–low molecular weight soluble polymer. The size measurement of microscopic particles in suspension can be performed by light beating spectroscopy, after certain modifications of the standard equipment, in accordance with the experimental requirements, have been introduced.

The mechanism of retarded precipitation must deal with crystallization processes in which both nucleation and growth are occurring. No comprehensive nucleation theory exists which takes the supersaturated solution as a starting point, as the mathematical difficulties encountered in such systems seem now to be insurmountable. The nucleation rates in solutions can be computed by the equations postulated for vapor phase nucleation with appropriate corrections. That is, they could be, if the nucleation process in solution were, as a rule, homogeneous. In practice, however, nucleation in solution is in most cases heterogeneous, except at artificial conditions of rapid mixing, and therefore additional corrections for the foreign substance on which the nucleus is formed must be introduced.

The models for heterogeneous nucleation in solutions deal with substrates which are, on an atomic scale, of infinite dimensions. They usually include walls of the reactor, macroscopic dust particles or foreign substances such as mica, sillicates, sparingly soluble carbonates, sulfates, etc. Turnbull and Vonnegut[2] assume a modification to energy barrier of nucleation due to the internal distortions in the nucleus, which are caused by the mismatch between the lattices of the substrate and the nucleus. Upreti and Walton[3] argue that it is not certain that ions upon joining a nucleus are already completely desolvated. Hence the nucleus is unlikely to possess macroscopic properties such as elastic modulus, surface energy, or even a normal crystal lattice. Their model is also based on the assumption of an infinitely large substrate. The systematic experimental studies of heterogeneous nucleation were carried out, almost exclusively, on substrates with well-developed, and preferably perfect, faces.

Nevertheless, no crystal surface can be perfect on the atomic scale, and photomicrographs of crystals grown on substrates show that only certain sites on the surface of a substrate are used for nucleation. Nucleation would presumably also occur if those sites were separated from the bulk and isolated from each other, provided they retained their special structural properties. It follows that very small, active fragments of matter could be prepared which would have the required degree of matching with the crystal lattice, on which heterogeneous nucleation could take place. In this study soluble polymers were used for this purpose. They have a distinct advantage over active sites on a bulk substrate, because their number can be known.

It was ascertained that the polymer actively participated in the crystallization process of the sparingly soluble salt, retarding precipitation and modifying the crystal habit,[4] while its monomer was almost inactive.[5]

In order to investigate the system "solution–salt particles", which presumably have nucleated by a heterogeneous process on polymeric molecules, a light scattering method was employed. Diameters of the particles and their relative numbers were calculated and changes in these parameters were observed at 1-min intervals for a period of about 1 hr.

Experimental Section

Materials. The crystallizing salt employed was strontium sulfate obtained by mixing clear, 0.2-μm millipore filtered solutions of strontium chloride and sodium sulfate.

The polymer used was poly(vinyl sulfonate), which has a sulfonic group at every alternating carbon. The average molecular weight of a macromolecule was 17 000 corresponding to about 300 carbon atoms in a chain. The employed concentrations were 10 and 20 ppm corresponding to 5.8×10^{-7} and 1.17×10^{-6} M concentrations, respectively.

Preparations of Solutions. The clear solutions of strontium chloride and of sodium sulfate, the latter premixed with the polymer solution, were placed in two separate arms of a three-armed container, shaped like an inverted Y.[6] The beginning of the crystallization process was marked when the solutions were mixed and transferred into an optical cell. The optical cell was introduced into a light scattering apparatus which is described elsewhere.[1]

Results and Discussion

The concentrations of strontium sulfate solutions employed in this study were 0.0156 and 0.0168 M which correspond to 18- and 19-fold supersaturation ratios, respectively. These supersaturations are sufficient to induce the precipitation of the solute excess in about 1 min, to be followed by a quick sedimentation. Poly(vinyl sulfonate), like certain other polyelectrolytes, stabilizes these supersaturated solutions; in their presence the precipitate forms very slowly and for a prolonged period of time no sedimentation is detected.[5,6] The effect is fairly specific, but when it exists, the higher the concentration of the additive, the longer the induction period. The concentrations of poly(vinyl sulfonate), 10 and 20 ppm, were selected for their mutual compatibility with the above-mentioned strontium sulfate concentrations to fulfill several conditions which are almost contradictory to each other, but which are required for this type of investigation. The particles of strontium sulfate had to be large enough to be detectable by the available equipment of light scattering, but small enough to remain suspended in the solution for a length of time sufficient for observation. It was desirable to follow the process of growth, i.e., changes in the values of the diameters; but the changes had to be slow enough to permit spectrum analysis of the scattered light at essentially stationary conditions. The range of the strontium sulfate concentration which complies with the requirements is rather narrow.

Figure 1 shows the sizes of the diameters of strontium sulfate particles formed in the presence of 10 and 20 ppm of poly(vinyl sulfonate). The determinations were made at intervals of 1 min. The first result was obtained 1 min after mixing, therefore the particles "seen" then were adult crystals well past the nucleation stage. The dots which compose the curves in Figures 1 and 2 show the statistical scattering of the determined values. The appreciable scattering of results is due to the very high sensitivity of the detecting system to any disturbances caused by stray dust particles, currents in the solution, vibrations, etc. as well as by deviations from monodispersity. Each experiment was run twice or thrice, every time from freshly filtered solutions. The curves are reproducible, but the degrees of deviations vary a little.

Curves A and B in Figure 1 represent the average diameters of strontium sulfate particles in 0.0168 M solutions with 10 and 20 ppm of poly(vinyl sulfonate). The zones of deviations from these curves do not overlap. The diameters of the particles in the 10 ppm solution (curve A) are about 1.3 times larger than those in the 20 ppm solution. This means that the ratio of the volumes and of the respective

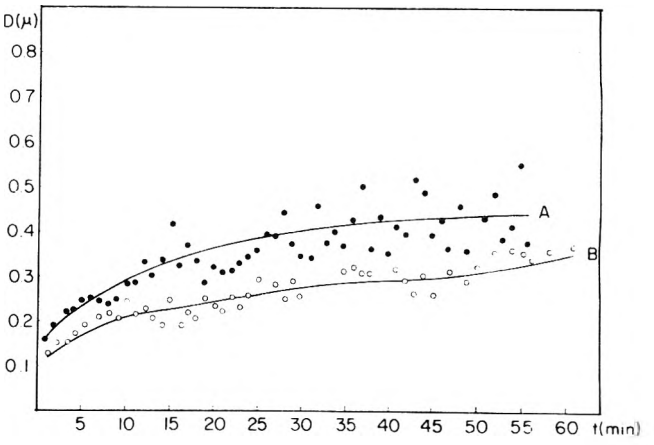

Figure 1. Diameters of strontium sulfate particle in 0.0168 M solution vs. time with admixture of 10 ppm (curve A) and 20 ppm (curve B) poly(vinyl sulfonate).

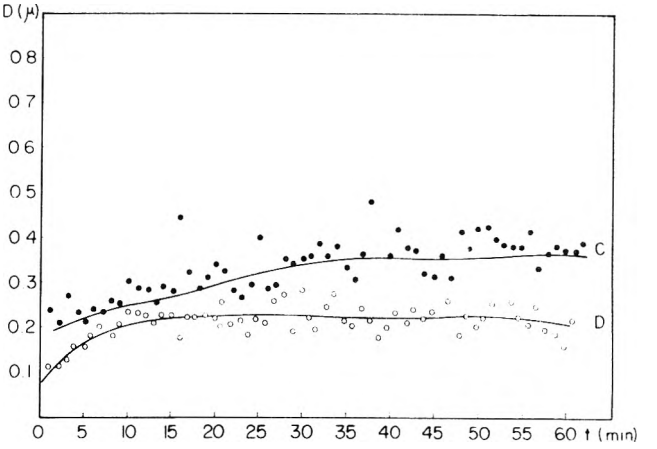

Figure 2. Diameters of strontium sulfate particles in 0.0156 M solution vs. time with admixture of 10 ppm (curve C) and 20 ppm (curve D) poly(vinyl sulfonate).

weights of the particles is 2.2. The proximity of this number to the inverse ratio of the polymer concentrations seems to be significant.

This result was checked in a second series of determinations, in solutions of 0.0156 M concentrations of strontium sulfate. Curve C, Figure 2, represents the diameters of the particles with 10 ppm poly(vinyl sulfonate) admixture and curve D, with 20 ppm. In this case also, the diameters of the particles formed in the presence of 20 ppm additive are smaller, by about the same factor as in the former case, than those formed with 10 ppm. Curve D lies below curve C and both curves are outside the deviation limits of each other.

Comparing curves which represent diameters of strontium sulfate particles formed in the presence of constant poly(vinyl sulfonate) concentration, in Figures 1 and 2, one can see that curve C which represents the lower concentration of strontium sulfate lies below curve A, which represents the higher concentration. The limit zones of both curves overlap. The same may be said about curves B and D.

The fact that the weights of the particles in the solution are in inverse ratio to the concentrations of the additive can be readily explained on the basis of the heterogeneous nucleation mechanism, when each polymeric species, or a

definite part of the polymeric molecules, are considered as microsubstrates, i.e., as likely nucleation sites. If the number of the nucleation sites is doubled, by raising the polymer concentration from 10 to 20 ppm, and the supply of the precipitating solute remains constant, by keeping the same strontium sulfate concentration, the particle weights will be halved, or the diameter will be diminished by a factor of $\sqrt[3]{2}$. This is exactly what is shown in both Figures 1 and 2. As for comparison between the two figures, if the supply of the solute is decreased by lowering the concentration of strontium sulfate but the number of the sites is kept constant (compare curves A and C), the result will be decrease of weight, or decrease of diameter, of the average particle.

The second test of this approach is to count the number of particles in each solution. Although no absolute values can be determined, the relative numbers of particles in the examined solutions were found at constant experimental conditions. In Figure 3 the relative numbers of particles grown in the presence of 10 and 20 ppm of poly(vinyl sulfonate) are shown. The broken lines of some parts of the curves intend to show that in these regions the determined values are widely scattered. However, both from the trends of the broken lines and of unbroken lines which represent the number of particles within a narrow range of deviation, it is clearly evident that the number of particles in the 20 ppm poly(vinyl sulfonate) is, at any given time, higher than their number in the 10 ppm solution. The same results were obtained for both 0.0168 and 0.0156 *M* strontium sulfate solutions.

The proposed heterogeneous-nucleation-on-macromolecules approach simply predicts that the number of crystals in the 20 ppm poly(vinyl sulfonate) solution will be greater by a factor of 2 than their number in the 10 ppm solution.

The number of particles in the solution, according to Figure 3, decreases with time. This may be due to partial coagulation, or to the completion of Ostwald ripening.[7] The coagulated particles, which suddenly become relatively large, are swept by sedimentation, and on their way down they may give sharp signals, thus both raising the average value of the diameters' sizes and increasing the uncertainty pertaining to the diameters' sizes in the late part of the process (see the scattering of results in Figures 1 and 2).

In the solutions employed there is, after mixing, an excess of about 2.7 mg of strontium sulfate per milliliter. The diameter of a strontium sulfate particle in the beginning of the process is about 0.1 μ. The volume of such a particle is $5.24 \times 10^{-4}\ \mu^3$ and its weight is 2.1×10^{-12} mg, taking into account the specific gravity of the bulk strontium sulfate mineral which is 3.96. If all the excess solute was distributed on the available nucleation sites and all the particles reached, after 1 min, the 0.1-μ diameter size, their number should have been 1.3×10^{12}. If only a part of this number of particles reached the 0.1-μ diameter size, the rest of them would be smaller than 0.1-μ and their total number would be larger than 1.3×10^{12}. Particles smaller than 0.1-μ are undetectable. The smallest particles would dissolve later on, nurturing the biggest particles present, thus completing the Ostwald ripening process and accounting for the gradual increase of the visible precipitate and for the decrease of the number of particles.

The concentration of 20 ppm poly(vinyl sulfonate) of 17 000 molecular weight corresponds to a 1.18×10^{-6} *M* concentration or to $[(1.18 \times 10^{-6})\ (6 \times 10^{23})]/10^3 = 6 \times 10^{14}$ molecules per milliliter. Thus 10 ppm corresponds to the concentration of 3×10^{14} molecules per milliliter. This means that there are enough available microsubstrates to act as nucleation centers in the system.

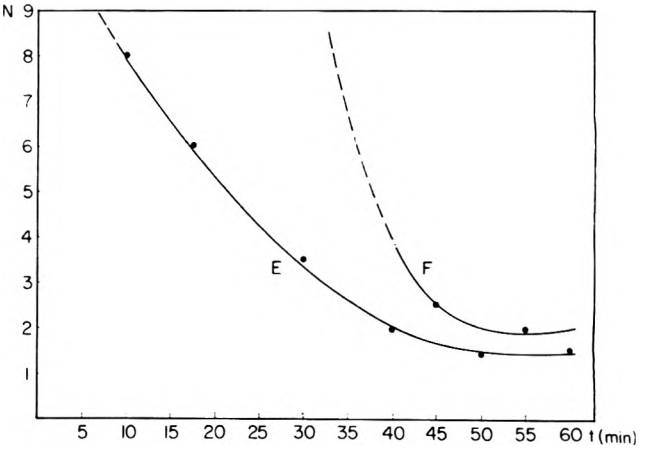

Figure 3. Relative number of particles in 0.0168 *M* strontium sulfate solution vs. time with admixture of 10 ppm (curve E) and 20 ppm (curve F) poly(vinyl sulfonate).

On the other hand, the possibility exists that the polymer molecules, which are 100-fold more numerous than the 0.1-μ sized particles, will adsorb on the particles and retard both Ostwald ripening and coagulation.

The retardation-through-adsorption theory has two important facets: the adsorption of ionic impurities on the critical or subcritical nuclei and the adsorption of surface active agents on grown crystallites with already developed crystal faces. Regrettably, these two approaches are often confused.

Simple arithmetic can show that the concept of retardation of growth of subcritical nuclei is unrealistic. A critical nucleus of strontium sulfate is thought to contain 35 ion pairs,[8] and the molarity of 20 ppm poly(vinyl sulfonate) is 1.18×10^{-6}. This means that the molarity of the inactivated strontium sulfate would be 4.13×10^{-5} *M*, a mere 0.246% of the 1.68×10^{-2} *M* concentration and 0.265% of the 1.58×10^{-2} *M* concentration. The fundamental fact of precipitation retardation, in the first place, cannot be explained by the mechanism of adsorption on nuclei. Secondly, the very insignificant difference between the inactivation of 0.246% of the solute excess by 20 ppm poly(vinyl sulfonate) solution and the 0.123% inactivation in the 10 ppm solution cannot explain the consistent differences between the sizes and the numbers of the particles in the respective solutions.

The second mechanism, which envisages termination of growth of adult crystallites, could not be as easily disproved as the first one. It is well known that surface active agents can retard the precipitation of sparingly soluble salts. It is also known that such agents can adsorb on a crystallite only after crystallographic faces have been developed, i.e., after the crystals are relatively large. In order to refute the possibility that this was the controlling mechanism of retardation, in this case the presented system should have been thoroughly examined to decide whether the experimental data can be explained by retardation-through-adsorption on growth sites at some stage of the crystallization process. This would mean that the macromolecule should patiently wait until a crystal first nucleates on a rare and noncharged substrate, then wait until

the crystal subsequently grows to a certain size, and only at this stage block the growth sites.

The retardation-through-adsorption mechanism has, however, one straightforward attractive feature. It states that in the absence of the additive we have immediate heavy precipitation, but in the presence of the additive the precipitation is retarded; the inhibition of growth is caused by the adsorption of the additive on the crystallites while they are very small. How is this basic fact of precipitation retardation to be explained by the presented mechanism of nucleation on microsubstrates?

It has already been mentioned that the employed solutions were 18- and 19-fold supersaturated. It was shown that only at very special conditions of fast mixing and at supersaturations of 100 and higher, true homogeneous nucleation of strontium sulfate can occur in solution.[8] The heterogeneous nuclei are formed on the walls of the container, on stray specks of dust, and on occasional unspecified impurities. The number of heterogeneous nuclei is usually in the range of 10^7–10^9/ml in clean solutions. If this is the number of nuclei formed in the first second, they can nurture on all the available excess of solute and, in the presented system, reach the ultimate weights of 2.7×10^{-7} to 2.7×10^{-9} mg. However if 6×10^{14} suitable microsubstrates per milliliter are introduced the excess of solute will be nearly equally distributed and the crystallites formed of 4.5×10^{-13} mg average weight and about 0.06-μ diameter will be too small to precipitate or to be detected. Only after a period necessary for partial coagulation and Ostwald ripening can regular precipitation take place. This delay constitutes the retardation effect in the presence of microsubstrates.

When microsubstrates are introduced to a system, the ordinary heterogeneous nucleation process evidently breaks down. It may be the sheer effect of quantities: the 10^7–10^9 centers per milliliter are negligible when compared to 10^{14} likely nucleation centers. The other possibility is that the ordinary nucleation centers are rendered inactive by association with the artificially introduced effective microsubstrates.

Poly(vinyl sulfonate) polymers are especially suited to act as microsubstrates for strontium sulfate. The polymer has negatively charged functional groups 0.4–0.5 nm apart on the free flexing chain. The intercationic distances in strontium sulfate are 0.435 nm, and this makes the two substances an almost perfect match.

The light scattering technique enables us to simultaneously determine the diameter of a particle and the relative number of particles in a solution. However even this powerful tool does not overcome the basic difficulty of nucleation research: the crystallites are measured and counted after a period of time which is infinitely long when related to nucleation events. Investigators of nucleation in solutions usually draw their conclusions about the nucleation events from the analysis of the precipitate. Investigation of particles in the solution in which they were born and continue to grow is a distinct improvement on the "post-mortem" technique.

Acknowledgment. The authors wish to thank Professor V. Barboy for his interest in this work and for stimulating discussions.

References and Notes

(1) Part I of this paper is entitled A Method for Rapid Measurement of Particle Size and Relative Number Density of Particles in Suspension. N. Ben-Yosef, O. Ginio, D. Mahlab, A. Weitz, and S. Sarig, *J. Phys. Chem.*, preceding article in this issue.
(2) D. Turnbull and B. Vonnegut, *Ind. Eng. Chem.*, **44** 1292 (1952).
(3) M. C. Upreti and A. G. Walton, *J. Chem. Phys.*, **44**, 1936 (1966).
(4) S. Sarig, *J. Crystal Growth*, **24/25**, 338 (1974).
(5) S. Sarig and F. Tartakovsky, *Isr. J. Chem.*, **12**, 905 (1974).
(6) S. Sarig and M. Raphael, *J. Crystal Growth*, **16**, 203 (1972).
(7) R. H. Doremus, *J. Phys. Chem.*, **74**, 1405 (1970).
(8) A. E. Nielsen, *Krist. Tech.*, **4**, 17 (1969).

Ultraviolet Spectra and Structure of Complexes of Pyridine 1-Oxide and Oxygen Acids[1]

Maurice M. Kreevoy* and Kwang-chou Chang

Chemical Dynamics Laboratory, University of Minnesota, Minneapolis, Minnesota 55455 *(Received September 22, 1975)*

Publication costs assisted by the National Science Foundation

The uv spectra of complexes formed by pyridine 1-oxide with carboxylic and sulfonic acids of various strengths are not combinations of the spectra of the protonated and the unprotonated base. Rather, the complexes with acids of intermediate strength show bands in intermediate positions. Neither fully protonated nor unprotonated base is present. Instead, these complexes have two partial O–H bonds, the relative strength of which varies continuously with the strength of the acid.

There are a considerable number of solids now known to contain hydrogen bonds in which two basic oxygens are 2.5–2.4-Å apart.[2] X-Ray and neutron diffraction studies of these substances suggest that the hydrogen is either centrally located between the two oxygens or else oscillates rapidly between positions only slightly displaced from the center. In solution, on the other hand, as judged by their uv spectra, hydrogen-bonded substances appear to be mixtures of tautomers in which the hydrogen is localized near one or the other of the two basic atoms,[3,4] as shown in eq 1.

$$AH \cdots B \rightleftharpoons {}^{-}A \cdots HB^{+} \quad (1)$$

The rate constant for the interconversion of the tautomers appears to be below 10^{11} s^{-1} when the equilibrium constant is of the order of unity.[3] This implies that a barrier to proton transfer of at least 2 kcal mol^{-1} exists, which would be hard to reconcile with the crystallographic evidence cited above. There are, however, several differences between the two kinds of compounds. Most of the solids in which the hydrogens are centrally located are chemically symmetrical or nearly so,[5] while A and B are quite different in the tautomeric cases. Most of the centrosymmetric cases involve only oxygens as the basic atoms, while one nitrogen is involved in each of the tautomeric equilibria. Finally, the hydrogen, conceivably, might be "centralized" by crystal forces in the solids.

The present paper describes the uv spectra of hydrogen-bonded complexes of the type 1, where A is a carboxylate or sulfonate ion, in tetrahydrothiophenedioxide (sulfolane) as solvent.

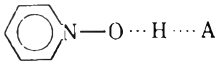

1

Experimental Section

Sulfolane, pyridine 1-oxide, DMSO, and the various acids were all purchased from standard sources and purified by distillation. They had appropriate boiling points, ir spectra, and NMR spectra. The various complexes needed for uv spectra were formed by dissolving appropriate quantities of pyridine 1-oxide and an acid in sulfolane. The uv spectra of the complexes were obtained from thin films of sulfolane solutions between sapphire plates. The thickness of the films was deduced from the ir intensity of one of the C–H stretching bands of the sulfolane. (Sapphire is transparent in the ir down to ~2200 cm^{-1}.) The intensity of this band was previously measured in a conventional ir cell of known path length. The uv spectra were determined with a Beckman DK-2 spectrophotometer which was calibrated with a benzene solution in hexane. Only air was in the reference beam. The uv spectrum of pure sulfolane was determined in the same way and showed no significant absorptions.

Results

The uv spectra of pyridine 1-oxide and its complexes with a series of acids of varying strength are shown in Figure 1. In Figure 2 is shown the spectrum of a solution containing a twofold molar excess of pyridine 1-oxide over trifluoromethanesulfonic acid.

Discussion

The ir spectra and freezing point depressions of solutions such as these show that they do, indeed, contain 1:1 hydrogen-bonded complexes which are not further aggregated.[6-8] The freezing point depressions in sulfolane preclude further aggregation.[6,7] The formation of symmetrical ions, as shown in eq 2, has been suggested,[9,10] and is not precluded

$$2AH + 2B \rightarrow AHA^{-} + BHB^{+} \quad (2)$$

by the freezing points if the ions dissociate. However, tetramethylammonium bis(trifluoro)acetate, which necessarily contains the same anion as the product in eq 2, shows two bands in the carbonyl region, at 1795 and 1740 cm^{-1}.[8]

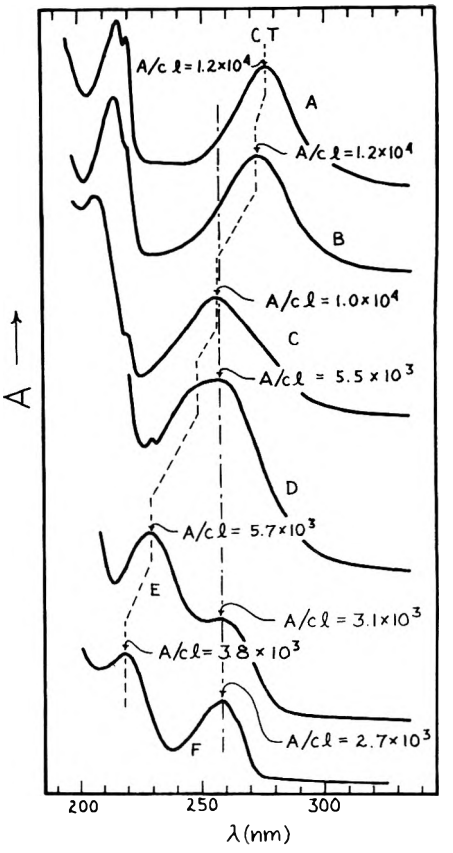

Figure 1. Uv spectra of pyridine 1-oxide and a series of its complexes with carboxylic and sulfonic acids in sulfolane solution: curve A is for 0.081 M pyridine 1-oxide, path length, 5.01 μm; curve B, for 0.065 M complex with CH_3COOH, path length 6.15 μm; curve C, for 0.076 M complex with $CHCl_2COOH$, path length 6.73 μm; curve D, for 0.101 M complex with CF_3COOH, path length 14.0 μm; curve E, 0.151 M complex with CH_3SO_2OH, path length 8.87 μm; curve F, 0.093 M complex with CF_3SO_2OH, path length 14.3 μm. The progressive blue shift of the charge transfer band is indicated by - - - -; the location of the benzenoid band by – – – –. Because both the concentration and the path length were variable, the molar absorptivities, *A/cl*, are indicated at one or more points on each spectrum to make a comparison of intensities easier.

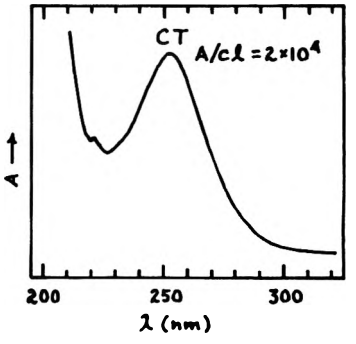

Figure 2. The uv spectrum generated by a solution of 0.148 M pyridine 1-oxide and 0.074 M CF_3SO_2OH, in sulfolane. The path length is 5.91 μm. The molar absorptivity is indicated.

The trifluoroacetic acid complex of pyridine 1-oxide shows only one, at 1780 cm^{-1}.[8] Moreover, the structure of the crystalline complex of trichloroacetic acid with pyridine 1-oxide has been determined by x-ray crystallography, and it is *not* that of the symmetrical ions but rather that of the

simple binary complex, 1.[5] The uv spectra shown in Figures 1 and 2 further support this view. The spectrum shown in Figure 2, generated by a solution containing 2 mol of pyridine 1-oxide for each mole of trifluoromethanesulfonic acid, is clearly not the sum of the spectra of the base and the protonated base, in equal proportions or in any other proportions. In view of the strong tendency of pyridine 1-oxide to form hydrogen bonds,[11,12] it is, almost certainly, the spectrum of the BHB^+ ion or the $BHB^+ \cdot A^-$ ion pair. Each 1:1 complex has its own spectrum, all of which are different from the spectrum of the BHB^+ ion. These observations sustain no doubt that we are dealing with complexes of structure 1.

The acid dissociation constant of protonated pyridine 1-oxide in water is about 0.1.[13] Since trifluoromethanesulfonic acid is one of the strongest acids known, largely ionized even in very weakly basic solvents,[14] its complex with pyridine 1-oxide should be completely ionized. Confirming this, the uv spectrum of the complex is very similar to that of the base in 1 *M* aqueous perchloric acid. The acetic acid complex, on the other hand, has a uv spectrum almost identical with that of the uncomplexed base, so that it must be entirely un-ionized. For the acids of intermediate strength the uv spectra shown in Figures 1 and 2 are incompatible with the formulation of the complexes as systems in tautomeric equilibrium. It should be possible to approximate the spectrum of a mixture by making a linear combination of the spectra of its constituents. Such approximations fail entirely for the spectra shown in Figures 1 and 2. Rather, the strong band found at 280 nm in the uncomplexed and acetic-acid-complexed pyridine 1-oxide is steadily blue-shifted by the stronger acids till it reaches 220 nm in the complex with trifluoromethanesulfonic acid. It is also somewhat diminished in intensity. A band found at 217 nm in the uncomplexed base is also blue-shifted by complexing and disappears from the accessible region of the spectrum for acids stronger than dichloroacetic. In the complexes with the stronger acids a new band, of lower intensity, at 258 nm, is exposed. The band found at 280 nm in the uncomplexed base is due to a transition from an orbital of π symmetry largely localized on oxygen to a π orbital spread over the ring,[15-17] describable as a charge transfer band. The band at 258 nm is present in benzene and all its derivatives.[18] It is due to a $^1B_{2w} \leftarrow {}^1A_g$ transition in benzene. It is never very strong and its position is rather insensitive to substitution in the aromatic ring.[18] In the present case its intensity appears to increase with the strength of the acid. The progressive blue shift of the charge transfer band with the strengthening of the acid indicates a progressive strengthening of the interaction of the electrons of the oxygen with the proton, so that the exitation of one of them to a more remote orbital requires progressively more energy. A coordinated weakening of the H-A bond is implied.

These results do not indicate whether there is one or two minima between the two basic oxygens in the potential function for the hydrogen. However, if there are two, the residence time of the hydrogen in one of them can be no more than about 10^{-15} s.[19] Such a residence time is of no chemical significance. If there is a double minimum potential function, the barrier between the two minima must lie almost entirely below the first allowed vibrational level. This result is entirely consistent with Speakman's view of the hydrogenic potential function in symmetrical ions having "class A" structures.[2] It shows that such potential functions require neither exact chemical symmetry nor the crystalline state. Previous observations of tautomeric mixtures in solution[3,4] must be related to other structural features; quite possibly to the replacement of one of the oxygens by nitrogen.

These results are inconsistent with a previously held view[20,21] that the very broad, hydrogenic vibrational spectrum which such complexes generate reflects exchange broadening. It has been suggested[22] that proton transfer to electron pairs in delocalized orbitals is generally slow. The photoelectron spectrum of pyridine 1-oxide,[16,17] the crystal structure of its trichloroacetic acid adduct,[5] and the intensity of the charge transfer band all show that the electron pair which accepts the proton in the present case is of π symmetry. While this orbital is concentrated on oxygen, it has a very substantial admixture of carbon and nitrogen $2p\pi$ orbitals.[17] Since there is no chemically significant barrier to proton transfer at all in the present case, a localized acceptor orbital cannot be a necessary condition for fast proton transfer reactions.

It may be of interest to note that the species described in this paper are analogous to "nonclassical ions".[23]

References and Notes

(1) Supported, in part, by the U.S. National Science Foundation through Grant No. GP-31360X.
(2) J. C. Speakman, *Struct. Bonding (Berlin)*, **12**, 141 (1972).
(3) D. Eustace and E. Grunwald, *J. Am. Chem. Soc.*, **96**, 7171 (1974).
(4) R. A. Hudson, R. M. Scott, and S. N. Vinogradov, *J. Phys. Chem.*, **76**, 1989 (1972).
(5) However the pyridine 1-oxide complex of trichloroacetic acid has recently been reported to have a very short O · · · O distance in the solid state, and to show an ir spectrum characteristic of a centrally located hydrogen: L. Galic, D. Hadzi, and F. Lazarini, *Chem. Commun.*, 860 (1971); D. Hadzi, private communication.
(6) J. Husar and M. M. Kreevoy, *J. Am. Chem. Soc.*, **94**, 2902 (1972).
(7) J. Husar, Ph.D. Thesis, University of Minnesota, 1971.
(8) K. Chang, Ph.D. Thesis, University of Minnesota, 1975.
(9) M. Szafran and Z. Dega-Szafran, *Rocz. Chem.*, **44**, 793 (1970).
(10) M. Szafran and M. Rozwadowska, *Rocz. Chem.*, **44**, 1465 (1970).
(11) E. M. Arnett, E. J. Mitchell, and T. S. S. R. Murty, *J. Am. Chem. Soc.*, **96**, 3875 (1974).
(12) R. W. Taft, D. Gurka, L. Joris, P. v. R. Schleyer, and J. W. Rokshys, *J. Am. Chem. Soc.*, **91**, 4801 (1969).
(13) H. H. Jaffe and G. O. Doak, *J. Am. Chem. Soc.*, **77**, 4441 (1955).
(14) 3M Brand trimsylate acid, technical information bulletin FC-24, anonymous, The 3M Co., St. Paul, Minn., 1970, p 2.
(15) H. H. Jaffe and M. Orchin, "Theory and Applications of Ultraviolet Spectroscopy", Wiley, New York, N.Y., 1962, pp 381-382.
(16) J. P. Maier and J.-F. Muller, *Tetrahedron Lett.*, 2987 (1974).
(17) J. P. Maier and J.-F. Muller, *J. Chem. Soc., Faraday Trans. 2*, **70**, 1991 (1974).
(18) Reference 15, p 257.
(19) The maximum residence time at which the uv bands of the two will be merged if they would be 5000 cm^{-1} apart in otherwise analogous, long-lived species; ref 3. Bands at 220 and 280 nm are separated by ~10 000 cm^{-1}.
(20) J. M. Williams and M. M. Kreevoy, *J. Am. Chem. Soc.*, **89**, 5499 (1967).
(21) J. Husar and M. M. Kreevoy, *J. Am. Chem. Soc.*, **94**, 2902 (1972).
(22) A. J. Kresge and G. L. Capen, *J. Am. Chem. Soc.*, **97**, 1795 (1975).
(23) P. D. Bartlett, "Nonclassical Ions", W. A. Benjamin, New York, N.Y., 1965.

Surface Acidity of Cation Exchanged Y-Zeolites

W. Kladnig

Centro de Petróleo y Quimica, Instituto Venezolano de Investigaciones Científicas, Apartado 1827, Caracas, Venezuela
(Received June 24, 1975)

Instituto Venezolano de Investigaciones Cientificas

Measurements of the surface acidity of Y zeolites containing Na, K, Ca, Sr, La, and Gd ions have been carried out by means of amine titrations, observing the color change of adsorbed Hammett indicators in the H_0 range +6.8 to −8.2 in benzene solution. A good correlation between the acid strength and physical parameters (e/r ratios) of the cations in 86% exchanged Y zeolites was detected. While a completely K exchanged Y zeolite had no observable acidity, La and Gd exchanged species exhibited strong acidity even at lower degrees of exchange. Zeolites containing alkaline earth ions had the same acidity as NaY in the range 0–55% exchange, indicating that the alkaline earth cations were in inaccessible sites. Lanthanum ion exchanged forms showed a marked rise in acidity at higher degrees of exchange, evidently due to partial migration of La ions into S_I sites. Acidic centers in the zeolite examined were presumed to be mainly Brönsted, but, on the basis of the results, Lewis and cationic centers also have to be considered.

Introduction

It has become obvious in recent years that in many catalytic reactions acidic centers on the catalyst surface play an important role. Especially for cracking, isomerization, alkylation, alcohol dehydration, and polymerization considerable surface acidity is necessary.[1-3]

The great acidity and catalytic activity of some cation-exchanged zeolites, mainly faujasites and mordenites, have made them of great importance to the petroleum industry. In a number of publications, and especially in those where infrared spectroscopy has been used, different types of acidic centers (Brönsted and Lewis) and total acidity have been correlated with the type of exchanged cation, the silica to alumina ratio, and different pretreatment conditions.[4,5] On the other hand, less attention has been paid to the acidity of zeolites by means of titration with a base in nonaqueous solutions.

The aim of the present work was, therefore, to examine the influence of the type of exchanged cation, degree of exchange, and pretreatment temperatures on the surface acidity of a synthetic faujasite, type Y. For this purpose a SK-40 molecular sieve was exchanged with different charged cations of approximately the same cation radius, e.g., K (1.33 Å), Ca (0.99 Å), La (1.016 Å), and Gd (0.938 Å). The resulting changes in acidity were related to the original sodium containing material.

Method. The acidity was determined by the microtitration method with *n*-butylamine as described by Benesi[6] and Johnson[7] using the color changes of adsorbed Hammett indicators.[8] Surface acidity is thus expressed by the Hammett and Deyrup H_0 function,[8] with

$$H_0 = -\log [a_{H^+}(f_B/f_{BH^+})]$$

a_{H^+} in this equation expresses the proton activity of the solid acid, and f_B and f_{BH^+} give the activity coefficients of the basic and acidic form of the adsorbed indicators.

As Walling[9] has pointed out, color changes of adsorbed indicators are not and cannot be strictly assigned to a proton-donating process, since, depending on the material, Lewis (electron accepting) centers also play a role in forming a colored complex with Hammett indicators. In this case the Hammett function is expressed by[9]

$$H_0 = -\log [a_A(f_B/f_{AB})]$$

with a_A being the activity of the Lewis acid, f_B and f_{AB} being the activity coefficients of the indicator base and the complex formed with the Lewis acid, respectively. It can be assumed, therefore, that with zeolites centers other than Brönsted sites, Lewis centers (tricoordinated aluminum) or the cations themselves can also take part in producing the acidic color of the indicator. This will be discussed later.

Experimental Section

Material. The Y zeolite used was a SK-40 molecular sieve from Union Carbide. The material was sieved and washed thoroughly several times with deionized water until no more sodium ions could be detected in the washing water. Afterwards the zeolite was exchanged twice with 1 N NaCl solutions, washed free of chloride ions, and dried under vacuum (10^{-2} Torr) at 200–220°C.

The cake so obtained was ground and, after repeated drying under the same conditions, stored in a desiccator over saturated NH_4Cl solution (79.4% relative humidity at 22–23°C). A constant moisture content of 25.9 wt % could be obtained after storage for 1 week.

The chemical analysis of the pretreated material gave the following: Na (10.09%), Al (11.84%), and Si (29.93%) or Na_2O (13.60%), Al_2O_3 (22.37%), SiO_2 (64.03%), with SiO_2/Al_2O_3 = 4.84 or Si/Al = 2.43 according to formula $Na_{56}Al_{56}Si_{136}O_{384}$.

Ion Exchange. In order to exchange sodium the zeolites were placed in contact with the appropriate aqueous solutions of metal chlorides in polyethylene bottles in a thermostated bath at 25 ± 0.1°C for 24 h to obtain exchange equilibrium. The concentrations of the salt solutions were chosen in such a way that the normality of the solution was equal to the equivalent ratio of the exchanging ion to sodium in the zeolite. So 18.885 g of the water containing zeolite (25.9% H_2O) was contacted with 66 ml of the 0.25, 0.5, 1.0, 1.5, 2.0, 2.5, 3.0, 3.5, . . . 5.0 N solutions of the chlorides,

whereby these concentrations equally expressed the equivalent ratio of the exchangeable ion relatively to the sodium in the zeolite (Me^+/Na^+ ratio). All solutions were checked for their salt concentrations by chloride titration. After equilibrium was reached, the phases were separated by filtration and the zeolite washed free of adsorbed chloride with deionized water. The extent of exchange was determined by atomic absorption of the sodium ions in the solution after equilibrium, considering the Na and moisture content of the starting material.

Since the majority of cations do not enter the sodalite cages of the zeolite during exchange at 25°C, some exchanges have been performed at 60°C with 2 N salt solutions, twice repeated (with exception of gadolinium; once only, 1 N solution at 100°C).

Zeolite Pretreatment. Before measuring the acid strength the zeolites were calcined under vacuum (10^{-2} Torr) at 250°C and further treated in a muffle oven in the temperature range 350–500°C, raising the temperature every hour by 50°C. At 500°C the temperature was held for 3 h. According to TGA measurements all physisorbed water was eliminated from the zeolite by this process.

Acid Strength Measurement. The titration of acid strength was determined according to Benesi[6] and Johnson.[7] Calcined zeolite (0.1 g) was weighed in test tubes (7-ml screw cap septum vials, Pierce Chem. Corp.), recalcined after the weighing process under the same conditions described above, and stored in a desiccator. To the cool probes 5 ml of dry benzene (analytical grade, redistilled and stored over Molecular Sieve 3A) was added. Afterwards 3 drops of 0.1% solutions of the indicators in dry benzene was added and the adsorption process accelerated by immersing the sealed test tubes in a water filled ultrasonic tank. This process was found to accelerate the adsorption process of the indicators considerably. Time of adsorption depended strongly on the indicator used as well as on the type of exchanged ion and the degree of exchange. In the case of strong acidic zeolites adsorption times of up to 3 days were necessary until equilibrium has been reached.

The titration was carried out in two steps. First *n*-butylamine (0.1 N) was added in 0.1-ml amounts to a number of vials. The color changes were observed visually after the *n*-butylamine had come into equilibrium with the indicators. The approximate range of the color change could be determined in this way. The final point was reached by adding the butylamine titer in 0.01-ml steps to a new series of catalyst samples in the approximate range of the end point. Time of neutralization varied with the acidity of the zeolite and the indicator.

The titrations were performed with a microburet (Buret Type A, Kimble Corp.), containing a needle point to pierce the sealed caps of the test tubes in order to avoid air moisture. With this procedure roughly 10–15 g of zeolite was necessary per indicator.

Indicators. All indicators were Eastman Kodak products, used without further purification and dissolved in dry, redistilled benzene of analytical grade. In Table I the indicators used are listed, together with their color changes, pK_a's, and corresponding sulfuric acid composition, as determined experimentally by Hammett and Deyrup.[8]

In the cases of neutral red and 4-(*p*-ethoxyphenylazo)-*m*-phenylenediamine, which were only available in form of their hydrochloride salts, the indicator bases were obtained by precipitation of their aqueous solutions with 0.1 N NaOH, filtration, and careful drying under vacuum. The pK_a's were taken from the literature.[3,6]

Neutral red deserves to be mentioned here since the neutralization reaction using this indicator was problematic in cases of high acidic zeolites. End points could only be determined after a neutralization time of up to 1 week, since the indicator was found to be strongly adsorbed. In contrast to zeolites, these difficulties were not observed with silica–alumina in our laboratories. With all other indicators titrations could be performed easily.

Results and Discussion

A. Ion Exchange. Figures 1 and 2 show the ion exchange isotherms as determined for the exchange Na → K, Ca, Sr, La, Gd in the range of 0–5 equiv Me^{n+}/Na^+.

Table II gives the relative selectivity coefficients for the exchange of a given ion pair as calculated by the formula $K_s = (X_A c_B)/(X_B c_A)$ from results obtained experimentally. X_A and X_B are the ion fractions of the cations in the crystal ($X \times 100$ = percent exchange) at equilibrium and c_A/c_B gives the equivalent ratio of $[Na]_{zeolite}$:$[ion]_{soln}$ before ion exchange. The constants are salt concentration dependent.

The ion exchange selectivity in the SK-40 zeolite is therefore Gd > Ca, Sr > La > Na > K. This sequence is, with the exception of La, in accordance with the exchange selectivity expected on a thermodynamic basis[10] in the range of low concentrations with nearly ideal exchange behavior. Figures 1 and 2 further show that the exchange possibilities for Sr, Ca, La, and Gd at 25°C have a limit even when the salt concentrations of exchangeable ions become very high. Table III gives the values obtained for maximum exchanges at different temperatures. The values for the exchanges at 25°C are in very good agreement with the results obtained by Sherry[11] for Ca and Sr and for La.[12] Exchanges with gadolinium have not been reported in literature. Due to its lower cation radius a higher degree of exchange should result as in the case of La. This was not observed, probably due to hydrolysis of $GdCl_3$ at higher salt concentrations.

At a 25°C exchange the solvated Ca, Sr, La, and Gd ions therefore cannot enter the small cages, which are equivalent to the S_I sites as defined by Breck.[13] The explanation of this phenomenon as given by Sherry[10] lies in a stripping effect of those solvated ions whereby large hydration radii as well as high hydration enthalpies prohibit entrance through the 2.2-Å windows of the sodalite cages.

Raising the temperature of the exchange system allows an easy 100% exchange with K, in accordance with the literature,[14] while the higher charged ions show difficulties in entering the small pores. As reported by Sherry,[12] 100% exchange with La was only possible after a 47-day treatment at 100°C.

B. Acidity. Table IV gives the zeolites used for acidity measurements after a calcination temperature of 500°C. The table includes total acidity as approximately calculated from the results obtained.

Acidity of K-Y. The acidity distribution of different K exchanged Y zeolites is shown in Figure 3. It is clear from this distribution that with rising K exchange the surface acidity becomes lower until at a 100% exchange no more acidic function of the zeolite is observable. In Figure 4 the correlation between degree of ion exchange and butylamine titers at H_0 +6.8 and +4.0 are shown. The curve at H_0 +6.8 bends sharply down at about 85% K exchange, which could be explained by the complete filling of S_I and S_{II} sites

TABLE I: Indicators for Determining Acid Strength

Indicator	Color		pK_a	Wt % H_2SO_4[a]
	Basic	Acidic		
Neutral red	Yellow	Red	+6.8	8×10^{-8}
4-(*p*-Ethoxyphenylazo)-*m*-phenylenediamine	Yellow	Red	+5.0	
4-Phenylazo-1-naphthylamine	Yellow	Red	+4.0	5×10^{-5}
4-*o*-Tolylazo-*o*-toluidin	Yellow	Red	+2.0	5×10^{-3}
4-Phenylazodiphenylamine	Yellow	Purple	+1.5	2×10^{-2}
2-Nitrodiphenylamine	Orange	Purple	−2.1	
Dicinnamalacetone	Yellow	Red	−3.0	48
Chalcone	Colorless	Yellow	−5.6	71
Anthraquinone	Colorless	Yellow	−8.2	90

[a] Reference 3.

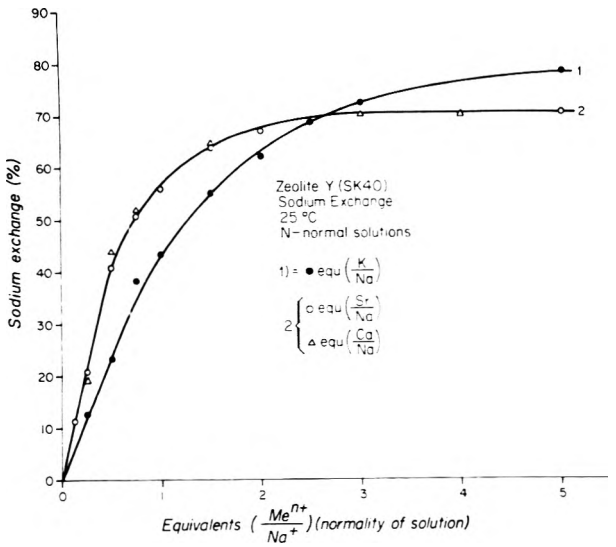

Figure 1. Sodium exchange in SK-40 molecular sieve with *N* normal solutions of KCl, $SrCl_2$, and $CaCl_2$ at 25°C (24 h).

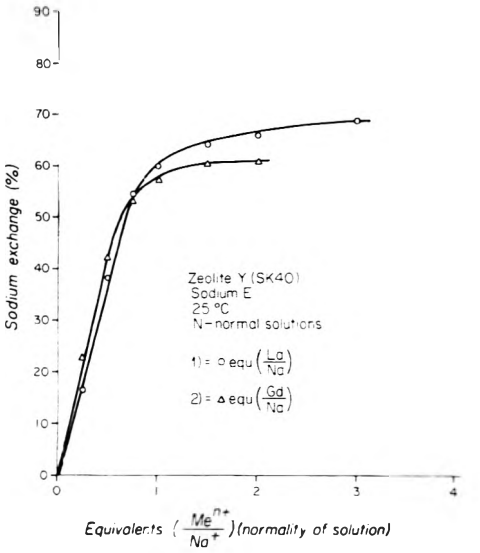

Figure 2. Sodium exchange in SK-40 molecular sieve with *N* normal solutions of $LaCl_3$ and $GdCl_3$ at 25°C (24 h).

TABLE II: Selectivity of Exchange $K_s = (X_A c_B)/(X_B c_A)$

c_A	B = Na A = K	B = Na A = Ca,Sr	B = Na A = La	B = Na A = Gd
0.125		1.0600		
0.25	0.6014	1.0709	0.8739	1.2018
0.3	0.5747	1.157	0.9424	
0.5	0.6164	1.3915	1.2415	1.4632

TABLE III: Maximum Ion Exchange in SK-40 Molecular Sieve

Ion	T, °C	c_A, N	Exchange	
			Time, h	%
K	25	5.0	24	78.64
Ca	25	3.0	24	70.05
Sr	25	5.0	24	70.05
La	25	3.0	24	68.73
Gd	25	2.0	24	61.64
K	60	2.0	24 repeated	100.00
Ca	60	2.0	24 repeated	86.14
Sr	60	2.0	24 repeated	86.14
La	60	2.0	24 repeated	76.90
Gd	100	1.0	24	75.00

(85.8% theoretically). Completing the exchange (at 100%) eliminates all detectable acidic functions in the zeolite. K therefore can be considered as a typical catalyst poison as has been described by Danforth.[15] Catalytic reactions with K exchanged zeolites thus cannot include carbonium ion mechanisms in which an acidic surface is considered to be necessary. In investigating the condensation reactions of toluene and methanol at about 500°C, Sidorenko et al.[16] describe preliminary styrene and ethylbenzene formation with K exchanged X and Y zeolites that is typical of a radical process.[17]

Acidity of Sr-Y. In changing sodium against strontium no change in acidity occurs until the degree of exchange reaches approximately 55%. Figure 5 shows the acidity distributions in H_0 range from +6.8 to −5.6 for various Sr exchanged Y zeolites. With rising degree of exchange, acidity becomes considerably higher than that of NaY. Figure 6 gives the correlation between the percentage of ion exchange and butylamine titers. It can be clearly seen that the acidity of SrNaY is equal to that of NaY until 55% ex-

TABLE IV: Accumulated Acidities in Ion Exchanged SK-40 Molecular Sieves after Calcination at 500°C

Y zeolite	Butylamine titer, mmol/g, in H_0 range: +6.8 to +4.0	+4.0 to +1.5	+1.5 to −5.6	<−5.6	Total in the range +6.8 to −5.6
Na	0.35	0.12			0.47
$K_{13}Na_{87}$	0.40	0.05			0.45
$K_{78.6}Na_{21.4}$	0.31	0.01			0.32
K_{100}	0.03				0.03
$Sr_{21.1}Na_{78.9}$	0.36	0.11	0.01		0.48
$Sr_{50.9}Na_{49.1}$	0.43	0.14	0.06		0.63
$Sr_{56.2}Na_{47.8}$	0.42	0.18	0.12	0.05	0.77
$Sr_{70.1}Na_{29.9}$	0.63	0.20	0.24	0.08	1.15
$Sr_{86.2}Na_{13.8}$	0.60	0.22	0.20	0.38	1.40
$Ca_{19.5}Na_{80.5}$	0.35	0.11	0.01	0.01	0.48
$Ca_{52.2}Na_{47.8}$	0.38	0.19	0.08	0.05	0.60
$Ca_{64.8}Na_{35.2}$	0.50	0.18	0.22	0.13	1.03
$Ca_{70.1}Na_{29.9}$	0.48	0.21	0.27	0.21	1.17
$Ca_{86.2}Na_{13.8}$	0.45	0.30	0.35	0.48	1.58
$La_{17.9}Na_{82.1}$	0.30	0.20	0.17	0.03	0.70
$La_{31.7}Na_{68.3}$	0.27	0.17	0.23	0.05	0.72
$La_{54.5}Na_{45.5}$	0.49	0.23	0.28	0.10	1.10
$La_{68.7}Na_{31.3}$	0.43	0.10	0.36	0.34	1.23
$La_{76.9}Na_{23.1}$	0.32	0.09	0.41	0.75	1.57
$Gd_{23.1}Na_{76.9}$	0.37	0.06	0.13	0.09	0.65
$Gd_{42.3}Na_{57.7}$	0.50	0.13	0.17	0.20	1.00
$Gd_{57.2}Na_{42.5}$	0.41	0.21	0.27	0.41	1.30
$Gd_{61.5}Na_{38.5}$	0.38	0.15	0.37	0.48	1.38
$Gd_{75.0}Na_{25.0}$	0.45	0.22	0.43	0.80	1.90

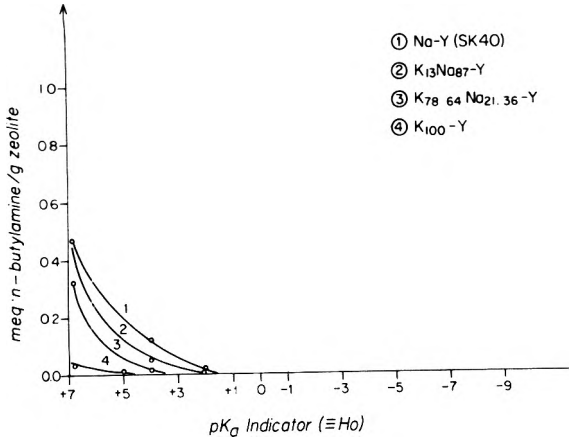

Figure 3. Acidity distribution in KNaY zeolites.

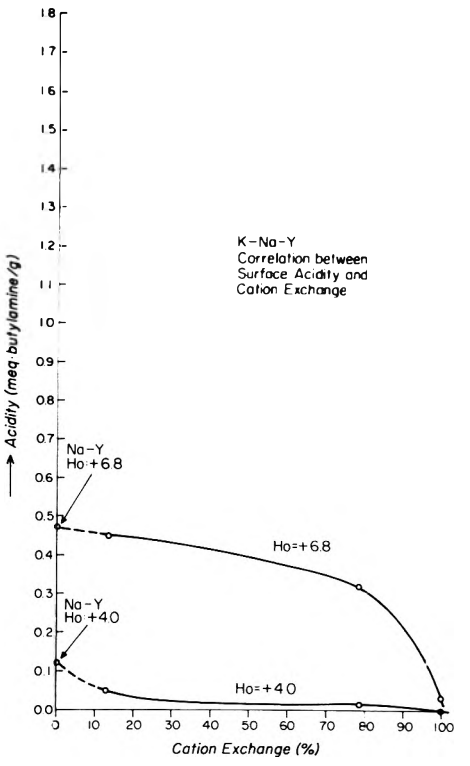

Figure 4. Comparison between milliequivalents of butylamine at H_0 +6.8 and +4.0 with degree of cation exchange in KNaY zeolite.

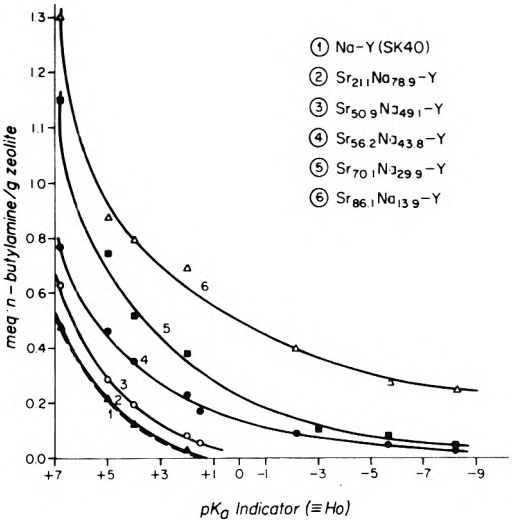

Figure 5. Acidity distribution in SrNaY zeolites.

change, above which a sharp rise in acidity occurs. Strong acidic centers are formed at exchanges greater than 70% which must be consistent with the occupation of S_{III} sites. Since surface acidity shows no difference between NaY until 55% exchange, the strontium ions first fill up the S_I sites of the zeolite. However one has to consider that the exchange procedure has been carried out at 25°C where Sr_{aq}^{2+} cannot enter the sodalite cages. A strontium ion migration during the calcination process therefore must have occurred, indicating the strong preference of alkaline earth ions for these sites.

Acidity of Ca-Y. Calcium exchanged SK-40 has a very similar behavior to the strontium one. Figure 7 gives the acidity distribution for the Ca exchanged zeolites. Again in the lower range of Ca exchange no difference in the acidity compared with NaY is observable (curve 2 in Figure 7). Figure 8 shows a sharp rise in acidity at exchanges greater than 50%. Compared with SrNaY, CaNaY gives greater surface acidity. Strong acidic centers ($H_0 < -5.6$) already become evident at exchanges greater than 20% (Figure 8). As in the case of SrY the calcium ions must have migrated into S_I positions during the calcination process.

The observation that alkaline earth ions in S_I positions do not show much acidic function has been reported on different occasions in the literature. In infrared investigations Ward[18,19] describes no observable acidity in $Me^{2+}HY$ zeolites in the exchange range 35–55%. Similarly in *o*-xylol isomerization at 260°C these zeolites showed no acidity. Rouse and Stone[20] could not obtain any activity in *n*-bu-

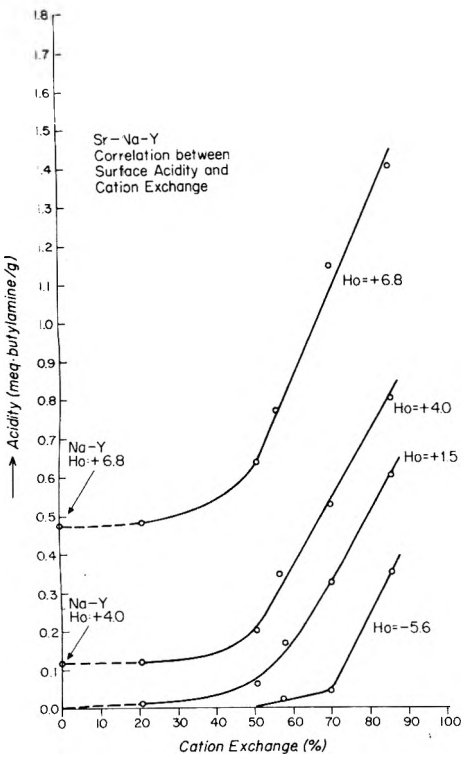

Figure 6. Comparison between milliequivalents of butylamine at H_0 +6.8, +4.0, +1.5, and −5.6 with degree of exchange in SrNaY zeolite.

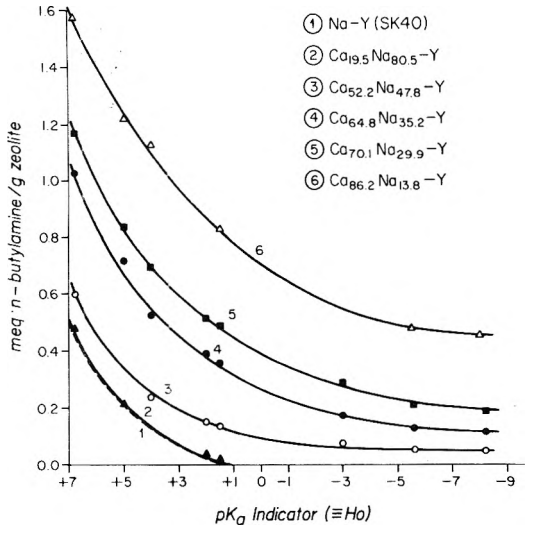

Figure 7. Acidity distribution in CaNaY zeolites.

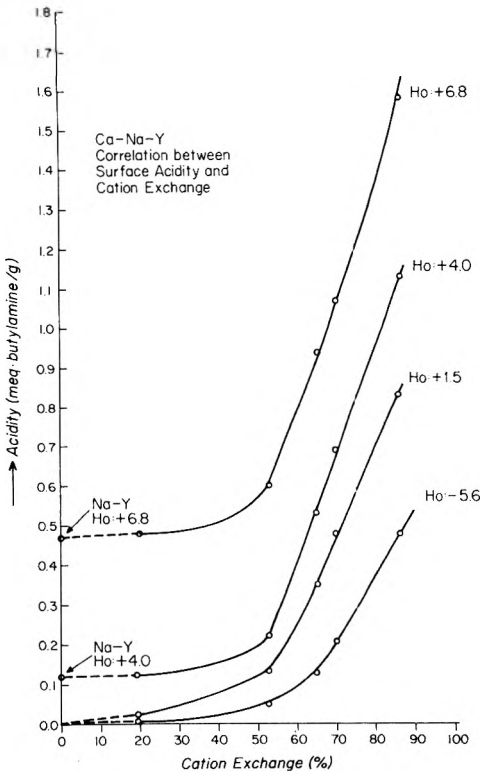

Figure 8. Comparison between milliequivalents of butylamine at H_0 +6.8, +4.0, +1.5, and −5.6 with degree of exchange in CaNaY zeolite.

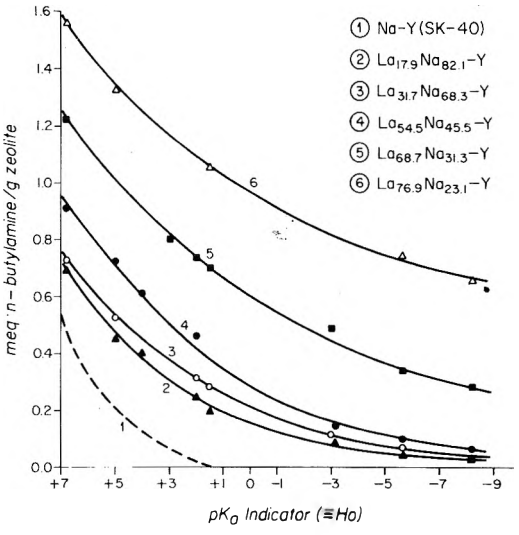

Figure 9. Acidity distribution in LaNaY zeolites.

tene isomerization until the exchange of Ca in CaNaY had become greater than 50%. Tung and McIninch[21] describe graphically that cracking and isomerization activity in CaNaY are observed for exchange in excess of 60%. Tsutsumi and Takahashi[22] observed no change in electrostatic fields of CaNaY zeolites, calculated from heats of immersion in different organic solvents, until the degree of exchange became greater than 40%. In investigating the catalytic activity of CaNaY zeolites with different Si/Al ratios, the same activity as NaY in cumene cracking resulted in all cases until the degree of Ca exchange reached 50%.[23]

All these cases show that Ca ions have a strong preference for S_I sites which they tend to fill up completely. In occupying these places the cations no longer exhibit any catalytic effect.

Acidity of La-Y. Lanthanum exchanged Y zeolites behave differently. In Figure 9 the acidity distribution of LaNaY zeolites is given. In contrast to SrNaY and CaNaY, LaNaY shows considerable acidity at very low degrees of exchange. In Figure 10 the correlation between amount of butylamine and cation exchange is given. A great number of centers of middle (H_0 +1.5) and low (H_0 +4.0 and +6.8) acidity is observable at small exchange levels. No sharp rise at a 50% exchange is seen. Instead a strong enhancement of

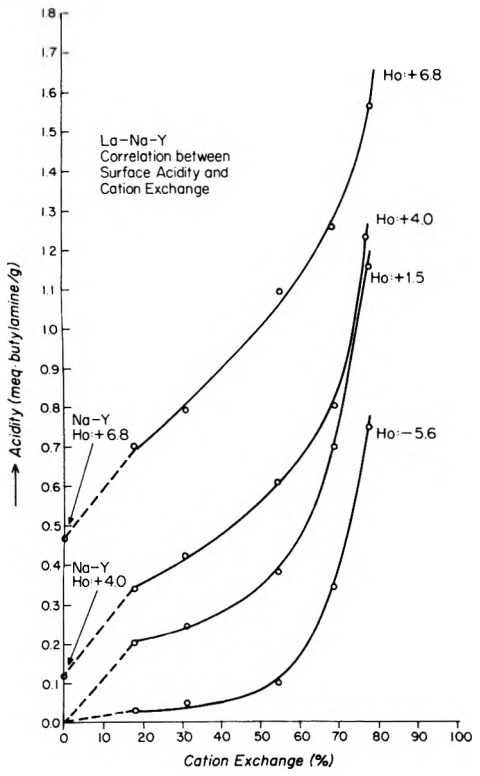

Figure 10. Comparison between milliequivalents of butylamine at H_0 +6.8, +4.0, +1.5, and −5.6 with degree of exchange in LaNaY zeolite.

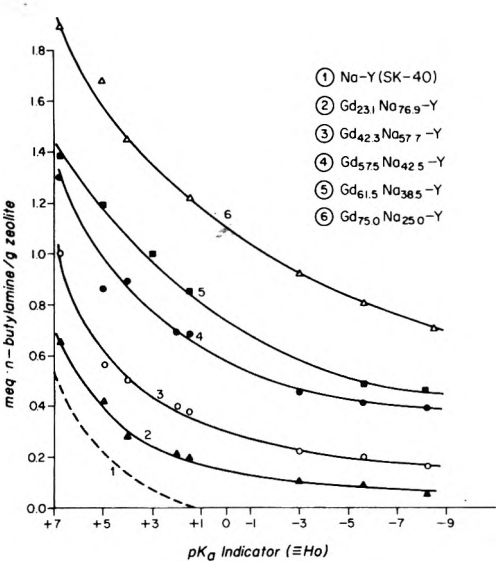

Figure 11. Acidity distribution in GdNaY zeolite.

acidity occurs at exchanges greater than 70%, when strong acidic centers are formed. This fact must have its explanation in a partial migration of lanthanum ions into S_I sites during the calcination process. Theoretically at 85.8% exchange all available S_I sites could be occupied by La ions. However Smith[23] gives a cation distribution for two 75–80% exchanged La faujasites, as calculated from x-ray data, with 11.8 (11.7) in S_I sites, 2.5 (2.5) in S_I', and 1.5 (1.4) in S_{II} after calcination at 420°C. This would be consistent with about 70–72% lanthanum ions in S_I places, indicating the strong preference of trivalent ions to fill up the sodalite

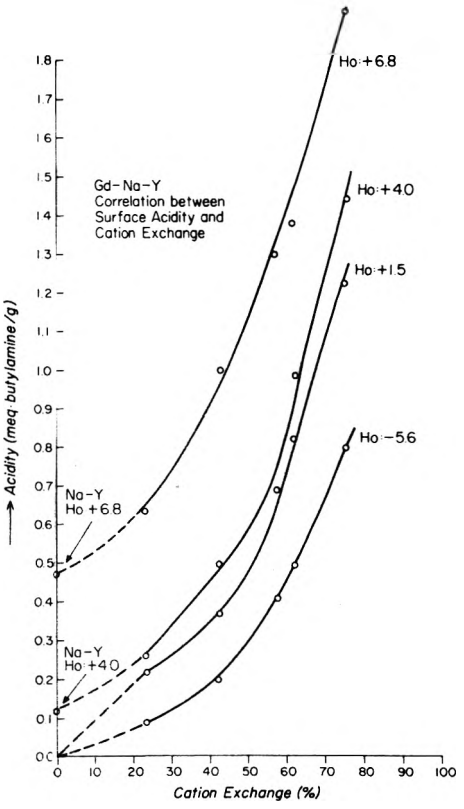

Figure 12. Comparison between milliequivalents of butylamine at H_0 +6.8, +4.0, +1.5, and −5.6 with degree of exchange in GdNaY zeolite.

cages. Lanthanum ion migration during calcination process has been reported by Bennett and Smith.[25,26] The partial occupation of S_I sites explains the higher acidity of LaNaY at lower degrees of exchange. For purposes of catalyst preparation lanthanum containing zeolites of greater than 70% must be prepared in order to obtain strongly acidic material. Tsutsumi and Takahashi[23] report a strong rise in cumene cracking activity with LaNaY zeolites of exchanges greater than 50%. Ikemoto et al.,[27] who examined surface acidity of La-Y by means of butylamine titration, also observed a strong rise in acidity at exchange levels greater than 60%. In studying the isooctane cracking activity Ballivet et al.[28] could not observe considerable changes in the activity of LaNaY in the exchange range 20–71%.

Acidity of Gd-Y. The properties of gadolinium exchanged faujasites are not reported in the literature. Comparing the acidity distribution of GdNaY and LaNaY one notes the higher values of Gd exchanged Y zeolite, especially in the range of high acidic centers (Figure 11). Figure 12 illustrates how considerable formation of strong acidic centers occurs even at low degrees of exchange. Gadolinium exchanged faujasite does not show much marked change in acidity with the occupation of the zeolite lattice by cations as the lanthanum forms. The bending of the acidity curves in H_0 ranges +1.5 and +4.0, as seen in Figure 12, indicates that above about 55% Gd exchange acidity becomes more significant. One suspects that Gd ions are occupying the S_I sites to a lesser extent than La ions, which is surprising since Gd^{3+} has a lower cation radius than La^{3+}. In repeating the calcination procedure at 500°C and above, we could observe how the number of strong acidic centers diminished. After a temperature treatment of some days at 550°C a 75% exchanged Gd zeolite did not give any colora-

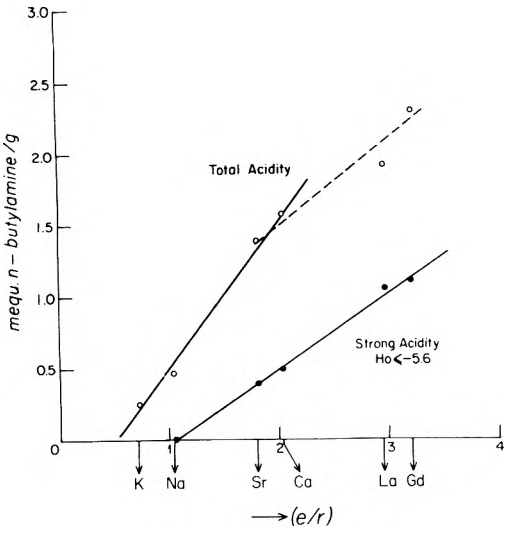

Figure 13. Correlation between physical parameter *e/r* of the exchanged cation in Y zeolites of equal degree of exchange (86%) and 500°C calcination temperature with the total acidity and amount of strong acidic centers.

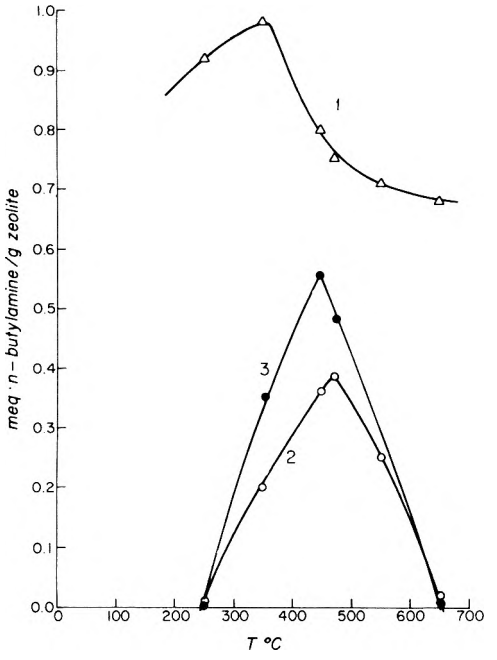

Figure 14. Dependence of titer (milliequivalents of butylamine/am) at H_0 −5.6 vs. pretreatment temperature in LaNaY (76.90% exchange) and SrCaY (86.14% exchange): △ LaNaY (1), ○ SrNaY (2), ● CaNaY (3).

tion with antraquinone. The gadolinium ions must have migrated completely into S_I sites after the rigorous temperature treatment.

Conclusions

The examples described show clearly that in accordance with the results of other and different physical methods the distribution of the cations in the zeolite's unit cell are of importance for their acidic function. The detected changes in acidity with the degree of exchange agree with the steric arrangements of the cations as given by Breck.[13] A cation migration during the calcination process into S_I sites must

TABLE V: Total Acidities in Ion Exchanged SK-40 Molecular Sieves after Calcination at 500° C

Y zeolite	Total acidity, mequiv butylamine/g	Σ acidic centers/ g of zeolite
$Ka_{86}Na_{14}$	0.26[a]	0.16×10^{21}
$Sr_{86}Na_{14}$	1.40	0.84×10^{21}
$Ca_{86}Na_{14}$	1.58	0.95×10^{21}
$La_{86}Na_{14}$	1.90[b]	1.14×10^{21}
$Gd_{86}Na_{14}$	2.30[b]	1.38×10^{21}
Na	0.47	0.28×10^{21}

[a] Interpolated at $pK_a = +6.8$. [b] Extrapolated at $pK_a = +6.8$.

be considered due to electrostatic, coordinative, and energetical considerations and has often been reported in the literature. With cations in S_{II} and S_{III} positions a strong enhancement of the acidity results, due to lower electrostatic shielding[29,30] in these positions, and to the asymmetric charge distributions caused by higher charged cations.

If this holds, a correlation between the physical parameters of the cations with their acidic function in high exchanged zeolites must be detectable. A nearly linear relationship between the *e/r* ratios of the exchanged cations and both the total acidities (maximum titer at H_0 +6.8) and the number of strong acidities could be found as shown in Figure 13. The broken line in total acidity of Figure 13 indicates a marked loss of titer if the LaNaY and GdNaY zeolites are precalcined at 500°C.

The nature of the active sites that can be Brönsted or Lewis or the cations themselves has been intensively studied, especially by infrared techniques. Due to investigation of the relations between acidity, the types of acidic centers, and the pretreatment temperatures, as mainly carried out by Ward,[3] it is known that alkaline earth exchanged zeolites show a maximum Brönsted acidity at about 450–500°C calcination temperature. No Lewis acidity was detectable in this temperature range. In contrast rare earth exchanged zeolites are reported to exhibit Lewis acidity at a 480°C pretreatment temperature.

In order to find a relation between surface acidity and pretreatment temperature, the 500°C calcined zeolites have been readsorbed with water by storing them in a desiccator over saturated NH_4Cl, as described in the Experimental Section, and after predrying under vacuum (10^{-2} Torr) at 200°C, calcining stepwise at different temperatures in the range 250–650°C. Figure 14 shows the relation of butylamine titer at $pK_a = -5.6$ with calcination temperatures of the Sr and La exchanged zeolites. LaY and CaY gave a similar picture. So CaY and SrY have maximum acidity at 450 and 470°C, respectively, while LaY gave maximum acidity at a 350°C calcination temperature pretreatment. This is in accordance with the findings of Ward[3] but not with the results of Hopkins,[31] who found maximum catalytic activity of LaY and CaY at a 350°C calcination temperature.

The titrated surface acidity in the zeolites by means of Hammett indicators therefore must mainly consist of reversible Brönsted centers. Lewis centers and the cations themselves must play an inferior role especially with the alkaline earth ions. However with rare earth exchanged zeolites (LaNaY in Figure 14) one observes a high rest-acidity of the zeolite even if the probe gets calcined up to 650°C. This may be indicative that the cation itself plays an important role in formation of the acidic function.

Calculating the approximate sum of acidic centers as has

been found in this work, by using maximum titers the results of Table V were obtained. As may be seen from Table V and Figure 13, surface acidity in rare earth exchanged Y zeolites is approximately twice that of alkaline earth exchanged ones. The scheme of formation of acidic centers, as already proposed by Hall,[32] considering the dissociative power of the cation on chemisorbed water, with $Me^{2+}(OH_2) \rightleftharpoons Me(OH)^+ + H^+$ in production of Brönsted centers, applied in our case. The dehydration studies with RE-Y zeolites, as shown in Figure 14, rather indicate that rare earth ions tend to bind one molecule of water, as proposed by Bolton.[33]

The relation of total to strong acidity in $Me^{2+}Y$ and $Me^{3+}Y$ has found to be roughly 3:1, so that about 30% of all acidic groups are strongly acidic, corresponding to >70 wt % H_2SO_4 (Figure 13).

The values obtained for the sum of acidic centers per gram of zeolite (Table V) are higher than the values given by Uytterhoeven et al.,[5] calculated from deuterium exchange reactions. This suggests that Lewis centers and cations are also involved in the adsorption of the Hammett indicators, although to a lesser extent than Brönsted centers. This already has been suggested by Walling,[9] who measured surface acidity of diverse oxides and halides. Uv spectroscopic studies of adsorbed azobenzene molecules on 500°C calcined X and Y zeolites as performed by Kiselev et al.[34] confirm this suspicion, since these authors observed bands of the adsorbed species that have been attributed to proton-donor as well as electron-acceptor acid centers. The observation in the work described here, that adsorption and neutralization kinetics of the different indicators, as well as the visually observed color changes, differed somewhat with the type of exchanged cation, is in agreement with this assumption.

Acknowledgment. The author acknowledges the assistance of Mr. P. Diaz, who carried out many of the experimental operations.

References and Notes

(1) C. L. Thomas, *Ind. Eng. Chem.*, **41**, 2564 (1949).
(2) A. G. Oblad, T. H. Millikan, and G. A. Mills, *Adv. Catal.*, **3**, 199 (1951).
(3) K. Tanabe, "Solid Acids and Bases—Their Catalytic Propterties", Academic Press, New York, N.Y., 1970.
(4) J. W. Ward, *J. Catal* **9**, 225 (1967); **10**, 34 (1968); **11**, 238 (1969); **14**, 365 (1969).
(5) J. B. Uytterhoeven, L. G. Christner, and W. K. Hall, *J. Phys. Chem.*, **69**, 2117 (1965).
(6) H. A. Benesi, *J. Am. Chem. Soc.*, **78**, 5490 (1956).
(7) O. Johnson, *J. Phys. Chem.*, **59**, 827 (1955).
(8) L. P. Hammett and A. J. Deyrup, *J. Am. Chem. Soc.*, **54**, 2721 (1932).
(9) Ch. Walling, *J. Am. Chem. Soc.*, **72**, 1164 (1950).
(10) H. S. Sherry, *Adv. Chem. Ser.*, **101**, 350 (1971).
(11) H. S. Sherry, *J. Phys. Chem.*, **72**, 4086 (1968).
(12) H. S. Sherry, *J. Colloid. Interface Sci.*, **28**, 288 (1968).
(13) D. W. Breck, *J. Chem. Educ.*, **41**, 678 (1964).
(14) H. S. Sherry, *J. Phys. Chem.*, **70**, 1158 (1966).
(15) J. D. Danforth, *J. Phys. Chem.*, **58**, 1030 (1954).
(16) Yu. N. Sidorenko, P. N. Galich, V. S. Gutyra, V. G. Lin, and I. E. Neimark, *Dokl. Akad. Nauk. SSR* (*Engl. Trans.*), **173**, 1–6, 188 (1967).
(17) J. T. Richardson, *J. Catal.*, **9**, 182 (1967).
(18) J. W. Ward, *J. Catal.*, **26**, 470 (1972).
(19) J. W. Ward, *J. Phys. Chem.*, **74**, 3021 (1970).
(20) I. M. Rouse, and F. S. Stone, Annual Meeting of the Chemical Society, Edinburgh, Apr 6–10, 1970, Preprints, Chapters 6 and 7.
(21) S. E. Tung and E. McIninch, *J. Catal.*, **10**, 166 (1968).
(22) K. Tsutsumi and H. Takahashi, *J. Phys. Chem.*, **74**, 2710 (1970).
(23) K. Tsutsumi and H. Takahashi, *J. Catal.*, **24**, 1 (1972).
(24) J. V. Smith, *Adv. Chem. Ser.*, **No. 101**, 171 (1971).
(25) J. M. Bennett and J. V. Smith, *Mater. Res. Bull.*, **3**, 633 (1968).
(26) J. M. Bennett and J. V. Smith, *Mater. Res. Bull.*, **4**, 7 (1969).
(27) M. Ikemoto, K. Tsutsumi, and H. Takahashi, *Bull. Chem. Soc. Jpn.* **45**, 1330 (1972).
(28) D. Ballivet, P. Pichat, and D. Barthomeuf, 3rd International Conference on Zeolites, Zurich, 1973, Reprints, Elsevier, Amsterdam, 1974, p 469.
(29) W. J. Mortier and H. J. Bosmans, *J. Phys. Chem.*, **75**, 3327 (1971).
(30) W. J. Mortier, H. J. Bosmans, and J. B. Uytterhoeven, *J. Phys. Chem.*, **76**, 650 (1972).
(31) P. D. Hopkins, *J. Catal.*, 12, 325 (1968).
(32) W. K. Hall, *J. Catal.*, **1**, 53 (1962).
(33) A. P. Bolton, *J. Catal.*, **22**, 9 (1971).
(34) A. V. Kiselev, D. G. Kitiashvili, and V. I. Lygin, *Kinet. Catal.*, (*Engl. transl.*), **14**, 1, 22 (1973).

Influence of Some Salts and Lower Alcohols on the Pfeiffer Effect. A Close Resemblance of the Pfeiffer Systems to Ionic Surfactant Solutions[1]

Katsuhiko Miyoshi, Yasushige Kuroda, and Hayami Yoneda*

Department of Chemistry, Faculty of Science, Hiroshima University, Hiroshima, Japan *(Received September 22, 1975)*

The influence of some inorganic salts and lower alcohols (methanol to pentanol) was examined on the following Pfeiffer-active systems at 25°; $[Zn(phen)_3]SO_4$–*d*-cinchonine hydrochloride and –*l*-strychnine hydrosulfate, $[Zn(bpy)_3]SO_4$–*d*-cinchonine hydrochloride, and $[Zn(phen)_3]SO_4$–ammonium *d*-α-bromocamphor-π-sulfonate systems in water (phen = 1,10-phenanthroline and bpy = 2,2′-bipyridine). It was found that, except for the last system, the logarithm of the Pfeiffer rotation α_p changes linearly with the logarithm of total counterion concentration C_j, α_p decreases linearly with added alcohol concentration C_A, and the logarithm of the rate of the decrease in α_p with C_A is a linear function of the number of carbon atoms in added alcohol molecules. These phenomena were interpreted to mean that added anions reduce the electrostatic repulsion between $[Zn(phen)_3]^{2+}$ or $[Zn(bpy)_3]^{2+}$ and *d*-cinchoninium or *l*-strychninium cation, thereby enhancing the Pfeiffer effect, and that added alcohol molecules penetrate into the aggregates composed of the above complex and chiral cations, thereby diminishing the Pfeiffer effect. It was proposed that the complex must come into direct contact with the chiral environment compound to exhibit the Pfeiffer effect. A close resemblance of the Pfeiffer systems to ionic surfactant solutions was also noted.

Introduction

The diastereomeric interaction between chiral compounds has been one of the most fascinating subjects of scientific study in chemistry.[2] Among them, the Pfeiffer effect,[3] a change in optical activity of a solution containing a chiral compound (called an environment compound), upon addition of a racemic mixture of a labile dissymmetric complex, is quite unique in that an enantiomerization of the complex takes place in favor of either the dextro or levo enantiomers,[4] depending on the spacial demand of the environment compound.[5] This "equilibrium shift" (enantiomerization) is usually ascribed to the diastereomeric interaction of the complex with the chiral environment compound. However, the nature of the interaction is not yet clearly elucidated. In particular, some authors[3e,6,7] have seemingly perplexing difficulty in interpreting the fact that the Pfeiffer effect is observed even for the systems of the same charge, such as the $[Zn(phen)_3]^{2+}$–*l*-stryH$^+$ and –*d*-cinchoH$^+$ systems in water, despite the electrostatic repulsion inevitably expected between them (phen = 1,10-phenanthroline, *l*-stryH$^+$ = *l*-strychninium, and *d*-cinchoH$^+$ = *d*-cinchoninium).

In our recent study on the Pfeiffer effect,[8,9] it was found that the addition of salts enhances the Pfeiffer effect to a great extent in the $[Zn(phen)_3]^{2+}$–*l*-stryH$^+$ system, and that the Pfeiffer rotation α_p[3] is slightly but definitely greater in D_2O than in H_2O (8% on an average) for the $[Zn(phen)_3]^{2+}$–*l*-stryH$^+$ and –*d*-BCS$^-$ systems (*d*-BCS$^-$ = *d*-α-bromocamphor-π-sulfonate). These findings led us to propose that added anions reduce the electrostatic repulsion between $[Zn(phen)_3]^{2+}$ and *l*-stryH$^+$, thereby facilitating their diastereomeric interaction, and that even cationic environment compounds can associate with the cationic complex $[Zn(phen)_3]^{2+}$, through the hydrophobic bonding[10] just as ionic surfactant molecules can form "micelles" against their mutual electrostatic repulsion. In this paper, the influence of some inorganic salts and lower alcohols was examined systematically on the Pfeiffer effect of the $[Zn(phen)_3]^{2+}$–*d*-cinchoH$^+$, –*l*-stryH$^+$, and –*d*-BCS$^-$, and the $[Zn(bpy)_3]^{2+}$–*d*-cinchoH$^+$ systems in water (bpy = 2,2′-bipyridine) and the convincing evidence was presented suggesting that the Pfeiffer systems bear a close resemblance to ionic surfactant solutions. Since the zinc complex systems give an instantaneous Pfeiffer rotation, they are well-suited to our purpose.

Experimental Section

Materials. Purity of commercially available *l*-stryH·$0.5SO_4$ and *d*-cinchoH·Cl was checked by both elemental analysis and optical rotation measurements. NH_4d-BCS was prepared according to the method described by Kauffman[11] and its purity was also checked. The stock solution of $[Zn(phen)_3]SO_4$ or $[Zn(bpy)_3]SO_4$ was prepared by directly dissolving $ZnSO_4·7H_2O$ and phen·H_2O or bpy in a mole ratio of 1:3 in water. Sample solutions were prepared by diluting respective stock solutions appropriately in volumetric flasks (25 ml). To these solutions were added methanol, ethanol, 1- and 2-propanol, 1- and 2-butanol, iso- and *tert*-butyl alcohol, 1-pentanol, NaCl, NaF, KCl, Na_2SO_4, and K_2SO_4, all of which were of reagent grade.

Optical Rotation Measurements. Optical rotations were measured at 405 nm in a 5-cm cell with a Union-Giken PM-71 polarimeter kept at 25 ± 0.1°.

Results and Discussion

Influence of Added Salts. In Figure 1 is plotted the Pfeiffer rotation α_p, defined as the observed rotation of the Pfeiffer system minus that of the chiral compound α_e, vs. the equivalent concentration of added salts for the $[Zn(phen)_3]^{2+}$–*l*-stryH$^+$ and –*d*-cinchoH$^+$ systems in water. Since α_e changes slightly with the salt concentration, the α_p's plotted are all values corrected for small changes in α_e. It is seen that all salts examined enhance the Pfeiffer effect to a great extent, and that anions are responsible for the increase in α_p, since the increment is dependent on the kind of anions but not of cations. This is interpreted to mean that added SO_4^{2-} or Cl^- ion effectively reduces the

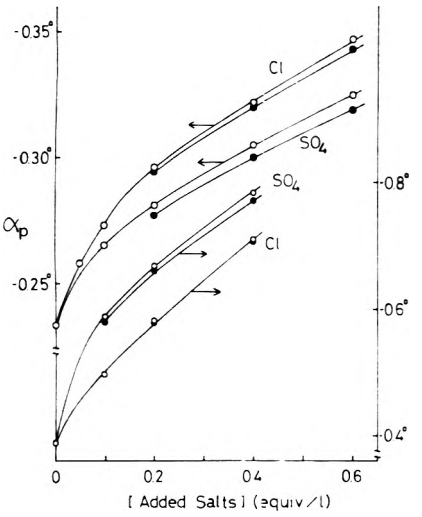

Figure 1. Plots of α_p vs. equivalent concentration of added salts for the $[Zn(phen)_3]^{2+}$ (0.01 M)–*l*-stryH$^+$ (0.01 M) and the $[Zn(phen)_3]^{2+}$ (0.015 M)–*d*-cinchoH$^+$ (0.01 M) systems (large and small circles, respectively). Open and filled circles refer to Na and K salts, respectively.

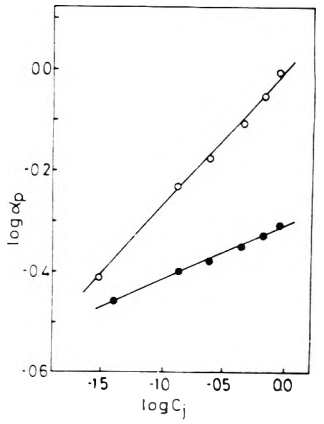

Figure 2. Plots of logarithm of α_p vs. logarithm of total equivalent concentration of counterions. Open and filled circles correspond to the $[Zn(phen)_3]^{2+}$ (0.01 M)–*d*-cinchoH$^+$ (0.01 M) and the $[Zn(phen)_3]^{2+}$ (0.015 M)–*l*-stryH$^+$ (0.01 M) systems, respectively. Their slopes are estimated to be 0.275 and 0.110, respectively by the least-squares method.

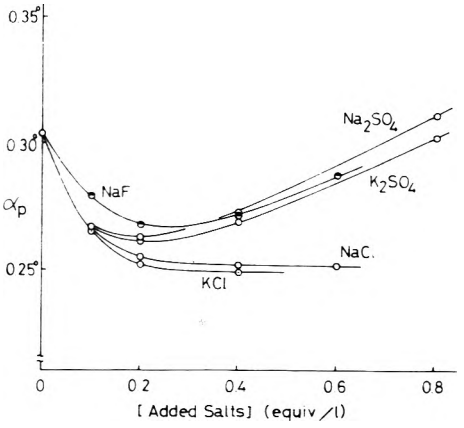

Figure 3. Plots of α_p vs. equivalent concentration of added salts for the $[Zn(phen)_3]^{2+}$ (0.01 M)–*d*-BCS$^-$ (0.02 M) system.

electrostatic repulsion between $[Zn(phen)_3]^{2+}$ and *l*-stryH$^+$ or *d*-cinchoH$^+$, thereby enhancing the Pfeiffer effect.

It is now well known that ionic surfactant molecules form aggregates called "micelles" through hydrophobic bonding against their mutual repulsion in water, and that the critical micelle concentration (cmc) is greatly influenced (lowered) by the addition of ions of the opposite charge to the surfactant ion.[12] This increased micelle stability is attributed to reduced electrostatic repulsion between surfactant ions by added ions. Thus, it is fairly plausible for $[Zn(phen)_3]^{2+}$ to form aggregates even with cationic environment compounds to exhibit additional optical activity if both cations bear hydrophobic character like surfactant molecules and if the medium is water.[13] Of course, the structure of the aggregates will be such that their repulsive force is a minimum.[14]

According to the theory for micelle formation,[12] the logarithm of the cmc changes linearly with the logarithm of the total counterion concentration C_j, i.e.,

$$\log \text{cmc} = -K_g \log C_j + \text{constant} \qquad (1)$$

where K_g is the ratio of the number of counterions to surfactant ions in the micelle. Then, log α_p is plotted in Figure 2 against log C_j (C_j in equiv/l.) for the $[Zn(phen)_3]^{2+}$–*l*-stryH$^+$ and –*d*-cinchoH$^+$ systems, to which varying amounts of Na_2SO_4 were added. A satisfactorily linear relationship[15] observed indicates that reduced electrostatic repulsion by added SO_4^{2-} ion leads to an increase in the number of the $[Zn(phen)_3]^{2+}$ ions interacting with the above chiral cation, the electrostatic repulsion between the two cations which have already associated with each other being unaffected. This will be further confirmed by examining the influence of added alcohols and salts on the Pfeiffer effect.

Salt effects on the $[Zn(phen)_3]^{2+}$–*d*-BCS$^-$ system are, on the other hand, quite different from those shown in Figure 1. When NaCl or KCl is added, α_p only decreases with salt concentration and ceases to decrease at high concentration, while with Na_2SO_4, K_2SO_4, and NaF, α_p at first decreases but begins to increase beyond ca. 0.2 equiv/l., as seen in Figure 3. Similar trends have been already found by Brasted et al.[3c] The first decrease is attributed to increased ionic strength, since ion association between a cation and an anion becomes less extensive as the ionic strength is increased according to a simple electrostatic theory.[16] The salt effect at high concentration is quite complicated and needs further study. However, we feel that the increase in α_p by Na_2SO_4, K_2SO_4, and NaF is due to their local salting-out effect,[17] since these salts are all known to salt out usual nonelectrolytes considerably[18] and both the complex and *d*-BCS$^-$ bear somewhat nonelectrolytic character.

Influence of Added Alcohols on the Pfeiffer Effect of the Same Charge. Table I lists the observed rotations at 405 nm of the Pfeiffer systems without added alcohols, where Na_2SO_4 is added to some of the systems. Code numbers are attached to identify the systems. In Figures 4 and 5 is plotted α_p as a function of molar concentration of added alcohols C_A for the $[Zn(phen)_3]^{2+}$–*d*-cinchoH$^+$ systems in water. Since α_e is slightly affected by added alcohols, α_p's plotted are all values corrected for small changes in α_e. Corresponding plots for the $[Zn(phen)_3]^{2+}$–*l*-stryH$^+$ and the $[Zn(bpy)_3]^{2+}$–*d*-cinchoH$^+$ systems are shown in Figures 6 and 7, and 8, respectively. It is seen that α_p decreases linearly with molar alcohol concentration C_A in all systems, and that the greater the Pfeiffer rotation and the longer the carbon chain in added alcohol molecules, the

TABLE I: Observed Optical Rotations at 405 nm of the Pfeiffer Systems[a]

Code no.	Racemic complex	Environment compd	Concn of added Na_2SO_4, equiv/l.	Rotation of environment compd, α_e, deg	Obsd rotation, α_{obsd}, deg	Pfeiffer rotation, α_p, deg
	$[Zn(phen)_3]SO_4$	*d*-cinchoHCl				
1a	0.01 M	0.01 M	0	+0.713	+0.326	−0.387
1b	0.01 M	0.01 M	0.1	+0.706[b]	+0.119	−0.587
1c	0.01 M	0.01 M	0.2	+0.706[b]	+0.037	−0.669
1d	0.01 M	0.015 M	0	+1.116	+0.573	−0.543
	$[Zn(phen)_3]SO_4$	*l*-stryH·0.5SO_4				
2a	0.015 M	0.01 M	0	−0.158	−0.509	−0.351
2b	0.015 M	0.01 M	0.1	−0.153[b]	−0.551	−0.398
	$[Zn(bpy)_3]SO_4$	*d*-cinchoHCl				
3a	0.03 M	0.03 M	0	+2.318	+1.980	−0.338
	$[Zn(phen)_3]SO_4$	NH_4*d*-BCS				
4a	0.01 M	0.02 M	0	+0.971	+1.275	+0.304

[a] In a 5-cm cell at 25°. [b] In the presence of Na_2SO_4.

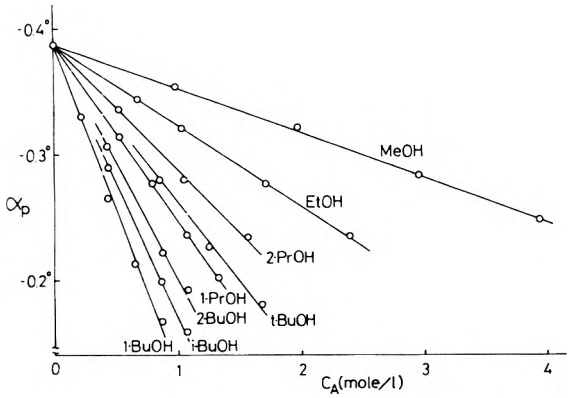

Figure 4. Plots of α_p as a function of molar concentration of added alcohols (system 1a in Table I).

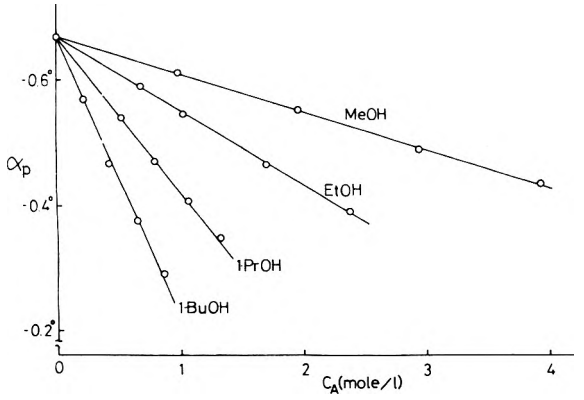

Figure 5. Plots of α_p as a function of molar concentration of added alcohols (system 1c in Table I).

steeper the slopes in these figures. These phenomena lead us to suppose that a certain fraction of added alcohols penetrates into the aggregates composed of the complex and the chiral compound, thereby diminishing the Pfeiffer effect,[19] i.e., added alcohols are distributed between water and the aggregates. Here, we coin the word "Pfeiffer oil" to denote the aggregates mentioned above, by analogy with surfactant micelles of oily character.

More than 20 years ago, Herzfeld et al.[20] and Shinoda[21] found that the cmc of ionic surfactant solutions decreases linearly with added alcohol concentration. Shinoda interpreted the effect of added alcohols in terms of the penetration of alcohol molecules into the micelle[22] and of the resulting decrease in the free energy brought about by both the entropy of mixing and the reduction of charge density on the micelle surface.[23] Thus, it seems appropriate to apply similar treatments to the Pfeiffer systems, since the complex and chiral ions must interact with each other against their mutual repulsion like ionic sufactant molecules.

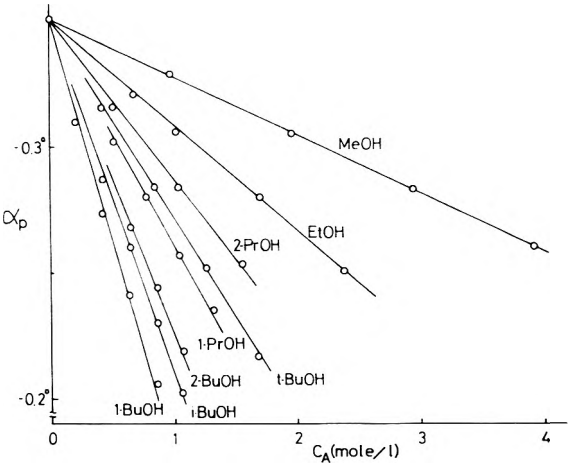

Figure 6. Plots of α_p as a function of molar concentration of added alcohols (system 2a in Table I).

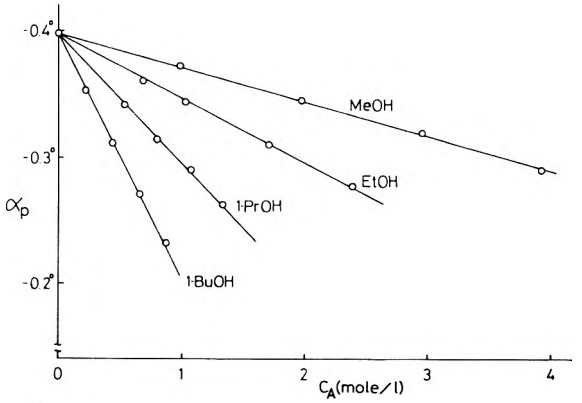

Figure 7. Plots of α_p as a function of molar concentration of added alcohols (system 2b in Table I).

TABLE II: Derived Values of $(d\alpha_p/\alpha_p\, dC_A)^a$ and $(\omega_w^{CH_2} - \omega_p^{CH_2})$

	Pfeiffer system						
	phen–*d*-cinchoH				phen–*l*-stryH		bpy–*d*-cinchoH
Added alcohol	1a	1b	1c	1d	2a	2b	3a
MeOH	9.13×10^{-2}	9.04×10^{-2}	9.07×10^{-2}	9.52×10^{-2} [b]	6.56×10^{-2}	6.73×10^{-2}	0.163
EtOH	1.67×10^{-1}	1.73×10^{-1}	1.78×10^{-1}	1.77×10^{-1}	1.22×10^{-1}	1.30×10^{-1}	0.303
1-PrOH	3.63×10^{-1}	3.60×10^{-1}	3.68×10^{-1}	3.61×10^{-1}	2.54×10^{-1}	2.55×10^{-1}	0.542
2-PrOH	2.59×10^{-1}				1.82×10^{-1}		
1-BuOH	6.71×10^{-1}	6.62×10^{-1}	6.75×10^{-1}	6.76×10^{-1}	4.89×10^{-1}	4.92×10^{-1}	0.904
2-BuOH	5.09×10^{-1}				3.54×10^{-1}		
i-BuOH	5.72×10^{-1}				3.99×10^{-1}		
t-BuOH	3.25×10^{-1}				2.25×10^{-1}		
1-PeOH							1.65
$(\omega_w^{CH_2} - \omega_p^{CH_2})$ [c]	$0.677RT$	$0.671RT$	$0.675RT$	$0.670RT$	$0.676RT$	$0.664RT$	$0.572RT$

[a] Somewhat different from the values reported earlier[1] because of the correction for α_e (see text). [b] Omitted in the calculation. [c] Calculated using the values for normal alcohols only.

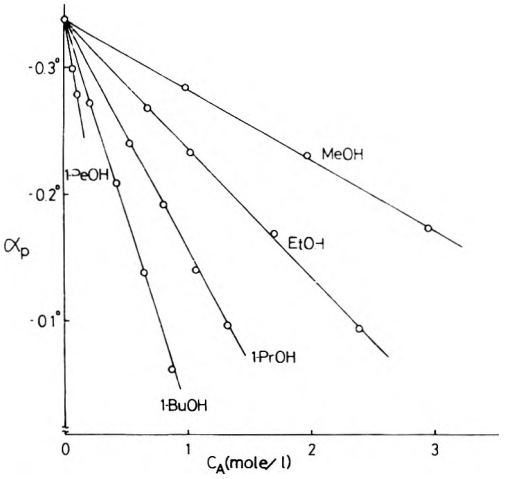

Figure 8. Plots of α_p as a function of molar concentration of added alcohols (system 3a in Table I).

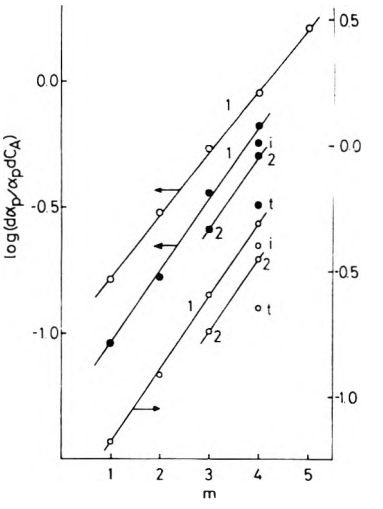

Figure 9. Plots of log $(d\alpha_p/\alpha_p\, dC_A)$ vs. the number of carbon atoms m in added alcohol molecules. Open (system 3a) and filled (system 1a) circles correspond to the left-hand scales. Small circ es (system 2a) to the right-hand scales.

According to the regular solution theory developed by Hildebrand,[24] the chemical potential of the alcohol dissolved in water, μ_w, is expressed as

$$\mu_w = \mu^0 + RT \ln x_w + m\omega_w^{CH_2} + \omega_w^{OH} \quad (2)$$

where symbols μ^0 and x have their usual meanings,[24] $\omega_w^{CH_2}$ is the enthalpy change per CH_2 group of the alcohol molecule on passing from the alcohol environment to water, ω_w^{OH} is the corresponding enthalpy change of the OH group,[25] and m is the number of carbon atoms in the alcohol molecule.[26] Then, overall enthalpy change is expressed in eq 2 as the sum of the contributions from CH_2 and OH groups instead of the solubility parameters generally used. The corresponding chemical potential in the Pfeiffer oil, μ_p, is expressed in a similar manner as

$$\mu_p = \mu^0 + RT \ln x_p + m\omega_p^{CH_2} + \omega_p^{OH} + E_{++} \quad (3)$$

where $\omega_p^{CH_2}$ and ω_p^{OH} denote the corresponding enthalpy changes from the alcohol environment to the Pfeiffer oil, and E_{++} represents the electrostatic energy change upon the penetration of the alcohol molecule into the Pfeiffer oil with positive charges, and it is assumed to be independent of m.[27,28] At distribution equilibrium, μ_p must be equal to μ_w. Then, from eq 2 and 3

$$\ln (x_p/x_w) = m(\omega_w^{CH_2} - \omega_p^{CH_2})/RT + (\omega_w^{OH} - \omega_p^{OH})/RT - E_{++}/RT \quad (4)$$

The molar alcohol concentration C_A is sufficiently low compared to that of water (55.5 M), and the amount of the alcohol transferred to the Pfeiffer oil is at most equal to or less than that of the complex or the environment compound present. Then, the mole fraction of the alcohol in water, x_w, is approximated to $C_A/55.5$. In addition, it is a reasonable assumption that the concentration of the Pfeiffer oil is proportional to the magnitude of α_p of the Pfeiffer system without added alcohols, and that of the alcohol in the Pfeiffer oil is, in turn, proportional to the change in α_p upon the addition of the alcohol. Then, the mole fraction of the alcohol in the Pfeiffer oil, x_p, is expressed as

$$x_p = K_i\, d\alpha_p/\alpha_p \quad (5)$$

where K_i is a proportionality constant and $d\alpha_p$ is the decrease in α_p when the added alcohol concentration is dC_A. Substituting the above relations, eq 4 is rearranged into

$$\ln (d\alpha_p/\alpha_p\, dC_A) = m(\omega_w^{CH_2} - \omega_p^{CH_2})/RT + (\omega_w^{OH} - \omega_p^{OH})/RT - E_{++}/RT + C_i \quad (6)$$

where C_i is a constant for a given Pfeiffer system. Equation 6 indicates that a linear relationship holds between the quantity on the left-hand side of eq 6 and m.

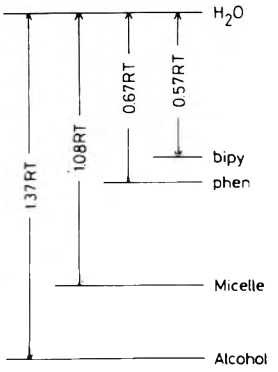

Figure 10. Energy diagram for the CH_2 group in different environments.

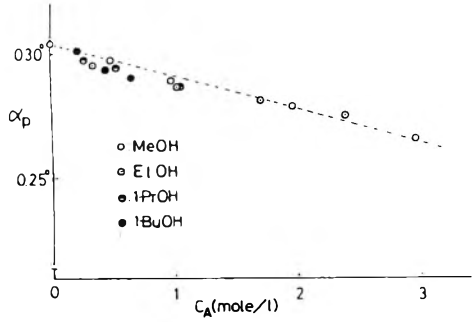

Figure 11. Plots of α_p as a function of molar concentration of added alcohols (system 4a in Table I).

In Table II are listed the values of $d\alpha_p/\alpha_p\, dC_A$, where the code numbers correspond to those in Table I. It is seen that for a given alcohol, the values of $d\alpha_p/\alpha_p\, dC_A$ are almost constant for a given system irrespective of the magnitude of its Pfeiffer rotation. This fact means that added salts enhance the Pfeiffer effect with the term E_{++} unaffected, and is consistent with our interpretation of the salt effect shown in Figures 1 and 2. In Figure 9 are shown the plots of log $(d\alpha_p/\alpha_p\, dC_A)$ vs. m for systems 1a, 2a, and 3a. It is seen that a good linear relationship is observed.[29] It should be also noted in Figure 9 that the slope for 2-propanol and 2-butanol is nearly equal to that for primary alcohols, and that α_p-decreasing order of butanol isomers follows the order of their solubilities in water. All these phenomena justify the validity of eq 6. From eq 6, the values of $(\omega_w{}^{CH_2} - \omega_p{}^{CH_2})$ corresponding to the enthalpy change of the CH_2 group on passing from the Pfeiffer oil to water were estimated by the least-squares method and are included in Table II. The value of $\omega_w{}^{CH_2}$ has been estimated to be $1.37RT$ by Shinoda et al.[30] from the solubility measurement of higher alcohols in water. In addition, the enthalpy change on transferring the CH_2 group from the micelles of usual surfactants to water has been reported also by Shinoda[21] to be $1.08RT$.[27] Then, the energy diagram for the CH_2 group in different environments is established as shown in Figure 10. It is seen that the Pfeiffer oil is not a so favorable environment to the CH_2 group as the surfactant micelles, but is much more favorable than water, and that the Pfeiffer oil of the phen complex is more "oily" than that of the bpy complex by ca. 60 cal/mol at 25°.

Influence of Added Alcohols on the $[Zn(phen)_3]^{2+}$*-d-BCS*$^-$ *System.* In Figure 11 is plotted the Pfeiffer rotation α_p of the $[Zn(phen)_3]^{2+}$-*d*-BCS^- system as a function of the molar concentration of added alcohols C_A. It is seen that α_p decreases only slightly with C_A and that the decrease seems independent of the kind of added alcohols. This suggests that added alcohols do not penetrate into the Pfeiffer oil of opposite charges, and that the slight decrease with C_A is probably due to an indirect medium effect.[31] In this case, the term E_{++} in eq 6 must be replaced by the term E_{+-} which represents the electrostatic energy change upon the penetration of alcohol molecules into the Pfeiffer oil of opposite charges, such as for the $[Zn(phen)_3]^{2+}$-*d*-BCS^- system. E_{+-} must be a positive quantity because it requires a certain amount of energy to separate a cation and an anion, while E_{++} is a negative quantity because the penetration of the alcohol molecules shields the electrostatic repulsion between the two cations. Therefore, it is the term E_{+-} that prevents added alcohols from penetrating into the Pfeiffer oil of the $[Zn(phen)_3]^{2+}$-*d*-BCS^- system, the terms $(\omega_w{}^{CH_2} - \omega_p{}^{CH_2})$ and $(\omega_w{}^{OH} - \omega_p{}^{OH})$ being superimposed on the term E_{+-} as minor contributions.

Conclusion

From the discussions presented above, it is concluded that the "Pfeiffer oil" is a much more favorable environment to the penetrating alcohol molecules than water, and that therefore, it seems necessary for the racemic complex and the chiral compound to come into direct contact with each other in order to exhibit the Pfeiffer effect, at least in the systems of the same charge. On the contrary, Bosnich and Watts[7] recently postulated that several water molecules intervene between the complex and chiral cations, with their electrostatic repulsion thereby being effectively reduced. However, if so, the value of $\omega_p{}^{CH_2}$ would be much larger, in other words, it would be almost equal to the value of $\omega_w{}^{CH_2}$, since the penetrating alcohols would find the interior of the Pfeiffer oil almost aqueous.[32] Therefore, their postulation can not be accepted.

Acknowledgment. One of the authors (K.M.) wishes to thank the Ministry of Education (Japan) for the financial support granted for this research.

References and Notes

(1) Preliminary results of this research are reported in K. Miyoshi, K. Sakata, and H. Yoneda, *J. Phys. Chem.*, **79**, 1622 (1975).
(2) E. E. Turner and M. M. Harris, *Quart. Rev., Chem. Soc.*, **1**, 299 (1947); P. E. Schipper, *Aust. J. Chem.*, **28**, 1161 (1975).
(3) (a) S. Kirschner and K. R. Magnell, *Adv. Chem. Ser.*, **No. 62**, 366 (1966); (b) S. Kirschner, N. Ahmad, and K. R. Magnell, *Coord. Chem. Rev.*, **3**, 201 (1968); (c) S. Kirschner and N. Ahmad, "Coordination Chemistry", S. Kirschner, Ed., Plenum Press, New York, N.Y., 1969, p 42; R. C. Brasted, V. J. Landis, E. J. Kuhajek, P. E. R. Nordquist, and L. Mayer, ibid., p 64; (d) S. Kirschner, *Rec. Chem. Prog.*, **32**, 29 (1971); (e) P. E. Schipper, *Inorg. Chim. Acta*, **12**, 199 (1975).
(4) S. Kirschner and N. Ahmad, *J. Am. Chem. Soc.*, **90**, 1910 (1968).
(5) S. Kirschner, *J. Indian Chem. Soc.*, **51**, 28 (1974).
(6) F. Basolo and R. G. Pearson, "Mechanisms of Inorganic Reactions", Wiley, New York, N.Y., 1958, p 275.
(7) B. Bosnich and D. W. Watts, *Inorg. Chem.*, **14**, 47 (1975).
(8) H. Yoneda, K. Miyoshi, and S. Suzuki, *Chem. Lett.*, **349** (1974); K. Miyoshi, K. Sakata, and H. Yoneda, *ibid.*, 1087 (1974).
(9) K. Miyoshi, K. Sakata, and H. Yoneda, *J. Phys. Chem.*, submitted for publication.
(10) W. Kauzmann, *Adv. Protein Chem.*, **14**, 1 (1959); G. Nemethy, *Angew. Chem., Int. Ed. Engl.*, **6**, 195 (1967).
(11) G. B. Kauffman, *J. Prakt. Chem.*, **33**, 295 (1966).
(12) K. Shinoda, "Colloidal Surfactants", K. Shinoda, B. Tamamushi, T. Nakagawa, and T. Isemura, Ed., Academic Press, New York, N.Y., 1963, Chapter 1.
(13) The hydrophobic interaction is characteristic of aqueous solutions. Confer, A. Ray, *Nature (London)*, **231**, 313 (1971).
(14) It is not yet certain whether only dimers of polyaggregates, such as micelles composed of the complex and the environment compound, are formed. However, their repulsive force is probably not so strong, since the charge of these bulky environment compounds is localized on the nitrogen atoms and the complex has low charge density.

(15) The cmc refers to the concentration of freely dispersed surfactant molecules, while α_p is proportional to the concentration of the aggregates composed of the complex and the environment compound. Therefore, it is not strange that added salts depress the cmc in the surfactant solutions, but enhance α_p in the Pfeiffer systems, through the same mechanism. Then a plot of eq 1 has a positive slope for the Pfeiffer system.
(16) R. A. Robinson and R. H. Stokes, "Electrolyte Solutions", Butterworths, London, 1959.
(17) By the term "local salting-out effect", it is meant that effective concentrations of solutes become higher as the number of water molecules available as a solvent decreases by hydration to added ions such as SO_4^{2-} and F^-. It is well confirmed that α_p is proportional to the concentration of both the racemic complex and the chiral environment compound.[3]
(18) F. A. Long and W. F. McDevit, *Chem. Rev.*, **51**, 119 (1952); P. K. Nandi and D. R. Robinson, *J. Am. Chem. Soc.*, **94**, 1299, 1309 (1972); A. Ray and G. Nemethy, *ibid.*, **93**, 6787 (1971).
(19) The addition of alcohols inevitably decreases the dielectric constant of the solution and thereby makes it electrostatically unfavorable for the two cations to associate with each other. However, such an effect may be a minor contribution to the decrease in α_p, because only a small amount of alcohols is added and the addition of urea[1] also diminishes α_p in spite of the accompanying increase in the dielectric constant of the solution. See, for example, M. F. Emerson and A. Holtzer, *J. Phys. Chem.*, **71**, 3320 (1967).
(20) S. H. Herzfeld, M. L. Corrin, and W. D. Harkins, *J. Phys. Chem.*, **54**, 271 (1950).
(21) K. Shinoda, *Bull. Chem. Soc. Jpn.*, **26**, 101 (1953); *J. Phys. Chem.*, **58**, 1136 (1954); **59**, 432 (1955).
(22) W. D. Harkins, R. W. Mattoon, and R. Mittelmann, *J. Chem. Phys.*, **15**, 763 (1947).
(23) Y. Ooshika, *J. Colloid Sci.*, **9**, 254 (1954); K. Shirahama and T. Kashiwabara, *J. Colloid Interface Sci.*, **36**, 65 (1971).
(24) J. H. Hildebrand and R. L. Scott, "The Solubility of Nonelectrolytes", 3rd ed, Reinhold, New York, N.Y., 1950.
(25) The OH group of the penetrating alcohol molecule is probably located at the exterior of the Pfeiffer oil, maintaining contact with water. Then, the environment of the OH group will not change drastically upon the penetration, i.e., the value of $(\omega_w^{OH} - \omega_p^{OH})$ will be small in magnitude.
(26) Strictly speaking, the interaction of the CH_3 group with water, alcohol, or the Pfeiffer oil should be different from that of the CH_2 group. However, their difference cannot be detected under our experimental conditions. Therefore, m can be set equal to the number of all carbon atoms in the alcohol molecule. Recently the group additivity of the enthalpy change on transferring some alcohols from one solvent to another has been discussed more quantitatively by C. V. Krishnan and H. L. Friedman, *J. Phys. Chem.*, **73**, 1572 (1969); **75**, 3598 (1971); by N. Laiken and G. Nemethy, *ibid.*, **74**, 3501 (1970); and by D. J. T. Hill and C. Malar, *Aust. J. Chem.*, **28**, 7 (1975).
(27) I. J. Lin and P. Somasundaran, *J. Colloid Interface Sci.*, **37**, 731 (1971).
(28) Recently, the enthalpy change of the CH_2 group of some alcohols on passing from nonionic micelles to water has been estimated to be $1.1RT$ which is close to the corresponding change from ionic micelles to water (see, N. Nishikido, Y. Moroi, H. Uehara, and R. Matuura, *Bull. Chem. Soc. Jpn.*, **47**, 2634 (1974)). Therefore, this assumption seems valid at least for surfactant micelles.
(29) When a considerable amount of Na_2SO_4 (e.g., 1 equiv/l.) is added, the final plot shifts upward with its slope unchanged. This is probably due to so-called salting-out[18] of alcohols by Na_2SO_4, which is attributed to the change in ω_w^{OH}. However, such an effect is not observed, when the amount of added Na_2SO_4 is less than or equal to 0.2 equiv/l., as seen in Table II. See, F. L. Wilcox and E. E. Schrier, *J. Phys. Chem.*, **75**, 3757 (1971); R. Aveyard and R. Heselden, *J. Chem. Soc., Faraday Trans. 1*, **71**, 321 (1975).
(30) K. Kinoshita, H. Ishikawa, and K. Shinoda, *Bull. Chem. Soc. Jpn.*, **31**, 1081 (1958).
(31) In general, the optical rotation of a chiral compound changes slightly with solvent.
(32) The recent NMR study by Nemethy et al. supports the view that the interior of the micelle is not exposed to water, though some conflicting results are reported by Muller et al. See. F. Podo, A. Ray, and G. Nemethy, *J. Am. Chem. Soc.*, **95**, 6164 (1973); N. Muller and R. H. Birkhahn, *J. Phys. Chem.*, **71**, 957 (1967); N. Muller and H. Simsohn, *ibid.*, **75**, 942 (1971).

Carbon-13 Hyperfine Splittings in the Electron Paramagnetic Resonance Spectra of β-Substituted Ethyl Radicals[1]

J. C. Scaiano[2] and K. U. Ingold*

Division of Chemistry, National Research Council of Canada, Ottawa, Canada K1A OR9 *(Received August 5, 1975)*

Publication costs assisted by the National Research Council of Canada

Carbon-13 α and β hfsc are reported for a number of 2-substituted ethyl, 2-substituted 1,1-di-*tert*-butylethyl, and 1,1,2,2-tetrasubstituted ethyl radicals. The $^{13}C_\beta$ hfsc are normally in the range 11–14 G and are not much affected by polar factors, by the conformation of the 2 substituent, or by distortion of the β carbon from tetrahedral geometry. The small $^{13}C_\beta$ hfsc's for $Me_3SiCH_2\dot{C}(CMe_3)_2$ (9.8 G) and for n-$Bu_3SiCH_2\dot{C}(CMe_3)_2$ (9.5 G) are attributed to distortion of the α carbon from planarity due to steric factors. The exceptionally small $^{13}C_\beta$ hfsc for $CF_3OCH_2\dot{C}(CMe_3)_2$ (6.1 G) is attributed to a homoconjugative interaction between the oxygen and the radical center.

The advent of EPR spectroscopy has made studies of the structures and conformations of alkyl radicals relatively straightforward.[3] The EPR spectra of a great many β-substituted alkyl radicals have been recorded under a variety of conditions[3-30] and there is little or no dispute about their actual conformations. However, the *reasons* that certain radicals take up particular conformations are still a matter for discussion.[6-22,25,28,29] β-Substituted alkyl radicals will normally adopt, or at least show a preference at low temperatures for either conformation 1, in which the β

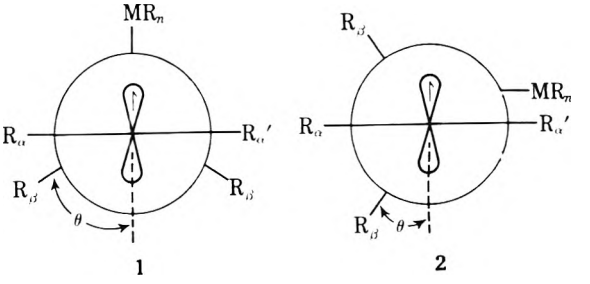

substituent, MR_n, occupies an eclipsed position relative to the C_α $2p_z$ orbital, or conformation **2**, in which the β substituent occupies a staggered position with respect to this orbital. Provided there is at least one proton attached to the β carbon, these two conformations can be easily distinguished by way of the β-hydrogen hyperfine splitting (hfsc) using the empirical relationship[3]

$$a^{H_\beta} = B_0 + B\cos^2\theta$$

where $B_0 \approx 2 \pm 2$, $B \approx 48 \pm 5$ G, and θ is the dihedral angle between the C_α $2p_z$ orbital and the C_β–H_β bond. Thus, a $R_nMCH_2\dot{C}(R_\alpha)_2$ radical in conformation **1** has a^{H_β} ca. 14 G, and in conformation **2** it has a^{H_β} ca. 38 G, and if it is freely rotating about the C_α–C_β bond it has a^{H_β} ca. 26 G.[5] For radicals that are rotating about the C_α–C_β bond under the conditions of measurement the conformation that would be preferred at sufficiently low temperatures can be determined from the temperature dependence of a^{H_β}.[5,7-15] A negative temperature coefficient for a^{H_β}, i.e., an increase in a^{H_β} with decreasing temperature, indicates a preference for conformation **2**, while a positive temperature coefficient indicates a preference for conformation **1**.

All 2-substituted 1,1-di-*tert*-butylethyl radicals, $R_nMCH_2\dot{C}(CMe_3)_2$, adopt conformation **1** for steric reasons.[27,28] However, for simple 2-substituted ethyl radicals, $R_nMCH_2\dot{C}H_2$, conformation **2** is preferred when M is carbon or oxygen, but conformation **1** is adopted when M is from row 2, 3, or 4 of the periodic table (e.g., Si, Ge, Sn, P, Cl, etc.).[4,15,17-27] The adoption by many $R_nMCH_2\dot{C}H_2$ radicals of conformation **1** has been variously attributed to the interaction of the unpaired electron with the C_β–M bond (hyperconjugation), and to its direct interaction with M via the d[6,7,9,31] or p[10,11,13,14,22-25] orbitals of M (homoconjugation). The potential importance of steric factors in inducing $R_nMCH_2\dot{C}H_2$ radicals to adopt conformation **1** has been largely ignored.

There have been relatively few measurements of $^{13}C_\alpha$ hfsc, and even fewer measurements of $^{13}C_\beta$ hfsc,[29,32-34] in carbon-centered radicals. With the hope that additional EPR data might provide some insight into the problem of the structure and conformation of substituted ethyl radicals we have determined the $^{13}C_\beta$ (and $^{13}C_\alpha$) hfsc for a number of $R_nMCH_2\dot{C}H_2$ and $R_nMCH_2\dot{C}(CMe_3)_2$ radicals.

Experimental Section

Materials. Unless otherwise indicated all reagents were commercial materials that were purified before use. Ethylene-*1,2*-$^{13}C_2$ (Merck Sharp and Dohme) had an isotopic purity of ca. 90%, the ^{12}C isotope being present mainly as ethylene-*1*-^{13}C.

Labeled 1,1-di-*tert*-butylethylene-2-^{13}C was prepared from methyl-^{13}C iodide (Merck Sharpe and Dohme, 90% isotopic purity) and 2,2,4,4-tetramethyl-3-pentanone.[35] It was purified by preparative VPC.

Methyl-*tert*-butyl peroxide was prepared by the method of Rust et al.[36] It was purified by distillation followed by passage through an alumina column.

Radical Generation. The radicals CF_3·, CCl_3·, CF_3O·, CF_3S·, Me_3Si·, *n*-Bu_3Si·, Cl_3Si·, $(EtO)_2\dot{P}{=}O$, C_6F_5·, and Cl· were generated by the methods previously reported.[29] Methoxy radicals were generated from methyl-*tert*-butyl peroxide and Cl_2CH· radicals were produced by uv irradiation of di-*tert*-butyl peroxide–dichloromethane mixtures.

EPR Spectra. The spectra were recorded on a Varian-E4 EPR spectrometer provided with a variable temperature controller and a quartz insert.

In the case of 1,1-di-*tert*-butylethylene-2-^{13}C about 10% of the ^{12}C impurity radical was usually observed. Attempts to resolve the spectra resulting from addition of C_6F_5· and Cl· to this olefin were not successful, because of the great complexity of the spectra and the limited quantity of the labeled compound.

In the case of ethylene-*1,2*-$^{13}C_2$ two (impurity) radicals resulting from the two possible modes of addition to ethylene-*1*-^{13}C were present in ca. 10% abundance each. Only the Cl_3C· radical was observed during an attempt to add Cl_3C· radicals to this ethylene. When we tried to add CH_3O· to ethylene at concentrations reasonable for an experiment with the ^{13}C labeled ethylene we obtained a radical with a^H = 13.2 G (1 H) and a^H = 3.5 G (2 H) to which we assign the structure $Me_3COOCH_2\dot{C}HOOCMe_3$. The addition of Cl· to the ethylene gave spectra too poor to be useful.

Results

The EPR parameters for the radicals observed in this work are given in Tables I and II. The sign and magnitude of the H_β temperature coefficients for the $R_nMCH_2\dot{C}H_2$ radicals (which indicate the preferred conformation of the radical, see Introduction), are also given in Table I. These were almost the only hfsc that showed any appreciable change with temperature. The present EPR parameters and those reported in the literature[7-9,14,28,29] are generally in excellent agreement.

Discussion

The C_β hfsc for alkyl radicals (Tables I and II) vary by just over a factor of 2, increasing from a low of 6.1 G for $CF_3OCH_2\dot{C}(CMe_3)_2$ to a high of ≥13.7 G for $CF_3OCH_2\dot{C}H_2$ at its low temperature limit. This change is considerably larger than the ca. 25% variation in the C_α hfsc, which increase from 37.1 G for $Me_3SiCH_2\dot{C}H_2$ to a high of 47.4 G for *n*-$Bu_3SiCH_2\dot{C}(CMe_3)_2$.[37]

For the $R_nMCH_2\dot{C}H_2$ radicals, the ranges in the magnitudes of the H_α, C_α, and C_β hfsc (1.9, 2.6, and 2.3 G, respectively) are quite small despite the changes in electronegativity and steric size of the R_nM groups and despite the various conformations of the individual radicals. We may note that when the C_α hfsc is large ($CF_3OCH_2\dot{C}H_2$) the C_β and H_α hfsc are also large, and that when the C_α hfsc is small ($Me_3SiCH_2\dot{C}H_2$) the C_β and H_α hfsc are also small. This can be simply explained on the basis that the C_α, C_β, and H_α nuclei all interact with the unpaired electron only by spin polarization (*assuming* a planar C_α) and so the magnitudes of the three hfsc depend only on the spin density in the C_α $2p_z$ orbital.[40] It is not clear whether the changes in the spin density in this orbital on going from $CF_3OCH_2\dot{C}H_2$ to $Me_3SiCH_2\dot{C}H_2$ are due to polar effects or to some other factor.

For the $R_nMCH_2\dot{C}(CMe_3)_2$ radicals, the $^{13}C_\beta$ hfsc vary much more dramatically (6.1 to 13.0 G) than the $^{13}C_\alpha$ hfsc (45.5 to 47.4 G), but with the exception of $R_nM = CF_3O$, these C_β hfsc are of generally similar magnitude to the values found for the $R_nMCH_2\dot{C}H_2$ radicals. A plot of the $^{13}C_\beta$ hfsc against the H_β hfsc for the $R_nMCH_2\dot{C}(CMe_3)_2$ radicals goes through a distinct maximum (see Figure 1).[41] We suggest that a C_β hfsc of 12–13 G and an H_β hfsc in the range 11–14 G are "normal" and correspond to a *relatively* undistorted $R_nMCH_2\dot{C}(CMe_3)_2$ radical in conformation **1**.

TABLE I: Hyperfine Splittings (Gauss) in 2-Substituted Ethyl Radicals[a]

Radical and preferred conformation		Temp range, K	$a^{H\beta}$	$a^{H\alpha}$	$a^{^{13}C\beta}$	$a^{^{13}C\alpha}$	a^{other}
$CF_3\dot{C}H_2CH_2$	2	133–173	26.2(−9)[b]	22.7	13.0	39.1	0.33 CF_3
$CF_3O\dot{C}H_2CH_2$	2	122–160	30.9(−34)[b]	22.4	13.7	39.7	1.6 CF_3
$CF_3S\dot{C}H_2CH_2$	1	141–201	12.7(+22)[b]	21.7	11.3	38.0	4.3 CF_3
$Me_3Si\dot{C}H_2CH_2$	1	128–178	17.1(+13)[b]	20.8	10.4	37.1	37.4 *Si*[c]
$Cl_3Si\dot{C}H_2CH_2$	1	122–160	16.5(+21)[b]	21.9	12.2	38.8	0.46 $SiCl_3$
$(EtO)_2(O)P\dot{C}H_2CH_2$	1	181–211	19.0(+16)[b]	22.1	11.7	*d*	90.6 *P*(−1.10)[b]
$CH_3\dot{C}H_2$[e]		95	26.9	22.4	13.6	39.1	

[a] Hfsc are given at the lowest temperature employed. [b] Temperature coefficient in mG/K. [c] Value for $Et_3SiCH_2\dot{C}H_2$ from ref 6. [d] Not resolved. [e] Data from ref 32.

TABLE II: Hyperfine Splittings (Gauss) in 2-Substituted 1,1-Di-*tert*-butylethyl Radicals and in some 1,1,2,2-Tetrasubstituted Ethyls[a]

Radical	$a^{H\beta}$	$a^{^{13}C\beta}$	$a^{^{13}C\alpha}$	a^{other}[b]
$CF_3CH_2\dot{C}(CMe_3)_2$	12.2	12.2	45.5	0.90 CF_3; 30.1 CF_3; 11.5 C_γ, 0.45 H_γ
$CCl_3CH_2\dot{C}(CMe_3)_2$	10.7	12.0	45.6	2.1 CCl_3; 34.0 CCl_3; 10.4 C_γ, 0.42 H_γ
$CHCl_2CH_2\dot{C}(CMe_3)_2$	12.8	12.1	c	0.69 H_γ
$CH_3OCH_2\dot{C}(CMe_3)_2$	11.7	12.6	c	0.6 H_γ
$CF_3OCH_2\dot{C}(CMe_3)_2$	7.2	6.1	45.5	3.0 CF_3; 0.61 H_γ
$CF_3SCH_2\dot{C}(CMe_3)_2$	10.4	9.9	c	5.0 CF_3; 0.47 H_γ
$Me_3SiCH_2\dot{C}(CMe_3)_2$	15.8	9.8	46.4	35.0 *Si*; 10.2 C_γ; 0.36 H_γ
n-$Bu_3SiCH_2\dot{C}(CMe_3)_2$	15.6	9.5	47.4	30.9 *Si*; 10.1 C_γ
$Cl_3SiCH_2\dot{C}(CMe_3)_2$	14.6	12.2	c	77.2 *Si*; 2.2 $SiCl_3$; 0.43 H_γ
$(EtO)_2(O)PCH_2\dot{C}(CMe_3)_2$	14.0	13.0	c	109.4 *P*; 10.4 C_γ; 0.42 H_γ
$HC(SiMe_3)_2\dot{C}(CMe_3)_2$	0	11.2	42.9	30.6 Si_2
$HC(Si$-n-$Bu_3)_2\dot{C}(CMe_3)_2$	0	11.5	43.5	28.7 Si_2
$HC(SiCl_3)_2\dot{C}(CMe_3)_2$	0	12.8	41	56.6 Si_2
$HC(SiMe_3)_2\dot{C}(SiMe_3)_2$	0	8.4	26.4	13.7 α-Si_2; 27.6 β-Si_2

[a] Hfsc are essentially temperature independent, see ref 29. [b] C_γ and H_γ refer to the methyls of the two *tert*-butyl groups. [c] Not resolved.

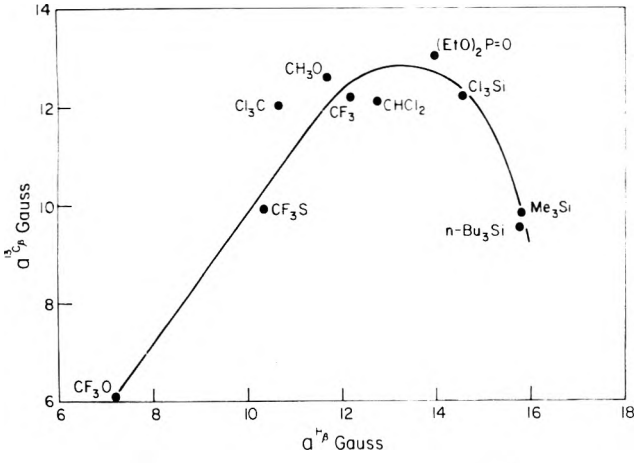

Figure 1. Plot of $^{13}C_\beta$ hfsc against H_β hfsc for $R_nMCH_2\dot{C}(CMe_3)_2$ radicals.

Some of the variation in the H_β hfsc may be due to the different R_nM groups having different effects on the ability of the β hydrogens to hyperconjugate with the unpaired electron.[42] However, large variations in the H_β and $^{13}C_\beta$ hfsc probably reflect distortion of C_β and C_α from their "normal" tetrahedral and trigonal geometries. Thus, when the R_nM group is large and bulky (e.g., Me_3Si) the radical's structure will be distorted by sterically induced repulsion between R_nM and the two *tert*-butyl groups, as indicated in **3**. This repulsion will increase the H_β hfsc since it will force these protons closer to the C_α $2p_z$ orbital. It will reduce the C_β hfsc since it will force this carbon slightly out of the C_α $2p_z$ nodal plane. This will allow positive spin to reach C_β and thus partly offset the negative spin which it acquires by spin polarization. It will also increase the C_α hfsc since the α carbon will become slightly nonplanar (thus, the C_α hfsc is ~45.5 G for R_nM = CF_3 or CCl_3, but is 46.4 for Me_3Si and 47.4 for n-Bu_3Si). In addition, this repulsion will decrease the M hfsc since the separation between M and the C_α $2p_z$ orbital will increase (thus, $a^{^{29}Si}$ = 35.0 for Me_3Si but only 30.9 for n-Bu_3Si).

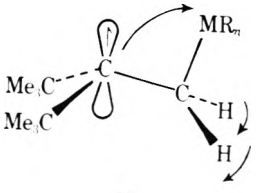

3

The $CF_3OCH_2\dot{C}(CMe_3)_2$ radical (and, to a lesser extent $CF_3SCH_2\dot{C}(CMe_3)_2$) would also appear to be distorted from structure **1**. Unusual behavior by a β-CF_3O in simple alkyl radicals has been described previously by Chen and Kochi[14] who discovered that while $CF_3OCH_2\dot{C}H_2$ has a preference for conformation **2**, the $CF_3OCH_2\dot{C}HCH_3$ radical has a preference for conformation **1**. It was suggested that this behavior was due to an enhanced homoconjugative interaction between the p orbitals on oxygen and the radical center in the secondary alkyl, this interaction being promoted by the electron-withdrawing CF_3 group. In the $CF_3OCH_2\dot{C}(CMe_3)_2$ radical, this attractive interaction will bring the β hydrogens closer to the C_α $2p_z$ nodal plane, as

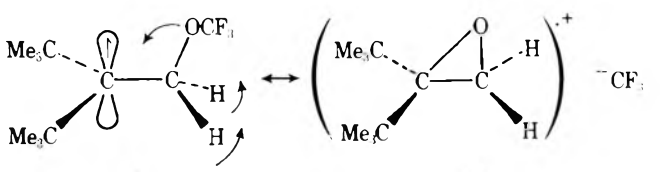

4 5

in **4**, which will reduce the H_β hfsc. In addition, the C_β hfsc will be reduced because some positive spin will reach this carbon via canonical structures such as **5**. The distortion of C_α from planarity due to this attractive interaction is probably not large since the $^{13}C_\alpha$ hfsc is the same as that found for $CF_3CH_2\dot{C}(CMe_3)_2$.

The four tetrasubstituted ethyls listed in Table II adopt conformation **2** with the β hydrogen lying in the nodal plane.[30] At least two of these radicals appear to have severely distorted tetrahedral geometry at C_β. That is, the dihedral angle, θ, between the C_β–Si bonds and the C_α $2p_z$ direction in the $HC(MR_n)_2\dot{C}(CMe_3)_2$ radicals can be calculated from the ^{29}Si hfsc given in Table II for the appropriate $R_nMCH_2\dot{C}(CMe_3)_2$ radicals ($\theta = 0°$) by the usual $\cos^2\theta$ relation.[3] The undistorted angle would be 30°. The calculated angles are 21, 16, and 31° for R_nM = Me_3Si, n-Bu_3Si, and Cl_3Si, respectively. Since these three radicals all have "normal" C_β hfsc we conclude that a simple distortion of C_β from a tetrahedral geometry is without appreciable effect on its hfsc. For the $HC(SiMe_3)_2\dot{C}(SiMe_3)_2$ radical the C_β and C_α hfsc are both about 35% smaller than the values found for the other three tetrasubstituted ethanes. This can be attributed to the known ability of α-silicon substitution to reduce the spin density at the α carbon.[29,30,38,39]

In conclusion, $^{13}C_\beta$ hfsc are disappointingly insensitive probes for identifying the structure and conformation of β-substituted ethyl radicals since they are not appreciably influenced by polar factors, by the conformation of the β substituent, nor by distortion of the β carbon. However, they may, on occasion, help to identify deviations from a planar geometry at the radical center.

References and Notes

(1) Issued as N.R.C.C. No. 15006.
(2) N.R.C.C. Visiting Scientist 1975. On leave from Departmento de Quimica y Fisica, Universidad Nacional de Rio Cuarto, Rio Cuarto, Cordoba, Argentina.
(3) (a) P. B. Ayscough, "Electron Spin Resonance in Chemistry", Methuen, London, 1967; (b) H. Fischer in "Free Radicals", Vol. II, J. K. Kochi, Ed., Wiley, New York, N.Y., 1973, Chapter 19.
(4) R. W. Fessenden and R. H. Schuler, *J. Chem. Phys.*, **39**, 2147 (1963).
(5) R. W. Fessenden, *J. Chim. Phys. Physicochim. Biol.*, **61**, 1570 (1964).
(6) P. J. Krusic and J. K. Kochi, *J. Am. Chem. Soc.*, **91**, 6161 (1969).
(7) P. J. Krusic and J. K. Kochi, *J. Am. Chem. Soc.*, **93**, 846 (1971).
(8) P. J. Krusic, P. Meakin, and J. P. Jesson, *J. Phys. Chem.*, **75**, 3438 (1971).
(9) T. Kawamura and J. K. Kochi, *J. Am. Chem. Soc.*, **94**, 648 (1972).
(10) T. Kawamura, D. J. Edge, and J. K. Kochi, *J. Am. Chem. Soc.*, **94**, 1752 (1972).
(11) D. J. Edge and J. K. Kochi, *J. Am. Chem. Soc.*, **94**, 6485 (1972).
(12) D. J. Edge and J. K. Kochi, *J. Am. Chem. Soc.*, **95**, 2635 (1973).
(13) K. S. Chen, I. H. Elson, and J. K. Kochi, *J. Am. Chem. Soc.*, **95**, 5341 (1973).
(14) K. S. Chen and J. K. Kochi, *J. Am. Chem. Soc.*, **96**, 1383 (1974).
(15) I. H. Elson, S. W. Mao, and J. K. Kochi, *J. Am. Chem. Soc.*, **97**, 335 (1975).
(16) M. C. R. Symons, *Tetrahedron*, **18**, 333 (1962).
(17) A. R. Lyons and M. C. R. Symons, *Chem. Commun.*, 1068 (1971).
(18) A. R. Lyons and M. C. R. Symons, *J. Chem. Soc., Faraday Trans. 2*, **68**, 622 (1972).
(19) A. R. Lyons and M. C. R. Symons, *J. Am. Chem. Soc.*, 93, 7330 (1971).
(20) M. C. R. Symons, *J. Am. Chem. Soc.*, **94**, 8589 (1972).
(21) M. C. R. Symons, *Tetrahedron Lett.*, **793** (1975).
(22) M. C. R. Symons, *Chem. Phys. Lett.*, **19**, 61 (1973).
(23) A. J. Bowles, A. Hudson, and R. A. Jackson, *Chem. Phys. Lett.*, **5**, 552 (1970).
(24) J. Cooper, A. Hudson, and R. A. Jackson, *Tetrahedron Lett.*, 831 (1973).
(25) I. Biddles and A. Hudson, *Chem. Phys. Lett.*, **18**, 45 (1973).
(26) T. Shiga, *J. Phys. Chem.*, 69, 3805 (1965).
(27) T. Shiga, A. Boukhors, and P. Douzou, *J. Phys. Chem.*, **71**, 3559 (1967).
(28) D. Griller and K. U. Ingold, *J. Am. Chem. Soc.*, **95**, 6459 (1973).
(29) D. Griller and K. U. Ingold, *J. Am. Chem. Soc.*, **96**, 6715 (1974).
(30) D. Griller and K. U. Ingold, *J. Am. Chem. Soc.*, **96**, 6203 (1974).
(31) J. H. Mackey and D. E. Wood, *Mol. Phys.*, **18**, 783 (1970).
(32) R. W. Fessenden, *J. Phys. Chem.*, **71**, 74 (1967).
(33) G. A. Russell, D. F. Lawson, H. L. Malkus, and P. R. Whittle, *J. Chem. Phys.*, **54**, 2164 (1971).
(34) H. Paul and H. Fishcher, *Helv. Chim. Acta*, **56**, 1575 (1973).
(35) M. S. Newmann, A. Arkell, and T. Kukunaga, *J. Am. Chem. Soc.*, **82**, 2498 (1960).
(36) F. F. Rust, F. H. Seubold, and W. E. Vaughan, *J. Am. Chem. Soc.*, **72**, 338 (1950).
(37) The $HC(SiMe_3)_2\dot{C}(SiMe_3)_2$ radical is excluded from consideration since α-silicon substituents "mop-up" a good deal of spin density and always produce very small C_α hfsc values (see, e.g., ref 29, 30, 38, and 39).
(38) A. R. Bassindale, A. J. Bowles, M. A. Cook, C. Eaborn, A. Hudson, R. A. Jackson, and A. E. Jukes, *Chem. Commun.*, 559 (1970).
(39) J. W. Cooper, D. Griller, and K. U. Ingold, *J. Am. Chem. Soc.*, **97**, 233 (1975).
(40) The orientation of R_nM with respect to the C_α $2p_z$ orbital should not affect spin polarization to the β carbon.
(41) There is no point in attempting to correlate $^{13}C_\beta$ and H_β hfsc for $R_nMCH_2CH_2$ radicals (even when they do prefer conformation 1) because of the marked temperature dependence of the H_β hfsc.
(42) See, e.g., ref 17 and J. A. Brivati, K. D. J. Root, M. C. R. Symons, and D. J. A. Tinling, *J. Chem. Soc. A*, 1942 (1969).

Interaction Forces between Tetramethyluric Acid and Aromatic Molecules. A Proton Nuclear Magnetic Resonance Study

Antonio Donesi, Livio Paolillo, and Piero Andrea Temussi*

Istituto Chimico, University of Naples, Naples, Italy *(Received August 4, 1975)*

^{1}H NMR is used to study the type of forces stabilizing complexes between 1,3,7,9-tetramethyluric acid (TMU) and aromatic hydrocarbons. Equilibrium quotients for complexes of TMU and benzene, naphthalene, phenanthrene, pyrene, and benzopyrene are calculated through chemical shift data. These data are used to evaluate a geometric model which demonstrates the predominance of dipole-induced dipole forces and excludes the existence of charge-transfer complexes in solution.

Introduction

Molecular complexes between purines and aromatic hydrocarbons have been investigated rather intensively during the last years, both in solution[1-11] and in the solid state.[12-15] The motivation of all these studies is twofold: physicochemical with respect to the forces responsible for the stabilization of molecular complexes in general and biophysical with respect to the role that some aromatic hydrocarbons are suspected to play in carcinogenesis.[16] In spite of all this effort no clear-cut conclusion on the nature of the forces responsible for complex formation has been reached. Charge-transfer forces have been invoked by many authors either on the basis of theoretical considerations[1,3] or as an interpretation of diffraction[14] and ir[15] studies in the solid state. It is significant however that other authors on the basis of similar (or even the same) experimental data discard the existence of charge transfer in favor of dipole-induced dipole interactions[12] or of dispersion forces.[9] The whole issue is complicated by the difficulty of comparing solid-state and solution studies, since most of the latter fail to give conclusive information on the geometry of the complexes. The best technique for studying molecular geometries in solution is probably NMR spectroscopy, but the only NMR study reported in the literature on purine–aromatic hydrocarbons complexes[11] deals with an unfavorable system and reaches no definite conclusion either on the geometry of the two complexes studied or on the forces responsible of complexation. Here we report a systematic NMR investigation on complexes of 1,3,7,9-tetramethyluric acid (henceforth called TMU) with aromatic hydrocarbons of increasing size, from benzene to 3,4-benzopyrene. These systems were chosen mainly for two reasons: (i) the existence of refined crystal structures of TMU complexes[12,13] can lead to a detailed comparison of solid-state and solution studies; (ii) the presence on TMU of four isolated methyl groups makes this molecule an ideal probe for the determination of the geometry of the complexes. On the other hand, TMU is substantially different from the purinic bases of nucleic acids, which makes all results of this study not directly transferable to the biological problem of carcinogenesis. It is fair to assume, however, that any new piece of information on the nature of the forces between purines and aromatic hydrocarbons may be significant in connection with all biological problems dealing with the action of aromatic hydrocarbons on nucleic acids.

Experimental Section

Materials. 1,3,7,9-Tetramethyluric acid was purchased from Fluka AG (Buchs, Switzerland) and used without further purification. Spectrograde benzene was purchased from Merck (Darmstadt), naphthalene and phenanthrene were purchased from Merck (Darmstadt), and pyrene and 3,4-benzopyrene were from Fluka AG (Buchs, Switzerland). Naphthalene, phenanthrene, and pyrene were purified by means of repeated sublimations. All other reagents were used without further purification.

Procedure. All solutions were prepared in such a way that the molar concentration of TMU remained approximately constant in each series examined, while the molality of the hydrocarbon increased up to the highest possible molar ratio (moles of hydrocarbon per mole of TMU) compatible with hydrocarbon solubility. A standard solution of TMU, 0.0302 M, in $CDCl_3$ (with 1% TMS) was used for 3,4-benzopyrene; standard solutions, always close to 0.08 M, were used for all other hydrocarbons. Appropriate amounts of the solid hydrocarbons were weighed in stoppered flasks, 1.0-ml aliquots of the standard solutions were added, and the flask was reweighed to determine the exact molality of the hydrocarbon. Benzene solutions were prepared in a slightly different way to account for the volume of added benzene. Variable volumes of standard solutions were used in this case, to keep the benzene:TMU molar ratio high enough for the relationship between shifts and molality to hold (vide infra).

^{1}H NMR spectra were recorded on a Varian Associates HA-100-15 spectrometer. Chemical shifts were measured with respect to internal TMS and are accurate to better than 0.2 Hz (the line widths of the methyl resonances being always very sharp). All measurements were made at 29.0 ± 0.5°C.

Equilibrium Quotients. It has been shown by Hanna et al.[17,19] that the upfield shifts induced by aromatic hydrocarbons upon complexation, with *N*-alkylamides, can be used to estimate both the equilibrium quotient and the shift of the pure complex in systems in which a 1:1 complex is formed. The ^{1}H NMR data can be analyzed by the equation

$$\frac{1}{(\Delta_{obsd})_i} = \frac{1}{Q\Delta_C}\frac{1}{m_i} + \frac{1}{\Delta_C}$$

where $(\Delta_{obsd})_i = \delta_0 - \delta_i$ is the observed difference in chemical shift between acceptor (TMU in our systems) protons in a solution with donor (hydrocarbon in our systems) concentration m_i and the chemical shift of the same protons in a solution without donor. Δ_C is the corresponding shift for the pure complex and Q is the equilibrium quotient for association of the complex. It is an implicit assumption of eq

TABLE I: Maximum Observed Shifts of the TMU Methyl Groups in Several Aromatic Hydrocarbons

Donor	[TMU], M	Range of donor concn, m	Max obsd shifts, Hz			
			$CH_3(9)$	$CH_3(3)$	$CH_3(7)$	$CH_3(1)$
Benzene	0.089_3	0.609–7.191	71.7	68.4	12.7	11.1
Naphthalene	0.089_8	0.453–1.660	100.2	91.5	19.1	17.7
Phenanthrene	0.081_5	0.392–1.976	172.2	159.5	49.0	46.9
Pyrene	0.089_8	0.499–1.110	218.0	202.3	65.0	60.3
3,4-Benzopyrene	0.030_2	0.120–0.216	130.5	118.9	50.3	48.2

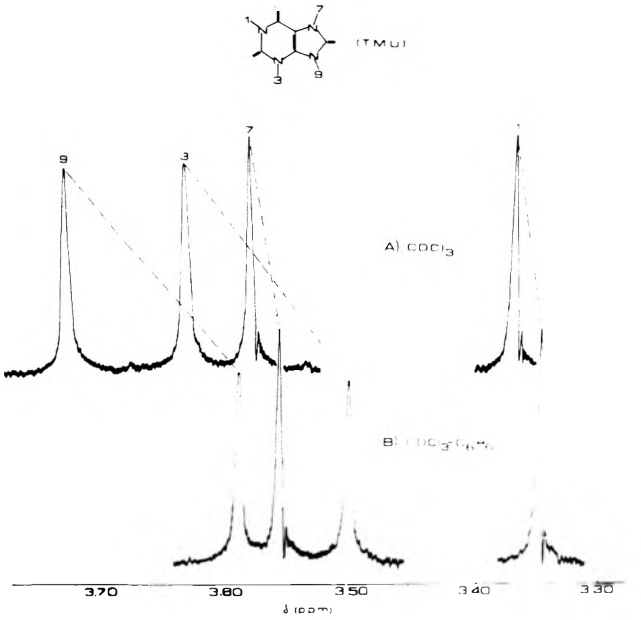

Figure 1. The 100-MHz spectra of TMU methyl groups in $CDCl_3$ (A) and in $CDCl_3$–C_6H_6 (B).

1 that the systems examined are ideal solutions, in which case Q coincides with the equilibrium constant, or that the ratio among activity coefficients of the species in solution remains constant over the concentration range studied. Another obvious requirement for eq 1 to be valid is that in all solutions $m_D \gg m_A$.

Results

The ^1H NMR spectrum of TMU, shown in Figure 1A, contains only four sharp peaks, attributable to the N-methyl groups. In spite of the simplicity of the spectrum, assignment of the resonances is not trivial since the four groups are isolated and are in very similar chemical environments. On the other hand, a correct assignment is crucial for the subsequent interpretation of donor-induced shifts in terms of possible complexes' geometries. A tentative assignment based on literature data on variously methylated xanthines[11,20] and thioxanthines[20] was confirmed by an NOE experiment. The peak at δ 3.37 can be easily assigned to 1-CH_3, since in all methylated xanthines this methyl group gives rise to the highest field peak.[20] Another characteristic feature of the NMR spectra of methylated xanthines is the marked downfield shift of the 3-CH_3 peak induced by the presence of a methyl in the 9 position.[20] Accordingly we have assigned the peaks at δ 3.58, 3.62, and 3.72 to 7-CH_3, 3-CH_3, and 9-CH_3 respectively. Such an assignment is also consistent with the line shape of the four resonances. It is shown by Figure 1A that the two downfield peaks have a slightly larger half-height width, as would be the case for a small long-range coupling and/or for a through-space interaction. These effects can be predicted in the case of TMU only for the adjacent 3-CH_3 and 9-CH_3 groups. In order to confirm the existence of a small albeit detectable interaction between these methyls we performed an NOE experiment. A small intensity enhancement was actually observed for the peak at δ 3.72 when irradiating at δ 3.62 and vice versa, while irradiation of either upfield peak had no effect on the intensities of the other resonances. Addition of aromatic hydrocarbons to N-alkylamides, as anticipated in the Experimental Section, induces large upfield shifts in the resonances of the alkyl groups.[17,19] Figure 1B shows the displacements of the TMU peaks upon addition of a small amount of benzene. A similar behavior was observed for all systems studied, with very large shifts for 3-CH_3 and 9-CH_3 and relatively smaller shifts for the other two methyls. The maximum observed shifts are reported in Table I, along with the ranges of hydrocarbon concentrations. In all cases the linear dependence of the reciprocal of the shift (Δ_{obsd}^{-1}) vs. $1/m$ was very good, so that one can rule out large contributions from complexes different from the 1:1. Figure 2 shows the graphs of the four methyl resonances for the system TMU–phenanthrene. The lines have been calculated by means of a least-squares analysis of the data that gave also the formation quotients and the limiting shifts for "pure" complexes. Table II summarizes the values of these parameters for each methyl group of every TMU–hydrocarbon pair. The main trend of the data of Table II is the monotonic increase of formation constants and limiting shifts as one goes from benzene to 3,4-benzopyrene. Such a behavior is consistent with the increase of ring current, resonance energy,[21] and polarizability[22,23] one expects from an increase in the number of benzene rings. On this basis, however, no clear-cut conclusion can be drawn on the nature of the forces stabilizing the complexes. In fact all types of forces suggested by various authors are compatible with the qualitative trend of polarizability and of resonance energy.

Our data, though, are amenable to a more detailed analysis in terms of molecular geometry which, in turn, can give us accurate information on the nature of the stabilizing forces. As mentioned in the Introduction, our systems are characterized by the presence of four "probes" (the methyl groups) well spaced on the purine molecule. Accordingly the number of relative orientations of the two interacting molecules that are consistent with the experimental shifts is very limited. Trial geometrical models of the complex between TMU and benzene were built on the basis of the atomic coordinates of TMU in the crystal structure[24] and of standard molecular parameters for benzene. The limiting shifts were calculated for each model by means of the formula of Waugh and Fessenden.[25] If we restrict our search to 1:1 complexes, there are essentially two limiting configurations we can start with, i.e., one with the molecular planes approximately parallel and another with the two

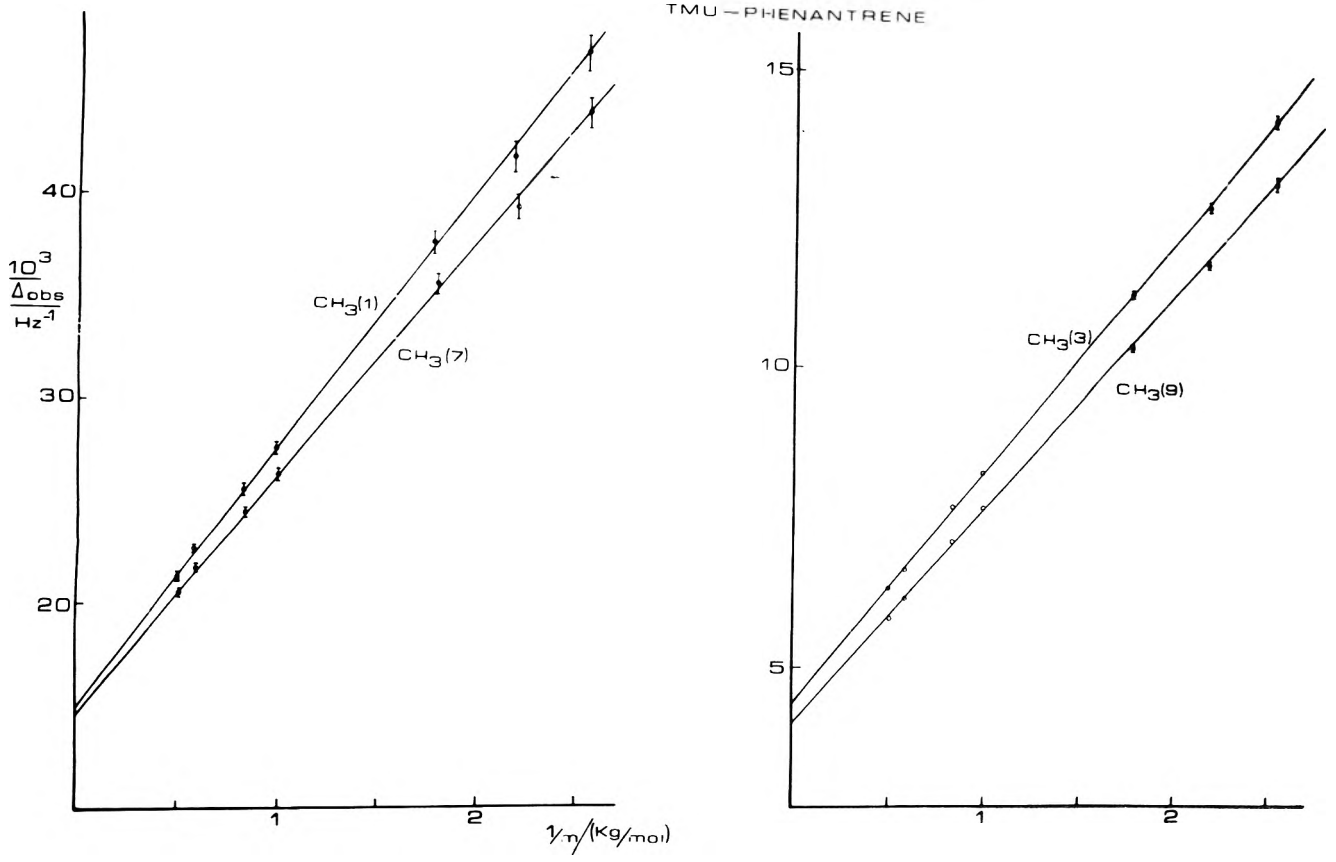

Figure 2. Plot of experimental methyl shifts of TMU vs. phenanthrene molality for the phenanthrene–TMU complex.

TABLE II: Results of a Least-Squares Analysis of Experimental Data[a]

	TMU–benzene		TMU–naphthalene		TMU–phenanthrene		TMU–pyrene		TMU–3,4-benzopyrene	
Methyl	Q, kg mol^{-1}	Δ_{AD}, Hz	Q, kg mol^{-1}	Δ_{AD}, Hz	Q, kg mol^{-1}	Δ_{AD}, Hz	Q, kg mol^{-1}	Δ_{AD}, Hz	Q, kg mol^{-1}	Δ_{AD}, Hz
1	0.29 ± 0.02	17 ± 1	0.60 ± 0.03	35 ± 2	1.20 ± 0.02	66 ± 1	1.56 ± 0.06	95 ± 2	2.2 ± 0.1	149 ± 6
7	0.22 ± 0.01	22 ± 1	0.58 ± 0.03	39 ± 2	1.28 ± 0.02	68 ± 1	1.77 ± 0.07	97 ± 2	2.8 ± 0.1	132 ± 4
3	0.212 ± 0.004	115 ± 2	0.58 ± 0.02	186 ± 8	1.12 ± 0.01	229 ± 2	1.69 ± 0.10	310 ± 7	2.8 ± 0.2	314 ± 18
9	0.217 ± 0.004	119 ± 2	0.59 ± 0.02	202 ± 8	1.14 ± 0.01	246 ± 3	1.7_6 ± 0.10	340 ± 10	2.7_7 ± 0.17	348 ± 16

[a] Computed equilibrium quotients (Q) and shifts for pure complexes (Δ_{AD}) between TMU and aromatic hydrocarbons are reported.

molecules approximately perpendicular. A sketch of the model with perpendicular arrangement is shown in Figure 3; the center of the benzene ring is coincident with the origin of the coordinate system and the molecular planes coincide with the xy and yz planes. In both models it is easy to find almost correct shifts for the 3-CH_3 and 9-CH_3 resonances by placing the center of the benzene ring equidistant from both methyl groups and at ca. 0.3 nm from the line joining them. Neither model however gives a reasonable agreement for the other two shifts. In fact, for the complex with parallel molecules, the two pairs of calculated shifts (1,7 and 3,9) are of opposite sign.

Numerous models with the molecular planes at angles (φ) ranging from 0 and 90° were examined at steps of the order of 5°, allowing for small displacements of the center of the benzene ring. The line joining methyls 3 and 9 was also slightly tilted to dissymmetrize the shifts of these methyl groups. As reported in Table III, a satisfactory agreement between calculated and observed shifts can be obtained for angles (φ) around 45° and a displacement of 0.05 nm of the benzene ring along the x axis.

TABLE III: Comparison between Experimental and Calculated Shifts of Pure Benzene–TMU Complex for Various Geometrical Arrangements[a]

	δ_1, Hz	δ_3, Hz	δ_7, Hz	δ_9, Hz
Exptl	17	115	22	119
φ = 90°	0	113	0	119
φ = 0°	−3	113	5	119
φ = 45°	4	113	29	119

[a] See text for definition of φ.

An even better agreement could be obtained by minor adjustments of the relative orientation. We decided against this refinement because on the basis of the experimental data it is not possible to exclude the presence in solution of very small amounts of other (1:1 or 2:1) complexes whose effect on the chemical shift changes might compensate the small discrepancies between calculated and observed shifts of Table III.

Before considering in detail the relationship between the geometry of the complexes and the possible intermolecular

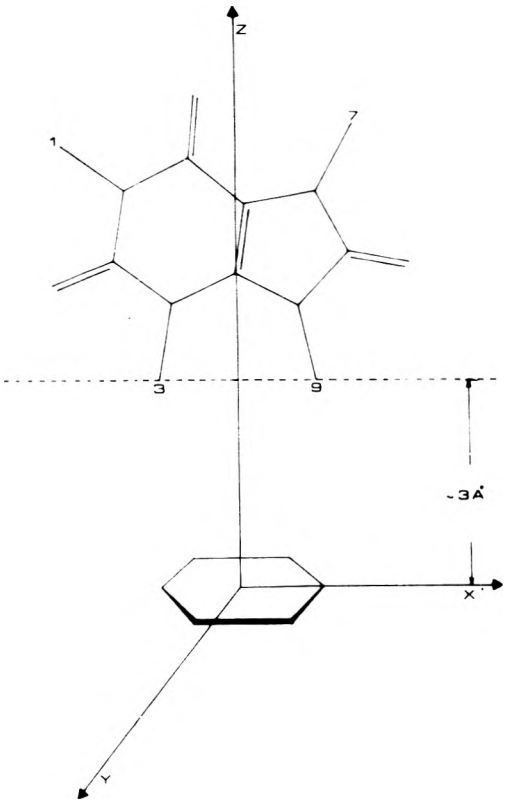

Figure 3. Model of the TMU–benzene complex with perpendicular arrangement.

forces it is appropriate to discuss the parameters measured for the other complexes in terms of the model found for the TMU–benzene complex. A quantitative calculation of the ring current shifts induced by the other hydrocarbons is not as easy as that for benzene and was not attempted since all NMR parameters can be interpreted, at least qualitatively, with reference to the benzene calculations. It can be seen from Table II that in all complexes the 3 and 9 shifts are always very similar and much larger than those of the pair 1,7. The simplest interpretation of this behavior is that the hydrocarbon is closer to the pair 3,9 and that the planes of the two molecules form an angle intermediate between 0 and 90°. It is true that for hydrocarbons with a very large area this interpretation may not be univocal, but the regular trend of the shifts along the series of the five hydrocarbons examined points to a substantial continuity of the geometrical model.

Discussion

The general features of the geometrical model we propose on the basis of the NMR results are not equally consistent with all types of forces previously proposed for these complexes. The essential feature of any charge-transfer complex is a good superposition of the π orbitals of the interacting molecules. It is clear then that any geometrical arrangement in which the planes of TMU and of the hydrocarbon are not nearly parallel cannot be stabilized by charge-transfer forces to any significant extent.

As mentioned above, such is the case for all our complexes and thus we must restrict our analysis to the other two main types of forces, i.e., dispersion forces and dipole-induced dipole forces. The latter are in fact consistent with the directions of total dipole moment and local dipole moments of TMU (vide supra) and we are inclined to attribute to these forces the major role in stabilizing the complexes studied. On the basis of our data, however, it is not possible to assess the contribution of dispersion forces with any degree of accuracy. It is only fair to say that dispersion forces may play an increasingly important role in the systems with larger hydrocarbons, but certainly dipole-induced dipole forces play an important role in all complexes studied and are responsible of the geometric arrangements compatible with the NMR shifts.

References and Notes

(1) B. Pullman and A. Pullman, *Biochim. Biophys. Acta*, **36**, 343 (1959).
(2) P. De Santis, E. Giglio, and A. M. Liquori, *Nature (London)*, **188**, 47 (1960).
(3) B. Pullman and A. Pullman, *Rev. Mod. Phys.*, **32**, 428 (1960).
(4) P. De Santis, E. Giglio, A. M. Liquori, and A. Ripamonti, *Nature (London)*, **191**, 900 (1962).
(5) A. M. Liquori, B. De Lerma, P. Ascoli, C. Botrè, and M. Trasciatti, *J. Mol. Biol.*, **5**, 521 (1962).
(6) E. Boyland and B. Green, *Br. J. Cancer*, **16**, 347 (1962).
(7) E. Boyland and B. Green, *Biochem. J.*, **84**, 54P (1962).
(8) B. L. Van Duuren, *J. Phys. Chem.*, **68**, 2544 (1964).
(9) B. Pullmann, P. Claverie, and J. Caillet, *Science*, **147**, 1305 (1965).
(10) B. L. Van Duuren, *Nature (London)*, **210**, 622 (1966).
(11) M. W. Hanna and A. Sandoval, *Biochim. Biophys. Acta*, **155**, 433 (1968).
(12) A. Damiani, P. De Santis, E. Giglio, A. M. Liquori, R. Puliti, and A. Ripamonti, *Acta Crystallogr.*, **19**, 340 (1965).
(13) A. Damiani, E. Giglio, A. M. Liquori, R. Puliti, and A. Ripamonti, *J. Mol. Biol.*, **20**, 211 (1966).
(14) I. Ikemoto, *Chem. Abstr.*, **72**, 71748 (1969).
(15) M. A. Slifkin, *Chem. Phys. Lett.*, **9**, 416 (1971).
(16) B. Pullmann, *Biopolym. Symp.*, **1**, 141 (1964).
(17) M. W. Hanna and A. L. Ashbaugh, *J. Phys. Chem.*, **68**, 811 (1964).
(18) A. A. Sandoval and M. W. Hanna, *J. Phys. Chem.*, **70**, 1203 (1966).
(19) P. J. Trotter and M. W. Hanna, *J. Am. Chem. Soc.*, **88**, 3724 (1966).
(20) D. Lichtenberg, F. Bergmann, and Z. Neiman, *J. Chem. Soc. C*, 1939 (1971).
(21) B. A. Hess, Jr., and L. J. Schaad, *J. Am. Chem. Soc.*, **93**, 2413 (1971).
(22) R. J. Le Fèvre and K. M. S. Sundaram, *J. Chem. Soc.*, 4442 (1963).
(23) C. G. Le Fèvre and R. J. W. Le Fèvre, *J. Chem. Soc.*, 1641 (1955).
(24) D. J. Sutor, *Acta Crystallogr.*, **16**, 97 (1963).
(25) J. S. Waugh and R. W. Fessenden, *J. Am. Chem. Soc.*, **79**, 846 (1957); **80**, 6697 (1958).

Analysis of the Charge Distributions in Molecules of the Types XCCH and XCN

Peter Politzer* and Stephen D. Kasten

Department of Chemistry, University of New Orleans, New Orleans, Louisiana 70122 *(Received July 21, 1975)*

A comparative analysis is presented of the electronic charge distributions in molecules of the types XCCH and XCN, using electronic density functions obtained from near-Hartree–Fock molecular wave functions. It is found that a significant fraction of the π electrons formally associated with triple bonds are actually in the neighboring bond regions; this accounts for the anomalous strength of single bonds adjacent to triple bonds. It is shown that conventional resonance structures can be misleading in their implications about bond strengths. Within each series of molecules, the charge distribution in the CCH or CN portion is found to be relatively little affected by the nature of X. For any given X, there is also a high degree of similarity in the X–C regions.

Introduction

The ethynyl group, –C≡CH, and the cyano group, –C≡N, have a certain formal similarity. They are isoelectronic, and they both contain a nominal triple bond. One may indeed view the –C≡CH group as related to –C≡N by the removal of a proton from the nitrogen nucleus to a point about 1.06 Å away, followed of course by a rearrangement of electronic charge.

It is interesting, therefore, to compare the electronic distributions in these two groups and how they are affected by various attached atoms. We have previously computed the atomic charges in a series of molecules of the types XCN and XCCH, where X included H, Li, F, Cl, and CN (in NCCN and HC_2CN).[1,2] We have also presented a preliminary discussion of the electronic charge distributions in acetylene and two of its derivatives.[3] Our purpose now is to analyze and compare in much greater detail the charge distributions in the XCN and XCCH series. We also include the diatomic species CN and CN^- in this study.

As before, electronic densities were computed from extended-basis-set self-consistent-field molecular wave functions.[4] Since these functions are of near-Hartree–Fock quality, it is anticipated that they will give good results for one-electron properties, such as electronic densities.[5]

Distribution of Electronic Charge among Internuclear Regions

A general picture of the charge distributions in the molecules being investigated, all of which are linear, can be obtained by integrating their valence electronic densities over the regions defined by hypothetical planes perpendicular to the molecular axes at the positions of the nuclei. The results, presented in Table I, represent the average quantities of valence electronic charge in the internuclear regions.

A striking feature of the data in Table I is that in every single instance of a molecule having an ostensible triple bond, the actual quantity of π charge in the internuclear region of the supposed triple bond is only 2.3–2.6 electrons. Thus, better than one-third of the four π electrons formally associated with a triple bond are *not* in the bond region. This observation has previously been made on a much more limited scale, for the molecules HCCH, FCCH, and LiCCH.[3] It appears now to be of quite general validity. To complete the picture, the quantities of π charge in the internuclear regions of CO and N_2 (which are isoelectronic with –C≡CH and –C≡N) have been computed and were found to be 2.41 and 2.49 electrons, respectively.[6]

If there were no interaction whatsoever between the atoms that form these "triple" bonds, there would still be essentially 2.0 π electrons in the internuclear regions. Thus, the formation of two π bonds involves the shifting of 0.3–0.6 electron into this region. This leaves approximately 0.8 π electron in each of the regions adjacent to the triple bond. The presence of these electrons in the neighboring bond regions should have the effect of strengthening these bonds.[7] This provides a very direct explanation of the well-known fact that a single bond is significantly strengthened by being next to a triple bond.[3,8,9] The origin of this phenomenon has been a matter of some controversy in the past.[8,9]

The data in Table I clearly indicate a considerable degree of π bonding in the X—C and H—C bonds of molecules of the types XCN and XCCH. This has been suggested before, the resonance structures $X^+{=}C{=}N^-$ and $X^+{=}C{=}C^-{-}H$ being invoked.[9,12] Since such structures are very unlikely when X is H, it might be anticipated that the C≡N and C≡C bonds in HCN and HCCH would be shorter and stronger than the corresponding bonds in the other XCN and XCCH molecules, into which the above resonance structures introduce some "double-bond" character. Instead, Table II shows that the C–N bond length in HCN is virtually identical with its values in the other XCN molecules, while the force constants are quite similar. The same holds true for the C–C bond lengths and force constants in HCCH and the XCCH molecules. The fact that the C–N and C–C bond lengths and force constants in HCN and HCCH differ so little from their values in the other XCN and XCCH molecules has been cited as evidence indicating that there is not a significant degree of π bonding in the X–C and H–C bonds in the XCN and XCCH series.[9,13] The integrated charge densities in Table I show, however, that there is inherently a certain amount of π bonding in the regions adjacent to a triple bond, even if the neighboring atom is a hydrogen. Since this is intrinsically associated with a triple bond, it does not imply any weakening of the latter, relative to some other existing situation. Conventional resonance structures are therefore misleading in regard to the XCN and XCCH molecules, in that they do require that any π contributions to the X–C bonds be accompanied by weakening of the C≡N or C≡C bonds.[14]

TABLE I: Quantities of Valence Electronic Charge in Molecular Regions

Diatomic molecules, AB		Molecular regions A	B	
CN	σ	1.06	2.14	1.79
	π	0.64	2.46	0.90
CN^-	σ	1.83	2.30	1.87
	π	0.51	2.42	1.07

Triatomic molecules, ABC		Molecular regions A	B	C	
HCN	σ	0.39	1.60	2.17	1.84
	π	0.02	0.69	2.42	0.86
FCN	σ	1.81	2.26	2.11	1.81
	π	1.82	2.75	2.52	0.91
ClCN	σ	1.67	2.36	2.15	1.83
	π	1.85	2.80	2.47	0.88
OCN^-	σ	1.83	2.21	2.15	1.82
	π	1.61	2.64	2.59	1.16
SCN^-	σ	1.69	2.30	2.19	1.83
	π	1.68	2.74	2.52	1.05

Four-atom molecules, ABCD		Molecular regions A	B	C	D	
NCCN	σ	1.84	2.15	2.02	2.15	1.84
	π	0.83	2.41	1.53	2.41	0.83
HCCH	σ	0.42	1.59	1.99	1.59	0.42
	π	0.03	0.80	2.34	0.80	0.03
FCCH	σ	1.82	2.27	1.92	1.58	0.41
	π	1.85	2.83	2.45	0.84	0.03
LiCCH	σ	0.03	1.87	2.08	1.59	0.44
	π	0.01	0.80	2.29	0.86	0.04
ClCCH	σ	1.68	2.36	1.96	1.58	0.41
	π	1.88	2.87	2.40	0.81	0.03

Five-atom molecules, ABCDE		Molecular regions A	B	C	D	E	
NCCCH	σ	1.84	2.15	2.03	1.98	1.60	0.40
	π	0.86	2.43	1.63	2.32	0.74	0.02

A somewhat similar situation exists in the cases of N≡C—C≡C—H and N≡C—C≡N. The C—C single bonds in both molecules are shorter than the average C—C single bond length, a fact which is explained in terms of conjugation between the triple bonds. But the appropriate resonance structures indicate that there should be a concomitant lengthening of the triple bonds. This does not occur, as can be seen from Table II by comparing these C≡N and C≡C bond lengths with those in HCN and HCCH. Table I shows that the quantities of both σ and π charge in the triple-bond regions of NCCCH and NCCN are almost exactly the same as in the corresponding regions in HCN and HCCH, which is consistent with the bond lengths being so nearly identical. Table I also shows the same phenomenon occurring here as has been discussed above; about 0.7–0.8 π electron is provided to the C–C region in each molecule from each of its neighboring triple bonds.[15] This added π bonding is presumably the reason for the shortening of the C–C single bond. This explanation of the effect of conjugated triple bonds upon the intervening single bond, as arising from the π charge inherently outside of the triple bond region, is more accurate than invoking resonance structures, since it does not involve the incorrect implication that there is a simultaneous lengthening of the triple bonds.[16]

TABLE II: Experimentally Determined Bond Properties

Bond	Molecule	Bond length,[a] Å	Force const, mdyn/Å
C–H	HCN	1.063	5.62,[b] 5.80,[c] 6.257[d]
C–H	HCCH	1.059	5.85[c]
C–H	FCCH	1.053	5.987,[e] 6.2[c]
C–H	ClCCH	1.052	5.961[e]
C–H	HCCCN	1.058	
C–H	C_2H_6	1.094	4.79[f]
C–C	HCCH	1.205	15.68,[g] 15.85[c]
C–C	FCCH	1.198	15.4,[c] 15.80,[h] 16.62[e]
C–C	ClCCH	1.205	15.81[e]
C–C	HC–CCN	1.205	
C–C	HCC–CN	1.378	
C–C	NCCN	1.380	
C–C	C_2H_6	1.534	4.50,[f] 4.92[g]
F–C	FCCH	1.279	8.213,[e] 8.64,[h] 8.8[c]
F–C	FCN	1.262	8.41,[i] 8.70[j]
F–C	C_2H_5F	1.375	5.96[k]
Cl–C	ClCCH	1.632	5.255,[e] 5.4[c]
Cl–C	ClCN	1.629	4.74,[i] 4.97,[b] 5.2[c]
Cl–C	C_2H_5Cl	1.777	3.64[k]
C–N	HCN	1.155	17.9,[c] 18.68,[d] 18.85[b]
C–N	FCN	1.159	17.44,[j] 17.92[i]
C–N	ClCN	1.155	16.7,[c] 17.92,[i] 18.45[m]
C–N	HCCCN	1.159	
C–N	CN	1.177	16.29[g]
C–N	NCCN	1.16	

[a] All bond lengths are taken from L. E. Sutton, Ed., *Chem. Soc., Spec. Publ.*, No. 18, Suppl. (1965), except those in FCN, FCCH, and HCCCN, which are from J. K. Tyler and J. Sheridan, *Trans. Faraday Soc.*, 59, 2661 (1963). [b] G. A. Thomas, J. A. Ladd, and W. J. Orville-Thomas, *J. Mol. Struct.*, 4, 179 (1969). [c] Reference 12. [d] H. C. Allen, E. D. Tidwell, and E. K. Plyler, *J. Chem. Phys.*, 25, 302 (1956). [e] K. Venkateswarlu and M. P. Mathew, *Z. Naturforsch., B*, 23, 1296 (1968). [f] B. L. Crawford and S. R. Brinkley, *J. Chem. Phys.*, 9, 69 (1941). [g] T. Shimanouchi in "Physical Chemistry," Vol. IV, D. Henderson, Ed., Academic Press, New York, N.Y., 1970, Chapter 6. [h] Reference 11. [i] Reference 9. [j] E. E. Aynsley and R. Little, *Spectrochim. Acta*, 18, 667 (1962). [k] W. G. Penney and G. B. B. M. Sutherland, *Proc. R. Soc. London, Ser. A*, 156, 654 (1936). [l] Y. Morino and E. Hirota, *Bull. Chem. Soc. Jpn*, 31, 423 (1958). [m] W. J. Orville-Thomas, W. J. Jones, and U. Opik, *J. Chem. Soc.*, 1625 (1959).

The preceding conclusions about the characters of the bonds in the XCN and XCCH molecules are fully supported by the calculated bond orders. These were obtained by extending to these linear polyatomic molecules an operational definition of bond order which was proposed originally for diatomic species.[17] This definition

$$\text{bond order} = 0.55747\sqrt{k/R}$$

requires only the force constant, k (mdyn/Å), and the bond length, R (Å), of the bond in question; it involves no wave function whatsoever. In Table III are listed the bond orders calculated using the experimental bond lengths and force constants given in Table II. The bond orders for all C≡N and C≡C bonds are in the range 2.00–2.27. This is fully consistent with the numbers of π electrons found in these bond regions, which suggest that relative to the σ bonds, the π bonds are more like half-bonds. As anticipated, the C≡N and C≡C bond orders in HCN and HCCH are exactly the same as in the other XCN and XCCH molecules, confirming the absence of any resonance-caused weakening of the latter. Finally, the bond orders of the X—C bonds

TABLE III: Calculated Bond Orders

Bond	Molecule	Bond order[a]	Bond	Molecule	Bond order[a]
C–H	HCN	1.28–1.35	F–C	FCN	1.44–1.46
C–H	HCCH	1.31	F–C	C_2H_5F	1.16
C–H	FCCH	1.33–1.35	Cl–C	ClCCH	1.00–1.01
C–H	ClCCH	1.33	Cl–C	ClCN	0.95–1.00
C–H	C_2H_6	1.17	Cl–C	C_2H_5Cl	0.80
C–C	HCCH	2.01–2.02	C–N	HCN	2.19–2.25
C–C	FCCH	2.00–2.08	C–N	FCN	2.16–2.19
C–C	ClCCH	2.02	C–N	ClCN	2.12–2.23
C–C	C_2H_6	0.95–1.00	C–N	CN	2.07
F–C	FCCH	1.41–1.46			

[a] The range of bond orders presented in this table for any given bond corresponds to the full range of force constants listed for that bond in Table II.

are invariably significantly greater when these are adjacent to a C≡N or C≡C bond than in the reference molecules (C_2H_6, C_2H_5F, and C_2H_5Cl) which have no multiple bonds. It is very gratifying that conclusions which had been reached by integrating electronic densities obtained from ab initio molecular wave functions are in such good agreement with those resulting from a completely independent consideration of experimentally determined bond lengths and force constants.

Effects of Substituents on Charge Distributions

In this section, the emphasis will be on the charge distributions in the C≡N and C≡CH portions of the XCN and XCCH molecules, taking everything to the right of the carbon nucleus as a single unit. Table IV gives the quantities of π and σ charge in these portions, obtained by simply summing the appropriate values in Table I. In general, these charges are quite similar in all of the cases, whether XCN or XCCH and regardless of the identity of X. For a given X, the amounts of σ charge are seen to be almost identical for XCN and XCCH. The amounts of π charge differ somewhat more, by 0.10–0.15 electron, with the XCN value always being the greater one. This is consistent with the greater electron-attracting power of the cyano group that has been noted, for example, by Brown.[18] The relative electron-attracting powers of the C≡N and C≡CH groups are particularly evident in the data for the molecule HC≡CC≡N, where the two groups are in direct competition with each other. Table IV shows that the quantity of σ charge is essentially the same in the C≡N and C≡CH portions of this molecule but that there is significantly more π charge (0.2 electron) in the C≡N portion.

The effects of substituents upon electronic distributions are often described in terms of various "substituent constants".[19] One of these, denoted σ_R^0, is interpreted as being a measure of the tendency of a substituent to donate electronic charge to the rest of the molecule through some sort of conjugative or resonance effect. In the case of the XCN and XCCH molecules, this would presumably be described in terms of contributions from the structures $X^+{=}C{=}N^-$ and $X^+{=}C{=}C^-{-}H$. An alternate view which has recently been proposed is that instead of charge being donated by the substituent, the effects observed are actually due to the strong repulsive interaction between electrons of the substituent and the π electrons of the remainder of the molecule.[20] Our present results seem to support this second view. If the indicated resonance structures did indeed play a key role, then the quantities of π charge in the X—C internuclear regions should show the same trend as the corresponding σ_R^0 values. Tables I and V show that this is not the case. However the quantities of π charge in the C≡N and C≡CH portions of the molecules (Table IV) do correlate linearly with σ_R^0, as is shown in Figure 1; the correlation coefficients are 0.983 and 0.979, respectively. This correlation can be interpreted as reflecting the repulsion between the electrons of the substituent and the π electrons of the –C≡N or –C≡CH group, which pushes the latter away from X and into the C≡N or C≡CH region. From Figure 1 and the data for HC≡CC≡N and LiC≡CH in Table I, σ_R^0 for the –C≡CH group is predicted to be 0.00, while for the Li atom the predicted σ_R^0 is −0.09.

TABLE IV: Quantities of σ and π Valence Electronic Charge and Positions of Centers of Charge in C≡N and C≡CH Portions of XCN and XCCH Molecules[a]

Molecule	Quantities of valence electronic charge		Positions of centers of valence electronic charge[b]	
	σ	π	σ	π
CN	3.94	3.36	2.031	1.602
HCN	4.01	3.29	2.026	1.564
FCN	3.92	3.43	2.039	1.587
ClCN	3.97	3.35	2.034	1.575
NCCN[c]	3.99	3.23	2.030	1.546
HCCH	3.99	3.17	2.392	1.605
FCCH	3.91	3.32	2.386	1.599
LiCCH	4.10	3.20	2.373	1.664
ClCCH	3.96	3.24	2.396	1.607
NCCCH[d]	3.97	3.09	2.379	1.552
HCCCN[d]	3.99	3.28	2.029	1.560

[a] The C≡N portion of an XCN molecule includes everything to the right of the hypothetical plane through the carbon nucleus. The C≡CH portion of XCCH includes everything to the right of the hypothetical plane through the carbon on the left. [b] These positions are given in atomic units relative to the carbon which begins the C≡N or C≡CH portion of the molecule. [c] NCCN is regarded as a molecule of the XCN type, in which X = CN. [d] HCCCN is included in this table twice, first as an XCCH molecule (X = NC) and then as an XCN molecule (X = HCC).

TABLE V: Substituent Constants[a]

Substituent, X	σ_R^0	Substituent, X	σ_R^0
F	−0.34	H	0.00
Cl	−0.23	CN	+0.13

[a] S. Ehrenson, R. T. C. Brownlee, and R. W. Taft, in *Prog. Phys. Org. Chem.*, 10 (1973).

Table IV also includes the calculated positions of the centers of both σ and π charge in the C≡N and C≡CH portions of the molecules. Within each series of molecules, these vary very little, even less than do the integrated quantities of charge in these regions, despite the fact that X includes such different entities as Li, H, F, and CN. The position of the center of σ charge in the C≡N portion varies only from 2.026 to 2.039 au and from 2.373 to 2.396 au in the C≡CH portion. The π charge is more mobile; its center shifts over ranges of 0.06 and 0.11 au, respectively.

Charge Distributions in the X–C Portions

It is interesting to compare, for a given substituent X, the charge distributions in the X–C portions of XCN and XCCH. (These are the entire regions of the molecules up to the boundary plane through the carbon nucleus.) The

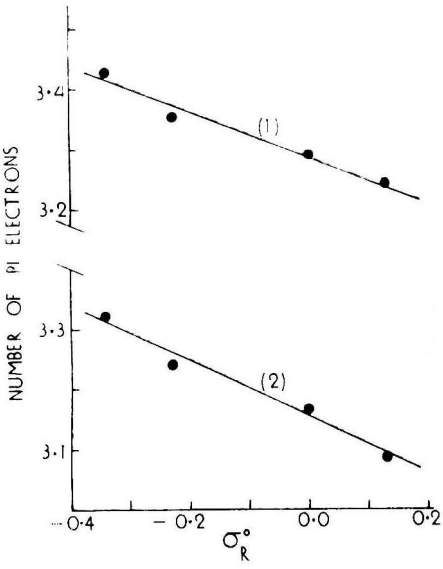

Figure 1. The relationship between the quantity of π-electronic charge in the C≡N or C≡CH region (Table IV) and the substituent constant σ_R^0 of substituent X (Table V). Line (1) is for XCN molecules; line (2) is for XCCH molecules. From left to right, the points are for X = F, X = Cl, X = H, and X = CN.

TABLE VI: Positions of Centers of Charge in X–C Portions of XCN and XCCH Molecules and in H–C Portions of XCCH Molecules

Molecule	Portion[a]	Positions of centers of valence electronic charge[b] σ	π
FCN	F–C	2.145	2.068
FCCH	F–C	2.177	2.076
ClCN	Cl–C	2.599	2.636
ClCCH	Cl–C	2.618	2.613
NCCN	NC–C	3.515	3.239
NCCCH	NC–C	3.518	3.204
HCN	H–C	1.337	0.599
HCCH	H–C	1.351	0.639
FCCH	H–C	1.345	0.635
ClCCH	H–C	1.342	0.642
LiCCH	H–C	1.376	0.673
NCCCH	H–C	1.331	0.600

[a] The X–C and H–C portions include everything up to a hypothetical plane through the nucleus of the carbon shown in the second column as forming the boundary of the region. [b] The distances are given in atomic units, measured from the carbon which forms the boundary of the portion of interest.

quantities of electronic charge in these portions of the molecules can be seen from Table I; the positions of the centers of charge are given in Table VI. These tables show that, for a given X, both the quantities of charge and the positions of the centers of charge are very similar in the X–C portions of XCN and XCCH. This close similarity is reflected in the experimentally determined bond properties given in Table II and in the bond orders in Table III.

A much more extensive comparison is possible for those X–C regions where X = H, since it can encompass not only HCN and HCCH but also the H–C portions of the other ethynyl molecules. These data are included in Table VI. A high degree of similarity is again observed, particularly with respect to the σ electrons. This relative insensitivity of the H–C portion of the XCN and XCCH molecules to the remainder of the molecule has been noted previously;[21-23] it can also be seen in the bond properties in Table II.

The Diatomic CN and CN^- Species

It is interesting to compare the electronic distributions in CN and CN^-, both with each other and with the results found for the XCN molecules; the latter comparison provides some insight into the effect of X. When CN gains an electron to form CN^-, the added electron occupies a σ molecular orbital. Table I shows the rearrangement of charge that accompanies this process. The primary effect is an increase of about 0.76 electron unit of σ charge in the carbon lone-pair region. Perhaps in response to this, the π charge becomes more polarized toward the nitrogen end.

Table I shows that the charge distributions in the CN portions of the neutral XCN molecules more closely resemble that in CN than that in CN^-. This suggests a relatively low degree of ionic character in the X–CN bond, which is consistent with the previously calculated atomic charges in the neutral XCN molecules.[1] The net charge of the CN portion was never found to be more negative than −0.18 (which was in HCN).

HCN is of particular interest in the present discussion because it is isoelectronic with CN^-. Its charge distribution therefore shows what rearrangement of charge takes place in CN^- when a proton is brought to a distance of 1.06 Å from the carbon, on the molecular axis. As anticipated, there occurs a general polarization of electronic charge toward the proton, although the total amount of charge moving past the hypothetical plane through the carbon is only 0.36 electron. More than half of this reflects movement of π charge out of the nitrogen lone-pair region. The data show that the proton approaches the carbon up to a point at which it has already penetrated the electronic charge in the carbon lone-pair region to quite a significant extent; in HCN there is 0.39 σ electrons behind the proton.

Acknowledgment. We are grateful to Mr. Jordan C. Band and his associates for their support of this work. We also thank the University of New Orleans Computer Research Center for its financial assistance (NSF Grant No. GJ-131).

References and Notes

(1) P. Politzer and P. H. Reggio, *J. Am. Chem. Soc.*, **94**, 8308 (1972).
(2) P. Politzer and A. Politzer, *J. Am. Chem. Soc.*, **95**, 5450 (1973).
(3) P. Politzer and R. R. Harris, *Tetrahedron*, **27**, 1567 (1971).
(4) A. D. McLean and M. Yoshimine, "Tables of Linear Molecule Wave Functions", IBM Corp., San Jose, Calif., 1967. The wave functions for CN and CN^- were very kindly provided by Professor Paul E. Cade.
(5) L. Brillouin, *Actual. Sci. Ind.*, **No. 71, 159, 160** (1933–1934); J. Goodisman, *J. Chem. Phys.*, **38**, 304 (1963).
(6) The CO wave function was taken from ref 4; the N_2 function was from P. E. Cade, K. D. Sales, and A. C. Wahl, *J. Chem. Phys.*, **44**, 1973 (1966).
(7) R. P. Feynman, *Phys. Rev.*, **56**, 340 (1939); T. Berlin, *J. Chem. Phys.*, **19**, 208 (1951).
(8) E. B. Wilson, Jr., *Tetrahedron*, **17**, 191 (1962), and references cited therein.
(9) E. J. Williams and J. A. Ladd, *J. Mol. Struct.*, **2**, 57 (1968).
(10) B. C. Curran and H. H. Wenzke, *J. Am. Chem. Soc.*, **59**, 943 (1937); P. A. Casabella and P. J. Bray, *J. Chem. Phys.*, **28**, 1182 (1958); J. Sheridan, J. K. Tyler, E. E. Aynsley, R. E. Dodd, and R. Little, *Nature (London)*, **185**, 96 (1960).
(11) J. K. Brown and J. K. Tyler, *Proc. Chem. Soc., London*, 13 (1961).
(12) G. R. Hunt and M. K. Wilson, *J. Chem. Phys.*, **34**, 1301 (1961).
(13) J. Duchesne, *J. Chem. Phys.*, **19**, 246 (1951).
(14) The important bonding effect that π electrons can have even in a region having no formal π bond has recently been emphasized by F. L. Hirshfeld and S. Rzotkiewicz, *Mol. Phys.*, **27**, 1319 (1974).
(15) It has been suggested, on the basis of spin-coupling constant measure-

ments, that there is an appreciable degree of π bonding in a C–C "single" bond which separates two multiple bonds: K. Frei and H. J. Bernstein, *J. Chem. Phys.*, **38**, 1216 (1963).
(16) A similar interpretation may be valid in the case of conjugation between double bonds. Thus, for example, while the C_2–C_3 distance in 1,3-butadiene is somewhat less than a typical C—C single bond, 1.48 vs. 1.54 Å, the C_1–C_2 and C_3–C_4 distances are almost exactly the same as the C=C bond length in ethylene, 1.336 vs. 1.337 Å, respectively: L. E. Sutton, Ed., *Chem. Soc., Spec. Publ.*, **No. 18**, Suppl. (1965).
(17) P. Politzer, *J. Chem. Phys.*, **50**, 2780 (1969); **51**, 459 (1969). The present extension of the original definition is supported by the recent work of N. K. Ray and R. G. Parr, *J. Chem. Phys.*, **59**, 3934 (1973).
(18) T. L. Brown, *J. Chem. Phys.*, **38**, 1049 (1963).
(19) P. R. Wells, S. Ehrenson, and R. W. Taft, in "Progress in Physical Organic Chemistry", Vol. 6, A. Streitwieser and R. W. Taft, Eds., Interscience, New York, 1968.
(20) P. Politzer and J. W. Timberlake, *J. Org. Chem.*, **37**, 3557 (1972).
(21) V. W. Weiss and W. H. Flygare, *J. Chem. Phys.*, **45**, 8 (1966).
(22) G. A. Thomas, G. Jalsovszky, J. A. Ladd, and W. J. Orville-Thomas, *J. Mol. Struct.*, **8**, 1 (1971).
(23) There has recently been made a detailed comparative study of various contributions to the bond energies in a series of nitriles, many of which also contain a C≡C bond: J. B. Moffat and K. F. Tang, *J. Phys. Chem.*, **79**, 654 (1975). It is interesting and pleasing to note how consistent these results are with the analysis and conclusions presented in this paper.

Theoretical Study of Borepinodithiophenes[1a]

Alfred T. Jeffries, III,[1b] and Cyril Párkányi*

Department of Chemistry, The University of Texas at El Paso, El Paso, Texas 79968 *(Received March 5, 1975; Revised Manuscript Received October 28, 1975)*

Publication costs assisted by The University of Texas at El Paso

The Pariser–Parr–Pople (PPP) type LCI–SCF–MO calculations (neglect of the penetration integrals, constant parameters, idealized geometry, a limited number of singly excited states in the configuration interaction, the *p* model for sulfur) have been used to study 4*H*-borepino[3,2-*b*:6,7-*b*′]dithiophene (**7**) and 4-hydroxy-4*H*-borepino[3,2-*b*:6,7-*b*′]dithiophene (**10**). The results of the calculations were employed to interpret and discuss some physical and chemical properties of the recently synthesized 4-methyl-4*H*-borepino[3,2-*b*:6,7-*b*′]dithiophene (**9**) and bis(4*H*-borepino[3,2-*b*:6,7-*b*′]dithienyl) ether (**8**) (electronic absorption spectra, NMR spectra, dipole moments, geometric structure, chemical reactivity). For the sake of comparison, a PPP calculation for *B*-phenylbenzo[*d*]borepin (**11**) has also been carried out.

Introduction

In recent years, an increased interest has been paid to various seven-membered ring π-electron systems in which one or several of the CH groups are replaced by a heteroatom. Thiepin (**1**) and 1*H*-borepin (**2**) may serve as examples of such systems which are isoelectronic with their hydrocarbon counterparts. The sulfur atom in the thiepin molecule contributes two π electrons into conjugation making thiepin an eight-π-electron system. Thus, thiepin can be considered as the simplest sulfur analogue of cyclooctatetraene in which the sulfur atom replaces a CH=CH group. On the other hand, if we assume that boron contributes no π electrons into the delocalized π-electron system, borepin is the heterocyclic analogue of the tropylium cation.

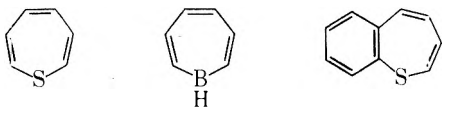

1 2 3

Thiepin itself has not yet been synthesized and its expected instability can be explained by the results of an LCI–SCF–MO (PPP) study. It is interesting to note that thiepin should possess a very low-lying triplet state.[2-4] On the other hand, fusion of one or two benzene rings to the thiepin ring stabilizes the molecule. The synthesis of benzo[*b*]thiepin (**3**) has been reported.[5,6] Benzo[*b*]thiepin is quite unstable and undergoes rapid thermal decomposition to naphthalene and sulfur. Dibenzo[*b*,*f*]thiepin (**4**) is a stable compound.[7,8] Also thiepin 1,1-dioxide (**5**) is known and is stable.[9,10]

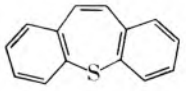

4

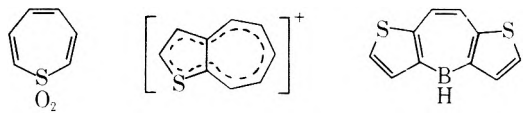

5 6 7

Thus, it would seem logical to try to increase the stability of the borepin ring by annelation of two stable π-electron rings. It is known that in the case of the tropylium ion benzoannelation decreases the stability of the system whereas fusion of a thiophene to the tropylium ion increases its stability. Thieno[*b*]tropylium cation (**6**) was recently studied by the LCI–SCF–MO (PPP) method and the experimental data on this compound (e.g., the electronic absorption spectrum) have been successfully interpreted on the basis of calculated quantum chemical data.[11,12]

The fusion of two thiophene rings to the borepin ring gives 4*H*-borepino[3,2-*b*:6,7-*b*′]dithiophene (**7**) which is iso-

electronic with the dithienotropylium cation and dibenzotropylium cation.

The synthesis of bis(4*H*-borepino[3,2-*b*:6,7-*b*']dithienyl) ether (**8**) and 4-methyl-4*H*-borepino[3,2-*b*:6,7-*b*']dithiophene (**9**) which are derivatives of **7** has recently been described.[13]

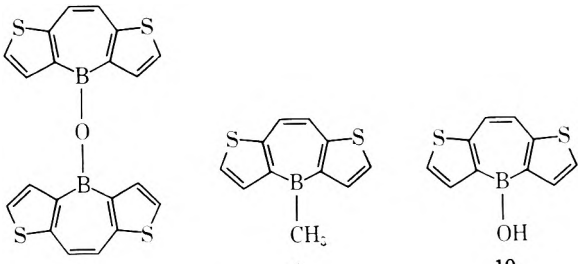

8 9 10

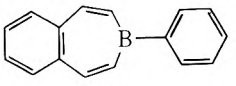

11

In the present contribution which is a continuation of the previous synthetic work,[13] we present a comparison of the experimental data with the results of LCI–SCF–MO (PPP) calculations carried out for the models of systems **8** and **9**, i.e., systems **10** and **7**, respectively. For the sake of comparison, an analogous calculation has been carried out for *B*-phenylbenzo[*d*]borepin (**11**).[14]

Methods

Compounds. The synthesis of compounds **8** and **9** has been published.[13] The synthesis of compound **11** has also been reported.[14]

Spectra. The electronic spectra of **8** and **9** were measured in cyclohexane on Unicam 800 and Cary 118 spectrophotometers. The proton NMR spectrum was determined in acetone-d_6 on a Varian A-60 spectrometer with tetramethylsilane as the internal standard, and the boron-11 spectrum was recorded in carbon disulfide using CAT and a Varian XL 100 instrument with boron trifluoride etherate as the external standard.[13]

LCI–SCF–MO (PPP) Treatment. In the calculations, compound **8** was approximated as 4-hydroxy-4*H*-borepino[3,2-*b*:6,7-*b*']dithiophene (**10**) and compound **9** as 4*H*-borepino-[3,2-*b*:6,7-*b*']dithiophene (**7**). The usual version of the PPP method was used. The parametrization and the method have been described elsewhere.[15] Interactions between monoexcited configurations formed by promotion of one electron from one of the four highest occupied MO's to one of the four lowest vacant orbitals MO's were considered. The systems studied were assumed to be planar and to have idealized geometry. All C–C, C–B, and C–S bond lengths were assigned to be 1.40 Å and the B–O bond length was taken as 1.36 Å. The rings were assumed to be regular heptagons and pentagons. SCF MO's served as the basis for CI calculations. Only resonance integrals between nearest neighbors were considered. The following parameters were used (values in eV).[11,16–18]

Atom, μ	I_μ	A_μ	$\gamma_{\mu\mu}$	Z_μ	$\beta_{C-\mu}$
C	11.22	0.69	10.53	1	−2.318
S	20.27	10.47	9.80	2	−1.623
B	2.00	−5.00	7.00	0	−1.800
O	27.17	12.59	14.58	2	−1.623 (β_{B-O})

TABLE I: Results of LCI Calculations

ΔE^1 [a]	f [b]	cos Φ [c]	Predominant confign i,j [d]	Wt	ΔE^3 [e]
4*H*-Borepino[3,2-*b*:6,7-*b*']dithiophene (**7**)					
3.425	0.830	1.000	1,−1	0.958	1.726
3.785	0.028	0.000	1,−2	0.761	2.577
4.657	0.061	0.000	2,−1	0.534	3.232
5.001	0.602	0.000	3,−1	0.445	3.502
5.020	0.015	−1.000	4,−1	0.781	3.616
5.366	0.037	0.000	1,−3	0.779	4.272
5.447	0.501	1.000	2,−2	0.908	4.632
5.531	0.380	1.000	3,−2	0.887	4.729
5.949	0.193	0.000	4,−2	0.893	5.359
5.987	0.049	1.000	1,−4	0.833	5.563
4-Hydroxy-4*H*-borepino[3,2-*b*:6,7-*b*']dithiophene (**10**)					
3.381	0.843	−1.000	1,−1	0.969	1.666
3.882	0.027	0.000	1,−2	0.729	2.551
4.669	0.052	0.000	2,−1	0.474	3.354
4.949	0.023	−1.000	4,−1	0.827	3.474
5.013	0.588	0.000	3,−1	0.314	3.680
5.367	0.119	0.000	1,−3	0.707	4.344
5.619	0.506	−1.000	2,−2	0.864	4.612
5.731	0.264	1.000	3,−2	0.913	4.814
5.901	0.050	−1.000	1,−4	0.827	5.560
6.012	0.184	0.000	4,−2	0.930	5.632

[a] Excitation energies (eV) for the ten lowest excited singlet states. [b] Oscillator strength. [c] Φ is the angle formed by the positive direction of the axis shown in the formula and the direction of the transition moment read counterclockwise. [d] A combination of two figures is used to label a configuration. A positive number refers to an orbital occupied in the ground state; a negative number, to a virtual orbital. [e] Excitation energies (eV) for the ten lowest excited triplet states.

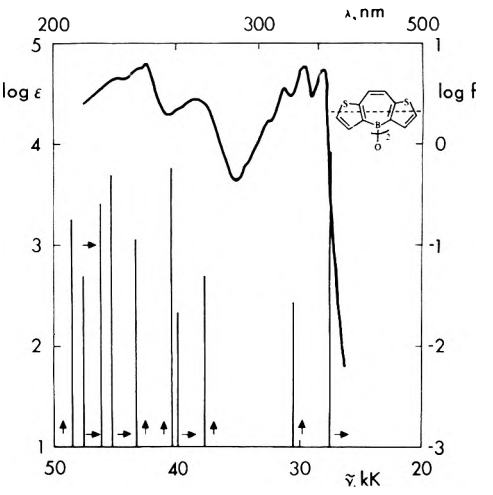

Figure 1. Electronic absorption spectrum (in cyclohexane) of bis(4*H*-borepino[3,2-*b*:6,7-*b*']dithienyl ether (**8**). Calculated LCI transition energies and intensities (for **10**) are shown as full straight lines. Scale for the calculated oscillator strength is shown on the right-hand side. The short arrows indicate the direction of polarization of the individual transitions.

I_μ and A_μ are the ionization potential and electron affinity of atom μ in the atomic valence state, respectively. The monocentric repulsion integrals and core integrals between nearest neighbors are represented by $\gamma_{\mu\mu}$ and $\beta_{C-\mu}$, respectively, and Z_μ is the core charge at atom μ. The bicentric electronic repulsion integrals have been calculated using the Mataga–Nishimoto formula[19]

$$\gamma_{\mu\nu} = \frac{14.399}{R_{\mu\nu} + 1.328}\ \text{eV}$$

where $R_{\mu\nu}$ (Å) is the distance between atoms μ and ν.

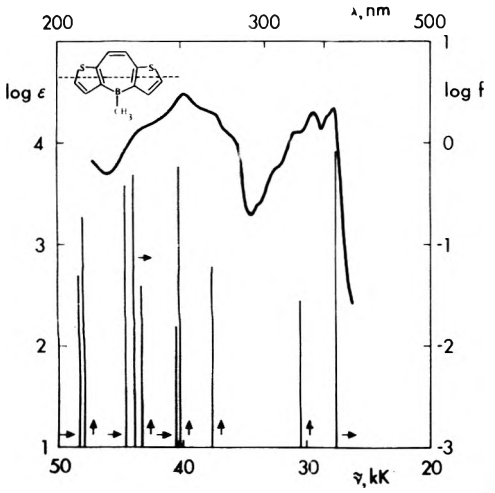

Figure 2. Electronic absorption spectrum (in cyclohexane) of 4-methyl-4*H*-borepino[3,2-*b*:6,7-*b*′]dithiophene (**9**) and the calculated transitions for **7**.

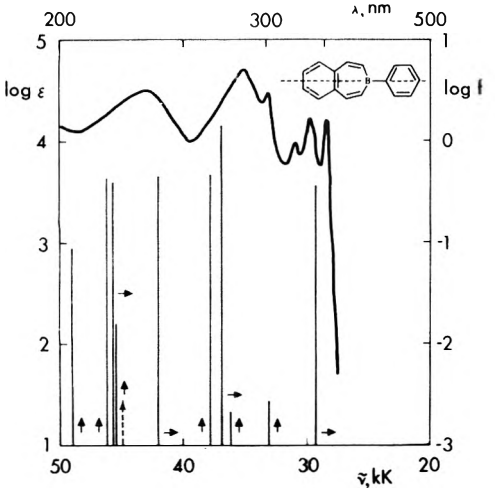

Figure 3. Electronic absorption spectrum (in cyclohexane, cf. ref 14b) and the calculated transitions for *B*-phenylbenzo[*d*]borepin (**11**). The broken-line arrow indicates a forbidden transition.

The calculations were performed on the CDC 3100 (borepinodithiophenes) and Univac 1108 (*B*-phenylbenzo[*d*]-borepin) computers.

For similar PPP calculations on borazaro analogues of benzenoid hydrocarbons, see ref 20.

Results and Discussion

Electronic Spectra. The results of PPP calculations on some of the spectral properties of compounds **7** and **10** are summarized in Table I and are compared with the experimental absorption curves for the compounds **9** and **8** in Figures 1 and 2. The experimental data are shown together with the calculated positions of 0–0 bands of the individual electronic transitions. When comparing calculated and experimental transition energies, it is necessary to remember that the former correspond to vertical transitions.

The experimental absorption curve for *B*-phenylbenzo[*d*]borepin[14] (**11**) and the calculated transitions are shown in Figure 3.[21]

The calculations yield several close-lying electronic transitions and this is an interesting result. Although fine structure is noticeable in some cases on the experimental absorption curves, most of the bands are broad thus revealing contributions to their intensity from more than one transition. The longest wavelength absorption band corresponding to the $S_0 \rightarrow S_1$ transition in the spectra of **8**, **9**, and **11**

TABLE II: ^{1}H and ^{11}B Chemical Shifts and the Corresponding π-Electron Densities in Borepinodithiophenes 8 and 9

Compd	Position[a]	Chem shift,[b] ppm	q^c
8	2	7.49 (^{1}H)	1.054
	3	7.29 (^{1}H)	1.040
	8	7.30 (^{1}H)	1.005
	4	−38.9 (^{11}B)	0.333
9	2	8.00 (^{1}H)	1.051
	3	7.80 (^{1}H)	1.034
	8	7.61 (^{1}H)	1.002
	4	−52.6 (^{11}B)	0.285

[a] The following numbering is being used throughout

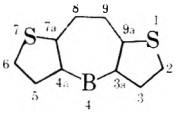

[b] Taken from ref 13. [c] SCF–MO π-electron densities for the models 10 and 7, respectively.

TABLE III: Experimental Bond Lengths in Bis(4*H*-borepino[3,2-*b*:6,7-*b*′]dithienyl) Ether (8)[a]

Bond, *i*–*j*	l_{ij}, Å	Bond, *i*–*j*	l_{ij}, Å	Bond, *i*–*j*	l_{ij}, Å
1–2	1.693	3–3a	1.426	4–oxygen	1.358
1–9a	1.725	3a–4	1.532	7a–8	1.428
2–3	1.345	3a–9a	1.387	8–9	1.330

[a] According to ref 28. Average values are given, ±0.005 Å. For numbering, see Table II.

TABLE IV: SCF–MO π-Electron Densities for Compounds 7 and 10[a]

Position, *i*	q_i	Position, *i*	q_i	Position, *i*	q_i
4*H*-Borepino[3,2-*b*:6,7-*b*′]dithiophene (7)					
1	1.755	3a	1.007	7a	1.008
2	1.051	4	0.285	8	1.002
3	1.034				
4-Hydroxy-4*H*-borepino[3,2-*b*:6,7-*b*′]dithiophene (10)					
1	1.754	3a	1.013	7a	1.015
2	1.054	4	0.333	8	1.005
3	1.040			Oxygen	1.904

[a] For numbering, see Table II.

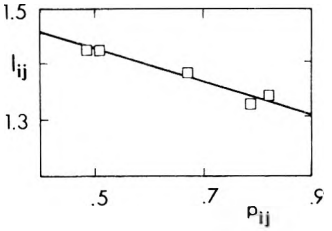

Figure 4. Experimental C–C bond lengths, l_{ij}, in bis(4*H*-borepino[3,2-*b*:6,7-*b*′]dithienyl) ether (**8**) plotted against calculated SCF–MO π-bond orders, p_{ij}. For experimental data, see ref 28. Regression line: l_{ij} (Å) = $-0.285p_{ij}$ + 1.570; correlation coefficient r = 0.975, number of points n = 5. All values are significant on 1% probability level.

appears at 28.5, 27.9, and 28.4 kK (3.534, 3.459, and 3.521 eV), respectively.

For certain transitions, the calculations predict considerable mixing of configurations, even of those of low energy. The squares of the expansion coefficient for the $\chi_{1,-1}$ configuration in the CI function for the first excited state are 0.958 and 0.969 for compounds **7** and **10**, respectively, but a considerable mixing is already observed in the second and third excited states.

It seems worth noting that, in agreement with the calculations, the overall character of the absorption curves, the positions of the absorption maxima, and their intensities for compounds **8** and **9** are quite similar and resemble the absorption curve of the π-isoelectronic 4*H*-cyclohepta[1,2-*b*:5,4-*b'*]dithiophene (**12**).[13]

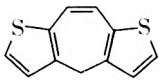

12

The calculated $S_0 \rightarrow T_1$ transitions for compounds **7** and **10** are at 13.92 and 13.44 kK (1.726 and 1.666 eV), respectively. No phosphorescence or singlet–triplet absorption spectra for this type of compounds are available so far. It should be pointed out that S–T and T–T transitions calculated by the PPP method are usually too low as compared to the experimental results and thus one would expect the $S_0 \rightarrow T_1$ transition for these systems at somewhat higher wavenumbers.

NMR Spectra. In several cases, successful correlations have been reported between proton or heteroatom chemical shifts observed in the NMR spectra of π-electron heterocycles and the calculated π-electron densities in the respective positions.[22-27] In other cases, attempts to find such a relationship failed.[11] Table II shows the measured chemical shifts and the SCF–MO π-electron densities for compounds **8** and **9**. A satisfactory qualitative agreement exists between these data but the small number of points prevents any meaningful quantitative correlation.

Dipole Moments. The π-electron contribution to the dipole moment is along the short axis in the cases of both **7** and **10** (orientation as shown). A considerable decrease of the dipole moment is predicted when going from the ground state to the first excited singlet state.

Structure. A classic criterion for the Hückel character of a system is its coplanarity. An x-ray determination of the structure of **8** has revealed that both halves of the molecule are essentially planar.[28] The only deviation from coplanarity in the whole molecule is due to the 152.5° angle formed by the B–O–B bonds.

The experimental bond lengths for compound **8** are shown in Table III. There is a good agreement between the calculated π-bond orders and the experimental C–C bond lengths (Figure 4).

Chemical Reactivity. The SCF–MO π-electron densities for **1** and **10** are given in Table IV and the corresponding π-bond orders in Table V.

The α position in the thiophene rings (position 2) should be the center of electrophilic reactivity of compounds **8** and **9**. In thiophene itself, electrophilic substitutions occur predominantly at the α position as well,[29,30] whereas annelation of benzene or tropylium rings to thiophene makes the β position most reactive toward electrophilic substitution.

According to the data in Table V, the 2–3 bond in the thiophene ring is most double in character and should be the bond at which the addition reactions would occur.

TABLE V: SCF–MO π-Bond Orders for Compounds **7** and **10**[a]

Bond, *i–j*	p_{ij}	Bond, *i–j*	p_{ij}	Bond, *i–j*	p_{ij}
4*H*-Borepino[3,2-*b*:6,7-*b'*]dithiophene (**7**)					
1–2	0.395	3–3a	0.502	7a–8	0.498
1–9a	0.386	3a–4	0.395	8–9	0.778
2–3	0.823	3a–9a	0.659		
4-Hydroxy-4*H*-borepino[3,2-*b*:6,7-*b'*]dithiophene (**10**)					
1–2	0.398	3–3a	0.507	4–oxygen	0.394
1–9a	0.385	3a–4	0.361	7a–8	0.486
2–3	0.820	3a–9a	0.670	8–9	0.786

[a] For numbering, see Table II.

As part of our efforts to confirm experimentally some of these predictions, we have tried to carry out two different electrophilic substitution reactions on the ether **8**. Our attempt at proton–deuterium exchange in dimethyl sulfoxide–D_2SO_4 resulted in almost complete decomposition of the substrate. Electrophilic bromination with pyridine perbromide hydrobromide in chloroform clearly introduced bromine into the thiophene rings but with a cleavage of the B–C bonds in the borepin ring.[31]

Acknowledgments. The financial support of the Robert A. Welch Foundation (Houston, Tex.) through Grant No. AH-461 is gratefully acknowledged. The authors are indebted to Dr. J. Michl for time on the Univac 1108 computer and to Dr. A. J. Leusink and Dr. B. Aurivillius for the provided information. The authors wish to express their sincere thanks to Mr. Mark A. Priesand for his help in developing a computer program for the evaluation of experimental absorption curves.

References and Notes

(1) (a) Presented at the 167th National Meeting of the American Chemical Society, Los Angeles, Calif., April 1–5, 1974. (b) R. A. Welch Postdoctoral Fellow.
(2) C. Párkányi, *Mech. React. Sulfur Compd.*, **4**, 69 (1969).
(3) C. Párkányi, paper presented at the First International Congress of Quantum Chemistry, Menton, France, July 4–10, 1973.
(4) C. Párkányi, to be submitted for publication in *Int. J. Sulfur Chem.*
(5) V. J. Traynelis, Y. Yoshikawa, J. C. Sih, L. J. Miller, and J. R. Livingston, Jr., *J. Org. Chem.*, **38**, 3978 (1973).
(6) I. Murata, T. Tatsuoka, and Y. Sugihara, *Tetrahedron Lett.*, 4261 (1973); *Angew. Chem., Int. Ed. Engl.*, **13**, 142 (1974).
(7) E. D. Bergmann and M. Rabinowitz, *J. Org. Chem.*, **25**, 828 (1960).
(8) R. Huisgen, E. Laschtuvka, and F. Bayerlin, *Chem. Ber.*, **93**, 392 (1960).
(9) W. L. Mock, *J. Am. Chem. Soc.*, **89**, 1281 (1967).
(10) H. L. Ammon, P. H. Watts, Jr., J. M. Stewart, and W. L. Mock, *J. Am. Chem. Soc.*, **90**, 4501 (1968).
(11) J. Fabian, A. Mehlhorn, and R. Zahradník, *J. Phys. Chem.*, **72**, 3975 (1968).
(12) J. Fabian and H. Hartmann, *Tetrahedron Lett.*, 239 (1969).
(13) A. T. Jeffries, III, and S. Gronowitz, *Chem. Scr.*, **4**, 183 (1973).
(14) (a) A. J. Leusink, W. Drenth, J. G. Noltes, and G. J. M. van der Kerk, *Tetrahedron Lett.*, 1263 (1967); (b) A. J. Leusink, private communication to A. T. Jeffries (1972).
(15) J. Koutecký, P. Hochman, and J. Michl, *J. Chem. Phys.*, **40**, 2439 (1964).
(16) C. Párkányi, E. J. Baum, J. Wyatt, and J. N. Pitts, Jr., *J. Phys. Chem.*, **73**, 1132 (1969).
(17) J. Michl, J. Koutecký, R. S. Becker, and C. E. Earhart, *Theor. Chim. Acta*, **20**, 41 (1971).
(18) R. Zahradnik, I. Tesařová, and J. Pancíř, *Collect. Czech. Chem. Commun.*, **36**, 2867 (1971).
(19) N. Mataga and K. Nishimoto, *Z. Phys. Chem. (Frankfurt am Main)*, **13**, 140 (1957).
(20) J. Michl, *Collect. Czech. Chem. Commun.*, **36**, 1248 (1971).
(21) Theoretical values concerning the model of compound **11** as well as additional quantities on compounds **7** and **10** can be obtained upon request from the authors.
(22) J. Kuthan and V. Skála, *Z. Chem.*, **6**, 422 (1966).
(23) J. Kuthan, J. Paleček, J. Procházková, and V. Skála, *Collect. Czech. Chem. Commun.*, **33**, 3138 (1968).
(24) J. Kuthan and J. Procházková, *Collect. Czech. Chem. Commun.*, **34**, 1190 (1969).
(25) T. B. Cobb and J. D. Memory, *J. Chem. Phys.*, **50**, 4262 (1969).

(26) H. Sterk, *Monatsh. Chem.*, **102**, 474 (1971).
(27) C. T. Goralski and W. B. Neely, *Theor. Chim. Acta*, **20**, 41 (1971).
(28) B. Aurivillius (University of Lund, Lund, Sweden), private communication to A. T. Jeffries (1973).
(29) R. Zahradnik, C. Párkányi, V. Horák, and J. Koutecký, *Collect. Czech. Chem. Commun.*, **28**, 776 (1963).
(30) F. Blicke in "Heterocyclic Compounds", Vol. 1, R. C. Elderfield, Ed., Wiley, New York, N.Y., 1950.
(31) After this paper had been submitted, there were published INDO calculations on several boron-containing compounds one of which was *B*-phenylbenzo[*d*]borepin (**11**): N. L. Allinger and J. H. Siefert, *J. Am. Chem. Soc.*, **97**, 752 (1975).

Transport Behavior of Glass-Forming Melts

N. Islam,* M. R. Islam, B. Waris, and Ismail K

Department of Chemistry, Aligarh Muslim University, Aligarh 202001, India *(Received September 23, 1974; Revised Manuscript Received August 11, 1975)*

Viscosities, η, of molten mixtures of cobalt(II) chloride and tetra-*n*-butylammonium iodide, measured as functions of temperature and composition, have been analyzed in terms of several analytical expressions and their empirical parameters computed. Linear increase in the secondary glass transition temperature, T_0, with successive increases in $[CoCl_2]$ has been attributed to an increase in the net cohesive forces. This is due to complex formation which leads to eventual supercooling to glassy states. Isothermal composition dependence of viscosities has been explained satisfactorily in terms of a parabolic expression which also describes the minimum obtained in the viscosity isotherms at N (mole fraction) $= -q/2r$, where q and r are computed parameters. A value equal to more than one for the ratio of activation energies, E_ϕ/E_Λ (ϕ and Λ stand for fluidity and equivalent conductance, respectively), and its agreement with the ratio of empirical parameters, k_ϕ/k_Λ, have been accounted for. The composition dependence of Walden's product has been discussed and a dynamic equilibrium between the free ions and the associated ion pairs has been postulated. Temperature dependence of Walden's product has been explained successfully in terms of analytical expressions and the corresponding empirical parameters computed. Identical $T_{0,\Lambda}$, $T_{0,\phi}$, and $T_{0,\Lambda\eta}$ as well as intrinsic volume $V_{0,\Lambda}$, $V_{0,\phi}$, and $V_{0,\Lambda\eta}$ reflect the thermodynamic nature of these parameters.

Introduction

Densities, viscosities, electrical conductances, and optical spectra have been measured in several molten salt systems.[1-7] Such measurements have also been reported[8-15] in the cases of glass-forming melts. Metal halide-rich mixtures of low-melting organic halides containing $(R_4B^+)_2MX_4^{2-}$ (B = N or P; M = Mn^{2+}, Co^{2+}, or Ni^{2+}) have been found to supercool to glassy states.[9-15] The degree of dissociation of MX_4^{2-} is negligible in pure $(R_4B^+)_2MX_4^{2-}$ as is apparent from the decreases in the electrical conductances[13,14] with increase in $[MX_n]$, where n denotes the charge on M. Because of the small intermolecular distances r, the species, $(R_4N^+)_{4-n}[MX_4]^{(4-n)-}$, appear to be held together at low temperatures. This results in a highly viscous liquid due to the presence of highly associated flowing entities of the form, $\{(R_4N^+)_{4-n}[MX_4]^{(4-n)-}\}_x$. The optical spectra and transport behaviors of such systems[15] suggest a relationship between the melts on one hand and the corresponding glassy state on the other.

Therefore, the electrical conductances, densities, and viscosities of molten mixtures of $CoCl_2$ and Bu_4NI have been measured with a view to understanding the differences in the ordinary melts and the supercooled materials and, also, the factors governing the glass-forming tendencies of these melts. The temperature and composition dependences of fluidities have been examined in terms of several models[8,16-18] proposed for describing the mechanism of kinematic viscous flow of Newtonian liquids. An attempt has also been made to describe such dependences of activation energies and Walden's products.

Experimental Section

Purified[19] toluene, *n*-octane (BDH), and quinoline (Riedel) were used as calibrating liquids. Tetra-*n*-butylammonium iodide was recrystallized[20] several times from purified[19] acetone–ether mixture and dried under vacuum over P_2O_5 at 50°C.

Several molten salt mixtures of anhydrous[21] $CoCl_2$ and Bu_4NI were prepared in a thermostated bath in an inert atmosphere.

Density and kinematic viscosity measurements were made with a dilatometer[15,17] of 0.005-ml divisions and calibrated Cannon-Ubbelohde viscometer,[22,23] respectively, in a relay-controlled thermostated glycerol bath of ±0.1° thermal stability.

The viscometer was filled with a required amount of the sample with a vacuum pump and was placed in a thermostated bath for 30 min to minimize the thermal fluctuations before recording the data. The viscosities of quinoline were determined with a calibrated viscometer ($\beta_I = 6.7 \times 10^{-5}$ cSt/s from 313 to 373.9 K using *n*-octane as a reference liquid, and were calculated between 373 and 418 K by extrapolating the plot of $10^3 \log \eta$ vs. $10^3/T$. These extrapolated values were used as a reference for the calibration of other viscometers ($\beta_{II} = 3.6 \times 10^{-4}$ cSt/s and $\beta_{III} = 5.2 \times$

10^{-4} cSt/s). These viscometers were employed for the determination of viscosities of molten salt mixtures in the said range of temperature. Measurements were made in a descending as well as in an ascending order of temperature. The time of flow of organic liquids was reproducible within ±0.1% while those of molten salt mixtures within ±1.0–3.3%.

The dilatometer and viscometer were cleaned by washing with hot nitric acid, chromic acid, a suspension of soap–water, and double distilled water, and dried for further use.

Results and Discussion

Temperature Dependence of Fluidity. Temperature dependence of fluidities were found to be explained by a Doolittle[24] type expression

$$\phi = A_\phi \exp[-B_\phi/(V - V_0)] \quad (1)$$

where A_ϕ and B_ϕ are empirical parameters while V and V_0 are molal and intrinsic volumes, respectively. Values of the computed parameters are given in Table I. Linear plots of log ϕ vs. $1/(V - V_0)$ (Figure 1) justify the applicability of the above expression.

Moreover, the temperature dependence of ϕ has been found to be described directly in terms of different analytical functions of the form

$$\phi = a + bt + ct^2 \quad (2)$$

$$\phi = a' \exp[-b'/(T - c')] \quad (3)$$

and

$$\phi = A_\phi' T^{-1/2} \exp[-k_\phi/(T - T_0)] \quad (4)$$

a, b, c, a', b', c', A_ϕ', k_ϕ, and T_0 are all empirical parameters.[25] The best-fit values of these parameters are listed in Table II[26] and III along with standard deviations in ϕ. Applicability of eq 4 in the present system has been emphasized by linear plots of log $\phi T^{1/2}$ vs. $1/(T - T_0)$ (Figure 2).

It may be noted that the free volume model[18] demands a critical void volume for the initiation of mass flow in glass-forming liquids. This, in turn, may manifest as a conventional activation energy for viscous flow. Accordingly, activation energies, E_ϕ's, were computed from the derivative of eq 4 and also from the slope of Arrhenius plots, and were averaged. The corrected activation energies, E_{cor} (Table IV),[26] were obtained by adding $(1/2)RT$ to the average values of E_ϕ as explained below.

From the Stokes–Einstein[27] equation, the activation energy for fluidity may be given as follows:

$$D_i = kT\phi/6\pi r_i \quad (5)$$

where D_i, r_i, and k are diffusion coefficient, ionic radius, and Boltzmann constant, respectively. Differentiating the logarithm of the above equation, we obtain

$$\mathrm{d} \ln D_i/\mathrm{d}(T^{-1}) = \mathrm{d} \ln \phi/\mathrm{d}(T^{-1}) - T \quad (6)$$

This gives the energy of activation for diffusion as

$$E_D = E_\phi + RT \quad (7)$$

In the light of Cohen and Turnbull's model[18]

$$\mathrm{d} \ln D/\mathrm{d}(T^{-1}) = -E_D/R = (-T/2) - k_\phi[T/(T - T_0)]^2 \quad (8)$$

Combining eq 7 and 8, we obtain

$$E_\phi + RT - (1/2)RT = k_\phi R[T/(T - T_0)]^2$$

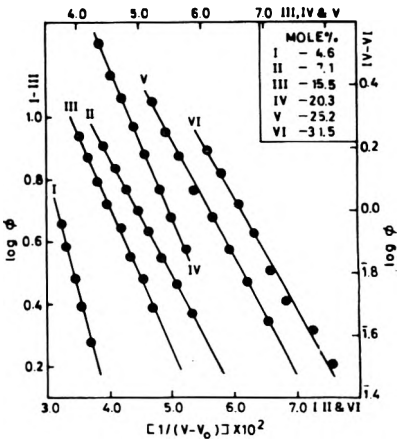

Figure 1. Plots of log ϕ vs. $1/(V - V_0)$ for molten mixtures of $CoCl_2$ and Bu_4NI.

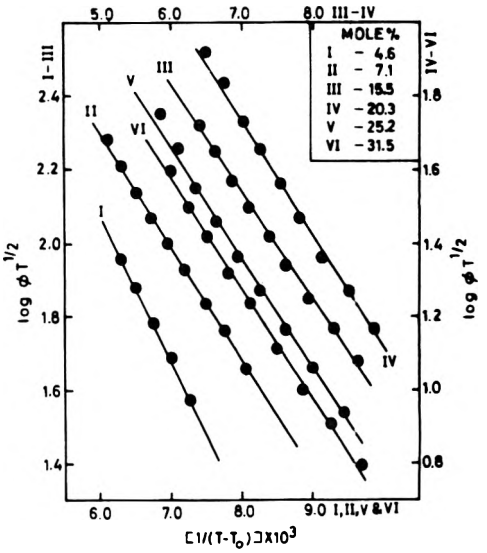

Figure 2. Plots of log $\phi T^{1/2}$ vs. $1/(T - T_0)$ for molten mixtures of $CoCl_2$ and Bu_4NI.

and

$$E_{cor,\phi} = E_\phi + (1/2)RT = k_\phi R[T/(T - T_0)]^2 \quad (9)$$

It is apparent from Figure 3 that the linear plots of E_{cor} vs. $[T/(T - T_0)]^2$ pass through the origin lending further support to the applicability of free volume model in describing the transport behavior in glass-forming melts.

Composition and temperature dependences of E_ϕ are illustrated in Figures 4 and 5. E_ϕ appears to decrease initially with an increase in $[CoCl_2]$ and passes through a minimum at ~10 mol % of $CoCl_2$ before it starts increasing with further increases in $[CoCl_2]$. The descending portion of the activation energy isotherms, corresponding to low $[CoCl_2]$, is comparable to similar behavior of Walden's product isotherms and may be due to dissociation of solvent molecules as discussed later. Probably, such a dissociation causes an easy flow thereby decreasing the value of E_ϕ; however, an increase in E_ϕ with $[CoCl_2]$ may be attributed to the formation of complex species. Moreover, an increase in E_ϕ with a decrease in temperature becomes more significant in the low temperature region and may account for the inadequacy of the free volume required for molecular migration at these temperatures.

TABLE I: Best-Fit Parameters for Equations $\phi,\Lambda = A_{\phi,\Lambda} \exp[-B_{\phi,\Lambda}/(V - V_{0,\phi,\Lambda})]$ for the Fluidity and Equivalent Conductance[a] of Molten Mixtures of $CoCl_2$ and Bu_4NI

Mol % Co^{2+}	A_ϕ	B_ϕ	$V_{0,\phi}$	Std dev in ϕ	A_Λ	B_Λ	$V_{0,\Lambda}$	Std dev in Λ
4.6	2044.30	188.45	285.00	0.034	46.371	102.94	288.37	0.013
7.1	271.50	89.36	279.00	0.019	21.786	77.23	279.00	0.009
15.5	856.12	120.50	254.11	0.109	22.968	85.00	255.50	0.032
20.3	451.94	112.14	247.50	0.049				
25.2	249.55	90.75	234.70	0.041				
31.5	153.84	82.30	222.50	0.033	17.441	76.41	222.50	0.004

[a] Values of $V_{0,\Lambda}$ were computed for comparison.

TABLE III: Best-Fit Parameters for Equations $\phi, \Lambda = A_{\phi,\Lambda}' T^{-1/2} \exp[-k_{\phi,\Lambda}/(T - T_{0,\phi,\Lambda})]$ for the Fluidity and Equivalent Conductance[a] of Molten Mixtures of $CoCl_2$ and Bu_4NI

Mol % Co^{2+}	A_ϕ'	k_ϕ	$T_{0,\phi}$	Std dev in ϕ	A_Λ'	k_Λ	$T_{0,\Lambda}$	Std dev in Λ
4.6	19724.0	854.60	250.20	0.131	1000.2	600.00	252.00	0.046
7.1	15306.0	723.31	253.79	0.113	1047.8	621.85	254.00	0.010
15.5	17975.0	715.42	258.32	0.149	868.5	609.71	260.00	0.038
20.3	9857.8	716.19	269.15	0.098				
25.2	7074.0	713.27	272.24	0.067				
31.5	4573.0	686.84	274.86	0.041	496.4	635.47	275.00	0.004

[a] Values of $T_{0,\Lambda}$ were computed for comparison.

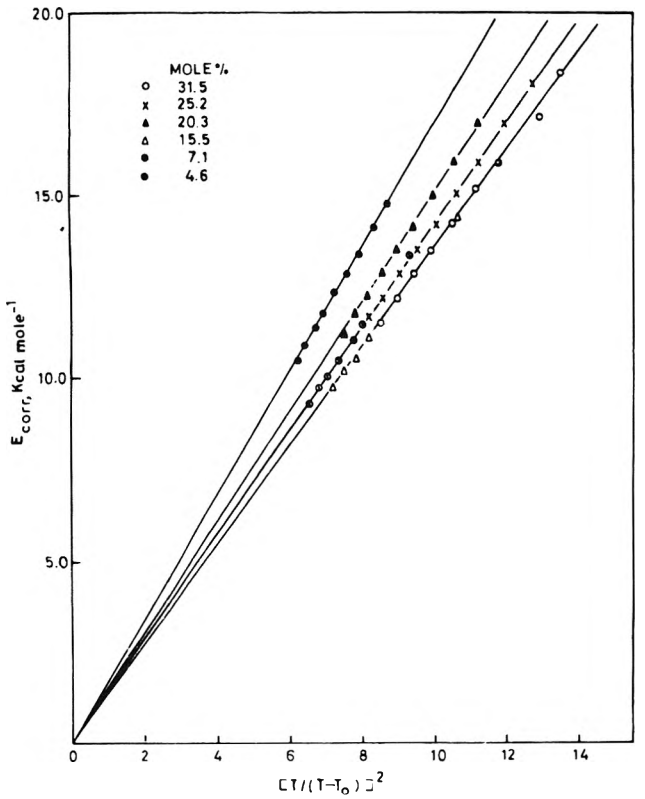

Figure 3. Plots of $E_{cor,\phi}$ vs. $[T/(T - T_0)]^2$ for molten mixtures of $CoCl_2$ and Bu_4NI.

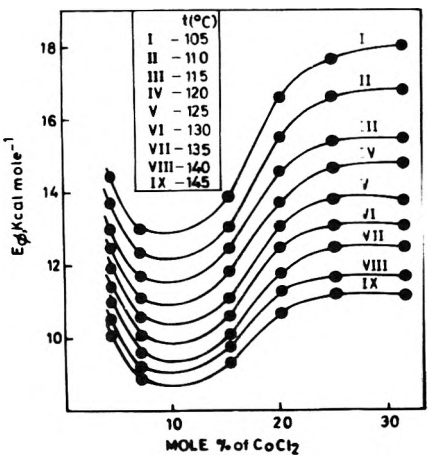

Figure 4. Energy of activation for fluidity as a function of composition for molten mixtures of $CoCl_2$ and Bu_4NI.

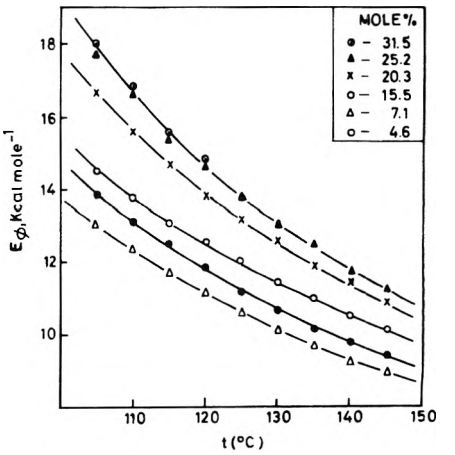

Figure 5. Energy of activation for fluidity as a function of temperature for molten mixtures of $CoCl_2$ and Bu_4NI.

Concentration Dependence of Fluidity. At a given temperature fluidity has been found to increase with successive decreases in concentration from 31.5 to 15.5 mol % of $CoCl_2$ in Bu_4NI and shows an abnormal decrease from 7.1 to 4.6 mol % of $CoCl_2$ (Figure 6).[26]

The composition dependence of viscosity from 15.5 to 31.5 mol % of $CoCl_2$ in molten Bu_4NI may be explained in

TABLE V: Best-Fit Parameters for Equation $\eta = p + qN + rN^2 + sN^3$ for the Viscosity of Molten Mixtures of $CoCl_2$ and Bu_4NI

T, K	Composition range (mole fraction)	p	q	r	s	Std dev in η
378.0	0.071–0.315	3.1347	−62.1240	377.8612	−576.0468	0.07
383.0		2.2870	−44.6443	271.2164	−407.4217	0.08
388.0	0.046–0.315	1.5713	−30.4471	187.2808	−275.6065	0.06
393.0		1.1579	−21.8551	133.0858	−189.1910	0.05
398.0		1.0025	−19.4355	121.4591	−184.2812	0.04
403.0		0.7379	−13.7007	84.9291	−124.7573	0.04
408.0		0.6357	−11.9564	75.0074	−113.5043	0.03
413.0	0.071–0.315	0.5809	−10.4264	62.4583	−91.3630	0.02
418.0		0.4825	−8.5896	51.5568	−76.1073	0.02

TABLE VI: Ratio of Corrected Activation Energies, E_ϕ/E_Λ, as a Function of Temperature for Molten Mixtures of $CoCl_2$ and Bu_4NI

	E_ϕ/E_Λ			
T, K	4.6 mol % Co^{2+}, k_ϕ/k_Λ = 1.424	7.1 mol % Co^{2+}, k_ϕ/k_Λ = 1.163	15.5 mol % Co^{2+}, k_ϕ/k_Λ = 1.173	31.5 mol % Co^{2+}, k_ϕ/k_Λ = 1.081
378.0	1.380	1.164	1.145	1.079
383.0	1.383	1.165	1.148	1.079
388.0	1.382	1.162	1.158	1.064
393.0	1.395	1.167	1.156	1.084
398.0	1.395	1.166	1.143	1.073
403.0	1.393	1.159	1.150	1.076
408.0	1.394	1.158	1.142	1.085
413.0	1.392	1.160	1.153	1.073

terms of various interactions. These interactions are not only dependent upon the type of the ions and the solvents used, but also upon the concentration of the ionic species present in the system. Formation of complex ions and associated species may increase such interactions thereby decreasing the fluidity with an increase in $[CoCl_2]$.

On the basis of the conventional transport theory, it has been suggested that the parameter T_0 is the controlling variable in the composition dependence of transport at low temperatures. T_0 reflects the cohesive forces in liquids, and in the case of charge unsymmetrical salt systems,[28] the cohesive energy of one component (1) may be much less than that of the other (2). In other words $T_{0(1)} \ll T_{0(2)}$ and, therefore, one can presume a linear relation between T_0 and composition. However, in the case of charge symmetrical salt systems, the cohesive energies of the two components may be similar and positive or negative departures from additivity may occur. A parallel behavior will be exhibited by T_0 thereby leading to positive or negative departures from additivity in the transport properties. In the present case of charge unsymmetrical molten salt system a linear relationship has actually been found between T_0 and the cationic potential (Figure 7) justifying the above assumption. Cationic potential has been defined as $\Sigma_i N_i Z_i/r_i$ where N_i = mole fraction, Z_i = ionic charge, and r_i = ionic radius of cation species i. An increase in T_0 with an increase in $[CoCl_2]$ may be attributed to an increase in net cohesion in the system due to complex formation which leads to an eventual supercooling to glassy states. Therefore, it appears that in the absence of crystallization, addition of an excess amount of a solute to any ionic solution results in glass formation and a sharp increase in viscosity.

A satisfactory representation of the composition dependence of viscosities in the present system may be displayed through an expression of the form

$$\eta = p + qN + rN^2 + sN^3 \qquad (10)$$

where p, q, r, and s are empirical constants. This expression represents a parabola (neglecting the last term) in which a maximum or minimum depends upon the magnitude r. For $r > 0$, one expects a minimum in the viscosity isotherm at $N = -q/2r$. Such values for N, viz. ~0.1 computed from the parameters q and r (Table V) are in good agreement with those obtained graphically (Figure 6).[26]

Comparison of Parameters Obtained from Conductance and Fluidity Measurements. Equation 4 based on the free volume model[18] has been used to describe the temperature dependences of both conductance and fluidity of glass-forming melts. It has been derived on the consideration that T_0 is a thermodynamic rather than a kinetic quantity. Therefore, values of T_0 obtained from the measurement of

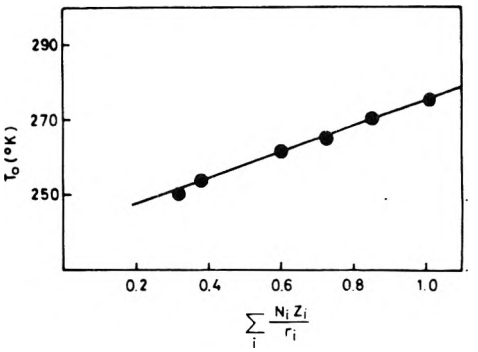

Figure 7. Relationship between T_0 and cationic strength for molten mixtures of $CoCl_2$ and Bu_4NI.

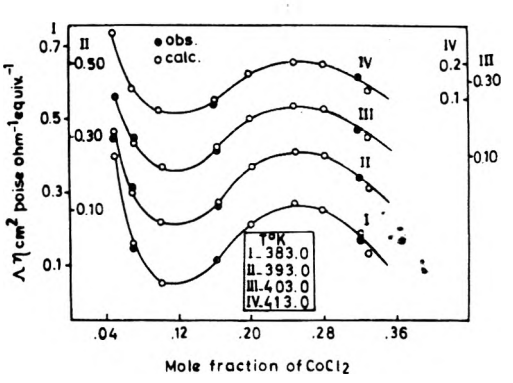

Figure 8. Walden's product as a function of composition for molten mixtures of $CoCl_2$ and Bu_4NI.

TABLE VII: Best-Fit Parameters for Equations $\Lambda\eta = A_1 \exp[B_1/(T - T_{0,\Lambda\eta})]$ and $\Lambda\eta = A_2 \exp[B_2/(V - V_{0,\Lambda\eta})]$ for the Walden's Product of Molten Mixtures of $CoCl_2$ and Bu_4NI

Mol % Co^{2+}	A_1	B_1	$T_{0,\Lambda\eta}$	Std dev in $\Lambda\eta$	A_2	B_2	$V_{0,\Lambda\eta}$	Std dev in $\Lambda\eta$
4.6	0.0370	296.63	250.00	0.003	0.0377	56.82	285.35	0.003
7.1	0.0694	97.83	255.00	0.002	0.0800	12.26	279.00	0.001
15.5	0.0570	75.30	259.00	0.003	0.0638	9.75	255.50	0.002
31.5	0.1253	34.57	274.11	0.008	0.1147	5.80	222.32	0.008

different transport properties must be identical, if the transport properties are measured over identical temperature ranges. The almost identical $T_{0,\Lambda}$ and $T_{0,\phi}$ obtained in the present case, therefore, reflect the thermodynamic nature of T_0. Similarly, $V_{0,\Lambda}$ and $V_{0,\phi}$ agree with each other, and, $k_\phi \approx 700$ and $k_\Lambda \approx 600$ seem to be almost composition independent parameters. These values are comparable to the universal values of k_ϕ and k_Λ found in the cases of several molten salt systems.[29] A higher value for k_ϕ reflects a larger value for critical void volume during viscous flow. This, in turn, accounts for a value more than one for the ratio E_ϕ/E_Λ as is apparent from Table VI. Moreover, a close resemblance (Table VI) between this ratio and k_ϕ/k_Λ is expected in the light of equations[30] of the type (9).

Walden's Product. Walden's products for the molten mixtures of $CoCl_2$ and Bu_4NI are plotted as a function of mole fraction of $CoCl_2$ at several temperatures (Figure 8). These plots show that the products pass through minima and maxima in going from 0.046 to 0.315 mole fraction of $CoCl_2$. Minima and maxima occur at ~0.1 and ~0.25 mole fractions of $CoCl_2$, respectively, and the nature of the curve is in accordance with that reported earlier.[31-33]

Initially, as the concentration increases, the electrostatic force holding an ion pair together is reduced due to the presence of a neighboring free ion. Thus the ion pair in the vicinity of a free ion (metal ion) may be more easily dissociated into ions upon a collision with a solvent molecule, thereby increasing the number of ionic species in the system. The occurrence of dissociation by such collisions depends on the number of free metal ions and the thermal energy of solvent.[33] Therefore, dissociation increases with an increase in concentration at constant temperature. This results in a decrease in viscosity which seems to be the controlling factor in Walden's product. The minimum $\Lambda\eta$ product corresponds to a point where dissociation becomes relatively more dominant. The minimum product has been reported[33] to depend on the dielectric constant of the medium and, therefore, one expects a shift in the minimum, if the solvent is changed for the same metal halide.

However, when the dissociation of solvent molecules increases, the solvent anions formed in this way are accumulated around the metal ion to form complex species such as CoX_4^{2-}, the presence of which has been supported by its ligand-field bands.[34] Moreover, as soon as the complex species such as CoX_4^{2-} are formed, they associate with the solvent cation, Bu_4N^+. This kind of simultaneous complexation and association may increase with an increase in $[CoCl_2]$ and, thereby, increase the viscosity of the system considerably. This may actually account for the increase in $\Lambda\eta$ product in the concentration range from ~0.1 to ~0.25 mole fraction of $CoCl_2$. Therefore, above ~0.1 mole fraction of $CoCl_2$ an equilibrium of the type, $CoX_4^{2-} + 2Bu_4N^+ \rightleftharpoons [Bu_4N^+]_2[CoX_4^{2-}]$, can be presumed.

Furthermore, it is pertinent to note that above ~0.25 mole fraction of $CoCl_2$, the Walden's product starts decreasing again. It appears that up to this concentration of $CoCl_2$, the viscosity of the system is the main controlling factor in determining the value of Walden's product. However, it is equally important to observe that the conductance decreases accordingly with increases in viscosity. Beyond ~0.25 mole fraction of $CoCl_2$ conductance may decrease remarkably owing to high viscosity of the medium and appears to predominate in determining the value of $\Lambda\eta$ product. Consequently, over this concentration range the product decreases with further increases in $[CoCl_2]$.

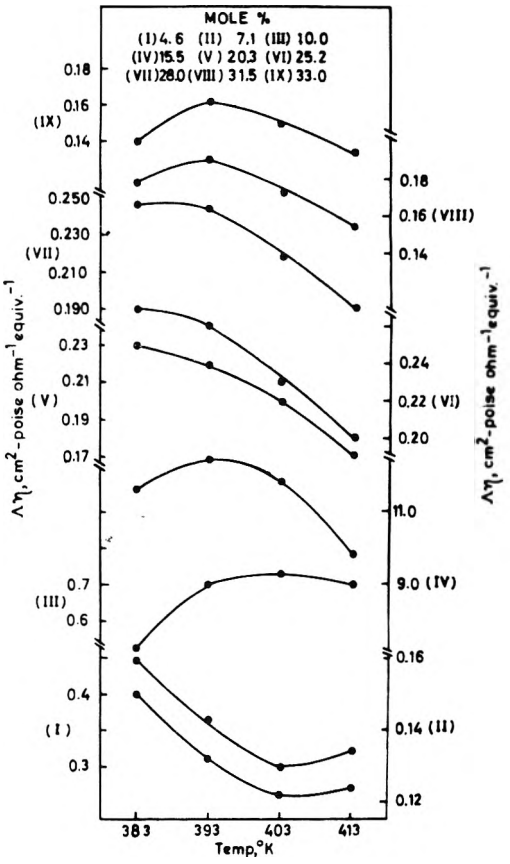

Figure 9. Walden's product as a function of temperature for molten mixtures of $CoCl_2$ and Bu_4NI.

The temperature dependence of Walden's product is shown in Figure 9. Changes in Walden's product with temperature may be explained through a structure making and breaking mechanism as suggested by Kay and Evans[35] to account for such a phenomenon in the cases of alkali and halide ions in aqueous solutions. Bu_4N^+ has been considered as an excellent structure maker.[35] As the temperature increases ions as well as ion pairs separate and, consequently, less structure will be available for making. Therefore, Bu_4N^+ will be less effective in increasing the local viscosity through structure making thereby causing a decrease in the

product with an increase in temperature. However, the maxima in the plots of Walden's product vs. temperature obtained in some cases may indicate that the mobility of the ions has been enhanced to such an extent by the rapid drop in local viscosity that equivalent conductance may predominate in the product.

A quantitative representation of the temperature dependence of Walden's product may be presented through expressions of the form

$$\Lambda\eta = A_1 \exp[B_1/(T - T_0)] \tag{11}$$

and

$$\Lambda\eta = A_2 \exp[B_2/(V - V_0)] \tag{12}$$

where A_1, B_1, A_2, and B_2 are empirical constants. These equations are basically obtained from those for Λ and η (eq 4 and 1). Best-fit values of the parameters are listed in Table VII along with standard deviation in $\Lambda\eta$. It appears that a simultaneous representation of the temperature dependences of Λ and η is more sound due to their interdependent nature. $T_{0,\Lambda\eta}$ and $V_{0,\Lambda\eta}$ obtained in this manner are in good agreement with those found independently from fluidity and conductance, i.e., $T_{0,\phi,\Lambda}$ and $V_{0,\phi,\Lambda}$ values, respectively, emphasizing further the thermodynamic nature of such parameters.

Acknowledgment. It is a pleasure to thank Professor W. Rahman, Head of the Department of Chemistry, for providing the necessary facilities during the progress of this work. Financial assistance of CSIR (New Delhi) to three of us (M.R.I., B.W., and I.K.) is gratefully acknowledged.

Supplementary Material Available: Tables II and IV and Figure 6 (3 pages). Ordering information is given on any current masthead page.

References and Notes

(1) R. P. Desieno, P. W. Greco, and R. C. Mamajek, *J. Phys. Chem.*, **75**, 1722 (1971).
(2) C. A. Angell and E. J. Sare, *J. Chem. Phys.*, **52**, 1058 (1970).
(3) C. A. Angell, *J. Phys. Chem.*, **68**, 1917 (1964).
(4) P. B. Macedo and A. Napolitano, *J. Chem. Phys.*, **49**, 1887 (1968).
(5) B. R. Hubble and J. L. Copeland, *J. Phys. Chem.*, **76**, 904 (1972).
(6) J. P. Frame, E. Rhodes, and A. R. Ubbelohde, *Trans Faraday. Soc.*, **55**, 2039 (1959).
(7) R. G. Gosshik and J. M. Sterels, *Inorg. Chem.*, **11**, 2180 (1972).
(8) C. T. Moynihan, C. R. Smalley, C. A. Angell, and E. J. Sare, *J. Phys. Chem.*, **73**, 2287 (1969).
(9) B. R. Sundheim and N. Islam, *Appl. Spectrosc.*, **27**, 285 (1973).
(10) B. R. Sundheim and N. Islam, *Appl. Spectrosc.*, **27**, 394 (1973).
(11) N. Islam, *Aust. J. Chem.*, **26**, 2371 (1973).
(12) G. P. Smith, C. H. Liu, and T. R. Griffiths, *J. Am. Chem. Soc.*, **86**, 4796 (1964).
(13) N. Islam and M. R. Islam, *Z. Phys. Chem. (Leipzig)*, **253**, 340 (1973).
(14) N. Islam and M. R. Islam, *Indian J. Chem.*, **12**, 705 (1974).
(15) N. Islam, M. R. Islam, S. Ahmad, and B. Waris, *Appl. Spectrosc.*, **29**, 68 (1975).
(16) C. T. Moynihan, *J. Phys. Chem.*, **70**, 3399 (1966).
(17) A. J. Barlow, J. Lamb, and A. J. Matheson, *Proc. R. Soc. London, Ser. A*, **292**, 322 (1966).
(18) M. H. Cohen and D. Turnbull, *J. Chem. Phys.*, **31**, 1164 (1959).
(19) I. Vogel, "Text Book of Practical Organic Chemistry", 3rd ed, Longmans, Green and Co., London, 1924, pp 163, 171, 189.
(20) D. F. Evans, C. Zawoyski, and R. L. Kay, *J. Phys. Chem.*, **69**, 3878 (1965).
(21) T. Moeller, *Inorg. Synth.*, **5**, 153 (1957).
(22) J. H. Kleinheksel and H. C. Kremers, *J. Am. Chem. Soc.*, **50**, 959 (1928).
(23) *Nat. Bur. Stand., Monogr.*, No. 55, p 8 (1962).
(24) A. K. Doolittle, *J. Appl. Phys.*, **22**, 1471 (1951).
(25) Equation 3 was first suggested by H. Vogel [*Phys. Z.*, **22**, 645 (1921)] and termed the Vogel–Tammann–Fulcher (VTF) expression. This has been used extensively in representing the temperature dependence of relaxation processes in glass-forming liquids. Equation 4 was originally developed by Cohen and Turnbull (see ref 18) for glass-forming molecular liquids on the basis of a free volume model and explains the significance of inserting a temperature term into the frequency factor of the VTF equation. Later on, Angell applied this equation satisfactorily to explain transport processes in fused salts [C. A. Angell, *J. Phys. Chem.*, **68**, 218 (1964); **69**, 2137 (1965); *J. Electrochem. Soc.*, **112**, 1224 (1965); *J. Phys. Chem.*, **70**, 3988 (1966)] as well as in glass-forming mixtures of molten salts [C. A. Angell, *J. Phys. Chem.*, **68**, 1917 (1964); C. T. Moynihan, C. R. Smalley, C. A. Angell, and E. J. Sare, *J. Phys. Chem.*, **73**, 2287 (1969)]. T_0 is a more significant factor known as "ideal glass transition temperature" at which free volume appears to originate [see ref 18; A. A. Miller, *J. Phys. Chem.*, **67**, 1031 (1963)] and is characteristic of the chemical system alone.
(26) See paragraph at end of paper regarding supplementary material.
(27) H. Bloom, "The Chemistry of Molten Salts", W. A. Benjamin, New York, N.Y., 1967, p 100.
(28) C. A. Angell, *J. Chem. Phys.*, **46**, 4673 (1967).
(29) C. A. Angell and C. T. Moynihan, "Molten Salts: Characterization and Analysis", G. Mamantov, Ed., Marcel Dekker, New York, N.Y., 1969, pp 347–352.
(30) $E_{cor,\Lambda}$ may be obtained in a similar manner as $E_{cor,\phi}$.
(31) L. C. Kenausis, E. C. Evers, and C. A. Kraus, *Proc. Natl. Acad. Sci. U.S.*, **48**, 121 (1962); **49**, 141 (1963).
(32) F. R. Longo, P. H. Daum, R. Chapman, and W. G. Thomas, *J. Phys. Chem.*, **71**, 2755 (1967).
(33) N. P. Yao and D. N. Bennion, *J. Phys. Chem.*, **75**, 3586 (1971).
(34) N. Islam, M. R. Islam, S. Ahmad, and B. Waris, *J. Am. Chem. Soc.*, **97**, 3026 (1975).
(35) R. L. Kay and D. F. Evans, *J. Phys. Chem.*, **70**, 2325 (1966).

Interactions of Multivalent Coions and Sodium Ions with Polyelectrolytes by Diffusion Studies

Marie Kowblansky and Paul Ander*

Department of Chemistry, Seton Hall University, South Orange, New Jersey 07079 *(Received July 31, 1975)*

Publication costs assisted by Seton Hall University

The interactions of coions with polyelectrolytes have been investigated in aqueous solutions of sodium poly(styrenesulfonate) containing NaCl, Na_2SO_4, and $Na_4Fe(CN)_6$. The behavior of sulfate ion in sodium poly(acrylate) solutions also has been studied. Self-diffusion coefficients are reported for the anions and cations of the simple salts in the concentration range 5×10^{-4} to 1×10^{-2} N, with the polyelectrolyte concentration ranging from 2×10^{-5} to 2×10^{-1} N. With polyelectrolyte present the self-diffusion coefficients of the coions and counterions are lower than those reported for aqueous solutions containing only the simple electrolyte. The self-diffusion coefficients of the simple ions are found to be dependent on the concentration ratio of polyelectrolyte to simple salt. Sodium ion self-diffusion coefficients are shown to be independent of the valence of the coion present in the solution. The experimental results are compared with those predicted from Manning's theory of polyelectrolyte solutions.

It is generally believed that counterions are affected to a great extent by the presence of polyions in solution[1-7] but that coions are little affected by the presence of the polyelectrolyte. From electric transport[8] and ionic activity coefficient[9] experiments of sodium poly(styrenesulfonate) (NaPSS) in aqueous sodium chloride solutions Nagasawa infers that coion–polyion interactions are not significant. Yet several other experimental investigations[7,10-18] have indicated that the coion does have a noticeable effect on the solution properties of polyelectrolytes. Also, the model for polyelectrolyte solutions developed by Manning predicts that coions, as well as the counterions that do not condense onto the polyion, interact with the polyion in a similar manner by Debye–Hückel interactions.[7,19-21] The theory has been shown to be successful for predicting the interactions of monovalent and divalent counterions with the polyion.[7,22,23] For coions, successful correlation with the theory has been reported only for the interaction of monovalent coions with the polyion.[24] To extend the studies of the behavior of coions in polyelectrolyte solutions, we have examined the interaction of multivalent coions with polyions by self-diffusion experiments. Here we discuss the results of self-diffusion measurements of Cl^-, SO_4^{2-}, $Fe(CN)_6^{4-}$, and Na^+ ions in aqueous solutions of sodium poly(styrenesulfonate) (NaPSS) at 25°C.

Experimental Section

Materials. Poly(styrenesulfonic acid) (HPSS) of molecular weight 70 000 was kindly supplied by the National Starch Co. The sample was purified by passing through cation and anion exchange columns in series (Rexyn 101 cation exchange resin and Rexyn 203 anion exchange resin) followed by tiration with NaOH to a pH of 7. The resulting NaPSS was reprecipitated three times by addition to 2-propanol. The sample was then dried in a vacuum oven at 80°C for 24 h and finally at 120°C just prior to use. The sulfur content of the sample was determined to be 14.44% by Schwarzkopf Analytical Laboratories, which corresponds to an equivalent weight of 222.0 ± 1.4 g. Analysis of the NaPSS by passage through a cation exchange resin and titration of the resulting HPSS with standardized NaOH solution to a phenolphthalein endpoint gave an equivalent weight of 220.6 ± 2.5 g. The average equivalent weight as determined by the two methods is 221.3 g, which corresponds to 93.1% sulfonation of the polystyrene.

Sodium poly(acrylate) (NaPA) of molecular weight 16 000 was prepared from poly(acrylic acid) (PAA), which was purchased from Pfaltz and Bauer. The sodium salt (NaPA) was prepared by titration of the PAA with NaOH. Titration of the PAA with standardized NaOH gave an equivalent weight of 98.8 ± 0.2 g for the NaPA, which corresponds to 95.2 ± 0.2% substitution.

$^{22}NaCl$, $Na^{36}Cl$, and $Na_4Fe(^{14}CN)_6$ were obtained from ICN Pharmaceuticals, Inc. and $Na_2{}^{35}SO_4$ was obtained from New England Nuclear Co.

Radioactive Solutions. Stock solutions of the sodium salts of $^{36}Cl^-$, $Fe(^{14}CN)_6{}^{4-}$, and $^{22}Na^+$ ions were prepared by diluting 0.1 mCi of each of the ions to 100 ml with distilled water. The stock solution of the sodium salt of $^{35}SO_4{}^{2-}$ was prepared by dissolving 1.0 mCi in 250 ml of distilled water.

One milliliter of the appropriate radioactive stock solution was transferred into a 10-ml volumetric flask and evaporated to dryness. To this flask, 10 ml of a radioactively inert NaPSS–simple salt solution of desired composition was added. Table I gives the percentages of the simple ions which were radioactively labeled in each of the resulting salt-containing polymer solutions. Where the concentration of the radioactive ion was greater than 0.3% of the total concentration of that ion, an appropriate amount of simple salt was added to the radioactively inert solution to make the concentrations of the two solutions identical.

Diffusion Measurements. All diffusion measurements were carried out in a constant temperature bath thermostated at 25.00 ± 0.01°C. The open and capillary method originally introduced by Anderson and Saddington[25] was employed without stirring to determine diffusion coefficients. Precision-bore capillary tubes of 1.0 ± 0.005 mm i.d. and 3.80 ± 0.005 cm length were filled with an aqueous solution containing the polyelectrolyte and simple salt, where the ion under investigation was radioactively labeled. After filling, each capillary tube was placed into a 100 × 13 mm

TABLE I: Percentages of the Simple Ions Radioactively Labeled in the Salt-Containing Polyelectrolyte Solutions

Normality of simple salt	NaCl % $^{36}Cl^-$	Na_2SO_4 % $^{35}SO_4^{2-}$	$Na_4Fe(CN)_6$ % $Fe(^{14}CN)_6^{4-}$	NaCl % $^{22}Na^+$
0.01000	5	0.01	0.1	0.00001
0.005000	10	0.01	0.3	
0.001000	50	0.1	1.4	0.0001
0.0005000	50	0.1	2.8	

test tube. Four to five milliliters of a solution, identical in chemical composition but not containing the radioactive ions, was then slowly added to the test tube containing the capillary. Prior to adding, the outer solution was thermostated at the bath temperature. After a sufficient amount of time was allowed for diffusion, the outer solution was carefully withdrawn by means of an aspirator and the radioactivity remaining in the capillary was determined by liquid scintillation counting and compared with the amount of radioactivity originally present. Diffusion coefficients were then calculated using an approximate solution of Fick's equation developed by McKay[26]

$$D = \frac{\pi}{4}\left(1 - \frac{C}{C_0}\right)^2 \frac{l^2}{t} \quad (1)$$

where C and C_0 are the final and initial activities of the capillary, respectively, t is the time allowed for diffusion, and l is the length of the capillary. When the ratio C/C_0 is equal to 0.5, an error of 0.3% results in the value of D from the approximation used in deriving eq 1. The higher is the ratio, the smaller is the error. However, the higher the ratio, the larger the error due to experimental manipulation. Therefore, the ratio was kept in the range of 0.6 to 0.7. This corresponds to diffusion times of approximately 24, 48, 72, and 48 h for Cl^-, SO_4^{2-}, $Fe(CN)_6^{4-}$, and Na^+, respectively.

Radioactive Counting. Upon removal of the capillary from the diffusion test tube, the outside of the capillary was wiped dry with tissue paper and its radioactive content was analyzed while still in the capillary tube using a Packard Tri-Carb liquid scintillation spectrometer Model 3385. Each sample was counted to a minimum of 20 000 counts. To eliminate the need of determining the values of C and C_0 for each capillary, precision bore capillaries matched to within ±0.005 cm length and ±0.005 cm i.d. were used. Four capillaries were used to determine one value of C_0, and a minimum of six capillaries were used to determine the value of one diffusion coefficient. Validation of the technique was accomplished by determining the diffusion coefficient of Cl^- in 0.030 N NaCl. The resulting value of 1.97 ± 0.03 cm^2/s, which is an average of ten determinations, compares well with the literature value of 1.96×10^{-5} cm^2/s reported by Wang and Miller.[27] The average standard errors of the diffusion coefficients reported below are 2, 3, 4, and 4% for Cl^-, SO_4^{2-}, $Fe(CN)_6^{4-}$, and Na^+ ions, respectively.

Results and Discussion

Self-diffusion coefficients for Cl^-, SO_4^{2-}, and $Fe(CN)_6^{4-}$ ions were determined in aqueous solutions of completely neutralized sodium poly(styrenesulfonate) (NaPSS) containing NaCl, Na_2SO_4, or $Na_4Fe(CN)_6$. At four simple salt concentrations, 0.01, 0.005, 0.001, and 0.0005 N, the polyelectrolyte concentration was varied between 5×10^{-5} and 0.16 N. Thus the values of X

$$X = n_e/n_s \quad (2)$$

where n_e and n_s are the equivalent concentrations of polyelectrolyte and simple salt, respectively, were kept in the range 0.1–16. To facilitate the comparison between the different coions, the results of the diffusion measurements are presented as the ratio D_i/D_i^0, where D_i is the observed diffusion coefficient of species i and D_i^0 is its value at infinite dilution in the absence of polyelectrolyte, as calculated by the Nernst relation.[28] Calculated D_i^0 values of 2.03×10^{-5}, 1.06×10^{-5}, and 0.738×10^{-5} cm^2/s were used for Cl^-, SO_4^{2-}, and $Fe(CN)_6^{4-}$, respectively. Figures 1, 2, and 3 present the experimental results obtained for the diffusion coefficients of Cl^-, SO_4^{2-}, and $Fe(CN_6)^{4-}$ as a function of X. It is evident from these figures that the presence of NaPSS in aqueous simple salt solutions results in a lowering of the diffusion coefficients of the coions as compared to their values at infinite dilution of simple salt. At constant simple salt concentration the coion diffusion ratio D_i/D_i^0 is found to decrease with increasing X, i.e., increasing polyelectrolyte concentration. As X increases, the decrease is sharp at low values of X, then more gradual at high X values. At the lowest concentrations of each of the simple salts employed (0.0005 N) the diffusion coefficients level off to a constant value at high values of X. Such trends have been observed recently for coion diffusion in aqueous Na_2SO_4 solutions containing sodium iotacarrageenan[29] and sodium alginate.[30] In NaPSS solutions containing 0.0005 N NaCl the diffusion ratio D_i/D_i^0 for Cl^- levels off at 0.90, which should be compared with a value of 0.98 for Cl^- in polyelectrolyte-free NaCl solutions of the same concentration.[31] This difference can only be interpreted as a result of interactions between the chloride ion and the polyelectrolyte. At a constant high value of X, where the polyelectrolyte concentration is high relative to the NaCl concentration, the diffusion ratio D_i/D_i^0 increases with decreasing simple salt concentration. At low X values, the coion diffusion ratio is less dependent on the simple salt concentration and the diffusion coefficients approximate each other more closely for all simple salt concentrations. The dependence of the coion diffusion ratio on the simple salt concentration is most pronounced for the $Fe(CN)_6^{4-}$ ion; the difference in the values of D_i/D_i^0 between 0.0005 and 0.01 N $Fe(CN)_6^{4-}$ is approximately 0.2 at high values of X, while for Cl^- or SO_4^{2-} ions it is less than 0.1. Of particular significance in our observations is that at a given value of X at low simple salt concentrations all the coions, regardless of their charge, interact with the polyion to the same extent; at high X values in 0.0005 N simple salt D_i/D_i^0 levels off at 0.90, 0.86, and 0.86 for Cl^-, SO_4^{2-}, and $Fe(CN)_6^{4-}$ coions, respectively, and at low X values nearly identical diffusion ratios are obtained.

To note the effect of the viscosity of the solution on the coion diffusion coefficient, $D_{Cl^-}/D^0_{Cl^-}$ ratios were determined using NaPSS of 3×10^6 molecular weight in 0.001 N NaCl. These were compared with the values obtained for NaPSS of 70 000 molecular weight. At $X = 10$ in 0.001 N NaCl the reduced viscosities are 160 and 1.80 dl/g for the high and low molecular weight samples, respectively. Figure 4 demonstrates that at low values of X, $D_{Cl^-}/D^0_{Cl^-}$ ratios were the same for both NaPSS samples within the experimental error. However, at X values greater than six, the coion diffusion ratios for the higher molecular weight NaPSS sample were approximately 10% lower. Dolar et al.[32] also observed only a small molecular weight dependence on the electrical conductivity of NaPSS in aqueous

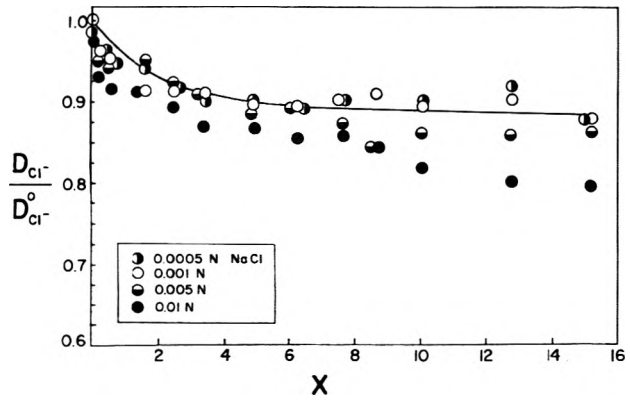

Figure 1. The dependence of the self-diffusion ratio of chloride ion on X in NaPSS solutions. The solid line is predicted from Manning's theory.

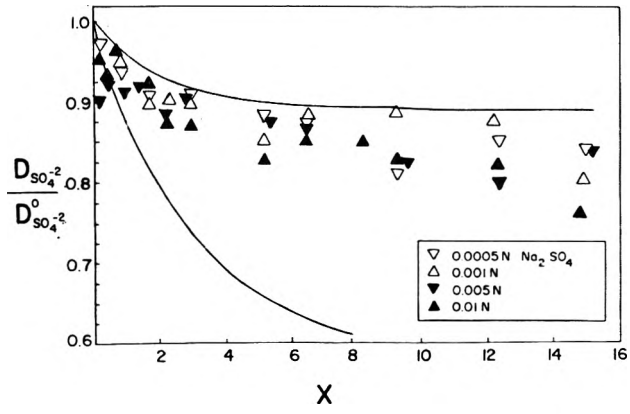

Figure 2. The dependence of the self-diffusion ratio for sulfate ion on X in NaPSS solutions. The solid lines are predicted from Manning's theory; the upper line is for monovalent coions and the lower line is for divalent coions.

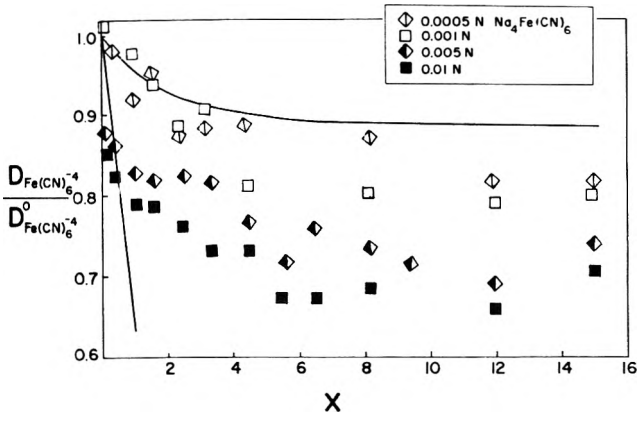

Figure 3. The dependence of the self-diffusion ratio for ferrocyanide coion on X in NaPSS solutions. The solid lines are predicted from Manning's theory; the upper line is for monovalent coions, the lower line is for tetravalent coions.

solution. It is interesting that the mobility of small molecules and ions in a given solvent medium have been found to be affected only to a small extent by the presence of nonionic macromolecules, although the viscosity of the macromolecular solution may be much higher than the viscosity of the polymer-free solution.[33]

To determine the effect of coion charge on counterion–

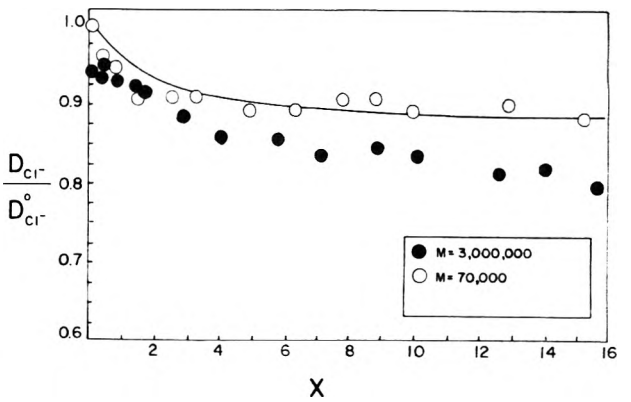

Figure 4. The effect of the molecular weight of two sodium poly(styrenesulfonate) samples on the self-diffusion ratio of the chloride ion.

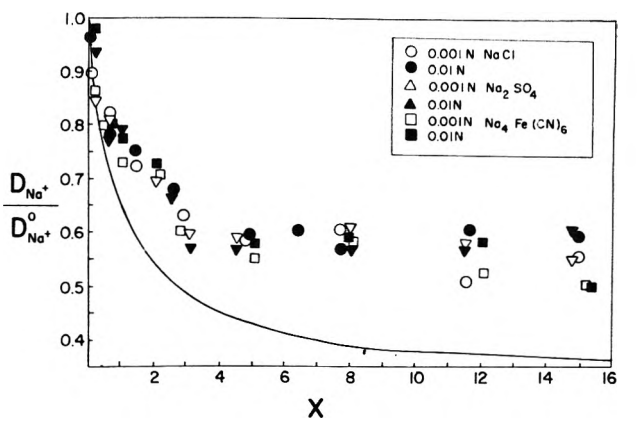

Figure 5. The dependence of the self-diffusion ratio of sodium ion in sodium poly(styrenesulfonate) solutions containing the sodium salts of chloride, sulfate, and ferrocyanide ions. The solid line is predicted from Manning's theory.

polyion interactions, the diffusion coefficients of Na^+ in NaPSS solutions containing the sodium salts of Cl^-, SO_4^{2-}, or $Fe(CN)_6^{4-}$ were also measured. The results are presented in Figure 5. As would be expected from electrostatic considerations, the counterion is seen to interact with the polyion more strongly than any of the coions investigated; i.e., the counterion diffusion ratio is more depressed from its value at infinite dilution ($D^0_{Na^+} = 1.33 \times 10^{-5}$ cm^2/s) than it is for the coions. From Figure 5 it is evident that the charge of the coion appears to have no effect on the interaction of the counterion with the polyion; the diffusion coefficient of the counterion is the same whether monovalent, divalent, or tetravalent coion is present in the solution. While the diffusion ratio of the coions is found to be dependent on the *total* concentration of polyelectrolyte and simple salt of the solution, no such dependence is observable for the counterion, within experimental error, even in ferrocyanide solutions where the effect was quite pronounced for the coion. The diffusion ratio of sodium ion appears to be primarily dependent on the ratio of equivalent concentrations of polyelectrolyte to simple salt, i.e., the concentration parameter X.

As mentioned in the introductory material, part of the stimulation for the present study was Manning's theory of polyelectrolytes inasmuch as it predicts different experimental values for counterions and coions of different valence type. Representing the polyion as an infinitely long

line charge, Manning formulated limiting laws describing the colligative and transport properties of polyelectrolyte solutions in the presence and absence of simple salts.[19-21] The theory was extended to polyelectrolyte solutions containing monovalent and multivalent counterions and coions by Manning and Devore.[34,35] Support for the rod-like model was presented by Schmitt and Varoqui.[36] They describe electrical and mass transport in salt-free polyelectrolyte solutions using nonequilibrium thermodynamics and conclude that the rod-like model best approximates the experimental data at high degrees of neutralization.

Central to Manning's theory is the dimensionless parameter ξ which is related to the charge density of the polyion

$$\xi = e^2/\epsilon kTb \tag{3}$$

where e is the charge on a proton, ϵ is the dielectric constant, k is the Boltzmann constant, T is the temperature, and b is the distance between adjacent charged groups on the polyion. At values of ξ greater than a critical value ξ_c given by

$$\xi_c = |z_p z_1|^{-1} \tag{4}$$

where z_p is the charge of a single charge-site on the polyion and z_1 is the charge of the counterion, counterions condense on the polyion to reduce the charge density to the critical value. For our sample of NaPSS $\xi = 2.65$ and $\xi_c = 1$. It then follows that for our system the fraction of charge neutralized on the chain by counterions is $(1 - \xi^{-1})$ and the fraction of uncondensed counterions is ξ^{-1}. Debye–Hückel interactions are assumed between all condensed ions and the polyion, and for $\xi_c = 1$ the diffusion of all uncondensed simple ions in solution is described by

$$D_i^{(u)}/D^0_i = 1 - \frac{z_i^2}{3} A(1,\xi^{-1}X) \tag{5}$$

where $D_i^{(u)}$ is the diffusion coefficient of uncondensed ion i, D^0_i is the limiting value at infinite dilution of ion i in the absence of polyelectrolyte, z_i is the charge of the ion i, and $A(1,\xi^{-1}X)$ is a function of the *effective* charge density ($\xi_c = 1$) of the polyion and the effective X value ($\xi^{-1}X$). The series $A(1,\xi^{-1}X)$ is

$$A(1,\xi^{-1}X) = \sum_{\substack{m=-\infty \\ (m,n)\neq(0,0)}}^{\infty} \sum_{n=-\infty}^{\infty} [\pi(m^2 + n^2) + |z_1|(|z_1| + |z_2|)\xi X^{-1}]^{-2} \tag{6}$$

where the subscripts 1 and 2 refer to the counterions and coions, respectively.

Since a fraction of the counterions in solution are condensed onto the polyion, the diffusion coefficient of the counterion D_1 is the sum of the diffusion coefficients of the condensed and uncondensed counterions

$$D_1 = (n_e + n_s)^{-1}[D_1^{(c)}(1 - \xi^{-1})n_e + D_1^{(u)}(\xi^{-1}n_e + n_s)] \tag{7}$$

where $D_1^{(c)}$ is the diffusion coefficient of the condensed counterions, which Manning assumed to be equal to zero, and $D_1^{(u)}$ is the diffusion coefficient of the uncondensed counterions interacting with the polyion by Debye–Hückel forces, given by eq 5. For monovalent counterions, the expression for the diffusion of the counterion, therefore, reduces to the following form

$$D_1/D^0_1 = [(\xi^{-1}X + 1)/(X + 1)][1 - \tfrac{1}{3}A(1,\xi^{-1}X)] \tag{8}$$

where $(\xi^{-1}X + 1)/(X + 1)$ represents the fraction of *total* uncondensed counterions. For the coion, no condensation occurs and the coion diffusion coefficient ratio D_2/D^0_2 is obtained in terms of Debye–Hückel interactions

$$D_2/D^0_2 = 1 - \frac{z_2^2}{3} A(1,\xi^{-1}X) \tag{9}$$

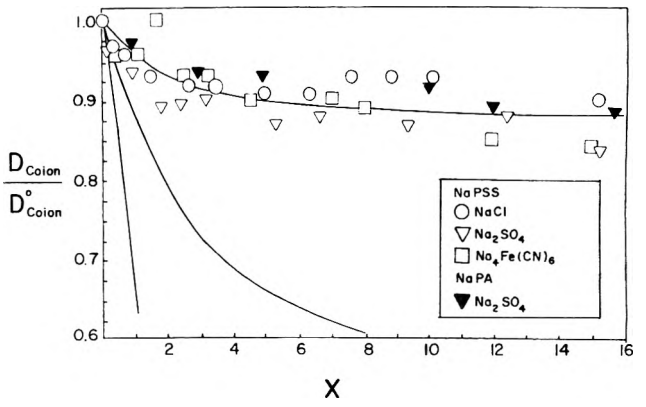

Figure 6. A comparison of the experimental coion self-diffusion ratios extrapolated to zero ionic strength. The solid lines are predicted from Manning's theory for monovalent, divalent, and tetravalent coions.

According to eq 9 a large decrease in D_2/D^0_2 (i.e., an increase in coion–polyion interaction) with increasing coion valence is predicted. The data for the diffusion of the monovalent coion presented in Figure 1 are in excellent agreement with theory, which is given by the solid line, particularly at the lowest concentrations studied. It is evident from Figures 2 and 3, that for higher-valent coions Manning's theoretical predictions given by the solid lines do not adequately describe the experimental findings. The extent of coion–polyion interaction is greatly overestimated. In fact, physically unreal negative diffusion ratios are theoretically predicted for coions of valence greater than 2, in the presence of monovalent counterions. While the Manning theory predicts a considerable difference in the behavior of coions of different valence type, our observations indicate that at low total concentrations of polyelectrolyte and simple salt the interactions of multivalent coions approximate those of the monovalent coions.

According to the theory, polyion–simple ion interactions depend upon the concentration ratio of polyelectrolyte to simple salt X and not upon the concentration of either. Yet our observations indicate that the coion ratio D_i/D^0_i not only depends on X, but also on the *total* concentration of ionic species, particularly for coions of higher valence type. Since Manning's predictions are limiting laws which are strictly valid in the limit of infinite dilution, where simple ion–simple ion and polyion–polyion interactions are not taken into account, it is not surprising that the diffusion data for Cl^- ion agrees more closely with theory at the lowest concentrations than at the higher ones. When X is constant, as n_s approaches zero, n_e must also approach zero. Therefore by extrapolating the diffusion data at a constant X to zero simple salt concentration, the total ionic strength is also necessarily approaching zero, and such extrapolated values should serve as a more valid test of the Manning theory. At a constant value of X a linear relationship is obtained between the diffusion coefficients and the square root of the concentration of simple salt, thereby allowing extrapolation to infinite dilution of simple salt. Figure 6 illustrates the comparison of theoretical D_i/D^0_i values for each coion studied and the extrapolated experimental

TABLE II: A Comparison of Theoretical and Experimental Values of $D_{Na^+}/D^0_{Na^+}$ and γ_{Na^+} in NaPSS–NaCl–H_2O Solutions of 25° C

Present study			Ref 38				Ref 37			Ref 39		
X	Exptl ($D_{Na^+}/D^0_{Na^+}$)	Theor (D_{Na^+}/D_{Na^+})	X	Exptl $\gamma_{\pm}$[a]	Exptl γ_{Na^+}[b]	Theor γ_{Na^+}	X	Exptl γ_{Na^+}	Theor γ_{Na^+}	X	Exptl γ_{Na^+}	Theor γ_{Na^+}
1	0.76	0.66	1	0.87	0.62	0.65	1	0.65	0.64	2.7	0.47	0.49
5	0.58	0.44	5	0.58	0.43	0.40						
10	0.56	0.39	10	0.53	0.40	0.34	10	0.40	0.32			
14	0.56	0.37	20	0.49	0.36	0.30	20	0.38	0.28			

[a] Values extrapolated at constant X to zero total ionic strength. [b] Calculated from extrapolated experimental $\gamma_{\pm}$ values and Manning's theoretical values for γ_{Cl^-}.

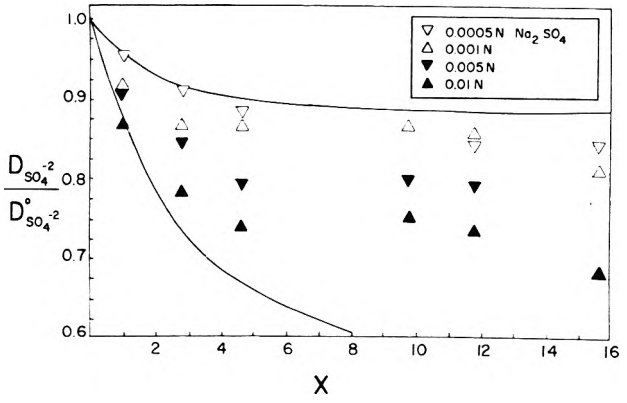

Figure 7. The dependence of the self-diffusion ratio of the sulfate ion on X in sodium poly(acrylate) solution. The solid lines are predicted from Manning's theory; the upper one for monovalent coions and the lower one for divalent coions.

values of D/D^0_i at constant X values. It can be concluded that at infinite dilution no specific effects due to coion charge are operative and that in the absence of simple ion–simple ion and polyion–polyion interactions all coions interact with the polyion to the same extent, regardless of their charge, i.e., according to Manning's prediction for monovalent coions.

To note if our results are valid for polyelectrolytes in general or are distinct for sodium poly(styrenesulfonate), diffusion measurements of SO_4^{2-} in NaPA solutions at the same concentration as those of the NaPSS–Na_2SO_4 solutions previously discussed are presented in Figure 7. The results further substantiate our conclusion that multivalent and monovalent coions interact with the polyelectrolyte to the same extent, and that this behavior is not unique for the poly(styrenesulfonate) polyion. Although a greater ionic strength dependence is observed than in the case of the NaPSS solutions, at the lowest concentrations of simple salt investigated (0.0005 N), $D_{SO_4^{2-}}/D_{SO_4^{2-}}$ was found to closely approach the Manning limiting law values for monovalent coions. Furthermore, the extrapolated values are also in excellent agreement with comparable extrapolated results for SO_4^{2-} in NaPSS solutions, as seen in Figure 6. Similar results were recently obtained for the diffusion of SO_4^{2-} in aqueous Na_2SO_4 solutions of sodium iota-carrageenan,[29] an ionic polysaccharide containing repeating sulfate groups, and sodium alginate,[30] an ionic polysaccharide containing repeating carboxyl groups. Thus, it can be concluded that the interaction of coions with polyions are independent of the specific nature of the charged groups on the polyion.

For the counterion, Manning's theory predicts that the charge of the coion should have a negligible effect on the counterion–polyion interaction. This has been confirmed by our observations shown in Figure 5. However, while agreement with the theory is good for low X values, our data indicate that for higher X values the interaction between uncondensed sodium ions and the poly(styrenesulfonate) polyion is not as strong as is predicted. While theory predicts that the diffusion ratio should attain a constant value of 0.38 at high values of X, experimentally a value of 0.58 is obtained. While quantitative agreement with theory at high values of X is not good, qualitatively the prediction that a constant fraction of counterions will remain uncondensed has been substantiated as is manifest by the fairly constant experimental values of $D_{Na^+}/D^0_{Na^+}$ at $X > 4$.

TABLE III: Comparison of $D_{Na^+}/D^0_{Na^+}$ in Aqueous Solutions with and without Simple Salt Present

Concn range, n_e	$D_{Na^+}/D^0_{Na^+}$ Exptl	Theor	Mol wt	Ref
0.01–0.1[a]	0.38–0.50[c]	0.31	40 000	32
0.01–0.1[a]	0.38–0.50[c]	0.31	100 000	32
0.01–0.1[a]	0.38–0.50[c]	0.31	500 000	32
0.01–0.1[a]	0.50–0.59	0.35	300 000	40
0.01–0.7[a]	0.39–0.52	0.33	300 0000	41
0.01–0.15[b]	0.57	0.38	70 000	This study

[a] Salt-free solutions. [b] Salt-containing solutions ($X > 4$). [c] From electric-transport experiments.

To further analyze our results of the self-diffusion of Na^+ in aqueous NaCl solutions of NaPSS, use will be made of reported ionic activity coefficients. Ueda and Kobatake[37] have measured single ion activity coefficients of chloride ions γ_{Cl^-} and of sodium ions γ_{Na^+} in aqueous solutions of NaPSS. At a constant value of X, their data show that $\gamma_{Cl^-}/\gamma^0_{Cl^-}$, the ratio of single ion activity coefficient in polyelectrolyte solution to that in polyelectrolyte-free solution is much more strongly dependent on the simple salt concentration than is $\gamma_{Na^+}/\gamma^0_{Na^+}$, i.e., at $X = 10$, $\gamma_{Cl^-}/\gamma^0_{Cl^-} = 0.96$ for 0.001 N NaCl and 0.83 in 0.01 N NaCl, while $\gamma_{Na^+}/\gamma^0_{Na^+} = 0.4$ and 0.35 for the same concentrations of NaCl, respectively. This shows a trend analogous to our diffusion results, as is evident from Figures 1 and 4. At $X = 10$, $D_{Cl^-}/D^0_{Cl^-}$ ranges from 0.82 to 0.91 and for $D_{Na^+}/D^0_{Na^+}$ no concentration dependence is observed. Mean activity coefficients $\gamma_{\pm}$ for NaCl in aqueous NaPSS–NaCl solutions determined by Kwak[38] show that at high values of X, $\gamma_{\pm}$ is not as dependent on the ionic strength as at low values of X. This is just as one would expect in view of our observations that diffusion coefficients for chloride ion are dependent on ionic strength and for sodium they are not; at high X values the sodium ion concentration is high as compared with that of the chloride ion, while at low values of X the

concentration of chloride ion approximates that of sodium ion in solution. Since it has already been demonstrated that Manning's predictions of D_i/D^0_i for Cl^- are in good agreement with experiment, it will be assumed that the predictions for the coion activity coefficients are equally good at infinite dilution (the same assumptions were utilized in the derivation of both properties). Therefore, using the experimental results of Kwak for $\gamma_\pm$ extrapolated to zero ionic strength, γ_{Na^+} can be calculated using the theoretical values of γ_{Cl^-} calculated from Manning's theory (eq 47 of ref 19). These calculated values, along with the results of several other studies, are correlated with our diffusion measurements in Table II. It becomes immediately apparent from the data in Table II that the measured values of γ_{Na^+} are in much better agreement with the Manning limiting laws than are the diffusion coefficients. In *salt-free* NaPSS solutions electric transport[32] and self-diffusion[40,41] data for sodium ions are also higher than predicted by the Manning theory. This is shown in Table III, where the diffusion coefficients of sodium ions in salt-free NaPSS solutions are compared with those obtained in the present study at high values of X. Such a comparison is valid since the properties of NaPSS solutions containing simple salt at high X values should approach those of salt-free solutions (where $X \rightarrow \infty$). Since the same electrostatic assumptions were utilized in the Manning theory for predicting both activity and diffusion coefficients it is surprising that the predictions for counterion activity coefficients agree well with experiment, while the predictions for counterion diffusion coefficients do not. This discrepancy leads one to suspect that the diffusion coefficient of the poly(styrenesulfonate) polyion may be greater than 10^{-7} cm/s (as is usually expected for macromolecules), and thus the assumption that $D_1^{(c)}$ is significantly smaller than $D_1^{(u)}$ in eq 7 would not be valid. This possibility is currently being investigated in our laboratory.

Acknowledgment. Professor G. S. Manning is gratefully acknowledged for his discussion pertaining to this work. This work was partially supported by NIH Research Grant No. GM 21234-01.

References and Notes

(1) S. A. Rice and M. Nagasawa, "Polyelectrolyte Solutions", Academic Press, New York, N.Y., 1961, Chapter 9.
(2) F. Oosawa, "Polyelectrolytes", Marcel Dekker, New York, N.Y., 1971, p 60.
(3) R. W. Armstrong and U. P. Strauss, "Polyelectrolytes" in "Encyclopedia of Polymer Science and Technology", Vol. X, Wiley, New York, N.Y. 1969.
(4) A. Katchalsky, *Pure Appl. Chem.*, **26**, 327 (1971).
(5) G. S. Manning, *Annu. Rev. Phys. Chem.*, **23**, 117 (1972).
(6) M. Nagasawa, *J. Poly. Sci.*, Symposium No. 49, 1 (1975).
(7) G. S. Manning in "Polyelectrolytes", E. Selegny, Ed., Reidel Publishing Co., Dordrect, Holland, 1974.
(8) M. Nagasawa, I. Noda, T. Takahashi, and N. Shimamato, *J. Am. Chem. Soc.*, **76**, 2286 (1972).
(9) M. Nagasawa, M. Izumi, and I. Kagawa, *J. Polym. Sci.*, **37**, 375 (1959).
(10) M. J. Pikal and G. E. Boyd, *J. Phys. Chem.*, **77**, 2918 (1973).
(11) P. H. von Hippel and T. Schleigh, *Acc. Chem. Res.*, **2**, 257 (1969).
(12) H. Eisenberg and G. R. Mohan, *J. Phys. Chem.*, **63**, 671 (1959).
(13) H. Eisenberg and D. Woodside, *J. Chem. Phys.*, **36**, 1844 (1962).
(14) A. Takahashi, S. Yamori, and T. Kagawa, *Nippon Kagaku Zasshi*, **83**, 11, 14 (1962).
(15) J. T. G. Overbeek, A. Vrij, and H. F. Huisman, In "Electromagnetic Scattering", M. Kerker, Ed., Macmillan, New York, N.Y., 1962, p 321.
(16) R. L. Gustufson, *J. Phys. Chem.*, **67**, 2549 (1963).
(17) T. J. Podlas and P. Ander, *Macromolecules*, **2**, 432 (1969).
(18) T. J. Podlas and P. Ander, *Macromolecules*, **3**, 154 (1970).
(19) G. S. Manning, *J. Chem. Phys.*, **51**, 924 (1969).
(20) G. S. Manning, *J. Chem. Phys.*, **51**, 934 (1969).
(21) G. S. Manning, *J. Chem. Phys.*, **51**, 3249 (1969).
(22) D. S. Dixler and P. Ander, *J. Phys. Chem.*, **77**, 2684 (1973).
(23) H. Magdelenat, P. Turq, and M. Chemla, *Biopolymers*, **13**, 1535 (1974).
(24) S. Menezes-Affonso and P. Ander, *J. Phys. Chem.*, **78**, 1756 (1974).
(25) J. C. Anderson and K. Saddington, *J. Chem. Soc.*, S381 (1949).
(26) R. McKay, *Proc. Phys. Soc.*, **42**, 547 (1930).
(27) J. H. Wang and S. Miller, *J. Am. Chem. Soc.*, **74**, 1611 (1952).
(28) R. A. Robinson and R. H. Stokes, "Electrolyte Solutions", Butterworths, London, 1959.
(29) R. A. Sasso and P. Ander, to be submitted for publication.
(30) A. Kowblansky and P. Ander, to be submitted for publication.
(31) P. Turq, Ph.D. Dissertation, University of Paris, 1970.
(32) D. Dolar, J. Span, and S. Isakovic, *Biophy. Chem.*, **1**, 312 (1974).
(33) H. Morawetz, "Macromolecules in Solution", Interscience, New York, N.Y., 1965.
(34) D. I. Devore, Ph.D. Dissertation, Rutgers, The State University, N.J., 1973.
(35) D. I. Devore, and G. S. Manning, *J. Phys. Chem.*, **78**, 1242 (1974).
(36) A. Schmitt and R. Varoqi, *J. Chem. Soc., Faraday Trans.*, **69**, 1087 (1973).
(37) T. Ueda and Y. Kobatake, *J. Phys. Chem.*, **77**, 2995 (1973).
(38) J. C. T. Kwak, *J. Phys. Chem.*, **77**, 2790 (1973).
(39) J. W. Lyons and L. Kotin, *J. Am. Chem. Soc.*, **87**, 1670 (1965).
(40) E. Baumgartner, S. Liberman, and A. Lagos, *Z. Phys. Chem.*, **61**, 211 (1968).
(41) R. Fernandez-Prini and A. E. Lagos, *J. Polym. Sci., Part A*, **2**, 2917 (1964).

Hydroxyl Relaxation in 2,6-Dinitrophenol and 2,6-Dinitro-4-methylphenol

S. P. Tay, J. Kraft, and S. Walker*

Department of Chemistry, Lakehead University, Thunder Bay, Ontario, Canada P7B 5E1 *(Received April 17, 1975)*

Publication costs assisted by Lakehead University

Dielectric absorption studies have been carried out on 2,6-dinitrophenol and 2,6-dinitro-4-methylphenol in a polystyrene matrix and for the latter also in a polyethylene matrix in the 10^2 to 10^8 Hz range at a variety of temperatures, and for the former also in *p*-xylene solution at eight to ten frequencies in the microwave range at three temperatures. *o*-Nitrophenol and *m*-dinitrobenzene have also been examined in the polystyrene matrix, and their enthalpies of activation for molecular relaxation are 12.2 and 25.0 kJ mol^{-1}, respectively. Evidence has been obtained for hydroxyl group relaxation for the two dinitrophenols in the matrices with an enthalpy of activation of ~35 kJ mol^{-1}, and the appreciable divergence of this enthalpy of activation from that of 2,6-dinitrophenol (10.0 kJ mol^{-1}) in the pure solid state could be accounted for in terms of the crystalline electric field.

Introduction

The hydroxyl group in *o*-nitrophenol is generally considered to be in the cis position. In support of this are (a) the NMR work in *o*-nitrophenol in carbon tetrachloride,[1] (b) the absence of an O–H stretching frequency in the 3600-cm^{-1} region,[2] and (c) the absence of overtones in the near infrared.[3] In fact, the O–H stretching frequency of the cis form is shifted by ~370 cm^{-1} to lower frequencies, the shift lying in between that for the o-halophenols (18–105 cm^{-1}), in which some trans form definitely exists,[4] and that for *o*-hydroxyacetophenone (~700 cm^{-1}), which appears to be totally in the cis form. This is borne out by dielectric studies by Antony and Smyth.[5] The *o*-halophenols have been regarded as having weak intramolecular hydrogen bonds while *o*-hydroxyacetophenone has a strong one.

The strength of the hydrogen bond in o-nitrophenol and 2,6-dinitrophenol has been the subject of different viewpoints. From uv absorption Dearden and Forbes[6] concluded that the intramolecular hydrogen bond could be explained in terms of an electrostatic model, that is, there is no need to postulate the presence of a covalent bond contribution; thus from this viewpoint it is to be inferred that the intramolecular bond is not a strong one. However, Flett[2] from infrared evidence classified the intramolecular hydrogen bond in *o*-nitrophenol to be of medium strength. The nuclear shielding parameter[7] for *o*-nitrophenol is considerably greater than that for *o*-chlorophenol, which has a weak hydrogen bond, and appears to indicate that the strength of the hydrogen bond in *o*-nitrophenol is of a similar order to that in methyl salicylate and significantly less than that for salicylaldehyde which Flett classified as having a strong intramolecular hydrogen bond.

Meakins[8] studied the dielectric absorption of a few phenols in the pure solid state with nitro substituents in the 2-, 2,6-, and 2,4,6- positions. No dielectric loss was detected in 2-nitrophenol in the frequency range between 5 Hz and 50 MHz. Two intriguing features from his study on 2,6-dinitrophenol, when the hydroxyl group relaxed by 180° from one planar position with the ring to the other, were: (i) there was an energy difference (ΔE) between the two planar forms, (ii) the enthalpy of activation ($\Delta H_2^{\ddagger}$) for the hydroxyl relaxation was only 10.0 kJ mol^{-1}, whereas for the very similar intramolecularly hydrogen bonded molecule, 2,6-dinitro-4-methylphenol, the $\Delta H_2^{\ddagger}$ is 41.8 kJ mol^{-1}. He tentatively suggested that the reason $\Delta E \neq 0$ might be attributed to a particular molecule being unsymmetrically placed with respect to the neighboring molecules in the crystal lattice. Meakins[9] also examined the dielectric absorption of these phenols in toluene solution at frequencies between 5 and 50 MHz and found that the loss factor increased toward higher frequencies. He considered that this loss was due in part to molecular relaxation and possibly hydroxyl relaxation. It seemed, though, that before definite conclusions could be made with respect to the hydroxyl relaxation in 2,6-dinitrophenol further work was necessary on: (a) dilute solutions of this in a nonpolar solvent at higher frequencies; (b) in the solid state where the influence of neighboring polar molecules is considerably reduced.

With respect to (a) we chose to examine the dielectric absorption of 2,6-dinitrophenol in *p*-xylene solution at several microwave frequencies. Particular emphasis was placed on the high frequencies measurements of about 70 and 140 GHz where the hydroxyl relaxation might have a bigger contribution than the molecular relaxation process.

With regard to (b) we chose to examine the 2,6-dinitrophenol in a polystyrene matrix where a low concentration of the solute could be monomolecularly dispersed[8,10] and, hence, any strong internal electric field, for example, in the crystalline solid, would be largely eliminated.

Experimental Section

The apparatus and procedures employed to determine the dielectric constants and losses of dilute liquid solutions in the microwave region at 1–2.5, 9–35, and 70–145 GHz have been described previously.[11–13] Static dielectric constants were measured at 2 MHz using a WTW dipolemeter.

The errors in ϵ' and ϵ'' by the bridge technique are of the order of ±0.5 and ±2%, respectively.[14] For the measurements at 70 and 145 GHz employing a Michelson interferometer the probable errors of the dielectric constant and loss are 0.2 and 2%, respectively.[13]

The apparatus and procedures employed in the dielectric measurements on dilute solid solutions in the 10^2–10^8-Hz range and the preparation of a polymer matrix have been described.[15]

All compounds were purchased from Aldrich Chemical

Co. and K & K Laboratory and were dried prior to use. The 2,6-dinitrophenol was purified by Soxhlet extraction followed by several recrystallizations from a *p*-xylene–cyclohexane solvent mixture. Purity was confirmed by agreement of the melting point with the literature value. Further checks on purity and presence of water were made by ir and NMR methods.

Results

For the microwave results of the dilute solutions the evaluation of the high-frequency dielectric constant (ϵ_∞), distribution coefficient (α), mean relaxation time (τ_0), discrete relaxation times (τ_1 and τ_2), weight factors (C_1 and C_2), and dipole moment (μ) has been described previously.[16] The use of Debye distributions to analyze the dielectric data of dilute solutions can be defended empirically and theoretically[17] and has been confirmed by experiment.[16] If the dielectric data are analyzed into contributions from two relaxation times, τ_1 and τ_2, the values of the dielectric constant (ϵ'_{calcd}) and the loss (ϵ''_{calcd}) calculated from the τ_1, τ_2, and C_1 values have to correspond with the measured values within the limits of the appropriate experimental error. In fact, for the systems listed in Table I there is, in general, good agreement between the calculated and experimental values within the limits of experimental error. The likely errors in τ_0, α, τ_1, τ_2, and C_2 have been considered as have the cases when the Budó analysis[18] may prove to be unsatisfactory.[16] It should be noted that it might prove equally feasible to analyze the results in terms of a mean relaxation time (τ_0) and a distribution parameter (α), where both this approach and the Budó one (i.e., analysis into τ_1, τ_2, and C_1) yield calculated values of the dielectric constant and loss which correspond with the observed ones within experimental error. However, the Budó analysis is acceptable only if a plausible physical mechanism can be associated with the evaluated parameters.[19]

The microwave dielectric data are presented in Table I. In Table II the values of τ_0, α, ϵ_∞, and ϵ_0 for 2,6-dinitrophenol in *p*-xylene are listed.

Figures 1–4 give the dielectric absorption curves for 2,6-dinitrophenol and 2,6-dinitro-4-methylphenol in polymer matrices in the 10^2–10^8-Hz range. The data were analyzed for a best linear fit to the Fuoss–Kirkwood equation:

$$\cosh^{-1}(\epsilon''_{max}/\epsilon'') = \beta(\ln f_{max} - \ln f)$$

Three parameters obtained were ϵ''_{max}, the maximum loss factor of the absorption, $\tau(= \frac{1}{2}\pi f_{max})$, the mean relaxation time characterizing the dipole motion giving rise to the absorption, and β, the inverse of which measures the width of the absorption relative to the Debye process. The Fuoss–Kirkwood β value may be related to the Cole–Cole α value by an equation given by Poley.[20]

$$\beta\sqrt{2} = (1 - \alpha)/\cos\{(1 - \alpha)\pi/4\}$$

In Table III the values of τ, β, and ϵ''_{max} are listed.

The energy barrier which must be surmounted in the motion of the dipole was evaluated in terms of Eyring enthalpy of activation, $\Delta H_E^\ddagger$, by assuming that the dipole relaxation could be represented by the Eyring rate equation:

$$\tau = \frac{h}{kT}\exp\left(\frac{\Delta H_E^\ddagger}{RT}\right)\exp\left(\frac{-\Delta S_E^\ddagger}{R}\right)$$

Figure 5 gives the log τT vs. T^{-1} plots from which $\Delta H_E^\ddagger$ and $\Delta S_E^\ddagger$, the entropy of activation, are evaluated, and the relaxation time (τ_{200}) at 200 K extrapolated (or interpolated). The free energy of activation $\Delta G_E^\ddagger$ ($= \Delta H_E^\ddagger - T\Delta S_E^\ddagger$) at 200 K was calculated for every system and listed with $\Delta H_E^\ddagger$, $\Delta S_E^\ddagger$, and τ_{200} in Table IV.

TABLE I: Dielectric Constant and Loss Data for 2,6-Dinitrophenol at 293, 313, and 333 K at Several Microwave Frequencies

$10^{-9}\ \omega$, radians sec^{-1}	ϵ'_{meas}	ϵ'_{calcd}	ϵ''_{meas}	ϵ''_{calcd}
		T = 293 K		
888.7	2.28	2.28	0.006	0.004
444.4	2.28	2.28	0.008	0.008
220.6	2.29	2.28	0.018	0.016
150.8	2.29	2.28	0.023	0.023
101.8	2.30	2.29	0.036	0.033
58.5	2.31	2.30	0.048	0.048
22.2	2.36	2.35	0.054	0.054
18.9	2.37	2.36	0.050	0.050
14.5	2.38	2.37	0.044	0.043
15.3	2.37	2.37	0.045	0.045
9.4	2.38	2.38	0.032	0.031
6.6	2.38	2.39	0.024	0.023
6.3	2.39	2.39	0.025	0.022
		T = 313 K		
888.7	2.24	2.25	0.012	0.007
444.4	2.25	2.25	0.011	0.012
150.8	2.26	2.26	0.031	0.031
101.8	2.27	2.27	0.042	0.041
58.5	2.28	2.29	0.050	0.052
15.3	2.35	2.35	0.034	0.035
12.6	2.35	2.35	0.030	0.030
9.4	2.36	2.35	0.024	0.024
7.9	2.36	2.36	0.021	0.021
		T = 333 K		
888.7	2.22	2.21	0.008	0.007
444.4	2.22	2.21	0.012	0.014
220.6	2.23	2.22	0.029	0.025
101.8	2.24	2.23	0.042	0.041
58.5	2.25	2.26	0.046	0.047
15.3	2.30	2.30	0.030	0.027
15.1	2.30	2.30	0.029	0.027
6.3	2.31	2.31	0.013	0.013

TABLE II: Relaxation Time (τ_0, psec), Distribution Parameter (α), Dielectric Constant at Very High Frequency (ϵ_∞), and Static Dielectric Constant (ϵ_0) for 2,6-Dinitrophenol in *p*-Xylene Solution at 293, 313, and 333 K

T, K	τ_0	α	ϵ_∞	ϵ_0
293	31.1	0.02	2.28	2.391
313	22.4	0.04	2.25	2.362
333	18.0	0.06	2.21	2.311

Discussion

For 2,6-dinitrophenol in *p*-xylene solution at 20, 40, and 60°C the distribution parameter (α) is not zero and, in fact, increases with rising temperature, being 0.02, 0.04, and 0.06, respectively. This increment with rising temperature is most unusual for solutions of a polar solute in a nonpolar solvent examined in the microwave region in that where a

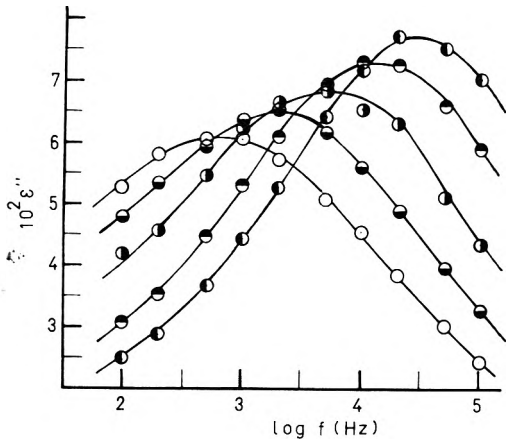

Figure 1. Dielectric absorptions of 0.70 *M* 2,6-dinitrophenol in polystyrene in 10^2–10^5-Hz range: O, 176 K; ◒, 185 K; ◑, 195 K; ◓, 205 K; ◐, 213 K.

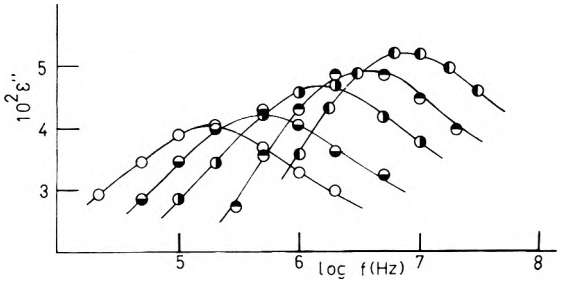

Figure 2. Dielectric absorptions of 0.40 *M* 2,6-dinitrophenol in polystyrene in 10^4–10^8-Hz range: O, 225 K; ◒, 240 K; ◑, 255 K; ◓, 270 K; ◐, 285 K.

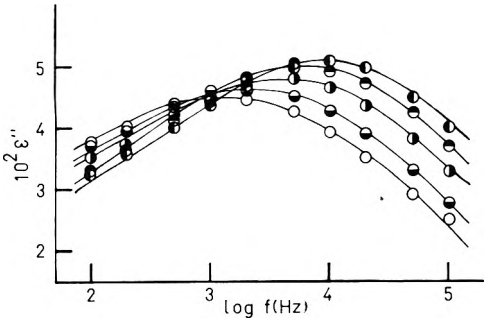

Figure 3. Dielectric absorptions of 0.45 *M* 2,6-dinitro-4-methylphenol in polystyrene in 10^2–10^5-Hz range: O, 186 K; ◒, 191 K; ◑, 196 K; ◓, 201 K; ◐, 206 K.

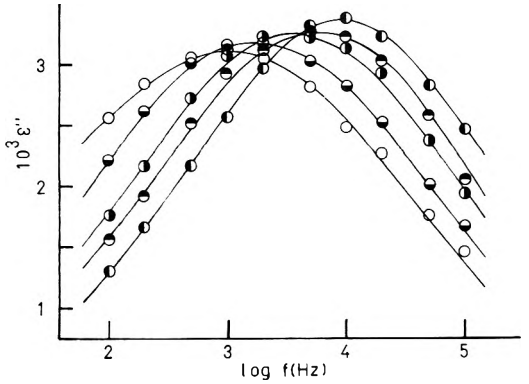

Figure 4. Dielectric absorptions of 0.02 *M* 2,6-dinitro-4-methylphenol in polyethylene in 10^2–10^5-Hz range: O, 186 K; ◒, 191 K; ◑, 196 K; ◓, 201 K; ◐, 206 K.

TABLE III: Relaxation Time (τ, sec), Distribution Parameter (β), and Maximum Dielectric Loss (ϵ''_{max}) for Some Intramolecularly Hydrogen Bonded Phenols and *m*-Dinitrobenzene in Polymer Matrices at a Variety of Temperatures

T, K	$10^6\ \tau$	β	$10^3\ \epsilon''_{max}$
0.70 *M* 2,6-Dinitrophenol in Polystyrene			
176	243	0.30	60.9
185	93.0	0.32	65.5
195	38.2	0.31	68.4
205	11.7	0.32	73.4
213	5.53	0.33	77.1
0.40 *M* 2,6-Dinitrophenol in Polystyrene			
225	0.802	0.38	40.1
240	0.301	0.39	42.6
255	0.097	0.39	46.5
270	0.046	0.42	49.3
285	0.019	0.45	53.1
0.45 *M* 2,6-Dinitro-4-methylphenol in Polystyrene			
186	148	0.27	45.0
191	83.8	0.27	46.4
196	44.7	0.27	48.0
201	27.2	0.25	49.4
206	15.7	0.25	50.7
0.02 *M* 2,6-Dinitro-4-methylphenol in Polyethylene			
186	171	0.30	3.1
191	95.1	0.31	3.1
196	41.9	0.34	3.3
201	28.6	0.34	3.3
206	17.7	0.35	3.4
0.53 *M* *o*-Nitrophenol in Polystyrene			
91	455	0.14	12.9
100	107	0.14	14.9
105	67.8	0.13	15.9
110	23.8	0.13	16.8
115	15.1	0.14	18.1
119	7.90	0.14	18.9
129	2.68	0.14	18.4
0.58 *M* *m*-Dinitrobenzene in Polystyrene			
136	1310	0.17	15.8
146	537	0.16	17.0
156	64.4	0.19	19.4
166	45.9	0.17	19.5
176	9.20	0.18	21.5
211	0.637	0.24	23.7
225	0.127	0.21	25.6
240	0.067	0.28	29.1
255	0.035	0.29	32.8

molecular and a group relaxation occur, α decreases with increasing temperature. As far as we are aware, this also applies to literature data. Magee[21] also found a nonzero distribution parameter for 2,6-dinitrophenol in *p*-xylene at 25, 37.5, 50, and 60°C. However, he employed only four microwave frequencies, the highest of which was 70 GHz, whereas our measurement has been made with eight to ten microwave frequencies, the highest of which is 145 GHz. There would seem little doubt that the distribution parameter is not zero in the temperature range examined and that it increases with increasing temperature.

TABLE IV: Activation Parameters and Relaxation Time at 200 K for Some Intramolecularly Hydrogen Bonded Phenols and *m*-Dinitrobenzene in Polymer Matrices

	$\Delta H_E^{\ddagger}$, kJ mol^{-1}	$\Delta S_E^{\ddagger}$, J K^{-1} mol^{-1}	$\Delta G^{\ddagger}_{200}$, kJ mol^{-1}	τ_{200}, sec
2,6-Dinitrophenol in polystyrene	35.7	+29.0	29.9	15.3×10^{-6}
2,6-Dinitro-4-methylphenol in polystyrene	35.2	+21.2	31.0	28.8×10^{-6}
2,6-Dinitro-4-methylphenol in polyethylene	36.4	+26.6	31.1	30.9×10^{-6}
o-Nitrophenol in polystyrene	12.2	−37.3	19.7	0.03×10^{-6}
m-Dinitrobenzene in polystyrene	25.0	− 2.6	25.5	1.08×10^{-6}

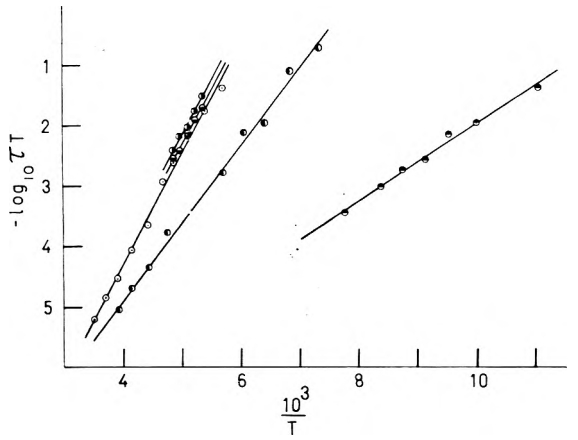

Figure 5. Eyring plots for activation energy in some systems: ○, 2,6-dinitrophenol–polystyrene; ◒, 2,6-dinitro-4-methylphenol–polystyrene; ◑, 2,6-dinitro-4-methylphenol–polyethylene; ●, *o*-nitrophenol–polystyrene; ◐, *m*-dinitrobenzene–polystyrene.

Budó analyses were attempted for our three temperatures and for Magee's four temperatures by a procedure outlined previously.[16] No meaningful analyses with a constant C_1 value were obtained for all seven temperatures. Our three sets of data could be analyzed for a $C_2 \sim 0.15$, whereas Magee's had C_2 values ranging from 0.4 to 0.15. In any case, according to Crossley, Tay, and Walker[16] little reliance can be placed on the τ_2 value from the Budó analysis when $C_1 \gg C_2$. Thus, although it is possible for 2,6-dinitrophenol in *p*-xylene solution that both molecular and group relaxation processes contribute to the dielectric absorption in the microwave region, the latter process cannot be regarded as having been established. Two feasible explanations of the nonzero distribution parameter values could be (a) both molecular and group relaxation processes occur, (b) molecular interaction with a variety of local environments. The latter case b would, however, seem the less probable as one might expect the variety of local environments to decrease with increasing temperature. In case a though, an increase in the τ_1/τ_2 ratio with increasing temperature could account for the increasing α value, and this could occur if $\Delta H_2^{\ddagger} \gg \Delta H_1^{\ddagger}$.

The enthalpies of activation for 2,6-dinitrophenol and *m*-dinitrobenzene in a polystyrene matrix are 35.7 and 25.0 kJ mol^{-1}, respectively, while for o-nitrophenol it is 12.2 kJ mol^{-1}. The wide frequency range, 10^2–10^8 Hz, employed in this study gave good linear plots (see Figure 5) of log τT vs. T^{-1}, even though two different types of apparatus and cells were employed in the frequency ranges of 10^2–10^5 and 10^4–10^8 Hz. For these measurements the error in $\Delta H_E^{\ddagger}$ is less than ±10% since the error in log f_{max} from a Fuoss–Kirkwood analysis is less than ±0.1. This magnitude of error is of the same order as that quoted by Davies and Swain.[10]

The enthalpy of activation of 12.2 kJ mol^{-1} for o-nitrophenol is to be compared with a value of 16.4 kJ mol^{-1} for *o*-dichlorobenzene[10] in a polystyrene matrix where the two solute molecules are fairly similar in size and shape. In view of this and of Meakin's finding that o-nitrophenol in pure solid state gave no dielectric loss, the dielectric absorption observed in the polystyrene would seem attributable to molecular relaxations. This is also supported by its much smaller $\Delta H_E^{\ddagger}$ value compared with those of the two dinitrophenols in the matrix. Higasi[22] considered 120 substances for which $\Delta H_E^{\ddagger}$ and $\Delta S_E^{\ddagger}$ are available for molecular relaxation processes and tentatively postulated that "$\Delta S_E^{\ddagger}$ is zero or has a negative value, if $\Delta H_E^{\ddagger}$ is below 13.4 kJ mol^{-1} ". Thus, negative entropies of activation are well known for molecular relaxation process, and four cases recently reported for polar solutes in a polystyrene matrix are cyclohexyl chloride, cyclohexyl bromide, anthrone, and camphor, where the $\Delta S^{\ddagger}$ values are −12.6, −20.0, −33.5, and −31.4 JK^{-1} mol^{-1}, respectively.[8,10]

2,6-Dinitrophenol and *m*-dinitrobenzene are almost identical in shape and size and have dipole moments of 3.89 and 3.86 D in benzene solution at 298 K, respectively.[23] Each would be expected to have a similar enthalpy of activation for molecular relaxation. However, the value for 2,6-dinitrophenol is 10.7 kJ mol^{-1} greater than that for the rigid *m*-dinitrobenzene which would not be expected if the process were molecular relaxation in each case. Enthalpies of activation for molecular relaxation in a polystyrene matrix are very sensitive to the length of the molecule on the long principal axis; for example, the enthalpies of activation of iodobenzene, *p*-bromotoluene, and 4-bromobiphenyl are 24.1, 30.0, and 59.9 kJ mol^{-1}, respectively (Morgan, Lakshmi, and McLellan, private communication, this laboratory). Thus, the fact that both 2,6-dinitrophenol and 2,6-dinitro-4-methylphenol have observed enthalpies of activation of ~35 kJ mol^{-1} rules out their being attributed to molecular relaxation since the latter molecule is a 2,6-dinitrophenol in which a para substituent has been inserted and thus it would have a considerably bigger enthalpy than the 2,6-dinitrophenol for molecular relaxation. Further, witness the study by Silver and Wood[24] on benzaldehyde and its ring substituents, the insertion of a *p*-methyl group would appear to have very little influence on the barrier to group rotation. A comparison of the similar relaxation times at 200 K for 2,6-dinitrophenol and 2,6-dinitro-4-methylphenol, which are 1.53×10^{-5} and 2.88×10^{-5} sec, respectively, strongly favors the group as opposed to molecular relaxation. A further experiment was carried out to distinguish between a molecular and an intramolecular process for the 2,6-dinitro-4-methylphenol by examining it in a polyethylene matrix. A molecular process exhibits appreciable variation in relaxation time and enthalpy by such a change in local environments, whereas an intramolecular process such as relaxation of a small hydroxyl group may

be expected to be reasonably independent of such a modification. The enthalpy of activation was 36.4 kJ mol^{-1} and the $\tau_{200} = 3.09 \times 10^{-5}$ sec. Hence, this close similarity to the results in polystyrene strongly favored an intramolecular process. Thus, the most reasonable interpretation of our data is that hydroxyl relaxation occurs in both 2,6-dinitrophenol and the corresponding *p*-methyl substituted molecule. The absence of the molecular relaxation is similar to the findings of Davies and Swain,[10] using similar temperature and frequency ranges, namely, that out of the ten flexible molecules which they examined only two yielded the molecular relaxation process, although the intramolecular one was detected in each case. These authors have indicated why the molecular process was not detected under the given conditions.[10]

A value of 35 kJ mol^{-1} for hydroxyl relaxation in 2,6-dinitrophenol and 2,6-dinitro-4-methylphenol in the matrix would seem reasonable for comparison with the value of 41.8 kJ mol^{-1} obtained by Meakins[9] for hydroxyl relaxation in 2,6-dinitro-4-methylphenol in the crystalline solid, whereas the value of 10.0 kJ mol^{-1} obtained by Meakins[9] for 2,6-dinitrophenol in the crystalline solid is hardly explicable in terms of group relaxation without invoking some additional factor. In fact, the suggestion by Fröhlich[25] that there is probably a variation in the barrier height in crystalline solids resulting from the varying relative positions of neighboring molecules would seem to be the most likely reason for the difference in behavior between the matrix and the crystalline solid.

It would seem likely that for 2,6-dinitrophenol in polystyrene that hydroxyl relaxation occurs from one planar hydrogen bonded position to the other. Thus, the transition takes place over an energy barrier which is strongly dependent on the energy required to break the intramolecular hydrogen bond. From the magnitude of its enthalpy of activation it would appear that the intramolecular hydrogen bond in 2,6-dinitrophenol is much closer to being a strong hydrogen bond than a weak one.

Acknowledgment. We wish to express our gratitude to Mr. B. K. Morgan for all his invaluable work on constructing the apparatus in the 10^2–10^8-Hz frequency range and to the National Research Council of Canada for financial support.

References and Notes

(1) J. A. Pople, W. G. Schneider, and H. J. Bernstein "High Resolution Nuclear Magnetic Resonance", McGraw-Hill, New York, N.Y., 1959, p 412.
(2) M. St. C. Flett, *Spectrochim. Acta*, **10**, 21 (1957).
(3) L. Pauling, "The Nature of the Chemical Bond" Cornell University Press, Ithaca, N.Y., 1944, p 319.
(4) C. N. R. Rao, "Chemical Applications of Infrared Spectroscopy", Academic Press, New York, N.Y., 1963, p 181.
(5) A. A. Antony and C. P. Smyth, *J. Am. Chem. Soc.*, **86**, 156 (1964).
(6) J. C. Dearden and W. F. Forbes, *Can. J. Chem.*, **38**, 1837 (1960).
(7) L. W. Reeves, E. A. Allan, and K. O. Stromme, *Can. J. Chem.*, **38**, 1249 (1960).
(8) M. Davies and A. Edwards, *Trans. Faraday Soc.*, **63**, 2163 (1967).
(9) R. J. Meakins, *Trans. Faraday Soc.*, **51**, 371 (1955).
(10) M. Davies and J. Swain, *Trans. Faraday Soc.*, **67**, 1637 (1971).
(11) S. E. Keefe and E. H. Grant, *Rev. Sci. Instrum.*, **39**, 1800 (1968).
(12) W. F. Hassell, M. D. Magee, S. W. Tucker, and S. Walker, *Tetrahedron*, **20**, 2137 (1964).
(13) S. K. Garg, H. Kilp, and C. P. Smyth, *J. Chem. Phys.*, **43**, 2341 (1965).
(14) M. D. Magee and S. Walker, *Trans. Faraday Soc.*, **62**, 3093 (1966).
(15) S. P. Tay and S. Walker, *J. Chem. Phys.*, **62**, 1635 (1975).
(16) J. Crossley, S. P. Tay, and S. Walker, *Adv. Mol. Relaxation Processes*, **6**, 69, 70 (1974).
(17) C. F. J. Böttcher, "Theory of Electric Polarization", Elsevier, Amsterdam, 1952, pp 374–378.
(18) A. Budó, *Z. Phys.*, **39**, 706 (1938).
(19) F. K. Fong and C. P. Smyth, *J. Chem. Phys.*, **40**, 2404 (1964).
(20) N. H. Hill, W. E. Vaughan, A. H. Price, and M. Davies, "Dielectric Properties and Molecular Behavior", Van Nostrand-Reinhold, New York, N.Y., 1969, p 292.
(21) M. D. Magee, Ph.D. Thesis, University of Aston in Birmingham, England, 1967.
(22) K. Higasi, "Dielectric Relaxation and Molecular Structure", Research Institute of Applied Electricity, Hokkaido University, Sapporo, Japan, 1961, p 11.
(23) A. L. McClellan, "Table of Experimental Dipole Moments", W. H. Freeman, San Francisco, Calif., 1963.
(24) H. G. Silver and J. L. Wood, *Trans. Faraday Soc.*, **60**, 5 (1964).
(25) H. Fröhlich, "Theory of Dielectrics", Oxford University Press, London, 1958, p 74.

Hydrogen Permeation in Palladium–Chromium Alloys

W. A. Swansiger,* J. H. Swisher, J. P. Darginis, and C. W. Schoenfelder

Sandia Laboratories, Livermore, California 94550 *(Received July 2, 1975)*

Publication costs assisted by the U.S. Energy Research and Development Administration

As part of a search for new palladium alloys with attractive permeation characteristics for hydrogen isotopes, alloys containing 9.3, 16.8, and 24.2 atom % chromium were evaluated in the temperature range from 322 to 449 K. The permeation coefficient, diffusion coefficient, and hydrogen solubility were all found to decrease with increasing chromium content. The solubility was found to obey Sievert's law in all alloys. The permeation coefficients deviated slightly from classical diffusion-controlled behavior. These deviations are attributed to slow molecular dissociation and adsorption of hydrogen on the surface at low pressures. In some preliminary experiments at high pressure, the Pd–16.8 atom % Cr alloy retained its structural integrity while a commercially available Pd–25 atom % Ag alloy was susceptible to cracking and blistering.

Introduction

Palladium has the scientifically interesting and practically important characteristic of having a very high permeation rate for hydrogen isotopes. At low temperatures and moderate hydrogen pressures, however, a phase change occurs on hydrogen absorption which adversely affects the mechanical properties of palladium. A number of Pd alloy systems have been studied for improved permeation and mechanical properties (see as examples ref 1–12). Alloying of palladium with silver has led to greatly improved properties,[1] and a Pd–25 atom % Ag alloy is now used commercially for hydrogen isotope purification and separation processes.

Because of the highly catalytic nature of Pd and Pd alloys, surface poisoning by impurities is a concern, particularly at low temperatures. For this reason, prior to 1965 there had been rather poor agreement between various investigators who measured permeation constants for hydrogen in Pd and Pd–Ag alloys. More recently, Holleck,[8] for example, has succeeded in obtaining permeation, diffusion, and solubility data which are internally consistent and free from anomalies attributable to surface defects.

Nearly all the published data are based on measurements made at pressure differentials less than 1 atm. A notable exception is the work of Ackerman and Koskinas,[7] who measured permeation rates through Pd–25 atom % Ag alloy tubes at high pressure and a temperature of 673 K. Our calculations show that if Holleck's results[8] are extrapolated by Sievert's law to a pressure of 68 atm, the agreement with Ackerman's results is within a few percent.

The only related work in the past on Pd–Cr alloys was done by Loebich.[3] He found that foils containing 5.0–26.5 atom % chromium were warp and fissure resistant when used for hydrogen purification at high temperatures. No permeation data were published by Loebich.

In the work described here, permeation and diffusion coefficient data were obtained for alloys containing 9.3, 16.8, and 24.2 atom % chromium. Some direct measurements of the hydrogen solubility and the pressure dependence of the permeation rate were obtained at one temperature, 449 K.

Experimental Section

The experimental alloys were prepared by arc melting buttons from mixtures of the two metals. The buttons were inverted and remelted several times to produce homogeneous material. The alloy compositions were obtained by chemical analysis. Hot and cold rolling were used to break up the cast structure and obtain the desired sheet thickness of approximately 0.06 cm (23 mils). Specimens in the form of disks approximately 2 cm in diameter were cut from the sheet, polished metallographically, and washed with distilled water and ethyl alcohol. The cold-rolled disks were sputter-cleaned before mounting in the permeation apparatus. One sample of each composition was used.

Permeation and diffusion coefficients were determined in an all-metal ion-pumped vacuum system using a gas permeation technique. The specimens were placed between two 0.10-cm thick copper gaskets, which in turn were placed between two Varian mini-conflat fittings. The assembly was bolted into the permeation apparatus and enclosed in a 7.6-cm diameter copper heat sink. The hydrogen pressure on the upstream side of the sample was held constant from 0.13 to 13 kPa (1 to 100 mmHg) by a servo-controlled leak valve receiving feedback from a capacitance manometer. Before admission to the upstream side of the system, the hydrogen was purified by passage through a heated Pd–25 atom % Ag tube. Hydrogen permeating into the downstream volume, which was continuously pumped, was detected by either a quadrupole mass spectrometer or an ionization gage. Permeation rates were determined by comparison with calibrated orifice leaks, while diffusion coefficients were determined by least-squares fits to the time-dependent hydrogen flux.

Solubility measurements were made by sealing specimens in glass capsules with known quantities of hydrogen gas. After holding for sufficient time to reach the equilibrium solubility at 449 K, the capsules were quenched in liquid nitrogen. The amount of hydrogen remaining in the gas phase was then measured volumetrically, and the amount of hydrogen absorbed by the specimens was measured after heating under vacuum to release the gas.

Results

Permeation. The temperature dependence of the steady-state permeation coefficient of hydrogen in the experimental alloys is shown in Figure 1 in the form of Arrhenius plots. Results obtained by Holleck[8] for unalloyed Pd and Pd–25 atom % Ag are shown for comparison. The experiments were all performed with an upstream pressure of

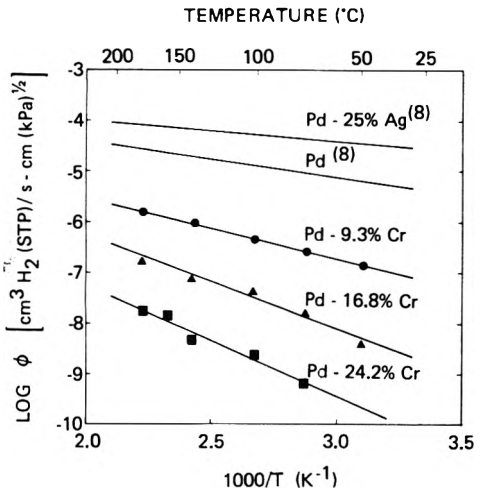

Figure 1. Temperature dependence of the permeation rate of hydrogen in Pd–Cr alloys.

13.33 kPa (100 Torr). As will be discussed later, there was a slight dependence of the permeation coefficient on pressure at 449 K. Figure 1 shows that the permeation coefficient decreases and the temperature coefficient of permeation increases with increasing chromium content. Least-squares calculations were used to obtain equations for the results in the form

$$\phi = \phi_0 \exp(-E_\phi/RT) \quad (1)$$

Values for ϕ_0 and E_ϕ for each alloy are given in Table I. The ϕ_0 values are within approximately a factor of 2 of each other, and E_ϕ increases approximately linearly with chromium content.

Diffusion. Corresponding data (determined at 13.33 kPa upstream pressure) for the temperature dependence of the diffusion coefficients are plotted in Figure 2. Again the diffusion coefficient decreases and the temperature coefficient for diffusion increases with increasing chromium content. The values of D_0 and E_D from equations of the form

$$D = D_0 \exp(-E_D/RT) \quad (2)$$

are given in Table I. The D_0 values are nearly the same for all alloys, and the E_D values increase linearly with chromium content. At 100 Torr upstream pressure the time-dependent hydrogen flux compared very well with the theoretical curve obtained by solution of Fick's second law.

Solubility. Experimental measurements of hydrogen solubility were made only at a single temperature (449 K). The data are plotted in Figure 3 as hydrogen concentration vs. $p^{1/2}$ to show conformance to Sievert's law. Only one value was obtained for the 24.2 atom % Cr alloy because the solubility was so low. A line corresponding to Holleck's results[8] for unalloyed Pd is given for comparison. His results were checked with our technique and the agreement was good; our value of 3.19 cm³ H_2/[cm³ metal kPa$^{1/2}$] was 5% less than a value of 3.36 obtained from Holleck's data.

A summary of the data obtained at 449 K for the variation of permeation coefficient, ϕ, diffusion coefficient, D, and solubility, S, with chromium content is given in Figure 4. Equations fitted to the results are

$$\log \phi = -4.68 - 0.120(\%\ \mathrm{Cr}) \quad (3)$$

$$\log D = -5.15 - 0.069(\%\ \mathrm{Cr}) \quad (4)$$

$$\log S = +0.47 - 0.051(\%\ \mathrm{Cr}) \quad (5)$$

TABLE I. Diffusion and Permeation Constants for Hydrogen in Pd and Pd Alloys

Alloy compositions	ϕ_0 [a]	E_ϕ [b]	D_0 [c]	E_D [b]
Pd–25 atom % Ag [d]	7×10^{-4}	7.96	2.2×10^{-3}	23.03
Pd [d]	1×10^{-3}	13.65	2.9×10^{-3}	22.02
Pd–9.3 atom % Cr	9×10^{-4}	23.49	1.0×10^{-3}	23.87
Pd–16.8 atom % Cr	2×10^{-3}	34.71	1.0×10^{-3}	28.72
Pd–24.2 atom % Cr	1×10^{-3}	42.12	1.3×10^{-3}	32.66

[a] ϕ_0 in cm³ H_2(STP)/sec cm (kPa)$^{1/2}$. [b] E_ϕ and E_D in KJ/g atom. [c] D_0 in cm²/sec. [d] Reference 8.

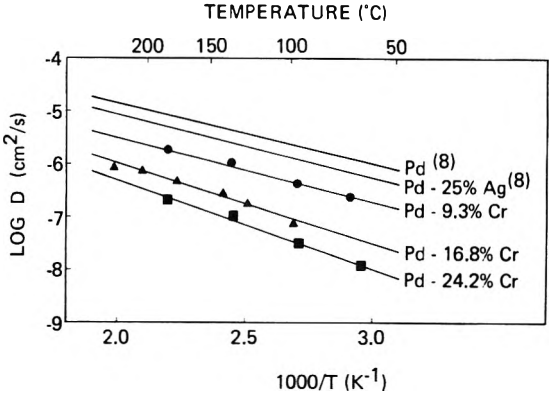

Figure 2. Temperature dependence of the diffusion coefficient of hydrogen in Pd–Cr alloys.

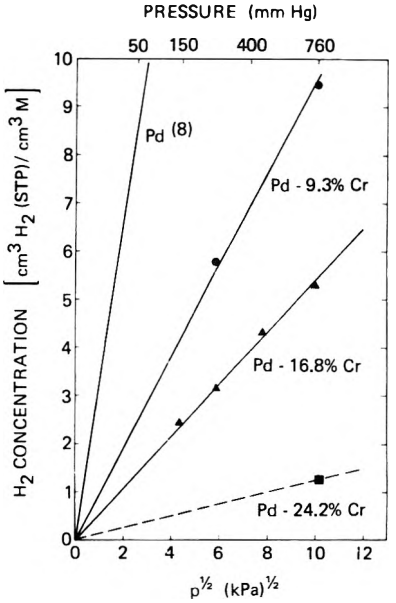

Figure 3. Hydrogen solubility in Pd–Cr alloys at 449 K.

Pressure Dependence of Permeation. As alluded to earlier, variation of the upstream pressure during permeation measurements at 449 K showed a relatively small but systematic effect on the permeation coefficient, ϕ. In principle, ϕ contains a $p^{1/2}$ term to make it a pressure-independent parameter. The observed effect of pressure on the permeation flux, J, is shown in Figure 5 in the form log J vs. log p. The linear behavior corresponds to a pressure depen-

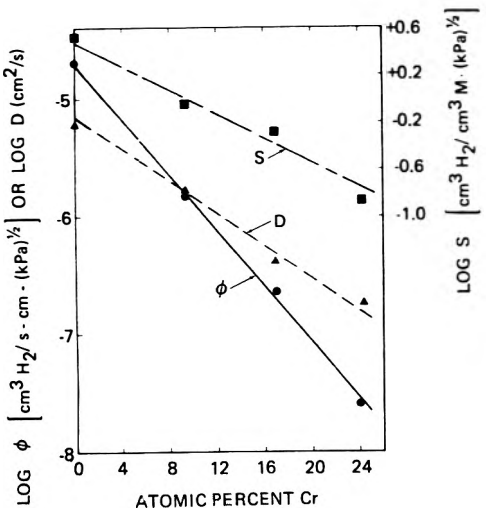

Figure 4. Permeation coefficient, diffusion coefficient, and solubility of hydrogen as a function of chromium content in Pd–Cr alloys at 449 K.

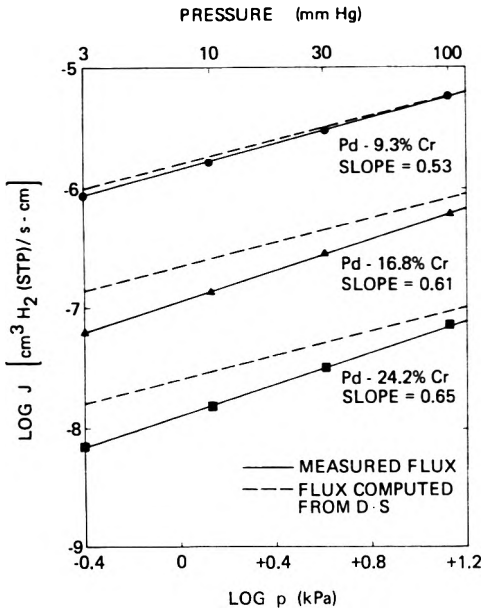

Figure 5. Permeation flux of hydrogen as a function of pressure in Pd–Cr alloys at 449 K.

dence of the type $J = Ap^n$, where $n = 0.53$ for 9.3 atom % Cr, 0.61 for 16.8 atcm % Cr, and 0.65 for 24.2 atom % Cr. The uncertainty in n is believed to be ±0.03. Values for n would probably vary with temperature.

Additional lines are shown in Figure 5 for fluxes computed from the relation $\phi = Jp^{1/2} = DS$, with D and S values taken from Figures 2 and 3. The differences between the computed and experimentally determined results are believed to be deviations from strictly diffusion-controlled permeation. Extrapolation of the results for the 16.8 and 24.2 atom % Cr alloys to higher pressures indicates that the experimental and computed lines should meet at pressures of a few atmospheres. As will be discussed, the deviations from classical behavior may be attributed to slow adsorption and/or dissociation of hydrogen molecules on the surface at low pressures.

High Pressure Experiments. A few experiments were performed at high pressure to investigate structural integ-

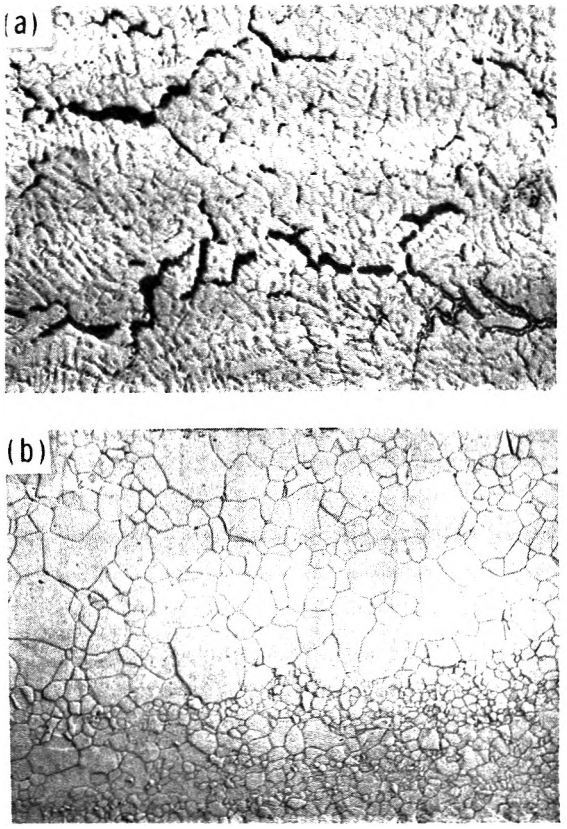

Figure 6. (a) Pd–25 atom % Ag specimen (75X) and (b) Pd–16.8 atom % Cr specimen (75X) after exposure to 50 MPa H_2 at 373 K for 2 days.

rity of the alloys. These tests consisted of exposing specimens of the commercial Pd–25 atom % Ag alloy and the experimental Pd–16.8 atom % Cr alloy at 373 K to a hydrogen pressure of 50 MPa. After holding under these conditions for 2 days, the specimens were examined metallographically for structural damage. As can be seen in Figure 6a and 6b, there was no evidence for damage in the Pd–16.8 atom % Cr specimen, but the Pd–25 atom % Ag specimen was badly cracked, due presumably to excessive swelling.

Discussion

In many permeation studies, the permeation and diffusion coefficients are determined independently, and the solubility is computed from the $S = \phi/D$ relationship. In our results, if the small pressure dependence effect is neglected, equations for S for the various alloys determined from ϕ/D for a pressure of 13.33 kPa (100 Torr) are

0 atom % Cr[8]	$S = 0.3 \exp(+8.37/RT)$	(6)
9.3 atom % Cr	$S = 0.9 \exp(+0.38/RT)$	(7)
16.8 atom % Cr	$S = 2.0 \exp(-5.99/RT)$	(8)
24.2 atom % Cr	$S = 0.8 \exp(-9.46/RT)$	(9)

S is given in units of cm^3 H_2(STP)/[cm^3 alloy $kPa^{1/2}$], and the constant in the exponential term is in kJ/g atom. The solubility decreases with increasing chromium content, and the temperature coefficient changes sign, becoming more negative with increasing chromium content. A change in sign of the temperature coefficient of solubility was also observed in the Pd–Ni system.[10]

Table II shows a comparison of the solubility values

TABLE II: Comparison of Hydrogen Solubility Values at 449 K Measured Directly and Computed from ϕ/D[a]

Atom % Cr	S (measd)	S (compd)
9.3	0.95	0.81
16.8	0.54	0.40
24.2	0.12	0.06

[a] S is given in units of cm³ H_2(STP)/[cm³ alloy $kPa^{1/2}$].

computed from eq 7–9 with values measured experimentally at 449 K. The agreement is reasonably good for the first two alloys. For the third alloy, the agreement is not as good; the measured value may be in error because of the difficulty in measuring the lower hydrogen concentration.

Rapid advances are being made in applying band theory to explain hydrogen solubility in metals.[13] Hydrogen solution in palladium can be considered basically to follow the proton model, in which the hydrogen electrons go into existing holes in the palladium d bands. In fact, 0.4 electrons per Pd atom can be accommodated in these holes,[14] but another 0.3 electrons per Pd atom go into new hydrogen–metal hybrid states created by the presence of hydrogen[15] (a feature of the anion model). Now, when the palladium is alloyed with another metal, the Fermi energy will change, causing either a decrease or increase in the number of holes in the d bands, depending on the metal added.

Using a rigid band approach, one would predict that the Fermi energy would increase with silver additions, i.e., the density of states at the Fermi energy would decrease.[16] If this occurred, the hydrogen solubility should decrease when silver is added to palladium. Experimental data show that the opposite occurs, so it is probable that silver additions create hybridized S-like bands below the Fermi energy (as hydrogen does in yttrium[17]), thereby providing effectively for more holes in the palladium d bands.

In the Pd–Cr system, a rigid band model could produce either an increase or a decrease in electron holes in the d band, depending on whether the Cr bands were Pd-like or the Cr electrons had to be put into existing holes in the palladium d band. Our experimental results suggest that some Cr electrons go into Pd d-band holes, since a decrease in hydrogen solubility is observed.

The solubility effects observed here can also be discussed in terms of a thermodynamic "interaction parameter" formalism developed for liquid iron alloys.[18] A large number of interaction parameters have been compiled for computing the effect of one alloying element on the solubility of another in liquid iron. While the model applies also to solid solutions, a compilation has not been made of available data.

In the interaction parameter model, the activity coefficient, γ, of a constituent in a ternary or multicomponent alloy is expressed as a series of terms. For the Pd–Cr–H system, the expression for γ_H is

$$\ln \gamma_H = \ln \gamma_H^0 + \epsilon_H^H N_H + \epsilon_H^{Cr} N_{Cr} \qquad (10)$$

where γ_H^0 is the activity coefficient of hydrogen at infinite dilution $\epsilon_H^H = \partial \ln \gamma_H/\partial N_H$, $\epsilon_H^{Cr} = \partial \ln \gamma_H/\partial N_{Cr}$, and the N's are concentrations in atom fraction. This model is strictly applicable only to very dilute solutions, but in practice it has been used successfully for moderately concentrated solutions. If γ_H is defined as p_{H_2}/N_H, it can be shown from the data for 449 K in Figures 3 and 4 that eq 10 reduces to

$$\ln \gamma_H = 3.57 + 11.9 N_{Cr} \qquad (11)$$

The second term in eq 10 is zero, which follows from Sievert's law, and the Cr–H interaction coefficient ϵ_H, is found to be +11.9. This value represents a relatively strong thermodynamic interaction of the repulsive type between Cr and H.

Equation 11 can be used to compute hydrogen solubility values for various hydrogen pressures and chromium concentrations at 449 K. There is some risk, however, in using the equation outside the range of the experimental measurements, especially for higher hydrogen pressures and higher chromium concentrations.

With respect to the diffusion coefficient data, the observed effects can be explained in terms of contraction of the crystal lattice of palladium by chromium. Hydrogen is known to dissolve interstitially in metals, so one of the parameters which affects the ease of migration of hydrogen in the material is the size of the interstitial holes. Grube and Knabe[19] have shown that the lattice parameter of palladium decreases continuously with additions up to 60 atom % chromium. Thus there is a correlation between contraction of the crystal lattice and lowering of the diffusion coefficient of hydrogen in Pd–Cr alloys. The size of the effect in Pd–Cr alloys is approximately the same as reported for Pd–Rh alloys.[11]

It is not felt that the size of interstitial holes is the only parameter of importance in affecting hydrogen diffusion rates. Band theory might shed more light on diffusion effects, but any conclusions drawn at the present time would be more speculative than for solubility effects and will not be attempted here.

Another topic that merits discussion is the pressure dependence of the permeation rate. The observation that the permeation rate at low pressures is lower than one would predict from the solubility and diffusion coefficient could be due to any one of several possible effects: (i) insufficient flux of hydrogen molecules impinging on the surface, (ii) low sticking coefficient of hydrogen,[20] (iii) deviations from Sievert's law behavior, (iv) slow dissociation of molecules to form chemisorbed hydrogen atoms. When calculations were made and consistency with the experimental results examined, explanations based on (i), (ii), and (iii) were dismissed. The formation of chemisorbed hydrogen on the surface appears to be the only process which is affecting the permeation rate. Smithells and Ransley[21] observed similar effects at low pressures and interpreted their results with the aid of the Langmuir adsorption equation. Our results in Figure 5 and those of others follow a so-called parabolic adsorption isotherm in which the volume of gas adsorbed varies logarithmically with pressure.[22,23]

It should be mentioned that the presence of chromium in palladium could play a significant role in adsorption behavior, particularly if the concentration of chromium atoms at the surface is higher than in the bulk due to surface energy considerations. Another potentially important effect is the presence of impurities on the surface. Auger spectroscopy showed the presence of sulfur, oxygen, and carbon on the specimen surfaces, all of which could reduce the sites available for hydrogen adsorption.

It is of interest to examine the pressure dependence effect using a chemical reaction model. The reaction under study is

$$H_2 \text{ (gas)} \rightleftharpoons 2H \text{ (adsorbed)}$$

The overall rate of this reaction is the difference between the rates of the forward and reverse reactions:

$$J = k_1 p_{H_2} - k_2[H]^2 \quad (12)$$

where k_1 and k_2 are rate constants and [H] is the concentration of hydrogen at the surface. At steady state, the overall rate of the chemical reaction must be equal to the permeation flux through the specimen. [H] will in general be lower than the value obtained from Sievert's law for the same pressure, and it can be evaluated from the measured permeation flux, specimen dimensions, and diffusion coefficient.

This model was tested by using two experimental data points to evaluate k_1 and k_2 from simultaneous equations derived from eq 12. In Figure 7, the curve obtained from the model is compared to the experimental curve. Even though the model is probably oversimplified, the agreement is rather good. The agreement was nearly the same when the model was applied to the data for the Pd–16.8 atom % Cr alloy. It should be mentioned that at higher pressures, the $[H]^2$ term dominates, the computed curve passes through a maximum and the model can no longer apply.

The last topic to be discussed is the behavior of palladium alloys under conditions of high hydrogen pressure and relatively low temperature. In unalloyed palladium at temperatures below approximately 673 K, a hydride phase forms at moderate to high hydrogen pressures. Addition of nonhydride-forming elements such as silver and chromium to palladium tends to suppress hydride formation. No phase equilibrium data are available on either system, but it is known that silver has a beneficial effect on the structural integrity of palladium when it is thermally cycled in a hydrogen environment. In the few experiments completed to date, it has been demonstrated that the Pd–25 atom % alloy is seriously degraded in 50 MPa H_2 at 373 K but the Pd–16.8 atom % Cr alloy is not (see Figure 6). For the Pd–16.8 atom % Cr alloy, no defects were present in the microstructure after the hydrogen was removed. Thus, while the permeation rate in the Cr alloy is not as high, it may be more suitable for high-pressure, low-temperature applications than the commercial Pd–Ag alloy because of better structural integrity. In addition to gas purification systems, Pd–Cr alloys might also have attractive properties as catalysts used in hydrogen at high pressures and low temperatures.

Summary

The hydrogen permeation behavior of three Pd–Cr alloys has been characterized at temperatures to 449 K and at low pressures. The permeation coefficient, diffusion coefficient, and hydrogen solubility all decrease substantially with increasing chromium content. The hydrogen solubility in the alloys was found to obey Sievert's law. Measurements of the pressure dependence of the permeation rate showed that the rates of surface adsorption and dissociation of hydrogen molecules had a slight effect on the overall rate. In a few hydrogen absorption experiments at 373 K and 50 MPa H_2, it was found that Pd–25 atom % Ag is susceptible to severe cracking while Pd–16.8 atom % Cr is not.

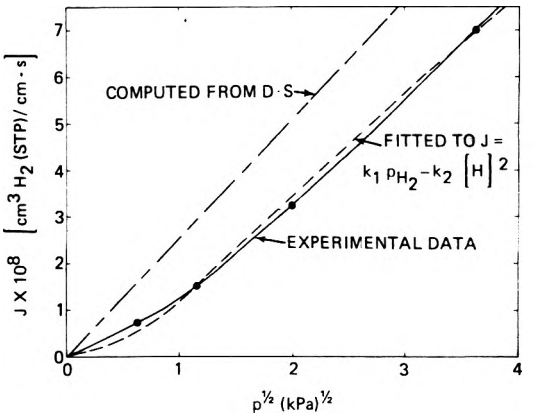

Figure 7. Comparison of pressure dependence of permeation flux with model for slow surface reaction.

Acknowledgments. The authors wish to acknowledge D. R. Folk for making the permeation measurements, L. A. West for Auger spectroscopy, T. L. Bryant for metallographic assistance, M. C. Nichols for x-ray diffraction measurements, R. B. Anderson for high pressure testing, and S. C. Keeton for comments on the application of band theory.

References and Notes

(1) J. B. Hunter, U.S. Patent No. 2 773 561, Dec 1956.
(2) D. L. McKinley, U.S. Patent No. 3 247 648, April 1966.
(3) O. Loebich, German Patent No. 1 533 234, June 1970.
(4) J. P. G. Farr and I. R. Harris, U.S. Patent No. 3 713 270, Jan 1973.
(5) J. W. Simons and T. B. Flanagan, *J. Phys. Chem.*, **69**, 3581 (1965).
(6) G. Bohmholdt and E. Wicke, *Z. Phys. Chem. (Frankfurt am Main)*, **56**, 332 (1967).
(7) F. J. Ackerman and G. J. Koskinas, *Ind. Eng. Chem., Fundam.*, **11**, 332 (1972).
(8) G. L. Holleck, *J. Phys. Chem.*, **74**, 503 (1970).
(9) R. A. Karpova and I. P. Tverdosvskii, *Zh. Fiz. Khim.*, **33**, 1393 (1959).
(10) V. A. Gol' Tsov, V. B. Demin, P. V. Gel'd, and G. E. Kagan, *Fiz. Khim. Mekh. Mater.*, **7**, 56 (1971).
(11) D. Artman and T. B. Flanagan, *J. Phys. Chem.*, **77**, 2804 (1973).
(12) K. D. Allard and T. B. Flanagan, *J. Phys. Chem.*, **74**, 298 (1970).
(13) R. B. McLellan and C. G. Harkins, *Mater. Sci. Eng.*, **18**, 5 (1975).
(14) F. M. Mueller, A. J. Freeman, J. O. Dimmoils, and A. M. Furdyna, *Phys. Rev. B.*, **1**, 4617 (1970).
(15) A. C. Switendick, *Ber. Bunsenges. Phys. Chem.*, **76**, 535 (1972).
(16) O. K. Anderson, *J. Appl. Phys.*, **41**, 1225 (1970).
(17) A. C. Switendick, *Solid State Commun.*, **8**, 1463 (1970).
(18) J. F. Elliott, M. Gleiser, and V. Ramakrishna, "Thermochemistry for Steelmaking", Vol. 2, Addison-Wesley, Reading, Mass., 1963, p 562.
(19) G. Grube and R. Knabe, *Z. Elektrochem.*, **42**, 739 (1936).
(20) H. Conrad, G. Ertl, and E. E. Latta, *Surface Sci.*, **41**, 435 (1974).
(21) C. J. Smithells and C. E. Ransley, *Proc. R. Soc. London, Ser. A*, **150**, 172 (1935); **152**, 706 (1963).
(22) H. Freundlich, "*Kapillarchemie*", **1**, 153 (1930).
(23) D. H. Baughm and F. P. Burt, *Proc. R. Soc. London, Ser. A*, **105**, 481 (1924).

Ultrasonic and Laser Temperature-Jump Studies of the Nickel Monocarboxylate Complex Formation Reactions in Solution

Shoji Harada, Tatsuya Yasunaga,* Kiyoshi Tamura, and Nobuhide Tatsumoto

Department of Chemistry, Faculty of Science, Hiroshima University, Hiroshima 730, Japan *(Received April 7, 1975)*

Ultrasonic absorption measurement of nickel acetate solution revealed two relaxation phenomena; one is in the kHz and the other in the MHz frequency range. The kHz frequency range relaxation phenomenon was studied in detail by the laser T-jump method. This relaxation phenomenon was interpreted by the stepwise complex formation mechanism. Rate constants and activation parameters obtained suggest that the rate-determining step of complex formation is the dehydration process of nickel ion. Results for the nickel complexes of acetate, propionate, butyrate, and β-chloropropionate indicate that the dissociation rate constants and the stability constants for the monocarboxylate complexes are intimately related to the acid dissociation constants of the protonated ligands. The MHz frequency range relaxation phenomenon was studied by sound absorption as a function of initial concentration of nickel acetate, acetate, and nickel ion concentrations, pH, temperature, and also in different solvents. The relaxation absorption was attributed to an intramolecular conversion of the nickel monocarboxylate complex and the rate constants and the activation parameters of this fast reaction were determined. Studies were also carried out for the nickel complexes of propionate, butyrate, acrylate, chloroacetate, and β-chloropropionate.

Introduction

In previous papers,[1-5] the authors studied the complexing reactions of many kinds of bidentate carboxylate complexes of nickel(II) by the pressure-jump method. In order to clarify the detailed mechanism of these reactions, kinetic informations on more simplified systems, i.e., monocarboxylate complexes, have been required. Few kinetic studies[6] have been carried out on the nickel monocarboxylate complex formation reactions, because of the lability of the complexes and the rapidity of the reactions in comparison to those of dicarboxylates.

The present ultrasonic absorption measurement of nickel acetate solution in the wide frequency range has revealed not only a relaxation absorption in the kHz frequency range but also another one in the MHz frequency range. The relaxation phenomenon of nickel acetate solution in the kHz frequency range was also observed by the laser T-jump method by Hoffmann et al.[7] and Koffer[8] but no systematic studies have been carried out. Nevertheless, the relaxation absorption of nickel carboxylate solution in the MHz frequency range is particularly interesting since the absorption occurs in the frequency range a few orders higher than that expected from the ordinary complex formation reactions of the nickel(II) ion and will provide some kinetic information on the very fast reaction in nickel carboxylate solution. This relaxation absorption has been reported by some workers. Jackopin et al.[9] and Atkinson et al.[10] have observed the relaxation absorption, but the relaxation frequency was below their measurable frequency range. Garza and Purdie[11] have also observed relaxation absorption but their frequency range was so restricted that the data were not precise enough to elucidate the relaxation mechanism.

The purpose of this paper is to assign these two relaxation phenomena and to obtain the kinetic parameters of the complex formation reactions. This information contributes not only to the elucidation of the reaction mechanism of monocarboxylate complexes but also aids in better understanding of the complicated reaction mechanism of dicarboxylate complexes.

Experimental Section

Samples. All chemicals used were of reagent grade and were used without further purification. Deionized water was used for aqueous solutions.

Sample solutions for ultrasonic studies were prepared as follows. Nickel acetate solution was prepared from $Ni(NO_3)_2$ and sodium acetate. Other nickel carboxylate solutions were prepared from $Ni(NO_3)_2$ and the corresponding carboxylic acids. The pH of the solution was adjusted to 6.0–6.5 by the addition of NaOH and HNO_3 solutions. Ionic strength, μ, was kept constant at $\mu = 2$ with some exceptions, by the addition of $NaNO_3$.

Sample solutions for the laser T-jump studies were prepared with care to avoid contamination of the nonreacting ions as follows. Nickel acetate solutions were made from nickel acetate. Nickel propionate, butyrate, and β-chloropropionate solutions were prepared from $NiSO_4$ and the equivalent amount of corresponding carboxylic acids. By addition of $Ba(OH)_2$, sulfate ion was precipitated out as $BaSO_4$. The pH was about 6.5 where most of the ligand is in the dissociated form. Each solution studied was prepared by diluting the stock solution to the desired concentration. No supporting electrolyte was added in order to avoid the decrease of the sensitivity of the conductivity bridge. Prior to the measurements, sample solutions were degassed by sonoration with a 400-kHz transducer under reduced pressure in order to avoid the cavitation effect caused by laser light.

Ultrasonic Measurements. Ultrasonic absorption was measured by the following two methods. In the frequency range 10–100 kHz, the reverberation method was used and in the frequency range 3.5–95 MHz, the pulse method was used. They are described elsewhere.[12] The velocity of sound was measured at 1.92 MHz by the sing-around method. The temperature was controlled to 0.01°C. Relaxation absorption spectra were represented by the single-relaxation equation

$$\alpha/f^2 = \frac{A}{1 + (f/f_r)^2} + B \qquad (1)$$

where α is the ultrasonic absorption coefficient, f the frequency, f_r the relaxation frequency, and A and B are the relaxing and nonrelaxing absorptions, respectively. More conveniently, however, the ultrasonic excess absorption per wavelength, $(\alpha'\lambda)$, is used for the relaxation equation

$$(\alpha'\lambda) = vf\left(\frac{\alpha}{f^2} - B\right) = \frac{Avf}{1 + (f/f_r)^2} \qquad (2)$$

where α' is the excess absorption coefficient, λ the wavelength, and v the velocity of sound. Values of f_r, A, and B were determined so as to give the best fit of the data to a single relaxation curve.

Laser T-jump Measurements. As a Q-switched laser source, a neodymium glass laser (Japan Electron Optics Laboratory Co. Ltd., Type JLS-G-3) was used. This laser flashed 1060 nm laser light as a 3 J/25 ns pulse. The concentration change of the species was followed by means of the electric conductivity method, i.e., the cell was set in one of the arms of a bridge circuit fed from a 1.25-MHz oscillator. The cell used in this work is shown in Figure 1. The laser light passes through a 3.2-mm diameter hole whose axis coincides with the direction of the laser beam. No windows were used and the sample solution was held by the surface tension. So as to avoid oscillations due to pressure reflection, a further vertical hole was introduced. Two 2-mm diameter platinum electrodes were introduced through the holes. The temperature was controlled to ±1°C by circulating thermostated water through the small bath mounted just behind the cell. The magnitude of the temperature jump was 0.1°C. The temperature constancy was examined and it was ascertained that the new temperature after the 0.1°C temperature jump is maintained for at least 20 ms. On the other hand, the relaxation effect retains for 1 ms for the longest. The bridge balance was controlled just before the temperature-jump because the change by the temperature-jump is masked by the slow but large temperature change of the thermostat. The measurements were carried out over the concentration range 0.03–0.50 M of nickel carboxylates at 25°C.

Results and Discussion

Figure 2 shows the ultrasonic absorption curve obtained for the 0.10 M nickel acetate solution in the entire frequency range. The relaxation spectrum is composed of at least two relaxation processes; one is in the kHz frequency range, and the other in the MHz frequency range. Then, kinetic studies were carried out for each relaxation phenomenon separately.

The kHz Frequency Range Relaxation Phenomenon Based on a Slow Reaction. As is seen in Figure 2, relaxation absorption was also observed in the solution of pH 3.80. This fact shows that the hydrolysis reactions of nickel and acetate ions are not related to this relaxation absorption. Unfortunately, the present ultrasonic measurements are restricted to a narrow frequency range and the relaxation frequency is located below this range so that the data imply only the existence of the relaxation absorption due to the nickel acetate complex formation reaction. Detailed kinetic studies of this process were carried out by the laser T-jump method.

In nickel acetate solution, the relaxation effect was also observed by the laser T-jump method in the same time range where the ultrasonic relaxation absorption occurs. The similarity of the time constants implies that the relaxation effect is based on the same reaction. In all of the concentration range studied, nickel acetate solution showed a relaxation spectrum characterized by a single relaxation phenomenon. The values of the reciprocal relaxation time, $1/\tau$, obtained are shown in Table I (available as supplementary material, see paragraph at end of text) with other experimental conditions. The values given are the mean of at least ten values measured.

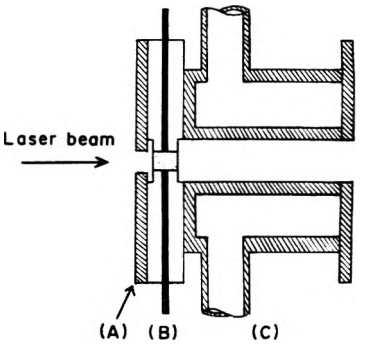

Figure 1. Sectional diagram of the laser T-jump cell: (A) aperture made of brass; (B) cell made of plastics; (C) thermostats both made of brass.

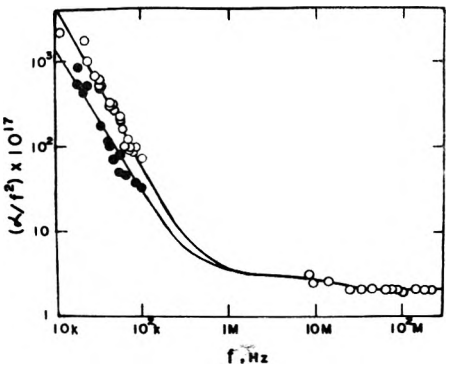

Figure 2. The ultrasonic absorptions of 0.10 M nickel acetate solutions at 25°C: (O) pH 6.05; (●) pH 3.80.

In an aqueous solution, nickel monoacetate complex formation may proceed according to the following stepwise mechanism

$$\underset{\text{I}}{Ni^{2+}} + Ac^- \underset{k_{21}}{\overset{k_{12}}{\rightleftharpoons}} \underset{\text{II}}{Ni^{2+}O\begin{matrix}H\\H\end{matrix}} Ac^- \underset{k_{32}}{\overset{k_{23}}{\rightleftharpoons}} \underset{\text{III}}{NiAc^+} \qquad (3)$$

where state I is the free ions, state II is the outer-sphere complex, and state III is the inner-sphere complex. The ion association and dissociation reaction, I ⇌ II, is very fast and the inner-sphere ligand substitution reaction, II ⇌ III, may be the rate-determining step. Then, the relaxation time for II ⇌ III may be expressed by

$$1/\tau = k_{23}[1 + \{K^0\Pi_f(C_{Ni} + C_{Ac})\}^{-1}]^{-1} + k_{32} \qquad (4)$$

where

$$\Pi_f = \frac{f_{Ni}f_{Ac}}{f_{NiAc^\ddagger}} \simeq f_{Ni} \qquad (5)$$

and K^0 is the outer-sphere complex formation constant, f_i is the activity coefficient of the species i and $f_{NiAc^\ddagger}$ is the coefficient of the activated complex which is assumed to be equal to that of acetate ion. K^0 was calculated by the Fuoss equation[13]

$$K^0 = \frac{4\pi Na}{3000} \exp(z_+ z_- e^2/a\epsilon k_B T) \quad (6)$$

where N is Avogadro's number, a the distance of the closest approach of the two ions, which is assumed to be 5 Å in this case, z_+e and z_-e the charges on the two ions, ϵ the dielectric constant, k_B Boltzmann's constant, and T the absolute temperature. The activity coefficients were calculated from the Davies equation.[14] As can be seen in eq 4, the rate constants k_{23} and k_{32} are obtained from the $1/\tau$ vs. $[1 + \{K^0\Pi_f(C_{Ni} + C_{Ac})\}^{-1}]^{-1}$ plot. Since the ionic strength was not kept constant, however, the values of K^0, f_{Ni}, and the stability constant, K, varied with ionic concentration. Assuming that the existence of $NiAc_2$ and other higher order complexes can be neglected in comparison with that of $NiAc^+$,[15] various parameters can be determined by the following procedure. At first, the stability constant at ionic strength zero, $K_{\mu=0}$, is assumed. The values of μ, f_i, K, and the ionic concentrations were calculated by the Davies equation and the following

$$K_{\mu=0} = \frac{f_{NiAc}}{f_{Ni}f_{Ac}} \frac{C_{NiAc}}{C_{Ni}C_{Ac}} = \frac{K}{f_{Ni}} \quad (7)$$

Then the bracketed term in eq 4 is calculated for each solution of various ionic concentration and $1/\tau$ values can be plotted. The plot will show a linear relationship and k_{23} and k_{32} are obtained from the slope and the intercept of the line, respectively. With k_{23}, k_{32}, and $K^0_{\mu=0}$, the value of $K_{\mu=0}$ is calculated by the equation

$$K_{\mu=0} = K^0_{\mu=0}\left(1 + \frac{k_{23}}{k_{32}}\right) \quad (8)$$

and the value should coincide with that assumed at first. The same procedure was repeated until all data coincided. Final plot of $1/\tau$ vs. $[1 + \{K^0\Pi_f(C_{Ni} + C_{Ac})\}^{-1}]^{-1}$ is shown in Figure 3 and the ionic concentrations and the ionic strength are tabulated in Table I.

From Figure 3, k_{23} and k_{32} were obtained to be 2.7×10^4 and 5.0×10^3 s^{-1}, respectively. The value of k_{23} is very close to the corresponding rate constants reported for various kinds of nickel complexes[16] and agrees also with the rate constant of the water exchange of nickel ion measured by NMR.[17,18] These coincidences suggest that the rate-determining step of the nickel acetate complex formation is the dehydration process of the nickel ion. From eq 8, $K_{\mu=0}$ was determined to be 34 M^{-1} which is very close to the Archer and Monk's value,[19] 27 M^{-1}, obtained from pH measurements.

Activation parameters were obtained by the following procedures. Equation 4 is simplified to be

$$1/\tau = k_{23}\left[f(c) + \frac{1}{K_{23}}\right] \quad (9)$$

where $K_{23} = k_{23}/k_{32}$ and f(c) is the concentration term. As the temperature dependency of the stability constant is relatively small,[20] the bracketed term in eq 9 may be assumed to be constant. Then, the temperature dependence of $1/\tau$ is ascribed to that of k_{23}. As is shown in Figure 4, a plot of log $[1/\tau T]$ vs. $1/T$ gives a straight line and the activation enthalpy $\Delta H^{\ddagger}_{23}$ was obtained to be 12 kcal mol^{-1} from the slope. By using Eyring's equation with the values of $\Delta H^{\ddagger}_{23}$ and k_{23} at 25°C, the activation entropy $\Delta S^{\ddagger}_{23}$ was calculated to be 2 cal deg^{-1} mol^{-1}. The coincidences of these values with those of the water exchange of the nickel ion obtained by NMR[17,18] also suggest that the present relaxation phenomenon is based on the equilibrium II $\rightleftharpoons$ III of reaction 3.

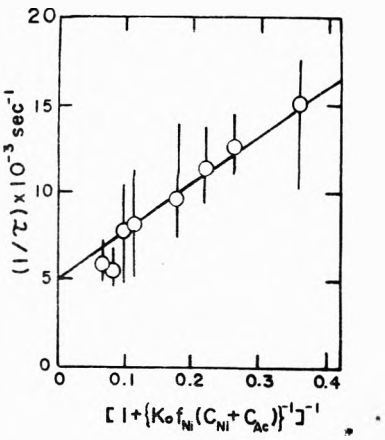

Figure 3. $1/\tau$ vs. $[1 + \{K^0 f_{Ni}(C_{Ni} + C_{Ac})\}^{-1}]^{-1}$ plot of nickel acetate system at 25°C.

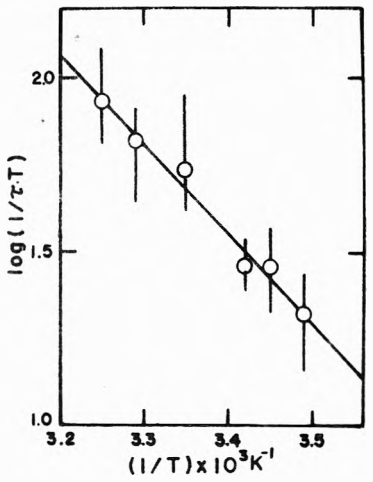

Figure 4. log $(1/\tau T)$ vs. $1/T$ plot of 0.40 M nickel acetate system.

The same studies were also carried out on the nickel complex solutions of propionate, butyrate, and β-chloropropionate. The results are shown in Figures 5–7 (available as supplementary material). The rate constants, k_{23} and k_{32}, and the stability constants obtained are summarized in Table II. The values of k_{23} are also very close to the rate constant of the water exchange on the nickel ion obtained by NMR.[17,18] Since the values of k_{23} obtained for these complexes are approximately constant, different values of the stability constant are reflected in the values of k_{32}. It has been shown that, for a homologous series of ligands, the stability constants are often inversely proportional to the acid dissociation constant, pK_a, of the protonated ligands.[22] These relationships between pK_a and k_{32} or the stability constant can be conjectured from Table II.

The Relaxation Phenomenon in the MHz Frequency Range Based on a Very Rapid Reaction. The relaxation absorption of nickel acetate solution in the MHz frequency range was studied by the pulse method as a function of total concentration of nickel acetate, acetate ion concentration, and nickel ion concentration. The results are tabulated in Table III (available as supplementary material) where two features may be noted. One is the independency of the relaxation frequency on ionic concentrations. The other is the increase of the absorption not only with increase of the total concentrations of nickel acetate and acetate ion but also with increase of the total concentration of

TABLE II: Rate Constants and Stability Constants for the Nickel Carboxylate Complex Formation Reactions at 25°C ($\mu \rightarrow 0$)

Ligand	k_{23}, 10^4 s^{-1}	k_{32}, 10^3 s^{-1}	K, M^{-1}	Acid pK_a[a]
Acetate	2.7	5.0	34	4.76
Propionate	2.4	5.5	30	4.88
Butyrate	2.4	4.5	35	4.82
β-Chloropropionate	2.6	7.5	24	4:08

[a] Reference 21.

nickel ion. The addition of acetate ion increases the concentrations of $NiAc^+$ and other higher order complexes while the addition of nickel ion decreases the concentrations of Ac^-, $Ni(Ac)_2$, and $Ni(Ac)_3^-$ and increases those of Ni^{2+} and $NiAc^+$. The latter features, then, suggest that the present relaxation phenomenon is not related to the higher order complexes but to the $NiAc^+$ complex. Moreover, another confirmation of this aspect is given by the fact that the ultrasonic absorption, $(\alpha'\lambda)_{max}$, is proportional to the concentration of $NiAc^+$ as shown in Figure 8.

The same kind of relaxation absorption as that of nickel acetate solution was also observed in the aqueous solutions of nickel complexes of propionate, butyrate, acrylate, chloroacetate, and β-chloropropionate. The measurements were carried out on solutions of the various ligand concentrations. The results are shown in Table IV (available as supplementary materal). In each case, the absorption increases with the addition of carboxylate ligand while f_r is kept constant. These features are similar to those of the nickel acetate solution. The ligand specificity can be observed both in f_r and the absorption.

Garza et al.[11] have measured the ultrasonic absorption of nickel acetate solution and assigned it to the intermediate step of the three-step complex formation mechanism (acetate ion desolvation step). Their data, however, contradict those presented here. Some of the reasons for the disagreement may be their small excess absorption due to low ionic concentrations, and their interpretation of the results as a double relaxation absorption. Therefore, the assignment of the present relaxation to one of the following reactions has been reinvestigated

$$M_w^{2+} + L_w^- \underset{k_{21}}{\overset{k_{12}}{\rightleftharpoons}} [M^{2+}(W)(W)L^-]_w \qquad (10)$$

$$[M^{2+}(W)(W)L^-]_w \underset{k_{32}}{\overset{k_{23}}{\rightleftharpoons}} [M^{2+}(W)L^-]_w \qquad (11)$$

$$[M^{2+}(W)L^-]_w \underset{k_{43}}{\overset{k_{34}}{\rightleftharpoons}} [ML^+]_w \qquad (12)$$

where M^{2+} is a metal ion, L^- a ligand ion, and W the coordinated water. The subscript indicates that the ions are hydrated. Under the conditions of k'_{12}, $k_{21} \gg k_{23}$, $k_{32} \gg k_{34}$, k_{43}, relationships between the relaxation frequencies (times) and the rate constants are given by

$$1/\tau_1 = 2\pi f_{r_1} = k_{12}\Pi_f(C_M + C_L) + k_{21} = k'_{12} + k_{21} \qquad (13)$$

$$1/\tau_2 = 2\pi f_{r_2} = k_{23}\frac{k'_{12}}{k'_{12} + k_{21}} + k_{32} = k'_{23} + k_{32} \qquad (14)$$

$$1/\tau_3 = 2\pi f_{r_3} = k_{34}\frac{k'_{23}}{k'_{23} + k_{32}} + k_{43} \qquad (15)$$

By the Debye-Eigen equations[23] concerning the ion association, the values of k_{12} and k_{21} can be calculated to be 1.1 × 10^{10} M^{-1} s^{-1} and 2.1 × 10^9 s^{-1}, respectively. From these

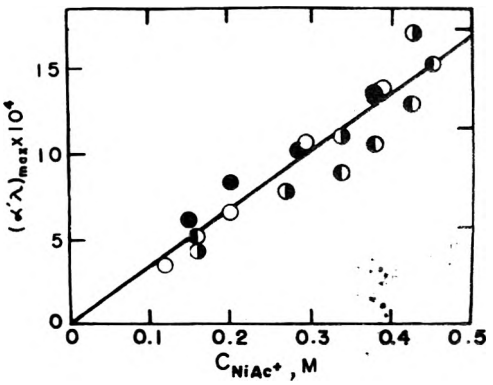

Figure 8. The relaxation absorption, $(\alpha'\lambda)_{max}$, vs. C_{NiAc^+} plot for nickel acetate system at 25°C: (○, ◑, ◐) Table I; (●) Table 5.

values and eq 13, the value of f_{r_1} was estimated to be above 300 MHz which is much higher than the present relaxation frequency. Moreover, eq 13 implies that f_{r_1} should exhibit some concentration dependency under the present experimental conditions. However, as shown in Tables III and IV, f_r remained constant. These inconsistencies indicate that the present relaxation absorption cannot be ascribed to reaction 10. On the other hand, reaction 12 was clarified as responsible for the relaxation absorption of the kHz frequency range as mentioned in the former part of this work.

The above considerations leave reaction 11 as the most plausible relaxation mechanism. Since the process is a dehydration step of the ligand, definite ligand dependency of the relaxation frequency as shown in Tables III and IV also seems to support this aspect. However questions still remain concerning the assignment of the present relaxation absorption to this process. Independencies of f_r on the ionic concentrations as shown in Tables III and IV should be in agreement with the interpretation. As is seen in eq 14, f_{r_2} turns out to be constant and independent of ionic concentration under the following extreme conditions:

(i) $$k'_{23} \simeq \text{constant} \left(\text{or } \frac{k'_{12}}{k'_{12} + k_{21}} \simeq 1\right)$$

(ii) $$k'_{23} \ll k_{32}$$

The following examinations were carried out to confirm whether one of these conditions would be fulfilled. First, under the present experimental conditions, k'_{12} = (3–30) × 10^8 M^{-1} s^{-1} and k_{21} = 2.1 × 10^9 s^{-1}, and then the value of $k'_{12}/(k'_{12} + k_{21})$ will be 0.1 to 0.6, which does not satisfy condition (i). Secondly, as shown by the laser T-jump studies, f_{r_3} (or $1/\tau_3$) varied with ionic concentration. This fact is caused by the relatively large variation of the term $k'_{23}/(k'_{23} + k_{32})$ in eq 15. Then, f_{r_2} (= $k'_{23} + k_{32}$) should also exhibit observable concentration dependency under the present experimental conditions. The above discussion confirms that reaction 11 is not preferable as the origin of the present relaxation absorption.

In order to elucidate the relaxation mechanism, further measurements were carried out with varying the experimental conditions for the nickel acetate solution. The effect of pH was studied on 0.50 M nickel acetate solution in the pH range 6.5–3.5. As shown in Table V, the absorption decreases with the decrease of pH (especially the effect is prominent below pH 5) while f_r increases slightly with lowering pH. To see the temperature effect, the ultrasonic absorption was measured on 0.50 M nickel acetate solution at 15, 25, and 35°C. The results are tabulated in Table VI

TABLE V: Ultrasonic Parameters for 0.50 M Nickel Acetate Aqueous Solutions at Various pH's and 25°C

pH	f_r, MHz	A, 10^{-17} s² cm⁻¹	B, 10^{-17} s² cm⁻¹	v, m s⁻¹	$10^{-4}\cdot(\alpha'\lambda)_{max}$
6.5	9.4	176	31.7	1583	13.1
6.0	10.3	161	31.1	1584	13.1
5.5	10.5	157	29.9	1581	13.0
4.5	11.2	117	28.8	1566	10.4
4.0	12.0	90	27.1	1563	8.4
3.5	13.0	62	25.3	1539	6.2

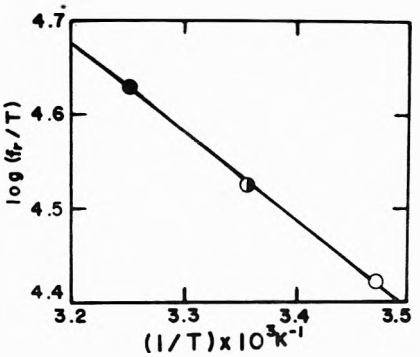

Figure 9. log (f_r/T) vs. 1/T plot of 0.50 M nickel acetate solution: (O) 15°C; (◑) 25°C; (●) 35°C.

(available as supplementary material). The temperature dependency of f_r is shown as a log (f_r/T) vs. 1/T plot in Figure 9. To see the effect of viscosity and dielectric constant, the absorptions were measured on 0.40 M nickel acetate solutions of 25 wt % glycerol, dioxane, and methanol. The results are shown in Table VII. The solvent effect on the absorption was studied on 0.40 M nickel acetate solutions of methanol, glycerol, dimethyl sulfoxide (DMSO), and dimethylformamide (DMF). The results are shown in Figure 10 and in Table VIII (available as supplementary material). Relaxation absorptions were observed in methanol and glycerol solutions; both absorptions were expressed by a single relaxation equation. In DMSO and DMF solutions, however, no relaxation absorption was observed. The solvent effect was also studied on 0.40 M nickel acetate solutions of methanol–water mixture. The results are shown in Figure 11.

In consideration of the relaxation mechanisms of the kHz frequency range studied above and the results of the relaxation absorption measurements in the MHz frequency range, the following stepwise complex formation mechanism is proposed as the most appropriate one

$$Ni_{aq}^{2+} + Ac_{aq}^{-} \underset{k_{21}}{\overset{k_{12}}{\rightleftharpoons}} [NiO(H)H\ Ac]_{aq}^{+} \quad (16)$$

$$[NiO(H)H\ Ac]_{aq}^{+} \underset{k_{32}}{\overset{k_{23}}{\rightleftharpoons}} [NiAc]_{aq}^{+} \quad (17)$$

$$[NiAc]_{aq}^{+} \underset{k_{43}}{\overset{k_{34}}{\rightleftharpoons}} [NiAc^{*}]_{aq}^{+} \quad (18)$$

Reaction 16 is the outer-sphere complex formation process whose f_r is much higher than 300 MHz as discussed above. Reaction 17 is the inner-sphere complex formation process which is the rate-determining step of all reactions. The relaxation phenomenon based on this process has been studied above.

TABLE VII: Ultrasonic Parameters for 0.40 M Nickel Acetate in Water, Dioxane–Water, and Methanol–Water Mixtures at 25°C

Solvent	f_r, MHz	A, 10^{-17} s² cm⁻¹	B, 10^{-17} s² cm⁻¹	v, m s⁻¹	$10^{-4}\cdot(\alpha'\lambda)_{max}$
Water	10.0	136	29.4	1559	10.6
25 wt % glycerol	10.0	119	53.0	1618	8.3
25 wt % dioxane	10.0	153	42.6	1575	12.1
25 wt % methanol	9.4	166	43.7	1610	12.5

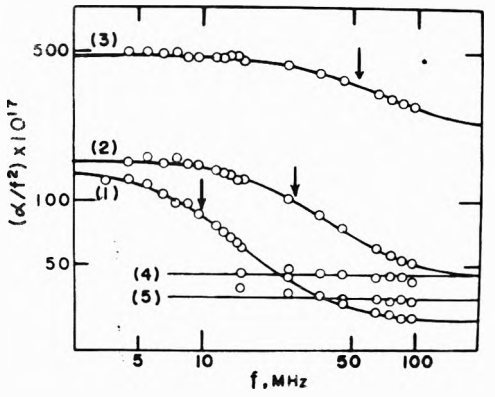

Figure 10. The ultrasonic absorption of 0.40 M nickel acetate in various solvents at 25°C: (1) water; (2) methanol; (3) glycerol; (4) DMSO; (5) DMF.

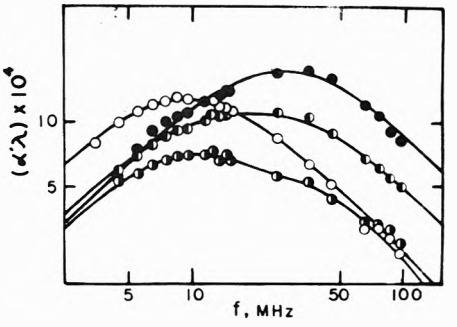

Figure 11. The ultrasonic absorption of 0.40 M nickel acetate solutions of methanol–water mixture at 25°C: (O) 25 wt %; (◑) 75 wt %; (◐) 85 wt %; (●) methanol.

Reaction 18 is assumed to be a very rapid intramolecular conversion reaction. Detailed discussions on this process are developed as follows.

(a) The relationship between the relaxation frequency and the rate constants for reaction 18 is given as

$$1/\tau = 2\pi f_r = k_{34} + k_{43} = k_{43}(K_{34} + 1) \quad (19)$$

where $K_{34} = k_{34}/k_{43}$. Calculations are shown in Appendix. As the concentration factor is not contained in this equation, f_r remains constant irrespective of the variation of ionic concentration. This fact is in agreement with the results in Tables III and IV.

(b) Maximum excess absorption per wavelength, $(\alpha'\lambda)_{max}$, for reaction 18 is given as

$$(\alpha'\lambda)_{max} = \frac{\pi(\Delta V)^2}{2\beta_0 RT}\left(\frac{1}{C_{NiAc}} + \frac{1}{C_{NiAc^*}}\right)^{-1} = \frac{\pi(\Delta V)^2}{2\beta_0 RT}\frac{C_{NiAc^*}}{1 + K_{34}} \quad (20)$$

Since the concentration term C_{NiAc^+} varies in proportion to the total concentration of $NiAc^+$, eq 20 indicates that the absorption, $(\alpha'\lambda)_{max}$ is proportional to the total concentration of $NiAc^+$. This consideration provides support for the present interpretation of the results shown in Figure 8.

(c) The effects of viscosity and the dielectric constant on the relaxation frequency and the relaxation absorption are prominent for ionic association reactions.[24] However, these effects on the present relaxation absorption are small, as shown in Table VII. The result implies that the absorption is not related to the ionic association reaction but to some others, e.g., reaction 18.

(d) The structure of $[NiAc^*]^+$ in reaction 18 can be assumed with reference to the crystal structure of nickel acetate[25] where the monodentated acetate ion forms a six-membered ring through the hydrogen bond with the coordinated water molecule. This structure may also be partly maintained in an aqueous solution and is shown in Figure 12. In this figure, $[NiAc]^+$ represents the complex where the coordinated acetate ion is also hydrogen bonded to the bulk water. The same kind of complexes of hydrogen bonded structure will be formed in alcohol whose hydroxyl group contributes to the hydrogen bond. This aspect may be supported by the fact that the relaxation absorption in the MHz frequency range is observed in water, methanol, and glycerol solution but not in DMSO and DMF solutions (Figure 10); the relaxation effects based on the inner-sphere complex formation reactions have been observed both in DMSO and DMF solutions.[26]

(e) Corsaro et al.[27] have reported that the formation and the rupture of hydrogen bond are catalyzed by protons. If we adopt this idea, the present mechanism may explain the pH effect on f_r, i.e., small increase of f_r with lowering pH, shown in Table V.

(f) By assuming that $k_{34} \ll k_{43}$, the temperature dependency of f_r gives the activation parameter of the backward process. From the plot in Figure 9, $\Delta H^{\dagger}_{43} = 4$ kcal mol^{-1} was obtained. This value is one third of that for the dehydration process obtained in the former part of this work but might be a reasonable one for the hydrogen bond rupture.[28]

(g) The results on the solutions of methanol–water mixture (Figure 11) show that, with increase of methanol fraction, the absorption at 10 MHz decreases while that at 27 MHz increases. Especially, in 75 and 85 wt % methanol solutions, double relaxation absorptions were observed. With further increase of methanol fraction, the absorption curve approaches to a single relaxation curve with $f_r = 27$ MHz. This solvent dependency of f_r indicates that the value of f_r depends not on the difference of dielectric constants but on other properties of the solvent, e.g., ability of hydrogen bond formation or steric factors for making a intramolecular hydrogen bonded structure.

(h) The lower the value of the pK_a of carboxylic acid is, the more labile is the complex, and the intramolecular hydrogen bond will also be more labile, i.e., k_{43} increases. If one assumes that $k_{34} \ll k_{43}$, eq 19 reduces to

$$2\pi f_r \simeq k_{43} \tag{21}$$

Then, the value of pK_a may be inversely proportional to f_r. The results on the many kinds of nickel carboxylates shown in Figure 13 exhibit the same proportionality between pK_a and f_r.

The above discussions, (a)–(h), lead to the conclusion that the ultrasonic relaxation absorption of nickel acetate

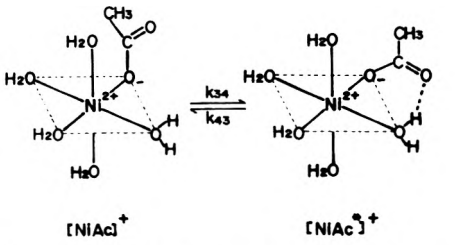

Figure 12. Two types $NiAc^+$ complexes in an aqueous solution.

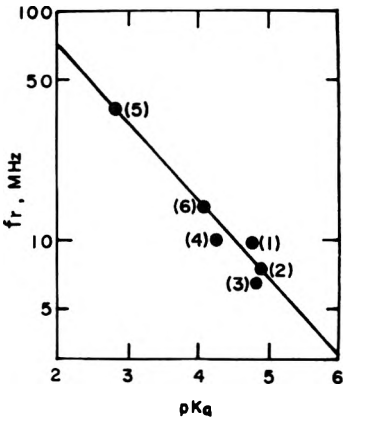

Figure 13. f_r vs. pK_a plot for a series of nickel carboxylates at 25°C: (1) acetate; (2) propionate; (3) butyrate; (4) acrylate; (5) chloroacetate; (6) β-chloropropionate.

solutions in the MHz frequency range is attributed to the intramolecular conversion of $NiAc^+$ complexes as shown in Figure 12. The absorptions of other nickel carboxylates may also be ascribed to the same reaction. Taking into account reaction 18, the relationship between the relaxation time and the rate constants used in eq 4, is partly changed to be

$$1/\tau = 2\pi f_r = k_{23}\frac{k'_{12}}{k'_{12} + k_{21}} + k_{32}\frac{k_{43}}{k_{34} + k_{43}} \tag{22}$$

This is, however, essentially the same as eq 4 where only reactions 16 and 17 are considered. Especially, if $k_{34} \ll k_{43}$, eq 22 reduces to eq 4. By assuming $k_{34} \ll k_{43}$, the values of k_{43} of a series of nickel carboxylates are calculated by eq 21 and are tabulated in Table IX. Unfortunately, the lack of the value of K_{34} prevents the estimation of the values of k_{34} and the volume change for reaction 18.

The kinetic informations obtained for the nickel monocarboxylate complex formation reaction will also be applicable for the nickel dicarboxylate system. Actually in the preliminary measurements on some of the nickel dicarboxylate solutions, similar relaxation absorptions have been observed. Furthermore, the proposed model is applicable not only to nickel complexes but also to other bivalent metal carboxylates. Preliminary studies on cobalt and copper acetate solutions indicate the existence of at least two relaxation processes. In case of these bivalent metal complexes, however, the rates of inner-sphere complex formation are much faster than that of Ni^{2+} and the relaxation will fall into the same time range as that of the intramolecular conversion. The distinction between two relaxations becomes very difficult. Relaxations based on high-order complex formations may also be observed around the same time range of that of the 1:1 complex formation. Detailed studies on these complexes are in progress.

TABLE IX: Rate Constants for the Nickel Carboxylate Complex Intramolecular Conversion Reactions at 25°C (μ = 2)

Ligand	k_{43}, 10^7 s^{-1}	pK_a[a]
Acetate	6.0	4.76
Propionate	4.7	4.88
Butyrate	4.1	4.82
Acrylate	6.3	4.26
Chloroacetate	8.8	4.08
β-Chloropropionate	23	2.81

[a] Reference 21.

Acknowledgment. The authors gratefully acknowledge the support of the TORAY Science Foundation.

Appendix

Equation 19 was obtained for the following equation where D ⇌ E is coupled to the much slower reaction C ⇌ D.

$$A + B \underset{k_{21}}{\overset{k_{12}}{\rightleftharpoons}} C \underset{k_{32}}{\overset{k_{23}}{\rightleftharpoons}} D \underset{k_{43}}{\overset{k_{34}}{\rightleftharpoons}} E \qquad \text{(A1)}$$

fast slow fast

In this case, the slow step is very much affected by the fast one; on the other hand, the fast step is not affected so much and becomes nearly equal to the uncoupled reaction. The reciprocal relaxation times are obtained as the eigenvalues of the following characteristic equation:

$$\begin{vmatrix} k_{12}' + k_{21} - 1/\tau & -k_{21} & 0 \\ -k_{23} & k_{23} + k_{32} - 1/\tau & -k_{32} \\ 0 & k_{34} & k_{34} + k_{43} - 1/\tau \end{vmatrix} = 0 \qquad \text{(A2)}$$

where $k'_{12} = k_{12}\Pi_f(C_A + C_B)$. When $1/\tau_I$ and $1/\tau_{III} \gg k_{23}$, k_{32}, we obtain

$$1/\tau_I = k'_{12} + k_{21} \qquad \text{(A3)}$$

$$1/\tau_{III} = k_{34} + k_{43} \qquad \text{(A4)}$$

and

$$1/\tau_{II} = k_{23}\frac{k'_{12}}{k'_{12} + k_{21}} + k_{32}\frac{k_{43}}{k_{43} + k_{34}} \qquad \text{(A5)}$$

Moreover, when $k_{34} \ll k_{43}$, eq A5 reduces tc eq 4.

Supplementary Material Available: laser T-jump data and ultrasonic parameters (8 pages). Ordering information is given on any current masthead page.

References and Notes

(1) S. Harada, K. Amidaizi, and T. Yasunaga, *Bull. Chem. Soc. Jpn.*, **45**, 1752 (1972).
(2) S. Harada and T. Yasunaga, *Bull. Chem. Soc. Jpn.*, **46**, 502 (1973).
(3) S. Harada, H. Tanabe, and T. Yasunaga, *Bull. Chem. Soc. Jpn.*, **46**, 2450 (1973).
(4) S. Harada, H. Tanabe, and T. Yasunaga, *Bull. Chem. Soc. Jpn.*, **46**, 3125 (1973).
(5) S. Harada, Y. Okuue, H. Kan, and T. Yasunaga, *Bull. Chem. Soc. Jpn.*, **47**, 769 (1974).
(6) H. Hoffmann, *Ber. Bunsenges. Phys. Chem.*, **73**, 432 (1969).
(7) H. Hoffmann, E. Yeager, and J. Stuehr, *Rev. Sci. Instrum.*, **39**, 649 (1968).
(8) H. Koffer, *Ber. Bunsenges. Phys. Chem.*, **75**, 1245 (1971).
(9) L. G. Jackopin and E. Yeager, Technical Report No. 35, ONR Contract No. 1439(04) Project NR 384-305, Case Western Reserve University, Cleveland, Ohio, June 1969.
(10) G. Atkinson, M. M. Emara, and R. F. Prini, *J. Phys. Chem.*, **78**, 1913 (1974).
(11) V. L. Garza and N. Purdie, *J. Phys. Chem.*, **74**, 275 (1970).
(12) N. Tatsumoto, *J. Chem. Phys.*, **47**, 4561 (1967).
(13) R. M. Fuoss, *J. Am. Chem. Soc.*, **80**, 5059 (1958).
(14) C. W. Davies, "Ion Association", Butterworths, London, 1962.
(15) Tanaka and Kato (ref 20) stated that only a 1:1 complex is found in the range of C_0 = 0.05~0.20 *M*. Many of the stability constants reported seem to be obtained by considering the 1:1 complex only (with some exceptions). However, in case of a very high electrolyte concentration, $Ni(Ac)_2$ may partly be produced. The deviations in high electrolyte concentrations in Figures 6 and 7 may based on this reason. Coincidences of the stability constants, obtained on this assumption, to that of the literature value will show that the assumption can be reasonably admitted.
(16) D. J. Hewkin and R. H. Prince, *Coord. Chem. Rev.*, **5**, 45 (1970).
(17) T. J. Swift and R. E. Connick, *J. Chem. Phys.*, **37**, 307 (1962). New data by Connick et al. (*J. Am. Chem. Soc.*, **94**, 3419, 8646 (1972)) do not seem to be the most plausible value because the activation parameters reported in it differs greatly from reported literature values.
(18) T. R. Stengle and C. H. Langford, *Coord. Chem. Rev.*, **2**, 349 (1967).
(19) D. W. Archer and C. B. Monk, *J. Chem. Soc.*, 3117 (1964).
(20) N. Tanaka and K. Kato, *Bull. Chem. Soc. Jpn.*, **32**, 516 (1959).
(21) R. C. Weast, "Handbook of Chemistry and Physics", The Chemical Rubber Co., Cleveland, Ohio, 1966.
(22) F. J. C. Rossotti, "Modern Coordination Chemistry", J. Lewis and R. G. Wilkins, Ed., Interscience, New York, N.Y., 1960.
(23) M. Eigen, *Z. Phys. Chem. (Frankfurt am Main)*, **3/4**, 176 (1954).
(24) J. Stuehr and E. Yeager, "Physical Acoustics", Vol. IIB, W. P. Mason, Ed., Academic Press, New York, N.Y., 1965.
(25) J. N. Niekerk and F. R. L. Schoning, *Acta. Crystallogr.*, **6**, 609 (1953).
(26) S. Harada and T. Yasunaga, unpublished data.
(27) R. D. Corsaro and G. Atkinson, *J. Chem. Phys.*, **55**, 1971 (1971).
(28) G. C. Pimental and A. L. McClellan, "The Hydrogen Bond", W. H. Freeman, San Francisco, Calif., 1960.

Dynamic Fluorine-19 Polarization in Fluorinated Strained Cyclic Alkanes and Alkenes

Richard D. Bates, Jr.,*

Chemistry Department, Georgetown University, Washington, D.C. 20057

Burkhard E. Wagner, and Edward H. Poindexter

U.S. Army Electronics Technology and Devices Laboratory (ECOM), Fort Monmouth, New Jersey 07703 *(Received September 2, 1975)*

Publication costs assisted by the Petroleum Research Fund and Army Research Office

Studies of dynamic polarization of ^{19}F nuclei in a series of perfluorocycloalkanes and perfluorocycloalkenes and their partially chlorinated analogues are reported. The experiments test effects that changes in the internal structure of the molecule have on the behavior of the peripheral fluorine atoms in nonaromatic species. With galvinoxyl interactions are dominated by dipolar coupling of the spins, with ultimate enhancements in the range −237 to −270. For the perfluorocycloalkanes enhancements are predominantly dipolar (−171 to −213 for bis(diphenylene)phenylallyl (BDPA), −182 to −227 for 2,2-diphenyl-1-picrylhydrazyl (DPPH)), with little variation for the four-, five-, and six-member ring species studied. The fluorines on the saturated carbons of the 1,2-dichloroperfluorocycloalkenes show more scalar coupling than the perfluorocycloalkanes (−143 to −158 for BDPA, −164 to −179 for DPPH), but the highest degree of scalar coupling is obtained for the perfluorocycloalkenes. The enhancements of the fluorines attached to unsaturated carbons are separated from the total observed enhancement and are shown to produce couplings significantly more scalar than others previously observed (+2 to −52 for BDPA, +256 to +223 for DPPH.) No evidence of correlation of DNP results for polarization of peripheral fluorine atoms on molecules when compared with high field NMR results is found.

Introduction

Ultimate NMR signal enhancements (U_∞) obtained in solution dynamic nuclear polarization (DNP) studies have been used to draw conclusions about intermolecular coupling, complexation, and preferential site occupation.[1-6] These enhancements are sensitive to the major changes in molecular electronic structure that affect the nature and chemical environment of the polarized nucleus, and to the availability of the polarizing free-radical unpaired electron.[1-4] However, the dominant dependence is on the molecular dynamics of the two interacting species.

The demonstration that the observed DNP enhancements do not depend significantly on the minor steric and electronic differences that govern high resolution NMR chemical shifts and spin–spin couplings is crucial to allow general application of the technique without the need to consider each coupling on a case by case basis. When compared with DNP investigations of saturated fluorocarbons, studies of aromatic fluorocarbons have indicated a significant increase in scalar coupling resulting from the polarization of the ring π structure.[4,7] However changes in substituent position of difluorobenzenes produced very small changes in DNP results.[4] Investigations of fluorine and phosphorus polarizations in phosphonitrilic fluorides and chlorides demonstrated similar behavior among the members of each series and a lack of conjugation of the ^{19}F nuclei to the ring π systems.[8,9] This paper reports the study of a series of perfluorocycloalkanes and perfluorocycloalkenes and their partially chlorinated analogues, for which there is considerable variation in the high-field NMR behavior.[10-12] The goal is to test effects that changes in the internal structure of the molecule have on the behavior of the peripheral fluorine atoms in nonaromatic species.

Additionally, one of the major disadvantages of DNP to date has been the inability to distinguish between chemically different ^{19}F atoms on the same receptor, as the chemical shifts at the low magnetic field strengths required for DNP experiments are too small to resolve signals. By comparison of the perfluorocycloalkenes with the corresponding species in which the carbons adjacent to the double bond are blocked by chlorine atoms, resolution of the contribution to the enhancements by the two chemically different nuclei may be possible. Finally, examining the relative amounts of dipolar and scalar coupling for samples in this series will elucidate (1) the influence of free-radical polarizers on the electronic structures of these species, and (2) the effect on intermolecular spin coupling of coplanarity of the fluorines and the carbon ring system.

Theory

Detailed accounts of the theory of DNP in free-radical solutions are available.[4,13,14] Equation 1 defines the observed enhancement, $G(P)$:

$$G(P) = \frac{A(P) - A(0)}{A(0)} = U_\infty^N f_N S_e(P) \quad (1)$$

$$U_\infty^N = \frac{\gamma_e}{\gamma_N} \frac{r - s + c}{2q + r + s + c} \quad (2)$$

$A(P)$ and $A(0)$ are the NMR signal amplitudes of nucleus N when the ESR line of the free radical is pumped or unpumped, respectively. The ultimate enhancement of nucleus N, U_∞^N, is the observed low-field enhancement extrapolated to complete saturation of the radical ESR line (limit of the saturation function, $S_e(P)$, going to one), and complete domination of the nuclear relaxation times by coupling with the radical (limit of the leakage factor, f_N, going to one). As shown in Figure 1, the terms r, s, and q, are the coupled electron–nuclear dipolar relaxation transition probabilities, and c is the corresponding relaxation induced

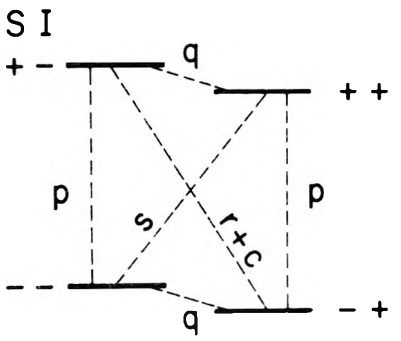

Figure 1. Combined energy states and relaxation probabilities for a system of unpaired electrons coupled weakly to spin $I = 1/2$ nuclei.

by a scalar mechanism. The electron and nuclear gyromagnetic ratios are γ_e and γ_N, respectively.

Values for U_∞^F are commonly obtained by the ratio method in which the ratios of the observed enhancement of the fluorine nucleus of interest to that of a proton in the same sample at the same applied radio-frequency power are averaged for several applied powers, as shown in

$$\frac{G^F(P)}{G^H(P)} = \frac{U_\infty^F f_F}{U_\infty^H f_H} = \frac{U_\infty^F}{U_\infty^H} = \frac{U_\infty^F}{-329.5} \quad (3)$$

Provided the radical concentration is high enough that proton and fluorine leakage factors are approximately one, the values for U_∞^F can be obtained from the ratio and −329.5, the ultimate enhancement obtained for low-field proton samples, to give sound results. The dipolar and scalar components can be resolved by using eq 2, as q, r, and s are in a ratio of 3:2:12 in the low-field limit, allowing a relative value of c to be obtained from U_∞^F.

One difficulty encountered with some of the samples in the present study is that they contain fluorine atoms of more than one type. As chemical shifts at the low magnetic fields used in the experiments are too small to resolve the different fluorine NMR signals, the enhancements obtained, and hence the values of U_∞^F, are composites of all contributing nuclei. The least sophisticated, and presently the only practicable, means to estimate the contribution of a given type nucleus to the total observed enhancement is to assume that the contribution of each type nucleus is simply proportional to the number of that type nucleus per molecule. This assumes that unpumped signal intensities are proportional solely to the number of atoms per molecule of a given type, that the leakage factors for all nuclei in different chemical environments are near one, and that the chemical shifts are so small that the two peaks are additive, both when polarized and when unpolarized. Then the ultimate enhancement of one type nucleus can be determined using eq 4 if the ultimate enhancement of the other nuclei contributing to the same signal can be estimated. $N_F(i)$ is the number of fluorine atoms of type i per molecule; $U_\infty^F(i)$ is the ultimate fluorine enhancement of that type of atom; U_∞^F(obsd) is the composite ultimate fluorine enhancement observed experimentally; and the sum over i is the sum over all types of fluorine atoms.

$$U_\infty^F(j) = \frac{1}{N_F(j)}\left[\left(U_\infty^F(\text{obsd})\sum_i N_F(i)\right) - \sum_{i\neq j} N_F(i)U_\infty^F(i)\right] \quad (4)$$

Experimental Section

Samples were prepared by dissolving a weighed portion of the free radical (for 0.02 m solutions) in a three-component mixture of (1) cyclic fluorocarbon, (2) benzene, and (3) carbon tetrachloride in a volume ratio of 1:1:4. This solvent combination, which has been used previously,[9] was necessary to ensure that (1) all four components are miscible at the conditions of the experiment, and (2) all samples are run in the same solvent system for reliable comparison. That the choice of solvent system may affect the relative degree of scalar coupling has been previously demonstrated,[4] and will be examined in depth in a forthcoming paper.[15] The variation is most significant for solvents with markedly different values of the cohesive energy density δ. For benzene, δ = 9.2, and for carbon tetrachloride, 8.6; typical values of this function for the perfluorocycloalkanes are between 5.7 and 6.1.[16,17] Thus the dissimilarity among the three solvent components may have some effect on the results obtained; however, as all the samples were run in the same solvent system, consistent results within the set should be obtainable.

The cyclic fluorocarbons were commercial products with stated minimum purity of 98%. The free radicals used in the study, the structures of which are shown in Figure 2, were chosen to provide a wide range of typical scalar to dipolar polarization ratios. Galvinoxyl (GALV) and 2,2-diphenyl-1-picrylhydrazyl (DPPH) were commercial products with stated purity of 98%. Bis(diphenylene)phenylallyl (BDPA) was synthesized by Professor C. F. Koelsch. Samples were degassed by several freeze–pump–thaw cycles before sealing. Samples of C_6F_6 and C_4F_8, both gases at room temperature, were prepared by trapping the gas at 77 K in a degassed mixture of radical, C_6H_6, and CCl_4, then sealed. Samples were run at 25°C and 75 G (7.5 mT) as described previously.[4]

Results and Discussion

Experimental values of U_∞^F, calculated from observed enhancements by using eq 1 and 3, are given in Table I for each fluorocarbon with the three free radicals. Observed fluorine enhancements for all the samples studied are highly negative, indicating that the coupling is dominated by the intermolecular electron–nuclear dipolar interaction rather than the scalar mechanism. The ultimate fluorine enhancements obtained with the radical GALV are among the most negative ever observed, nearly to the dipolar limit. Typically, ultimate fluorine enhancements with GALV have been in the range from −200 to −250, with the most negative value of −270 obtained with 1,1,1-trifluorotrichloroethane,[1,4] in which the fluorines are on a saturated carbon atom. These highly dipolar enhancements with GALV reflect the inaccessibility of the free-radical electron in the GALV structure.[4]

All polarizations produced by BDPA and DPPH are more positive (greater scalar contribution) than those produced by GALV. For BDPA and DPPH, the enhancements shown in Table I are most negative with cycloalkanes. The DPPH ^{19}F enhancements are slightly more dipolar than the BDPA values for all but one of the molecules in which the fluorines are bound to saturated carbons, including those cycloalkenes with the two unsaturated positions occupied by chlorine atoms. These results agree both in range and radical order with previous aliphatic samples for which comparisons can be drawn.[2,3]

Two types of chlorine-substituted species have been in-

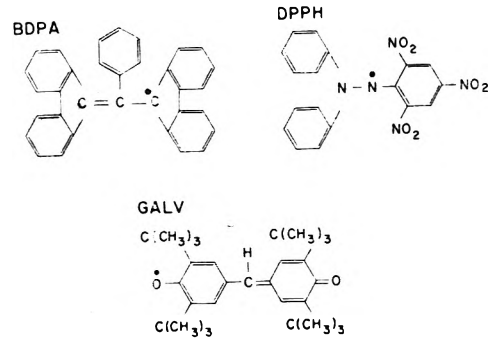

Figure 2. Structures of free radicals used in the investigation.

cluded in this study. Results with all three radicals for the two partially chlorinated perfluorocyclobutanes show little difference from the enhancements obtained for the perfluorocyclobutane itself. Thus, for these saturated cyclobutanes, the effect of partial chlorine substitution on the fluorine DNP is, if any, below the detectable limit in the current set of samples. High-field magnetic resonance studies have shown considerable differences in the chemical shifts of the fluorine nuclei of these species. Perfluorocyclobutane has a shift of +135.2 ppm relative to $CFCl_3$; 1,1,2,2-tetrachlorotetrafluorocyclobutane has a shift of +114.0 ppm relative to $CFCl_3$; and 1,2-dichlorohexafluorocyclobutane exhibits intermediate values for the different fluorine atoms.[10] Evidently, the intramolecular mechanisms giving rise to the differences in the chemical shifts have little effect on the intermolecular polarization of the fluorine nuclei by free radicals. For these fluorinated cyclobutanes, the fluorines are unaware of the nature of the rest of the molecule.

In contrast, the fluorines bound to the saturated carbons on the cycloalkenes which have the positions adjacent to the double bond blocked by chlorine atoms have enhancements with BDPA and DPPH which are significantly less dipolar than found for the corresponding perfluorocycloalkanes. For these chlorocycloalkenes the fluorine atoms one carbon removed from the double bond also show a downfield shift compared to the perfluorocycloalkane analogues. For example, the near fluorines on 1,2-dichlorooctafluorocyclohexene-1 lie at +110.6 ppm, and the far at +134.1 ppm, while C_6F_{12} gives +133.0 ppm for all fluorines, all with respect to $CFCl_3$.[11] In these chlorocycloalkenes the shifts are also comparable to those obtained with the chlorocycloalkanes, but definite differences are observed in the DNP results. Previously, an increase in scalar coupling for molecules containing chlorine atoms has been observed for several types of molecules (^{31}P in $POCl_3$, ^{13}C in CCl_4, ^{31}P in phosphonitrilic chlorides), but in these cases, the nucleus exhibiting the greater degree of scalar coupling has been attached directly to the chlorine.[8,18,19] Increased ^1H scalar coupling in $CHCl_3$ has been observed with the di-*tert*-butyl nitroxide radical, but this has been attributed to the tendency of the proton to hydrogen bond to the nitroxide, rather than the effect of the chlorine atom.[20,21] In the present study, the polarized fluorines observed are several atoms removed from the chlorines, yet the fluorine enhancements are markedly more scalar for BDPA and DPPH than in the corresponding perfluorocycloalkanes.

The BDPA and DPPH enhancements are more positive for the perfluorocycloalkenes than for the corresponding 1,2-dichloroperfluorocycloalkene-1 compounds. These perfluorocycloalkenes have two fluorines attached to nominally sp^2 carbons, which may exhibit markedly different enhancements from those of the sp^3 carbon fluorines on the same molecule. As a first approximation eq 3 may be used to resolve the two contributions to the enhancements obtained. The fluorine enhancements on these chloro compounds can be used as an approximation of the enhancements of the fluorines bound to the saturated carbons on the perfluorocycloalkenes, an approximation supported by the observation that partially chlorinated perfluorocyclobutanes behave analogously with the perfluorocyclobutanes themselves. The results of this calculation for the four-, five-, and six-member ring perfluorocycloalkenes are shown in Table II, along with the percent scalar coupling calculated by using eq 2. Despite the large uncertainties inherent in this method of resolving the two contributions to the observed enhancements, the percent scalar coupling for the BDPA and DPPH with the 1,2 fluorines is consistent for all three species investigated. The BDPA value of approximately 32% scalar coupling is nearly identical with the scalar contribution to the polarization of hexafluorobenzene, long the standard for comparison for unsaturated fluorine enhancements.[3] The planar BDPA with delocalized electron has been very versatile in inducing scalar polarization in aromatic fluorocarbons for which the possibility of plane–plane collisions exists.[2,3,5] For the same aromatics, enhancements with DPPH are typically slightly more dipolar than are BDPA enhancements, as, for example hexafluorobenzene is −2 with DPPH and +20 with BDPA.[3] Quite the contrary is observed for the sp^2 fluorines on the perfluorocycloalkenes. Here the DPPH polarizations are more than 50% scalar, and the enhancements which average around +230 are much more positive than any previously observed for ^{19}F nuclei with DPPH. The perfluorocycloalkene observed enhancements with DPPH are actually slightly more scalar than those with BDPA, in contrast to other fluorine enhancements for those homologous series which have been studied,[3] except for the phosphonitrilic fluorides.[9] However, the resolved enhancements due to the sp^2 fluorines are much more positive than for BDPA. DPPH, with its localized unpaired electron on the nitrogen atom, is far superior, when compared with BDPA, in polarizing by the contact route the fluorines attached to double-bonded carbons than it is in polarizing fluorines on aromatic fluorocarbons. The high-field NMR chemical shifts for the fluorines on the unsaturated carbons show some variation (C_4F_6, +130.4 ppm; C_5F_8, +150.2 ppm; and C_6F_{10}, +151.9 ppm; all with respect to $CFCl_3$), but all are shifted to higher field than the other fluorine atoms on the same molecule, approaching hexafluorobenzene at +162.6 ppm.[12] Again, the intermolecular coupling observed in DNP experiments does not parallel the intramolecular-based chemical shift data.

Conclusions

The interactions of all cyclic fluorocarbons studied with galvinoxyl free radical are dominated by the dipolar coupling of the fluorine nuclei with the free-radical unpaired electron.

With BDPA and DPPH, fluorine enhancements vary considerably with the nature of the fluorocarbon. For the perfluorocycloalkanes, enhancements are predominantly dipolar, with little variation evident for the four-, five-, and six-member ring species studied. Partial chlorination of

TABLE I: Ultimate Fluorine Enhancements from DNP Measurements for Cyclic Fluoroalkanes and -alkenes with the Free Radicals GALV, BDPA, and DPPH

Formula	Compound	$U_\infty F$ GALV	$U_\infty F$ BDPA	$U_\infty F$ DPPH
C_4F_8	Perfluorocyclobutane	−264 ± 7	−193 ± 7	−182 ± 7
$C_4Cl_2F_6$	1,2-Dichlorohexafluorocyclobutane	−270 ± 5	−171 ± 2	−193 ± 9
$C_4Cl_4F_4$	1,1,2,2-Tetrachlorotetrafluorocyclobutane	−251 ± 18	−177 ± 3	−220 ± 8
C_4F_6	Perfluorocyclobutene	−237 ± 5	−96 ± 1	−35 ± 1
$C_4Cl_2F_4$	1,2-Dichlorotetrafluorocyclobutene-1	−252 ± 6	−143 ± 9	−164 ± 6
C_5F_8	Perfluorocyclopentene	−261 ± 5	−118 ± 2	−71 ± 3
$C_5Cl_2F_6$	1,2-Dichlorohexafluorocyclopentene-1	−266 ± 4	−157 ± 9	−179 ± 8
C_6F_{10}	Perfluorocyclohexene	−262 ± 5	−137 ± 4	−86 ± 3
$C_6Cl_2F_8$	1,2-Dichlorooctafluorocyclohexene-1	−240 ± 4	−158 ± 9	−165 ± 6
C_6F_{12}	Perfluorocyclohexane	−265 ± 14	−213 ± 7	−227 ± 11

TABLE II: Ultimate Enhancements and Percent Scalar Coupling of ^{19}F Nuclei Bound to Unsaturated Carbons in Perfluorocycloalkenes by Correcting Observed Ultimate Enhancement for ^{19}F Nuclei Bound to Saturated Carbons on the Molecule

Species measd	Species used for cor	$U_\infty F$(BDPA)	% c-BDPA	$U_\infty F$(DPPH)	% c-DPPH
C_4F_6	$C_4Cl_2F_4$	−2 ± 21	33.2	+223 ± 15	56.1
C_5F_8	$C_5Cl_2F_6$	−1 ± 34	33.6	+253 ± 14	59.2
C_6F_{10}	$C_6Cl_2F_8$	−53 ± 56	28.1	+230 ± 39	55.9

perfluorocyclobutanes gives no change in fluorine enhancements.

Perfluorocycloalkenes show marked increase in ^{19}F scalar coupling when compared with the saturated analogues. Resolution of the signal component resulting from the fluorines bound to the unsaturated carbons shows that the enhancements for these fluorines are more positive with DPPH than for other ^{19}F nuclei that have been examined previously. This reversal of positions of BDPA and DPPH with respect to largest scalar contribution in polarizing ^{19}F nuclei has also been observed for the phosphonitrilic fluorides, another series of predominantly nonplanar, unsaturated ring compounds.[9,22,23] The fluorines out of the plane of the double bond in the 1,2-dichloro-substituted perfluorocycloalkene-1 compounds show increased fluorine scalar coupling as well with both BDPA and DPPH when compared to the corresponding perfluorocycloalkanes.

The trends observed in the polarization of fluorine nuclei by intermolecular coupling with the unpaired electron of the free radicals do not correlate with observed chemical shifts from high-resolution NMR experiments. Moreover, studies of the radical-induced fluorine relaxation showed no unusual behavior for these samples. The intermolecular interactions studied by DNP are a sensitive probe of the environment of the nucleus which is exposed to other molecules in the system, and are not necessarily reflections of the inner electronic structures of the molecule itself. Thus, DNP can serve as a useful means of investigating the intermolecular dynamics without the necessity of detailed concern with minor variations in the nature of the individual molecule.

Acknowledgment. The authors gratefully acknowledge the help of Anthony J. Montedoro in sample preparation and in operation of instrumentation, and the aid of Ruthann I. Bates for critically reading the manuscript.

One of the authors (R.D.B., Jr.) acknowledges the Donors of The Petroleum Research Fund, administered by the American Chemical Society, and AROD, under Grant No. DAHC04-75-G-0042, for partial support of this work.

References and Notes

(1) E. H. Poindexter, J. R. Stewart, and P. J. Caplan, *J. Chem. Phys.*, **47**, 2862 (1967).
(2) J. R. Stewart, E. H. Poindexter, and J. A. Potenza, *J. Am. Chem. Soc.*, **89**, 6017 (1967).
(3) J. A. Potenza and E. H. Poindexter, *J. Am. Chem. Soc.*, **90**, 6309 (1968).
(4) J. Potenza, *Adv. Mol. Relaxation Process*, **4**, 229 (1972).
(5) B. E. Wagner, J. N. Helbert, R. D. Bates, Jr., and E. H. Poindexter, *Chem. Commun.*, 748 (1973).
(6) B. E. Wagner, R. D. Bates, Jr., and E. H. Poindexter, *Inorg. Chem.*, **14**, 256 (1975).
(7) W. Müller-Warmuth and A. Yalciner, *Ber. Bunsenges. Phys. Chem.*, **75**, 763 (1971).
(8) R. A. Dwek, N. L. Paddock, J. A. Potenza, and E. H. Poindexter, *J. Am. Chem. Soc.*, **91**, 5436 (1969).
(9) E. H. Poindexter, R. D. Bates, Jr., N. L. Paddock, and J. A. Potenza, *J. Am. Chem. Soc.*, **95**, 1714 (1973).
(10) J. Feeney, L. H. Sutcliffe, and S. M. Walker, *Mol. Phys.*, **11**, 117 (1966), and references cited therein.
(11) J. Feeney, L. H. Sutcliffe, and S. M. Walker, *Mol. Phys.*, **11**, 137 (1966), and references cited therein.
(12) V. W. Gash and D. J. Bauer, *J. Org. Chem.*, **31**, 3602 (1966).
(13) E. H. Poindexter, P. J. Caplan, B. E. Wagner, and R. D. Bates, Jr., *J. Chem. Phys.*, **61**, 3831 (1974).
(14) R. D. Bates, Jr., E. H. Poindexter, and B. E. Wagner, *J. Chem. Phys.*, **59**, 3031 (1973).
(15) J. A. Potenza and J. W. Linowski, personal communication.
(16) J. Hildebrand, J. M. Prausnitz, and R. C. Scott, "Regular and Related Solutions", Van Nostrand-Reinhold, New York, N.Y., 1970, p 213.
(17) R. L. Scott, *J. Am. Chem. Soc.*, **70**, 4090 (1948).
(18) R. D. Bates, Jr., B. E. Wagner, and E. H. Poindexter, *Chem. Phys. Lett.*, **17**, 328 (1972).
(19) J. A. Potenza, E. H. Poindexter, P. J. Caplan, and R. A. Dwek, *J. Am. Chem. Soc.*, **91**, 4356 (1969).
(20) R. D. Bates, Jr., E. H. Poindexter, and B. E. Wagner, 166th National Meeting of the American Chemical Society, Chicago, Ill., Aug 1973, No. Phys. 3.
(21) K. Endo, B. Knuettel, I. Morishima, T. Inubushi, and T. Yonezawa, *Chem. Phys. Lett.*, **31**, 387 (1975).
(22) P. J. McQuillin, "Alicyclic Chemistry", Cambridge University Press, London, 1972, p 24.
(23) C. H. Chang, R. F. Porter, and S. H. Bauer, *J. Mol. Struct.*, 7, 89 (1971).

Effects of Ionization of a Hydroxyl Substituent on Vicinal Proton–Proton Coupling Constants

A. Jaworski, D. Shugar,* and E. Darżynkiewicz

Department of Biophysics, Institute of Experimental Physics, University of Warsaw, 02-089 Warsaw, Poland, and Department of Cell Biology and Experimental Therapeutics, Institute of Oncology, 02-061 Warsaw, Poland

(Received July 28, 1975)

The SCF finite perturbation method (FPM) in the INDO molecular orbital approximation has been employed to evaluate the influence of ionization of a hydroxyl substituent on vicinal proton–proton coupling constants, $^3J(^1H–^1H)$, using for this purpose the simplest possible model, the ethanol molecule. The changes in coupling constants resulting from ionization were calculated for dihedral angles over the range 0–360°. These results were then used to derive some qualitative predictions for several arabinonucleosides, which adopt a C(2′)endo conformation on ionization of the sugar hydroxyls; for these the effects due to ionization are not expected to exceed 0.5 Hz.

Introduction

It has been recently demonstrated[1] that the solution conformations of some pyrimidine 1-β-D-arabinofuranosyl nucleosides undergo appreciable modifications on transfer from neutral to highly alkaline medium where the sugar hydroxyls are known to undergo dissociation with pK values in excess of 12.[2] In particular, for such nucleosides as araC,[3] 3′-maraC, 3′-maraU, and araA, the conformations of which differ to a greater or lesser extent in neutral medium, dissociation of the 2′-hydroxyl leads in all instances to a common conformation for the pentose moiety. This conformation is of the form C(2′)endo and more than 80–90% gauche,gauche and is accompanied by formation of an intramolecular hydrogen bond with the 5′-OH as donor and the negatively charged 2′-O as acceptor, viz., 5′-OH···O(2′)$^-$. It is strikingly similar to that encountered for the neutral forms of araC and araU in the solid state, where the 2′-OH is the donor and the intramolecular hydrogen bond is of the form 2′-OH···O(5′)H.[4]

The conformations of the sugar moieties of nucleosides in solution are deduced from the vicinal coupling constants between protons attached to adjacent carbon atoms. The dependence of these coupling constants on the stereochemical relationship between coupled hydrogens has been extended to embrace the influence of various substituents (see, e.g., ref 5–8). No attempts appear to have been made to examine theoretically the effects of dissociation of a substituent such as a hydroxyl or carboxyl group.

In the studies referred to above on the conformation of arabinonucleosides in strongly alkaline medium,[1] the use of some reference compounds suggested that hydroxyl dissociation directly affected vicinal coupling constants to only a minor extent. Because of the potential applicability of these findings to studies on the properties of sugar hydroxyls in general and to conformational modifications associated with the dissociation of such hydroxyls, it appeared of interest to examine theoretically the possible effects of hydroxyl dissociation on vicinal coupling constants.

The choice of a simple model system for such calculations was based in part on subdivision of the pentose ring into two fragments, with replacement of C–C, C–R, and C–O bonds by C–H, to give ethanol (Figure 1). This model was selected for the following reasons. (a) It renders possible calculations of the dependence of vicinal coupling constants on dihedral angles over a range of 0–360°. (b) It also makes possible an examination of the effects of the oxygen lone pairs on the vicinal coupling constants for different orientations of the hydroxyl group, as well as a comparison of these effects with those resulting from hydroxyl ionization. (c) Although our method is time consuming, the cost of the computations is low with such a simple molecule. Introduction of the appropriate extrapolation procedure results in rapid convergence with the method used. In addition, the symmetry of the methyl group reduces by a factor of 3 the computing time required.

It is not to be anticipated that such a model will provide quantitative data directly applicable to nucleosides. Furthermore, the method of calculation employed is such that is usually predicts values for the vicinal coupling constants in ethanelike compounds which are too high.[7] In addition the difficulties associated with the use of approximate wave functions in the FPM scheme are well-known.[7-9] However one may expect this procedure to provide qualitatively the changes in the values of the coupling constants as a function of hydroxyl ionization.

Computational Procedure

This made use of the SCF finite perturbation method[10] in the INDO molecular orbital approximation.[11] The calculations were based on the Fermi contact coupling mechanism and were performed with the aid of a modified version of the QCPE-142 program[12] on a Control Data Corp. Cyber-72 computer.

Bond lengths and angles employed were standard values for model A of Pople and Beveridge,[13] with the exception of the C–O$^-$ bond in the ionic form. We have been unable to locate any data in the literature for the length of this bond; but model B of Pople and Beveridge (ref 13, p 131) cites a value of 1.36 Å for the C–O bond in radicals and radical ions. This value was checked by geometrical optimalization, which led to a value of 1.354 Å. All atomic coordinates were calculated with the aid of the QCPE-186 program.[14] The rigid rotor model was assumed. The methyl group was

* To whom correspondence should be addressed at the Department of Biophysics, Institute of Experimental Physics, University of Warsaw.

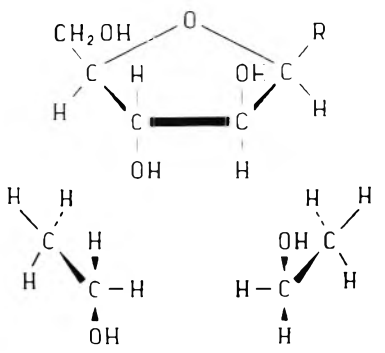

Figure 1.

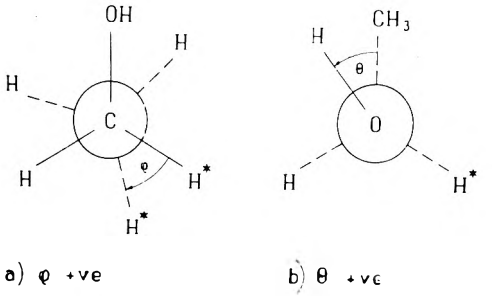

Figure 2.

rotated about the C–C bond, using the following convention: the dihedral angle (ϕ) was taken as zero when the protons denoted by an asterisk were cis and increased positively as the designated methyl proton was rotated relative to the oxygen atom as in Figure 2(a). A similar convention was followed for rotation of the proton about the C–O bond, so that the dihedral angle θ is zero when the hydroxyl proton is cis to the C–C bond and increases positively as this proton rotates away from the designated carbon-linked proton, as in Figure 2(b). Calculations were carried out at intervals of 12° or less for rotation of the methyl group of the ethanol molecule. For all computed points, the errors resulting from the finite convergence of the SCF procedure do not exceed 0.01 Hz.

Computed proton–proton coupling constants were analyzed in terms of a truncated Fourier-type expansion with the aid of a fitting procedure[15] for determining the analytical forms of the curves. The expansion employed was of the form[16]

$$^3J(\phi) = C_1 + C_2 \cos(\phi + D) + C_3 \cos 2(\phi + D) + C_4 \cos 3(\phi + D) + C_5 \sin(\phi + D) + C_6 \sin 2(\phi + D) + C_7 \sin 3(\phi + D) \quad (1)$$

All C_i coefficients are in hertz and the coefficient D is in degrees.

Results

For the ionic form trial runs showed that the Fourier-type expansion presented above could be simplified to the form[17]

$$^3J(\phi) = C_1 + C_2 \cos\phi + C_3 \cos 2\phi + C_5 \sin\phi + C_6 \sin 2\phi \quad (2)$$

The explicit use of the sine terms is necessary in order to reflect the different values of the function under examination in the neighborhood of the minima located in the vicinity of 80 and 280°.

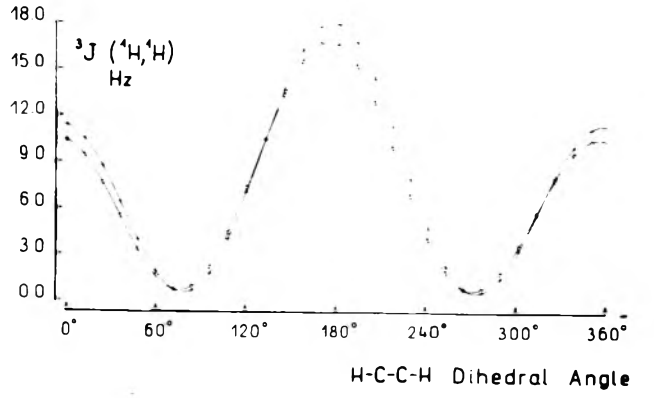

Figure 3. Plots of $^3J(^1H-^1H)$ vs. HCCH dihedral angle in ethanol for θ values of 180° (+) and 60° (◇). See test for further details.

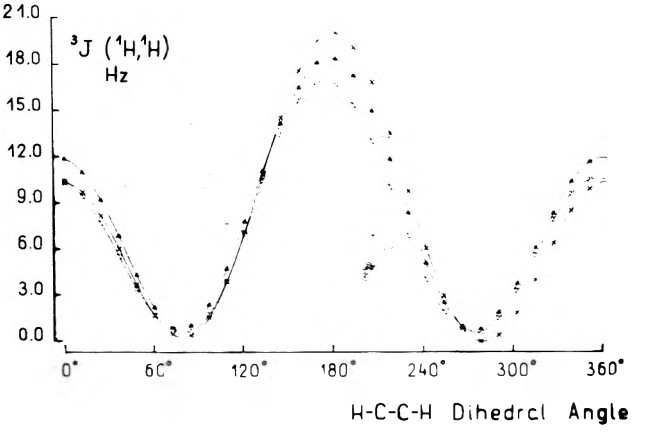

Figure 4. Dependence of $^3J(^1H-^1H)$ on HCCH dihedral angle for the ionized form of ethanol (×) and the upper (▲) and lower (□) limits of the coupling constant values for all orientations of the hydroxyl proton in the neutral form of the ethanol molecule.

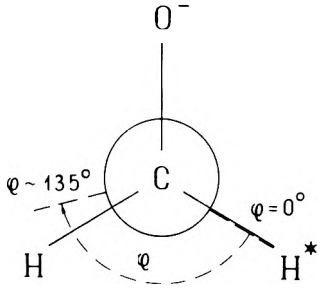

Figure 5.

For the neutral form the values of the coupling constants are dependent on the orientation of the hydroxyl proton (influence of the lone-pair electrons). Theoretical calculations[18] and experimental data[19] for ethanol both point to the existence of one principal and two local energy minima associated with rotation of the hydroxyl proton. In the case of the pentofuranose ring it is, of course, difficult to establish the orientations of the hydroxyl substituents since these are dependent, among other factors, on the nucleoside conformation. With this in mind, calculations on ethanol were conducted for six possible orientations of the

TABLE I: Constants for Eq 2

θ, deg	C_1	C_2	C_3	C_5	C_6	Rms dev
0	7.46	−3.01	6.45	0.41	−1.52	0.04
60	7.27	−3.06	6.21	0.43	−1.47	0.03
120	7.54	−3.45	6.49	0.48	−1.44	0.03
180	7.74	−3.27	6.91	0.28	−1.01	0.02
240	7.93	−3.20	7.08	0.21	−0.85	0.03
300	7.75	−3.37	6.85	0.31	−0.99	0.03
Anionic form (C–O⁻ = 1.36 Å)	7.80	−4.79	7.29	0.26	−0.29	0.07
Anionic form (C–O⁻ = 1.34 Å)	7.67	−4.97	7.19	0.29	−0.35	0.08
Anionic form (C–O⁻ = 1.41 Å)	8.09	−4.40	7.50	0.21	−0.15	0.06

TABLE II: Constants for Eq 3

θ, deg	C_1	C_2	C_3	D	Rms dev
0	7.46	−3.04	6.63	6.7	0.06
60	7.27	−3.09	6.38	6.7	0.06
120	7.54	−3.48	6.65	6.4	0.08
180	7.74	−3.28	6.98	4.2	0.04
240	7.93	−3.21	7.13	3.4	0.03
300	7.75	−3.38	6.92	4.2	0.06

hydroxyl proton, spaced at equal intervals of 60°. For the specific conformations calculated by Maciel et al.[7] (staggered form, hydroxyl proton cis (θ = 0°) and trans (θ = 180°) to the C–C bond), our own results were virtually identical.

From the Fourier expansion for the dependence of vicinal proton–proton coupling constants on the corresponding dihedral angles, it follows that only the even functions with common phase shifts are necessary. Each expansion may be expressed in the form[20]

$$^3J(\phi) = C_1 + C_2 \cos(\phi + D) + C_3 \cos 2(\phi + D) \quad (3)$$

so that only four parameters are required. In addition, for purposes of comparison, we present the *independent* expansions in the form (2) with explicit use of the sine functions. All of the C_i and D coefficients and the corresponding rms errors are presented in Tables I and II.

Figure 3 exhibits a plot of the dependence of coupling constants on dihedral angle for two orientations of the hydroxyl proton: trans (θ = 180°), the principal energy minimum for ethanol; and gauche (θ = 60°), corresponding approximately to one of the local minima. The curve for the second gauche minimum (θ = 300°) is closely similar to that shown for the trans form. Figure 4 shows three curves: one for the dependence of coupling constant on the dihedral angle for the ionized form and the other two for the minimal and maximal values of the coupling constants for all orientations of the hydroxyl proton in the neutral form.

Discussion

The criterion adopted for evaluating the results was that modification of the coupling constant as a result of ionization was of significance only when the calculated value fell outside the limiting curves for all orientations of the hydroxyl proton in the neutral form of the molecule. It will be noted that this occurs for dihedral angles in excess of 135°[21] when the influence of the ionized oxygen atom is most apparent[22] (Figure 5), but the computed differences do not exceed 2 Hz. For angles less than 135°, in particular in the region 65–105°, the differences are negative, but small.

Application of the foregoing findings to the arabinonucleosides referred to above requires some knowledge of the magnitudes of the dihedral angles between carbon-linked protons and their signs according to the convention adopted above.[23] With such data and the plots presented in Figure 4, it becomes possible to make some predictions about differences in coupling constants between the ionized and neutral forms of a given nucleoside with the same conformation.

For arabinonucleosides with free 2′ and 5′ hydroxyls, which adopt the conformation C(2′)endo on dissociation of the 2′-OH, J(1′–2′) should be minimally affected. Although applicability of our model to coupling between H(2′) and H(3′) is debatable, we predict a small decrease of less than 0.5 Hz. Dissociation of the "up" 2′-OH should not affect J(3′–4′) and J(4′–5′,5″), so that the observed modifications of the values of these coupling constants[1] should be due solely to conformational changes. Dissociation of the 3′-OH might be expected to affect J(3′–4′); in this instance we predict an increase of the order of 0.5 Hz.

It should be emphasized that, notwithstanding the uncertainty in the length of the C–O⁻ bond of the ethanol anion (from 1.34 to 1.41 Å), the conclusions derived above retain their validity. An increase in the C–O⁻ bond length leads to an increase in the values of the coupling constants in the neighborhood of the cis maximum by about 0.2 Hz/0.01 Å and smaller changes elsewhere. Shortening the C–O⁻ bond length to 1.34 Å decreases the range over which the coupling constants are unchanged on ionization from 0–135 to 15–135°, while an increase in bond length to 1.41 Å increases to the same extent the angular range within which ionization should not result in any modifications in $^3J(^1H–^1H)$.

Acknowledgments. We are indebted to Dr. B. L. Lesyng and Dr. J. S. Kwiatkowski for useful discussions. This investigation profited from the partial support of the Polish Academy of Sciences (Project 09.3.1) and The Wellcome Trust.

References and Notes

(1) E. Darżynkiewicz, M. Remin, A. Dworak, and D. Shugar, *Cancer Biochem. Biophys.*, **1**, 85 (1975); M. Remin, E. Darzynkiewicz, A. Dworak, and D. Shugar, *J. Am. Chem. Soc.*, in press; M. Remin, E. Darżynkiewicz, I. Ekiel, and D. Shugar, in preparation.
(2) P. A. Levene, L. W. Bass, and H. S. Simms, *J. Biol. Chem.*, **70**, 229

(1926); J. J. Fox and D. Shugar, *Biochem. Biophys. Acta*, **9**, 369 (1952); J. J. Fox, J. F. Codington, N. C. Yung, L. Kaplan, and J. O. Lampen, *J. Am. Chem. Soc.*, **80**, 5155 (1958); J. J. Christensen, J. H. Rytting, and R. M. Izatt, *J. Phys. Chem.*, **71**, 2700 (1967); E. Darżynkiewicz, H. Sierakowski, and D. Shugar, *Z. Naturforsch., C*, **30**, 565 (1975).
(3) Abbreviations employed: araC, 1-β-D-arabinofuranosylcytosine; araA, 9-β-D-arabinofuranosyladenine; araU, 1-β-D-arabinofuranosyluracil; 3'-maraC, 3'-*O*-methyl-araC; 3'-maraU, 3'-*O*-methyl-araU.
(4) P. Tollin, H. R. Wilson, and D. Young, *Acta Crystallogr., Sect. B*, **29**, 1641 (1973); A. K. Chwang and M. Sundaralingam, *Nature (London), New Biol.*, **243**, 78 (1973); P. P. Tougard and O. Lefebvre-Soubeyran, *Acta Crystallogr., Sect. B*, **30**, 86 (1974).
(5) M. Karplus, *J. Am. Chem. Soc.*, **85**, 2870 (1963).
(6) A. D. Cohen and T. Schaefer, *Mol. Phys.*, **10**, 209 (1966).
(7) G. E. Maciel, J. W. McIver, Jr., N. S. Ostlund, and J. A. Pople, *J. Am. Chem. Soc.*, **92**, 4497 (1970).
(8) P. D. Ellis and G. E. Maciel, *Mol. Phys.*, **20**, 433 (1971).
(9) G. E. Maciel, J. W. McIver, Jr., N. S. Ostlund, and J. A. Pople, *J. Am. Chem. Soc.*, **92**, 4151, 4506 (1970).
(10) J. A. Pople, J. W. McIver, Jr., and N. S. Ostlund, *J. Chem. Phys.*, **49**, 2960, 2965 (1968).
(11) J. A. Pople, D. L. Beveridge, and P. A. Dobosh, *J. Chem. Phys.*, **47**, 2026 (1967).
(12) P. A. Dobosh, Program No. 142, Quantum Chemistry Program Exchange, University of Indiana, Bloomington, Ind. 47401.
(13) J. A. Pople and D. L. Beveridge, "Approximate Molecular Orbital Theory", McGraw-Hill, New York, N.Y., 1970, pp 111, 112.
(14) M. J. S. Dewar and N. C. Baird, Program No. 186, Quantum Chemistry Program Exchange. University of Indiana, Bloomington, Ind. 47401.
(15) G. C. Sheppey, "A Program to Find Local Minima. . .Using Conjugate Directions (MINCON)", CERN 6600 Computer Library, Section D505 (CERN, Geneva, Switzerland, unpublished).
(16) The coefficients C_1 and D are not independent; an expansion of this form was used only for purposes of convenience and was subsequently converted to a more simplified form.
(17) Functions of this form to represent the calculated values of coupling constants (EHT method) were proposed previously: K. G. R. Pachler, *Tetrahedron Lett.*, 1955 (1970); *Tetrahedron*, **27**, 187 (1971); *J. Magn. Reson.*, **8**, 183 (1972).
(18) L. Random, W. J. Hehre, and J. A. Pople, *J. Am. Chem. Soc.*, **94**, 2371 (1972); J. A. Pople, *Tetrahedron*, **30**, 1605 (1974).
(19) Ch. O. Kadzhar, I. D. Isaev, and L. M. imanov, *Zh. Strukt. Khim.*, **9**, 445 (1968); M. Takano, Y. Sasada, and T. Satoh, *J. Mol. Spectrosc.*, **26**, 157 (1968); Y. Sasaoa, M. Takano, and T. Satoh, *Ibid.*, **38**, 33 (1971).
(20) Such a formulation of the angle, as well as substituent, dependence was also employed recently: K. G. R. Pachler, *J. Chem. Soc., Perkin Trans. 2*, 1936 (1972).
(21) There are two regions for angles greater than 135°. In the range 135–265° ionization leads to an increase in the $^3J(^1H-^1H)$ values, whereas in the range 265–360° there is a decrease.
(22) The dependence of the coupling constants in the neutral form of the molecule on the orientation of the hydroxyl group suggests that the electrons localized in the neighborhood of the oxygen atom participate in "transmission" of the orientation of proton spins to their coupled partners.
(23) Typical dihedral angles for the 2'-endo conformation were taken from the standard geometrical model[24] based on crystallographic data.[4]
(24) A modified version of the program QCPE-186.[14]

Electrical Conductance, Ultrasonic Relaxation, and Microwave Dielectric Relaxation of Sodium Perchlorate in Tetrahydrofuran

Herman Farber and Sergio Petrucci*

Departments of Chemistry and Electrical Engineering, Polytechnic Institute of New York, Brooklyn, New York 11201
(Received May 22, 1975)

Audiofrequency electrical conductance, radiofrequency ultrasonic absorption, and microwave complex permittivities have been measured for the system $NaClO_4$ in THF. Analysis of the electrical conductance data reveals the electrolyte to be strongly associated, giving association constants for both ion pairs and triple ions. Analysis of the ultrasonic data together with additional results for $AgClO_4$ and sodium picrate in THF suggests that a pseudo-first-order process, probably associated with anion desolvation (or solvation), is being observed. The complex permittivity data are described by a Cole–Davidson distribution function with distribution parameters $\beta = 0.9 \pm 0.1$ and 0.8 at c = 0.05 and 0.10 M ($NaClO_4$), respectively. These parameters may be predicted theoretically by a modified Glarum theory envisaging diffusion rotation of ion pairs coupled with dipole–dipole collision. To check the proposed mechanisms ethanol was added to $NaClO_4$ 0.1 M in THF, the ethanol:$NaClO_4$ molar ratio being $\simeq 30$. Both the ultrasonic and the dielectric relaxation frequencies shift to much lower frequencies. This phenomenon is interpreted as due to solvation of the electrolyte by ethanol (rather than to an increase in the solvent viscosity).

Introduction

Electrolytes in media of low permittivity have been investigated recently by relaxation methods such as ultrasonics by Hemmes et al.[1] and in this laboratory.[2] Many processes have been observed which are associated with the complex structure of the electrolytes in these media. The relative concentration of free ions is quite small and the electrolyte mainly consists of ion pairs and complexes including larger species such as triple ions and quadrupoles. This study extends the previous ones[1,2] to $NaClO_4$ in THF.

Electrical conductivity measurements were performed to calculate the extent of the association of this electrolyte in order to have structural information of this electrolyte solution. The results of these measurements gave estimates of the relative proportion of the species in solution.

It was also hoped that combination of two relaxation methods like ultrasonic and dielectric relaxation could give a more definite picture of the nature of the phenomena observed. The application of mechanical waves by ultrasonic techniques may shift existing equilibria in solution by forcing mutual interconversion of some of these species (provided the isothermal volume changes and the enthalpy changes are not both zero for the process studied). In particular, increasing the frequency eventually causes the re-

laxation of the observed process. Measurement of the relaxation time and its concentration and temperature dependence gives information on the rate constants and energy barriers for the process. Similarly application of electromagnetic waves to the same ionic systems forces charge transport in solution. If the majority of the ionic species are paired or complexed, the alternating field will mainly cause diffusional dipolar rotation. Increasing the frequency up to the microwave range will cause the relaxation of these rotational movements including the solvent dipoles at sufficiently high frequencies. Measurement of the dielectric relaxation times and of the difference $\epsilon_0 - \epsilon_\infty$ gives information about the size and the apparent dipole moment of the rotating entities.

In this paper radiofrequency ultrasonic relaxation measurements gave the kinetics of the mutual transformation of two solvated ion pairs.

Microwave dielectric relaxation measurements were used to study the relaxation rotational diffusion of these species. The effect of the change in medium, by the addition of ethanol, is shown by both the ultrasonic and the microwave data.

I. Electrical Conductance

Experimental Procedure. The details for making the measurements have been described previously.[2] Anhydrous $NaClO_4$ (Smith Co., Cleveland, Ohio) was dried at 140°C in an oven until no further change in weight occurred. THF was distilled in a nitrogen atmosphere over molten potassium in an all-glass system containing a 3-ft Vigreux column.

Solutions of concentrations greater than 0.01 M were prepared on the basis of weight and the molality was converted to molarity by measuring the density of the solutions. The electrical conductance of these individually prepared solutions was measured using an Erlenmeyer–Kraus conductance cell with a constant $K = 0.1142 + 4\chi_s$ cm^{-1}, χ_s being the conductivity of the solutions.

Lower molarity solutions were prepared by adding weighed portions of stock solutions to the weighed solvent directly in the conductance cell. This procedure eliminated errors resulting from weighing small quantities of salts.

All solutions were transferred in a dry nitrogen box. Temperature was maintained at 25.000 ± 0.001°C.

Results. The measured densities of the solutions with concentrations of 0.010, 0.025, 0.050, 0.10, and 0.15 M of $NaClO_4$ in THF were 0.8833_9, 0.8855_6, 0.8882_2, 0.8923_9, and 0.8972_3 g cm^{-3}, respectively. Equivalent conductance in the form of log Λ vs. log c is reported in Figure 1A. The plot of $\Lambda\sqrt{c}$ vs. c is shown in Figure 1B according to the 1933 Fuoss–Kraus[1] triple-ion theory[3]

$$\Lambda\sqrt{c} = \frac{\Lambda_0}{\sqrt{K_A}} + \frac{\Lambda^0{}_T K_T}{\sqrt{K_A}} c$$

The solid straight line (Figure 1B) is the best fit based on the least-squares computation. It has a slope of 0.8392 and an intercept of 1.683×10^{-2}. K_A is calculated as $9.9_3 \times 10^7$ M^{-1} using the intercept and $\Lambda_0 = 167.7$ Ω^{-1} cm^2 equiv^{-1} for $NaClO_4$ in THF. This value comes from $\lambda^0_{Na^+} = 48.2$ Ω^{-1} cm^2 equiv^{-1} [4] and from $\lambda^0_{ClO_4^-} = 119.5$ Ω^{-1} cm^2 equiv^{-1}.[5] Also from the slope of the line $\Lambda^0{}_T K_T = 8364$ and then $K_T = 149.6$ M^{-1} using the arbitrary assumption[3] that $\Lambda^0{}_T = \frac{1}{3}\Lambda_0 = 55.9$ Ω^{-1} cm^2 equiv^{-1}. No allowance has been made for the possible formation of quadrupoles in the above analysis which includes data for $C = 2.4 \times 10^{-5}$ M to $C = 0.0499$ M but excludes the results for $C = 0.1$ and 0.15 M.

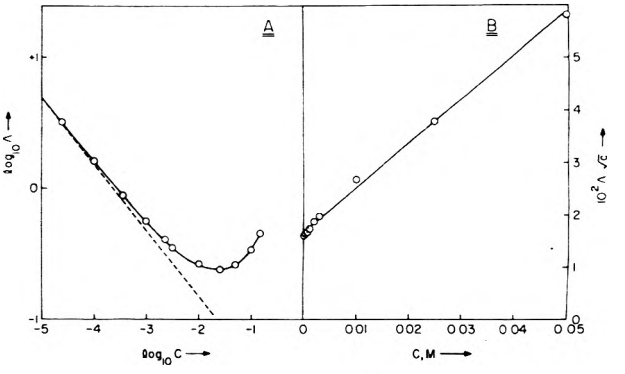

Figure 1. (A) log Λ vs. log c for $NaClO_4$ in THF at 25°C. (B) $\Lambda\sqrt{c}$ vs. the molar concentration c for $NaClO_4$ in THF at 25°C.

The slope of the line may be somewhat modified if quadrupoles were present,[6] and hence also the value of K_T.

II. Ultrasonic Relaxation

Experimental Procedure. The details of the instrumentation have been described in ref 2. The frequency range extended from 5 to 300 MHz and the concentration range of the electrolyte was from 0.05 to 0.15 M. In addition to the $NaClO_4$ solutions, solutions of $AgClO_4$ in THF and sodium picrate in THF were studied. Also, a mixed solvent C_2H_5OH–THF (3 M C_2H_5OH in THF) was studied, as well as a solution of 0.1 M $NaClO_4$ in this solvent. The solvent mixture was prepared on a weight basis.

Every effort was made to remove all traces of water from the materials used and to keep them moisture free. Solutions of weighed amounts of $AgClO_4$ and of $NaClO_4$ in THF were prepared by volumetric flasks in a drybox. The anhydrous C_2H_5OH was redistilled in a Vigreux column over aluminum amalgam collecting only the middle portion of the distillate. The THF was distilled over liquid potassium. The anhydrous $AgClO_4$ (Alfa Inorganics) was further dried at room temperature in vacuo (0.05 Torr) until a constant weight was achieved. The sodium picrate (Kodak) was dried using the same procedure. The temperature of the solutions was maintained at 25.0 ± 0.05 and 0.0 ± 0.05°C by means of a Forma Junior thermostatic bath. Temperatures of −15 ± 0.05 and −30 ± 0.05°C were maintained by means of the cryostat described elsewhere.[2]

Results. The results for the measurements on the solutions of $NaClO_4$ in THF are shown in Figure 2 as α/f^2 vs. frequency and μ vs. frequency. These two functions, valid for a single relaxation process[7] are

$$\alpha/f^2 = \frac{A}{1 + (f/f_R)^2} + B \qquad (1)$$

$$\mu = \alpha_{exc}\lambda = 2\mu_{max}\frac{f/f_R}{1 + (f/f_R)^2} \qquad (2)$$

with α being the sound absorption coefficient; $\alpha_{exc} = \alpha - Bf^2$, the excess sound absorption coefficient; B, the background absorption, at high frequency, of the solution; $A = 2\mu_{max}/uf_R$; u, the sound velocity approximated to the one of the solvent; λ, the wavelength of the sound wave, $\lambda = u/f$; f, the frequency; and f_R, the relaxation frequency.

The solid lines shown in Figure 2 have been calculated by an iterative process as follows. An initial value of B is chosen; μ is calculated from the experimental value of α at each frequency. Then eq 2 is rearranged into

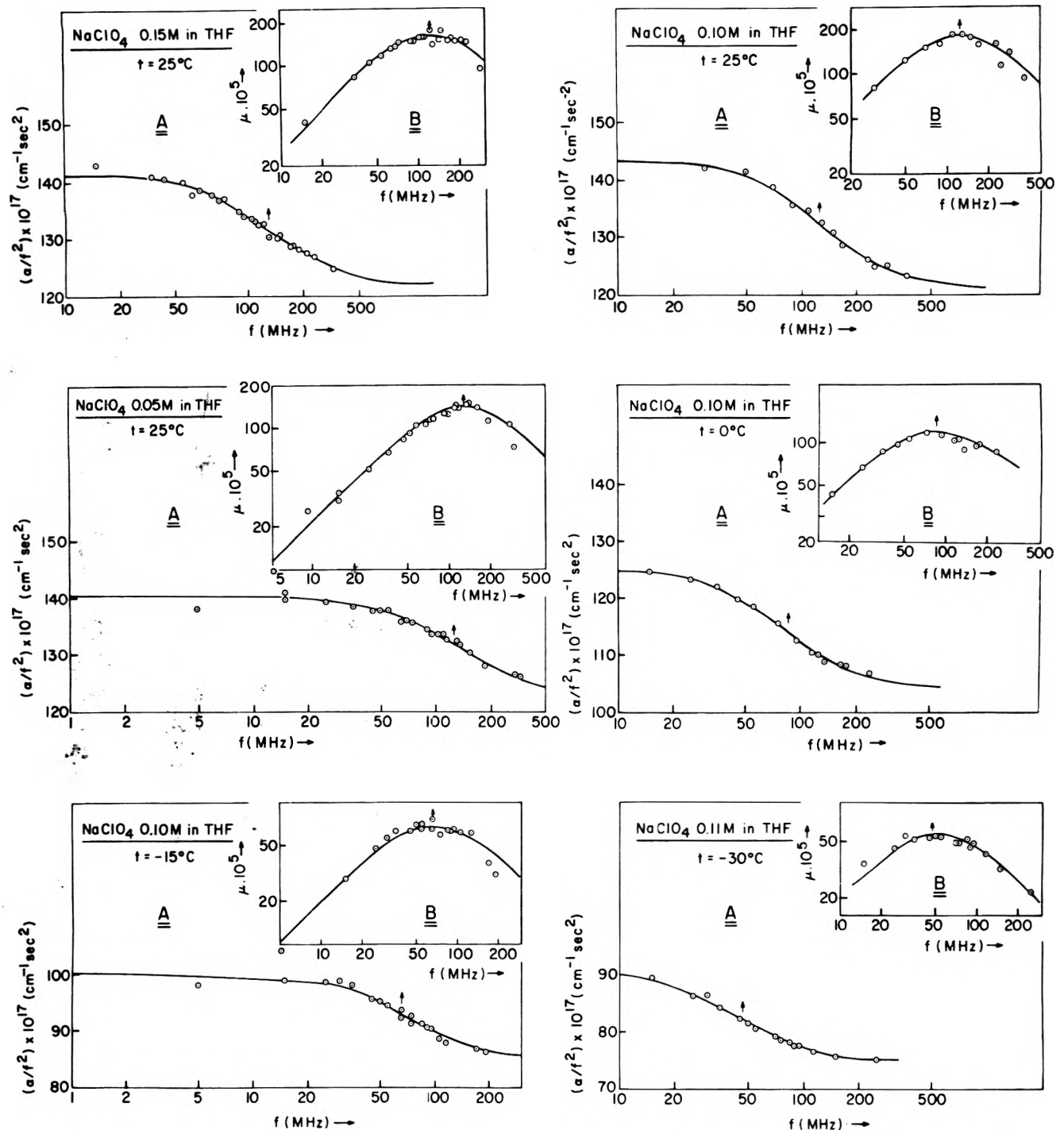

Figure 2. (A) α/f^2 vs. the frequency f for $NaClO_4$ in THF at 25, 0, −15, and −30°C. (B) μ vs. the frequency f for $NaClO_4$ in THF at 25, 0, −15, and −30°C.

$$\mu + \frac{\mu f^2}{f_R^2} = \frac{2\mu_{max}}{f_R} f$$

and

$$\frac{\mu}{f} = \frac{2\mu_{max}}{f_R} - \frac{\mu f}{f_R^2}$$

μ/f vs. μf is plotted and a best fit straight line is calculated using the least-squares method giving $-1/f_R^2$ as the slope and $2\mu_{max}/f_R$ as the intercept. Then eq 1 and 2 are used to reevaluate B from the calculated values of μ_{max} and f_R. This process is repeated until convergence is reached.

The results of the measurements made on $AgClO_4$ in THF solutions are plotted in Figure 3. A similar iterative procedure was used to evaluate B, f_R, and μ_{max}.

The results of both sets of computations, i.e., the converging values of B as well as A, μ_{max}, and f_R for the $NaClO_4$ and the $AgClO_4$ solutions, are tabulated in Table I.

The relaxation frequency appears to be independent of concentration for the $NaClO_4$ solutions which indicates a first-order or a pseudo-first-order kinetic process of the type

$$A \underset{k_R}{\overset{k_f}{\rightleftharpoons}} B \qquad (3)$$

TABLE I: Calculated Ultrasonic Relaxation Parameters for $NaClO_4$ and $AgClO_4$ in THF and for $NaClO_4$ in the Solvent Mixture THF–C_2H_5OH

t, °C	c, M	f, MHz	$10^5\mu_{max}$	$10^{17}A$, cm^{-1} s^2	$10^{17}B$, cm^{-1} s^2	$10^{-5}u$, cm s^{-1}
			$NaClO_4$ in THF			
25.0	0.15	127	155	18.9	122	1.269
0.10	0.10	127	183	22.6	121	1.269
	(2nd run)	127	187	23.2	121	1.269
	0.05	125	137	17.3	123	1.269
0.0	0.10	85	120	20.3	104	1.390
−15.0	0.10	66	69.6	13.8	85.5	1.457
−30.0	0.11	47.5	56.4	15.5	74.5	1.531
			$AgClO_4$ in THF			
25	0.14	105	119	17.9	126.5	1.269
	0.10	125.5	106.5	13.4	122	1.269
	0.05	109	95.2	13.7	124	1.269
−15	0.10	61	77.5	17.4	88.5	1.457
−30	0.11	54	73	17.7	76.5	1.531
			$NaClO_4$ in THF–C_2H_5OH; $X_{C_2H_5OH}$ = 0.226			
25	0.10	43	33.4	12.5	75.0	1.243

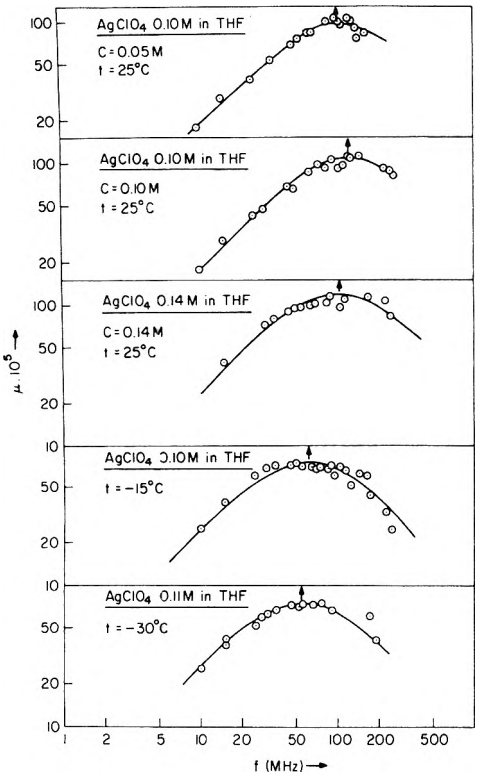

Figure 3. μ vs. the frequency f for $AgClO_4$ in THF at 25, −15, and −30°C.

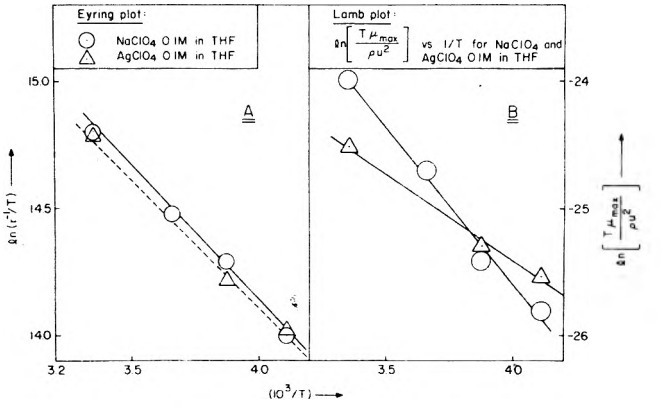

Figure 4. (A) ln (τ^{-1}/T) vs. $1/T$ for $NaClO_4$ and $AgClO_4$ in THF. (B) ln $(\mu_{max}T/\rho\mu^2)$ vs. $1/T$ for $NaClO_4$ in THF.

The energy barrier of the observed first-order process may be calculated from the temperature dependence of the relaxation frequency following the derivation partially outlined by Lamb.[8]

For a first-order process one has $\tau^{-1} = k_f + k_R$ with $K = k_f/k_R = [B]/[A]$ where τ is the relaxation time and K is the equilibrium constant. Then

$$\tau^{-1} = k_R(1 + K)$$

notice that if $K \ll 1$, the above expression reduces to $\tau^{-1} = k_R$, whereas if $K \gg 1$, $\tau^{-1} = k_f$. If one assumes either of the two positions ($K \ll 1$ or $K \gg 1$) and retains the Eyring theory, one has

$$\tau^{-1} = (kT/h)\exp(-\Delta H^{\ddagger}/RT)\exp(\Delta S^{\ddagger}/R)$$

and

$$\ln(\tau^{-1}/T) = [\ln(k/h) + \Delta S^{\ddagger}/R] - \Delta H^{\ddagger}/RT$$

from which it transpires that a plot of ln (τ^{-1}/T) vs. $1/T$ (Figure 4A) shall give as a slope d ln (τ^{-1}/T)/d$(1/T) = -\Delta H^{\ddagger}/R$ and as an intercept ln $(k/h) + \Delta S^{\ddagger}/R$.

In the absence of independent knowledge of the magnitude of K (and retention of either $K \ll 1$ or $K \gg 1$)), it would then remain undetermined whether the calculated activation parameters $\Delta H^{\ddagger}$ and $\Delta S^{\ddagger}$ refer to the forward or to the reverse process.

On the other hand, by making no assumption on the magnitude of K, one has

$$\tau^{-1} = [(kT/h)\exp(-\Delta H_R^{\ddagger}/RT)\exp(\Delta S_R^{\ddagger}/R)](1 + K)$$

and

$$\frac{d\ln(\tau^{-1}/T)}{d(1/T)} = -\frac{\Delta H_R^{\ddagger}}{R} + \frac{d\ln(1+K)}{d(1+K)}\frac{d(1+K)}{d(1/T)} = -\frac{\Delta H_R^{\ddagger}}{R} + \frac{K}{1+K}\frac{d\ln K}{d(1/T)}$$

$$\frac{d\ln(\tau^{-1}/T)}{d(1/T)} = -\frac{\Delta H_R^{\ddagger}}{R} - \frac{K}{1+K}\frac{\Delta H^{\circ}}{R}$$

the term $[K/(1 + K)](\Delta H°/R)$ can be determined from the temperature dependence of the excess sound absorption per wavelength μ_{max} as shown below. Hence $\Delta H_R^{\ddagger}$, $\Delta S_R^{\ddagger}$, and therefore $\Delta G_R^{\ddagger}$ can be determined independently by ultrasonic absorption measurements.

For $NaClO_4$ in THF the term $K/(1 + K)(\Delta H°/R) = -2490$ (see below). From Figure 4A the slope calculated by linear least squares is -1017. Then $-1017 = -\Delta H_R^{\ddagger}/R + 2490$ and $\Delta H_R^{\ddagger} = 6.97$ kcal/mol. Similarly the intercept 18.212 gives $\Delta S_R^{\ddagger} = -11.0$ eu. At $T = 298.15$ K $\Delta G_R^{\ddagger} = 6.97 + 3.28 = 10.25$ kcal/mol which gives $k_R = (kT/h) \exp(-\Delta G_R^{\ddagger}/RT) = 1.91 \times 10^5$. Because $f_R = 127$ MHz ($C = 0.05$ M, $T = 298.15$ K, Table I), $\tau^{-1} = k_f + k_R = 7.98 \times 10^8$ s^{-1} and $K \simeq 4.2 \times 10^3 \gg 1$. In fact, retention of this condition, hence $\tau^{-1} = k_f$, from Figure 4A gives slope $= -\Delta H_f^{\ddagger}/R = -1017$ and $\Delta H_f^{\ddagger} = 2.02$ kcal/mol whereas from the intercept $\Delta S_f^{\ddagger} = -11.0$ eu. From these parameters one can calculate, at $T = 298.15$ K, $\Delta G_f^{\ddagger} = \Delta H_f^{\ddagger} - T\Delta S_f^{\ddagger} = 5.3$ kcal/mol and retaining the Eyring theory

$$k_f = (kT/h) \exp(-\Delta G_f^{\ddagger}/RT) = 8.1 \times 10^8 \text{ s}^{-1}$$

For $AgClO_4$ in THF the term $K/(1 + K)(\Delta H°/R) = -1371$ (see below). From Figure 4A the slope calculated by linear least squares is -884.8. Then $-884.8 = -\Delta H_R^{\ddagger}/R + 1371$, which gives $\Delta H_R^{\ddagger} = 4.48$ kcal/mol. Similarly the intercept is equal to 17.725 which gives $\Delta S_R^{\ddagger} = -11.9$ eu. Then, at $T = 298.15$ K, $\Delta G_R^{\ddagger} = 4.48 + 3.55 = 8.03$ kcal/mol, which in turn gives $k_R = 0.81 \times 10^7$ s^{-1}. At 25°C the average relaxation frequency is $f_R = 113$ MHz; thus $\tau^{-1} = 7.1 \times 10^8$ s^{-1}. As in the case of $NaClO_4$ $k_f \gg k_R$ and $K \gg 1$. Retention of the condition $\tau^{-1} = k_f$ from Figure 4A gives $\Delta H_f^{\ddagger} = 1.75$ cal/mol and $\Delta S_f^{\ddagger} = -11.9$ eu. These two figures are clearly comparable to the corresponding ones for $NaClO_4$ (as the close parallelism and closeness of the two functions drawn in Figure 4A testify). The results of the above kinetic calculations are summarized in Table II.

We wish now to extract thermodynamic parameters from the ultrasonic spectra of $NaClO_4$ and $AgClO_4$ in THF. Following a procedure partially outlined by Lamb[8] for a first-order process of type (3) we may write

$$\mu = \frac{\pi(\Delta V_s)^2}{\beta RT}\left(\frac{1}{[A]} + \frac{1}{[B]}\right)^{-1} \frac{f/f_R}{1 + (f/f_R)^2}$$

where $\beta = 1/\rho u^2$ is the solvent compressibility and $\Delta V_s = \Delta V_T - (\theta/\rho c_p)\Delta H°$ with θ being the isobaric expansion coefficient and c_p the specific heat. At the relaxation frequency

$$\mu_{max} = \frac{\pi(\Delta V_s)^2}{2\beta RT} \frac{[A][B]}{[A] + [B]}$$

or

$$\mu_{max} = \frac{\pi(\Delta V_s)^2}{2\beta RT} [A] \frac{K}{1 + K} \tag{4a}$$

and

$$\mu_{max} = \frac{\pi(\Delta V_s)^2}{2\beta RT} c^* \frac{K}{(1 + K)^2} \tag{4b}$$

with $c^* = [A] + [B]$. Then one may write

$$\frac{\mu_{max} T}{\rho u^2} = \frac{\pi(\Delta V_s)^2}{2R} c^* \frac{K}{(1 + K)^2} \tag{5}$$

As in the kinetic treatment of the data above, one might assume $K \ll 1$ or $K \gg 1$. For $K \ll 1$, since $K = \exp(-\Delta G°/RT)$, one has

TABLE II: Summary of the Results of the Ultrasonic Analysis for $NaClO_4$ and $AgClO_4$ in THF

Electrolyte	k_f(298.15 K), s^{-1}	$\Delta H_f^{\ddagger}$, kcal/mol	$\Delta S_f^{\ddagger}$, eu	$K = k_f/k_R$
$NaClO_4$	8.1×10^8	2.02	−11.0	4.2×10^3
$AgClO_4$	8.1×10^8	1.75	−11.9	10^2

$$\ln\left(\frac{\mu_{max} T}{\rho u^2}\right) = \ln\left[\frac{\pi(\Delta V_s)^2 c^*}{2R}\right] - \frac{\Delta G°}{RT}$$

Thus the slope of the straight line obtained by plotting ln $(\mu_{max}T/\rho u^2)$ vs. $1/T$ is equal to $-\Delta G°/R$. Notice, however, that by retaining the condition $K \gg 1$, one has

$$\ln\left(\frac{\mu_{max} T}{\rho u^2}\right) = \ln\left[\frac{\pi(\Delta V_s)^2 c^*}{2R}\right] + \frac{\Delta G°}{RT}$$

Therefore lack of independent information on the magnitude of K (and retention of either $K \ll 1$ or $K \gg 1$) would leave the sign of $\Delta G°$ undetermined. However, if no position is taken on the magnitude of K, then from relation 4a and $K = [B]/[A]$ one may write

$$\ln\left(\frac{\mu_{max} T}{\rho u^2}\right) = \ln\left[\frac{\pi(\Delta V_s)^2}{2R}[B]\right] - \ln(1 + K)$$

In this case the slope of the function ln $(\mu_{max}T/\rho u^2)$ plotted vs. $1/T$ will be

$$\text{slope} = -\frac{d \ln(1 + K)}{d(1/T)} = -\frac{d \ln(1 + K)}{d(1 + K)} \frac{d(1 + K)}{d(1/T)} = -\frac{K}{1 + K} \frac{d \ln K}{d(1/T)} \tag{6}$$

$$\text{slope} = \frac{K}{1 + K} \frac{\Delta H°}{R}$$

which, combined with the kinetic data as shown above, allows the determination of the activation parameters of process 3. For $NaClO_4$ in THF the plot of ln $(\mu_{max}T/\rho u^2)$ vs. $1/T$ (Figure 4b) gives slope $= K/(1 + K)(\Delta H°/R) = -2490$ and intercept $=$ ln $[(\pi(\Delta V_s)^2/2R)[B]] = -15.636$. Because $K \gg 1$ as determined in the kinetic section, we can safely call slope $= \Delta G°/R = -2490$ and intercept $=$ ln $[(\pi(\Delta V_s)^2/2R)c^*]$ according to the derivation shown above for $K \gg 1$. Then $\Delta G° = -2490R = -4.95$ kcal/mol, which corresponds to $K = \exp(-\Delta G°/RT) = 4.2 \times 10^3$ at $T = 298.15$ K. Similarly for $AgClO_4$ in THF the plot of ln $(\mu_{max}T/\rho u^2)$ *vs.* $1/T$ (Figure 4B) gives slope $= K/(1 + K)(\Delta H°/R) = -1371$ and intercept $= -19.935$. Because also for $AgClO_4$ $K \gg 1$ as determined in the kinetic section, then $\Delta G° = -1371R = -2.73$ kcal/mol, which corresponds to $K \simeq 100$ at 298.15 K. Hence, whereas the kinetic forward activation parameters do not show appreciable differences between $NaClO_4$ and $AgClO_4$ in THF, the stability constants of the process investigated differ for the two systems as Figure 4B reveals.

The above implies, as a consequence, that also the product $(\Delta V_s)^2 c^*$ for the two processes is different. This is evident from the different intercepts of Figure 4B and from eq 5, the μ_{max} being of the same order of magnitude for the two systems (Table I). Unfortunately the quantity $c^* = [A] + [B]$ is unknown; the c^* is not to be identified with the stoichiometric concentration c as discussed below. This hinders the numerical evaluation of the ΔV_s's.

The experimental results shown in Tables I and II and in Figure 4A show that the first-order process that has been observed involves mainly the anion. In fact from Tables I and II, the relaxation frequencies and the activation pa-

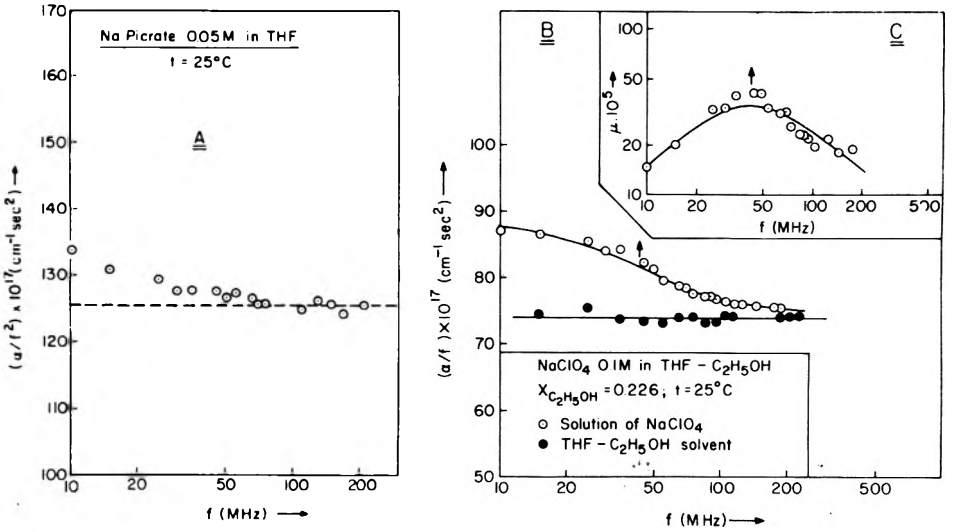

Figure 5. (A) α/f^2 vs. f for sodium picrate 0.05 M in THF at 25°C. (B) α/f^2 vs. f for $NaClO_4$ 0.1 M in a C_2H_5OH–THF mixture at 25°C. (C) μ vs. f for $NaClO_4$ 0.1 M in a C_2H_5OH–THF mixture at 25°C.

rameters for for $AgClO_4$ and $NaClO_4$ solutions are comparable.

Similar observations were made by Hemmes[1] on solutions of $LiNO_3$ and of Bu_4NNO_3 in THF. It seems therefore that the same process with an activation enthalpy close to the activation energy for viscous flow E_1 = 1.79 kcal/mol is observed for both $AgClO_4$ and $NaClO_4$.

The results of measurements on a 0.05 M sodium picrate solution (Figure 5A) show the onset of a relaxation only at the lower end of the available frequency range. This further demonstrates that ClO_4^- and not Na^+ is responsible for the observed relaxation near 100 MHz.

The hypothesis is advanced that we have observed the second step of the Eigen scheme (eq 7) corresponding to

$$Na^+S_x + ClO_4^-S_y \underset{k_{21}}{\overset{k_{12}}{\rightleftharpoons}} Na^+S_2ClO_4^- \underset{k_{32}}{\overset{k_{23}}{\rightleftharpoons}} Na^+SClO_4^- \underset{k_{43}}{\overset{k_{34}}{\rightleftharpoons}} NaClO_4 \quad (7)$$

step I step II step III

the anion desolvation and its reverse. (S = solvent molecule.) The first step is not observable by ultrasonics[1] because of the extent of ionic association, and to a good approximation process 7 could be written without step I.

The measured rate constants would then correspond to k_{23} or k_{32}, but there is no way to decide which one corresponds to the experimental k_f for a first-order process since the only experimental data we have are τ and its temperature dependence.

In order to test the proposed mechanism, an ethanol–THF solution (mole fraction $X_{C_2H_5OH}$ = 0.226) was prepared. A solution of $NaClO_4$ 0.1 M in this solvent ($[C_2H_5OH]/[NaClO_4] \simeq 30$) was also prepared. It was thought that if the observed process in pure THF is related to anion desolvation by adding an excess of polar solvent (with respect to the electrolyte), the relaxation phenomenon might be disturbed.

The results of the measurements of the solvent mixture and of 0.1 M $NaClO_4$ in the same mixture are reported in Figures 5B and 5C and in Table I. The relaxation frequency shifts, by a factor of about 3, to a lower frequency indicating a possible participation of ethanol in the process involving ClO_4^-. Ethanol, rather than THF, probably intervenes in the observed cation–solvent exchange around the anion in the ion pair. It is significant that the results shown below of the microwave dielectric measurements on $NaClO_4$ in the same ethanol–THF solutions tend to substantiate this conclusion. This concurrence of observations of two different phenomena restricts the choice of possible alternate explanations for the ultrasonic process.

The measured viscosity of the ethanol–THF mixture was 5.02% higher than the measured viscosity of pure THF. In fact, a Cannon viscometer (No. 0, manufacturer calibration constant A = 0.000972 according to the relation $\eta = A\rho t$) was recalibrated with freshly distilled THF and with C_2H_5OH. The calibration constant at 25°C resulted as A = 0.000971 ± 6 × 10^{-6} in good accord with the above calibration. The solvent mixture THF–C_2H_5OH of $X_{C_2H_5OH}$ = 0.226 resulted in viscosity η = 0.481 cP, its density being ρ = 0.8654 g cm^{-3}, whereas the viscosity of pure THF is η = 0.458 cP at 25°C.[2] Thus the increased viscosity could not account for the ultrasonic frequency shift.

Notice also that eq 5 may appear to imply that μ_{max} is proportional to the concentration c, which is not the case as shown in Table I. However, in our hypothesis, c^* = [A] + [B] = $[Na^+S_2ClO_4^-]$ + $[Na^+SClO_4^-]$ which is not the total concentration. Changes in the electrolyte concentration may change c^* in a nonlinear fashion by modifying the number and type of species present. The only assumption, made through the use of eq 5 (Figure 4B), is that at the total concentration c = 0.1 M ($NaClO_4$ or $AgClO_4$), the change in c^* is negligible in the temperature range investigated.

III. Dielectric Relaxation

Experimental Procedure. The dielectric constant and loss in the frequency range of 0.2–1.5 GHz were measured using a GR bridge, No. 1602 B,[9] and a microwave power reflection technique was used for the frequency range of 2–8.5 GHz.[9] The preparation of the materials and the solutions are described in the ultrasonic section. A Forma Junior thermostatic bath was used to maintain a temperature of 25 ± 0.05°C. The liquid temperature was checked in the dielectric cell after each measurement.

Results. The real and imaginary parts of the complex

TABLE III: Real and Imaginary Parts of the Permittivity in the Frequency Range Investigated for $NaClO_4$ 0.1 and 0.05 M in THF at 25°C[a]

f, GHz	ε′	ε″	f, GHz	ε′	ε″
$NaClO_4$ 0.1 M in THF; 25°C; $\chi_s = 2.65 \times 10^{-5}\ \Omega^{-1}\ cm^{-1}$					
0.30$_3$	8.71	0.42	1.50	8.36	0.78
0.50	8.68	0.40	2.00	8.20	0.80
0.60	8.65	0.43	3.00	7.88	0.90
0.90	8.59	0.59	4.00	7.73	1.03
1.20	8.42	0.63	8.52$_5$	7.24	1.03
$NaClO_4$ 0.05 M in THF; 25°C; $\chi_s = 1.30 \times 10^{-5}\ \Omega^{-1}\ cm^{-1}$					
0.30	8.21	0.28	2.00	7.85	0.58
0.60	8.26	0.38	3.00	7.77	0.74
0.90	8.15	0.45	4.00	7.56	0.76
1.20	8.14	0.50	8.53	7.21	0.96
1.50	7.99	0.52			
C_2H_5OH–THF Mixture; $X_{C_2H_5OH} = 0.226$; 25°C					
0.207	9.37	0.13	1.50	9.28	0.60
0.304	9.30	0.17	3.00	9.00	1.06
0.450	9.30	0.42	4.00	8.78	1.25
0.600	9.31	0.28	8.52	7.81	1.48
0.900	9.26	0.33			
$NaClO_4$ 0.1 M in C_2H_5OH–THF; $X_{C_2H_5OH} = 0.226$; $\chi_s = 2.61 \times 10^{-4}\ \Omega^{-1}\ cm^{-1}$					
0.189	12.24	2.69	1.50	10.01	1.61
0.304	11.92	2.27	2.00	9.57	1.86
0.468	11.38	1.99	3.00	9.12	1.97
0.600	10.90	1.81	4.00	8.95	2.13
0.900	10.44	1.51	8.52	7.71	2.27
1.200	10.19	1.58			

[a] χ_s is the audiofrequency electrical conductivity (Ω^{-1} cm^{-1}).

permittivity for 0.1 and 0.5 M solutions of $NaClO_4$ in THF are shown in Table III. The analysis of this data is similar to the one described in a previous paper.[9] The corrected values of ϵ_d' and ϵ_d'' are calculated from the contributions of the solvent relaxation and the conductivity using the relationships

$$\epsilon_d' = \epsilon'\omega + \epsilon_s' - \epsilon_s'(\omega)$$
$$\epsilon_d'' = \epsilon''(\omega) - \epsilon_s''(\omega) - \epsilon_x'' \qquad (8)$$

where $\epsilon'(\omega)$ and $\epsilon''(\omega)$ are the experimental values. ϵ_s' is the static permittivity of the solvent (7.40) at 25°C. $\epsilon_s'(\omega)$ and $\epsilon_s''(\omega)$ are the real and imaginary parts of the solvent permittivity at the angular frequency, ω. ϵ_x'' is the contribution to the loss due to the solution conductivity χ_s

$$\epsilon_x'' = \frac{1.8 \times 10^{12}}{f}\chi_s \qquad (9)$$

The approximation used in deriving equations 8 and 9, e.g., that the solvent relaxation is negligibly altered by the presence of the solute, and in retaining the audiofrequency conductivity have been discussed previously.[9] The approximations for the solvent corrections are probably acceptable in dilute solutions to 0.05–0.1 M.

The calculated values of ϵ_d' and ϵ_d'' for c = 0.1 M are shown in Figure 6A as a Cole–Cole plot. The solid line fits a Cole–Davidson distribution with a parameter $\beta = 0.8$, according to the function for the complex permittivity

$$\epsilon_d' - j\epsilon_d'' = \epsilon_\infty + \frac{\epsilon_0 - \epsilon_\infty}{(1 + j\omega\tau_D)^\beta} = \epsilon_\infty + \frac{\epsilon_0 - \epsilon_\infty}{[1 + j(f/f_R)]^\beta}$$

where ϵ_∞ has been set equal to ϵ_s' the static permittivity of the solvent; τ_D is the dielectric relaxation time. The fit has

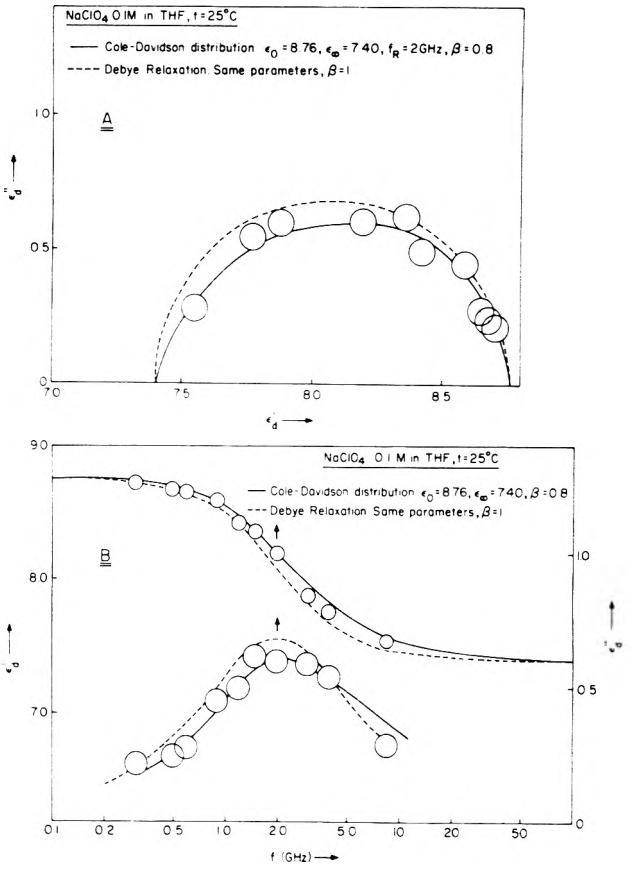

Figure 6. (A) Cole–Cole plot of ϵ_d'' vs ϵ_d' for $NaClO_4$ 0.1 M in THF at 25°C; relaxation parameters $\epsilon_0 = 8.76$, $\epsilon_\infty = 7.40$, $f_R = 2.0$ GHz, $\beta = 0.8$. (B) ϵ_d' vs. f and ϵ_d'' vs. f for $NaClO_4$ 0.1 in THF at 25°C.

been obtained for $\epsilon_0 = 8.76$, $f_R = 2.0$ GHz, and $\beta = 0.8$. In Figure 6B the same data are displayed by ϵ_d' and ϵ_d'' and plotted as functions of frequency. The results for the measurements on 0.05 M $NaClO_4$ solution are shown in Figure 7A and B. The parameters corresponding to the Cole–Davidson distribution functions were $\epsilon_0 = 8.30$, $\epsilon_\infty = \epsilon_s' = 7.40$, $f_R = 1.8$ GHz, and $\beta = 0.9 \pm 0.1$.

In the study on $LiClO_4$ in THF[9] the probability was discussed that the Cole–Davidson distribution was the result of an overlapping of two or more Debye relaxation processes which originate from the rotational relaxation of different solvated forms of ion pairs.

From the ultrasonic work for $NaClO_4$ in THF the ratio between the concentration of the two outer-sphere forms of the ion pairs results in $K = 4.2 \times 10^3$. However, from the ultrasonic work alone we cannot decide whether $K = [Na^+S_2ClO_4^-]/[NaSClO_4^-]$ or $K = [Na^+SClO_4^-]/NaS_2ClO_4^-]$, i.e., which form of solvated ion pairs predominates in the solution. Similarly the calculation of the outer-sphere formation constant K_{12}^{-1} (from the equations based on the electrostatic ionic potentials[10]) is too sensitive to parameter a, the minimum collision distance of free ions. Consequently it is not possible from these data alone to extract a meaningful value of K_{34}^{-1} from the Eigen relation[11]

$$K_\Sigma = K_{12}^{-1}(1 + K_{23}^{-1} + K_{23}^{-1}K_{34}^{-1}) \qquad (10)$$

where K_Σ is the overall formation constant; K_{23}^{-1} and K_{34}^{-1} are the formation constants of steps II and III of reaction 7.

In the absence of such precise structural information the

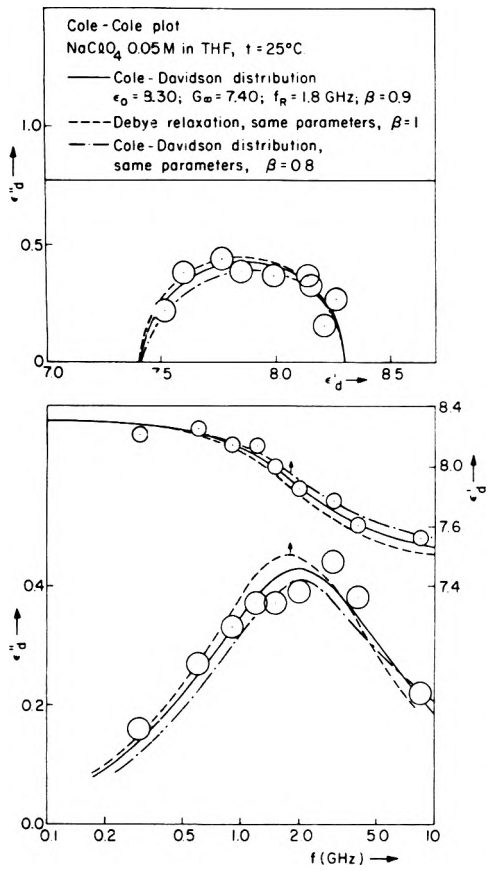

Figure 7. (A) Cole–Cole plot of ϵ_d'' vs. ϵ_d' for $NaClO_4$ 0.05 M in THF at 25°C; relaxation parameters $\epsilon_0 = 8.30$, $\epsilon_\infty = 7.40$, $f_r = 1.8$ GHz, $\beta = 0.9 \pm 0.1$. (B) ϵ_d' vs. f and ϵ_d'' vs. f for $NaClO_4$ 0.05 M in THF at 25°C.

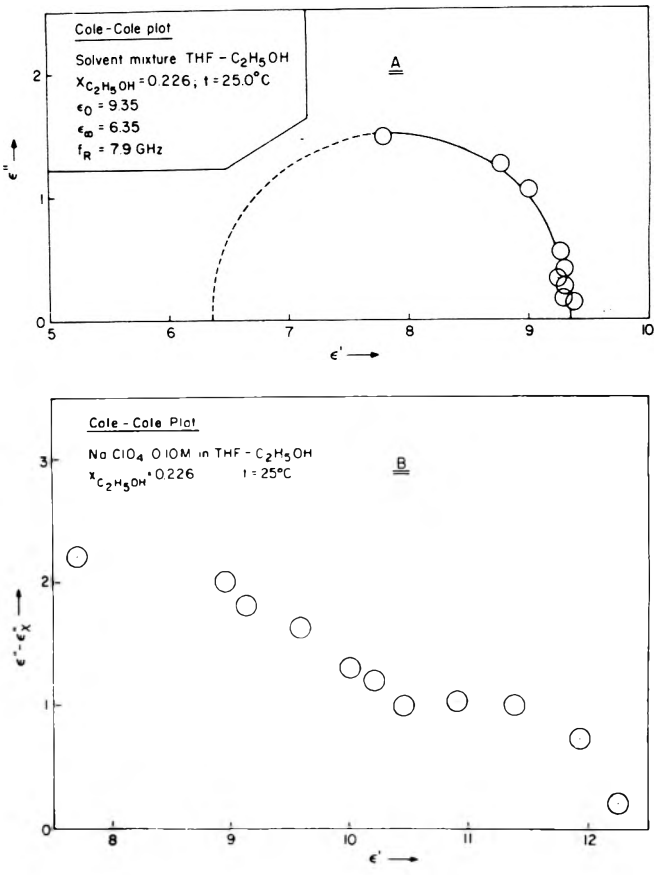

Figure 8. (A) Cole–Cole plot of ϵ'' vs. ϵ' for the solvent mixture C_2H_5OH–THF; $X_{C_2H_5OH} = 0.226$; $t = 25°C$. (B) Cole–Cole plot of $(\epsilon'' - \epsilon_x'')$ vs. ϵ' for $NaClO_4$ 0.1 M in the solvent mixture C_2H_5OH–THF; $X_{C_2H_5OH} = 0.226$; $t = 25°C$.

same calculation[9] of the Cole–Davidson distribution parameter β has been performed. It is assumed that the source of the Cole–Davidson relaxation distribution function is due to the diffusional rotation of ion pairs coupled with diffusional collisions between them. A modified Glarum theory[9] leads to the calculation of β as

$$\beta = \frac{(\tau_{dif}/\tau_D)^{1/2}}{1 + (\tau_{dif}/\tau_D)^{1/2}}$$

where $\tau_{dif} = l_0^2/D$, and l_0 is the average diffusion distance for the encounter of the rotating ion pairs, i.e. l_0 is the distance a rotating ion pair moves in either direction of a one-dimension diffusion walk[13] to encounter the next neighbor pairs assumed randomly distributed. D is the diffusion coefficient of the pairs. Numerically, for 0.1 M $NaClO_4$ $D \simeq 10^{-5}$ cm^2 s^{-1}[9] and $2l_0 = [1/\frac{1}{2}C_{pair}(10^{-3}L)]^{1/3} \simeq [1/\frac{1}{2}C(10^{-3}L)]^{1/3}$ where L is Avogadro's number. The resultant values are $l_0 = 16.07 \times 10^{-8}$ cm, $\tau_{dif} = 2.58 \times 10^{-9}$ s, and $\beta_{calcd} = 0.85$ (given $\tau_D = 7.96 \times 10^{-11}$ s) which is in agreement with $\beta_{exptl} = 0.8$. Similarly for a 0.05 M $NaClO_4$ solution the calculated values are $l_0 = 20.3 \times 10^{-8}$ cm, $\tau_{dif} = 4.12 \times 10^{-9}$ s ($\tau_D = 8.84 \times 10^{-11}$ s), and $\beta_{calcd} = 0.87$ whereas $\beta_{exptl} = 0.9 \pm 0.1$. The calculated values of β agree with the experimental values within the possible tolerances. The limited solubility of $NaClO_4$ prevents extending the measurements to higher concentrations. (In the case of $LiClO_4$, at higher concentrations the process becomes more cooperative and β tends to 0.5.)

At this stage of the research it was conceived that if the observed relaxation is mainly due to the rotation of ion pairs, one should observe a change in the relaxation phenomenon once the structure of these pairs is altered. In order to check on this hypothesis, the same solvent mixture, ethanol–THF, that was used for ultrasonic work was employed here. The results of these measurements (Table III) are plotted in Figure 8A for the solvent mixture alone and in Figure 8B for the 0.1 M $NaClO_4$ in the ethanol–THF solvent. The Cole–Cole plot in Figure 8A (maximum frequency was 8.5 GHz) may be described by a Debye single-relaxation function. However, it is anticipated that at frequencies higher than 8.5 GHz a single relaxation will not be sufficient to describe the data since pure THF has a separate relaxation at higher frequencies.[9,12] The apparent relaxation parameters of the solvent, calculated from a linear least-squares plot of ϵ' vs. f are $\epsilon_0 = 9.35$ and $f_R = 7.9$ GHz. (The extrapolated Debye function crosses the ϵ' axis at $\epsilon_\infty = 6.35$ in Figure 8A.) However, one has to keep in mind that the above parameters, especially f_R and ϵ_∞, fit the function without consideration of the contribution of the solvent THF relaxation. Hence they should be considered as approximate.

The Cole–Cole plot in Figure 8B reports for the ordinate the quantity $(\epsilon'' - \epsilon''_x)$, namely, the total imaginary part corrected for the conductance contribution

$$\epsilon''_x = \frac{1.8 \times 10^{12}\chi}{f}$$

(The conductance of the electrolyte solution was measured at 25.000°C giving $\chi = 2.61 \times 10^{-4}$ Ω^{-1} cm^{-1}). The frequency range was 0.189–8.52 GHz. From the trend of the

data in Figure 8B, it may be seen that (at least) two relaxation regions are discernible, one approximately comparable to the one for the solvent mixture ethanol–THF and an additional one at lower relaxation frequency.

A quantitative analysis of these data is not possible because of the unknown contribution of the solvent THF to the investigated relaxation processes. To this purpose it would be necessary to extend the frequency range to about 100 GHz. It is possible, however, to draw some qualitative conclusions from the above data. It seems that the relaxation at the higher frequency (Figure 8B) is comparable to the relaxation of the ethanol–THF mixture and the lower relaxation (centered around the relaxation frequency $f_R \approx 0.5$ GHz) is the result of the addition of $NaClO_4$ to the solvent mixture ethanol–THF. This relaxation frequency $f_R \approx 0.5$ GHz is lower by a factor of 4 than the average relaxation frequency shown by $NaClO_4$ 0.1 M in pure THF ($f_R = 2$ GHz). Since the viscosity increases only by 5% (with respect to pure THF) by the addition of ethanol, as in the ultrasonic studies, it seems likely that ethanol intervenes in solvating the ion pairs, consequently lowering their rate of rotation.

References and Notes

(1) H. Wang and P. Hemmes, *J. Am. Chem. Soc.*, **95**, 5115 (1973).
(2) P. Jagodzinski and S. Petrucci, *J. Phys. Chem.*, **78**, 917 (1974).
(3) R. M. Fuoss and C. A. Kraus, *J. Am. Chem. Soc.*, **55**, 2387 (1933).
(4) D. N. Bhattacharyya, C. L. Lee, J. Smid, and M. Szwarc, *J. Phys. Chem.*, **69**, 608 (1965).
(5) C. Micheletti, Thesis, University of Paris, 1972.
(6) H. Wang and P. Hemmes, *J. Am. Chem. Soc.*, **95**, 5119 (1973).
(7) S. Petrucci in "Ionic Interactions", Vol. II, Academic Press, New York, N.Y., 1971, Chapter II.
(8) J. Lamb in "Physical Acoustics", Vol. II, W. P. Mason, Ed., Academic Press, New York, N.Y., 1965, Part A, Chapter 4.
(9) H. Farber and S. Petrucci, *J. Phys. Chem.*, **79**, 1221 (1975).
(10) R. M. Fuoss, *J. Am. Chem. Soc.*, **80**, 5059 (1958); N. Bjerrum, *K. Dan. Vidensk. Selsk., Mat.-Fys. Medd.*, **7**, 9 (1926).
(11) M. Eigen and L. DeMaeyer in "Techniques of Organic Chemistry", Vol. VIII, Part II, S. L. Friess, E. S. Lewis, and A. Weissberger, Ed., 2nd ed, Interscience, New York, N.Y., 1963.
(12) J. P. Badiali, H. Cachet, A. Cyrot, and J. C. Lestrade, *J. Chem. Soc., Faraday Trans. 2*, **69**, 1339 (1973).
(13) Justifications for the approximation inherent in assuming a one-dimension system were discussed in the original theory: S. H. Glarum, *J. Chem. Phys.*, **33**, 639 (1960).

Thermodynamics of Caffeine Aqueous Solutions

A. Cesàro, E. Russo, and V. Crescenzi*

Institute of Chemistry, University of Trieste, 34127 Trieste, Italy

(Received August 2, 1974; Revised Manuscript Received November 3, 1975)

Publication costs assisted by the Consiglio Nazionale delle Ricerche

A rather complete description of the thermodynamic properties of caffeine in aqueous solution for a wide concentration range is afforded on the basis of calorimetry, vapor pressure osmometry, solubility, and density experiments. The whole set of data is compatible with an interpretation of the concentration dependence of properties considered in terms of multiple association equilibria of the solute. Data on complex formation between caffeine and the dye ethidium bromide in aqueous solution are also reported. The thermodynamics of caffeine self-dimerization as well as of the caffeine–ethidium bromide adduct formation is discussed and compared with that for a few different species known to dimerize and/or aggregate by "vertical stacking" in dilute aqueous solution.

Introduction

Pyrimidine and purine bases, as well as a number of their derivatives, are known to self-associate in aqueous solution with the formation of dimers or higher aggregates by "vertical-stacking". A thermodynamic characterization of this behavior has been achieved in many instances with considerable accuracy by means of vapor pressure osmometry,[1] ultracentrifugation,[2] and calorimetry.[3,4]

A common feature, apparently independent of the degree of stacking of the compound under consideration, is that both the enthalpy and entropy of each association step are quite large and negative. In particular, the negative (unitary) entropy change of such association, for which hydrophobic forces would be relevant, has been a matter of debate.[4]

In the context of this type of studies, caffeine (1,3,7-trimethyl-2,6-dioxopurine) seems a particularly suitable compound. The study of the concentration dependence of its properties should, in fact, be free from complications that arise in other aggregating systems due to electrostatic interactions and due to the possible existence of protolytic products in solution. Moreover, caffeine is reported to form 1:1 mixed molecular complexes with different organic compounds containing aromatic ring systems, a fact which has possible pharmacological implications.[5,6] There is, however, still some lack of quantitative information on the behavior of caffeine in water (for instance, according to Guttman and Higuchi[16] the self-association of caffeine would proceed to the dimeric and tetrameric species only, a conclusion questioned by Gill et al.[3]), and nothing is known on the thermodynamics of its interactions with aromatic compounds in aqueous solution.

Pursuant to our interest on the physical chemistry of nonionic compounds in aqueous solution[7,8] and in the light

of what was mentioned above, we have carried out a series of solubility, vapor pressure osmometry, density, and microcalorimetry experiments aiming at a better characterization of the caffeine–water system. The interaction of caffeine with the dye ethidium bromide and with urea has also been studied, principally by means of calorimetry.

Experimental Section

(a) *Materials.* Urea and caffeine (C. Erba, Italy) were recrystallized from water–ethanol (1:1) and from water, respectively. Hydrated caffeine crystals were obtained in this way at around room temperature. Thermogravimetric and differential scanning calorimetric analysis revealed that such crystals lose 1 mol of water per mole of caffeine at around 82 °C. Sublimation of caffeine leads to anhydrous crystals exhibiting x-ray powder diffraction spectra quite different from those of the monohydrate crystals.

Crystalline forms were used in the calorimetric heats of solution measurements of both hydrated and anhydrous materials. Sublimed caffeine (anhydrous) was employed in most of the other experiments.

(b) *Methods.* (1) Osmotic coefficients, Φ, were obtained at 29.8 and 35.0 °C by vapor pressure osmometry (Perkin-Elmer, molecular weight apparatus Model 115) using sucrose (A-grade) solutions (0–0.05 m) as standards, writing $\Phi = (\Delta R/m)_{\text{caffeine}}/(\Delta R/m)_{\text{sucrose}}$ where ΔR(ohm) is the difference in thermistor resistance readings for the solution of molality m and for water. The $(\Delta R/m)_{\text{sucrose}}$ value was independent of m, and equal to the value reached by $(\Delta R/m)_{\text{caffeine}}$ for $m = 0$. In our experience the reproducibility of the measurements rapidly deteriorates with decreasing working temperature using the above apparatus because of its poor temperature control near 25 °C (water as solvent). For this reason we shall not report Φ values for 25 °C as we consider these values of insufficient reliability.

(2) Saturated caffeine solutions were obtained by prolonged equilibration under continuous shaking with pure solid caffeine in unsaturated or supersaturated solutions in a thermostated bath. The equilibrium molality of caffeine was derived either by direct uv analysis (after appropriate dilution of a weighed amount of the equilibrated solutions) using a molar extinction coefficient of ϵ 9900 at 272 nm,[9] or by evaporation to constant weight at 90 °C. A faster method, following a modified Davies et al.[10] procedure, has yielded the same solubility data, well within experimental errors (±0.0003 m from 16 to 30 °C).

(3) Density measurements were carried out using an A. Parr Model DMA-02-D microdensimeter connected with a thermostated bath at 25 ± 0.0001 °C. Water and air were employed for routine instrumental calibration using literature data[11] for their densities at the temperature and pressure of the experiments.

(4) Calorimetric measurements were made at 25 °C with a LKB 10700 batch-type microcalorimeter with glass cells. In the heat of dilution experiments weighed amounts of caffeine solutions of known concentration (ca. 4 g) were mixed with weighed amounts of water (0.5–2 g) in the calorimetric cells. Experimental values of the heat of dilution ranged from 0.2 (at the highest dilution) to 55 mcal, with an estimated uncertainty of 0.1 mcal. In the heat of solution experiments solid anhydrous caffeine (ca. 3 mg) weighed with a semimicro analytical balance (Gibertini G-15; precision ±10 μg) was mixed with weighed amounts of water (or urea solution). The complete dissolution of crystalline caffeine takes place in less than 4 min under the experimental conditions employed. The final concentration was checked by uv absorption analysis. Caffeine hydrate crystals were kept in a saturated solution and wiped with a filter paper before use. The amount of caffeine hydrate in the heat of solution experiments was determined by uv analysis of the final solution. The interaction of caffeine (2×10^{-3} to 5.3×10^{-2} M) with ethidium bromide (4.84×10^{-4} M) was studied with a LKB flow-type calorimeter.[12] The net heat of interaction was obtained during the same experiment by subtracting the experimental heats of dilution of each substance. The enthalpy of complex formation (ΔH) was obtained from the relation

$$\Delta H = Q/MV$$

where Q is the net heat of interaction (in cal/s), M is the complex concentration in the flux V (in our experiments 9.58×10^{-6} l./s). The concentration of the 1:1 complex was evaluated using the equilibrium constant obtained from spectral measurements.

(5) Uv measurements were performed at room temperature with a Hitachi Coleman EPS-3t spectrophotometer using quartz cells of appropriate pathlengths. Spectra of ethidium bromide ($1–2 \times 10^{-4}$ M) in the presence of different caffeine concentrations (10^{-3} to 10^{-2} M) were recorded using 1-cm thermostated quartz cells.

Results and Discussion

(A) *Caffeine in Water.* The results of the measurements carried out on aqueous solutions of caffeine are listed in Table I.

Assuming that deviations from ideality of the water–caffeine system are essentially due to solute–solute interactions leading to caffeine association, the experimental osmotic coefficient, Φ, values (Table I) were used to calculate the association constant with the equation[1]

$$K = (1 - \Phi)/m\Phi^2 \qquad (1)$$

assuming a multiple equilibrium with $K = K_1 = K_2 = \ldots K_{n-1}$. The results are $K = 9.0 \pm 0.1$ m^{-1} (29.8 °C), and $K = 7.8 \pm 0.1$ m^{-1} (35.0 °C).

From the density data of Table I one deduces that the apparent molar volume of caffeine goes from $\Phi_v^0 = 144.2$ ($m \to 0$) to $\Phi_v = 142.15$ cm^3/mol for $m = 0.1$, at 25 °C. We interpret this Φ_v decrease in terms of association and write

$$\Phi_v = \sum_{i=1} X_i V_i,$$

where X_i is the mole fraction of solute species of aggregation number i having a molar volume V_i. To solve the problem one can assume that the molar increment in volume passing from i to $(i + 1)$ is a constant, v, independent of i, i.e. that $V_i = \Phi_v^0 + (i - 1)v$. On the basis of our density data and using the association equilibrium constant, K, given above, one then easily calculates $v = 138.3$ cm^3/mol. This implies, for instance, that the molar volume of caffeine dimers in water would be 282.5 cm^3/mol of dimer, which is less by 5.9 cm^3/mol of dimer than would be expected from simple additivity of the apparent volume of the monomer. Our results are in qualitative agreement with dilatometric data reported by Kasarda.[13]

With the same assumptions made in the analysis of the Φ data, the enthalpy of association, $\Delta H°$, can be evaluated using the relative apparent molal enthalpy (Φ_L) data of Table I and

$$\Delta H° = \Phi_L/(1 - \Phi) \qquad (2)$$

TABLE I: Physicochemical Properties of Caffeine Aqueous Solutions[a]

Solubility[b]		Osmotic coefficient[c]				Apparent rel molal enthalpy 25 °C[d]		Density 25 °C[e]		
		29.8 °C		35.0 °C						
t	m_{satd}, mol/kg H_2O	m	Φ	m	Φ	m	$-\Phi_L$, cal/mol	m	d, g/cm³	Φ_v, cm³/mol
16.60	0.0714	0.1116	0.622	0.1027	0.656	0.1051	1150	0.00626	0.997360	143.7
19.30	0.0827	0.0765	0.683	0.0895	0.680	0.0632	970	0.01054	0.997577	143.8
20.50	0.0905	0.0590	0.723	0.0702	0.720	0.0357	710	0.02018	0.998069	143.5
23.80	0.1026	0.0528	0.745	0.0509	0.755	0.0298	640	0.02864	0.998500	142.7
26.08	0.1126	0.0386	0.781	0.0296	0.837	0.0247	550	0.05419	0.999840	142.5
26.44	0.1166	0.0258	0.835	0.0203	0.877	0.0169	420	0.05477	0.999859	142.6
28.88	0.1309					0.0125	340	0.07629	1.000965	142.5
						0.0092	240	0.10472	1.002456	142.0
						0.0084	230	0.10754	1.002558	142.2
						0.0044	110			
						0.0028	60			

Heats of solution in water at 25 °C

Crystalline anhydrous				Crystalline hydrate			
mol of caffeine × 10⁶	g H_2O	Q, mcal	ΔH, kcal/mol	mol of caffeine × 10⁶	g H_2O	Q, mcal	ΔH, kcal/mol
11.5	4.1162	38.12	3.31	29.0	4.4290	148.6	5.08
13.1	4.5024	46.52	3.54	9.12	4.0647	43.49	4.78
14.1	4.0713	47.82	3.49	14.5	4.5195	76.02	5.22
13.3	4.0593	46.44	3.50	8.72	3.9289	43.36	4.97
11.6	4.0778	38.73	3.33	8.74	4.1301	44.80	5.12
Mean ΔH_{IS} = 3.4 ± 0.1 kcal/mol				Mean ΔH_{IS} = 5.0 ± 0.1 kcal/mol			

[a] In the case of solubility, osmotic coefficient, and density data, each value is an average of at least four determinations. [b] Maximum deviations from the mean value are $\pm 3 \times 10^{-4}$ m. [c] Maximum deviations from the mean value are $\pm 5 \times 10^{-3}$. [d] Maximum deviations from the mean value are ±10 cal/mol. [e] Maximum deviations from the mean value are $\pm 8 \times 10^{-6}$ g/cm³. Concerning the Φ_L data, ± 10 cal/mol represents the maximum deviation of the average Φ_L values from a graphical best fit interpolation of Φ_L against m plot.

using extrapolated[23] values of Φ. We obtain $\Delta H^0 = -3.17 \pm 0.10$ kcal/mol, at 25 °C. Elaboration of the same experimental data according to the procedure of Stoesser and Gill[14] yields a nonlinear plot for the highest caffeine concentrations; nevertheless the values −3.4 kcal/mol and 9.4 m^{-1} for the enthalpy and the constant of association (at 25 °C), respectively, could be extrapolated from the low concentration region.

Concerning the solubility vs. temperature data it is important to point out that equilibrium was attained in each case between saturated solutions and solid hydrated caffeine. From these data (Table I) we derive d log m_{satd}/d(1/T) = 1.86×10^3 K. Using for the differential heat of solution, ΔH_{DS}, the relationship

$$\Delta H_{DS} = 2.303R\,\mathrm{d}\log m_{satd}/\mathrm{d}(1/T)\left(\Phi_{satd} + m_{satd}\frac{\mathrm{d}\Phi}{\mathrm{d}m}\right)_{25°C} \quad (3)$$

and introducing the Φ and dΦ/dm values extrapolated[23] from the data of Table I (m_{satd} = 0.1092; Φ_{satd} = 0.602, and dΦ/dm = −1.32 ± 0.05), one obtains ΔH_{DS} = 3.90 ± 0.05 kcal/mol.

The same figure, within experimental error, can be independently derived from the calorimetric data of Table I. In fact at 25 °C $\Delta H_{DS} = \Delta H_{IS} + \Phi_L(m_{satd})$ = 3.9 ± 0.1 kcal/mol where ΔH_{IS} is the heat of solution at infinite dilution.[24]

Given the calorimetric heat of solution data for both the hydrate and anhydrous form of caffeine we finally evaluate (see Table I) ΔH = 1.6 ± 0.1 kcal/mol for the enthalpy of the reaction at 25 °C.

$$(\text{caffeine}\cdot H_2O)_S \rightarrow (\text{caffeine})_S + (H_2O)_L \quad (4)$$

This heat should reflect the breaking of the H bond linking one caffeine molecule (through its N_9) with one water molecule in the hydrate,[15] assuming that the crystal packing of caffeine is little affected by reaction 4. Unfortunately, however, no crystallographic data seem to be available for anhydrous caffeine in order to substantiate our qualitative conclusion.

In conclusion, the whole set of results reported here may be interpreted in terms of association of caffeine in aqueous solution. Our osmotic coefficient data cannot, however, support the lack of trimer formation suggested by Guttman and Higuchi[16] and are instead more compatible with the hypothesis of multiple association with identical equilibrium constants.

Our heat of dilution values at 25 °C are in good agreement with those reported by Gill et al.,[3] but they do imply a nonlinear plot of Φ_L against $(\Phi_L/m)^{1/2}$ which, in turn, would suggest that $\Delta H_2^\circ \neq \Delta H_3^\circ \neq \ldots$. As a matter of fact, using the limiting ($m \rightarrow 0$) value of ΔH° = −3.4 kcal/mol, one calculates K = 9.4 m^{-1} in agreement with the osmotic coefficient result, while *higher* K values are obtained with increasing m.

From our data it also appears that the entropy of caffeine dimerization (ca. −7 eu) may result solely from the contribution arising from the unit decrease in mole number upon association (ca. −8 eu, in water). Therefore the dimerization of caffeine is entirely enthalpy driven, and one can safely assume that the source of dimer stability resides in the optimization of van der Waals contacts between stacked molecules whose planes would be at a distance of 3.4×10^{-8} cm apart with C_2 symmetry.[17]

Comparison of our data with those from the literature indicates that the extent of dimer formation in aqueous caffeine solutions at 25 °C is similar to that of purine[3] and 6-methylpurine[4] but smaller than in the case of 6-dimethylaminopurine or of 6(methylamino)-9-methylpurine at the same temperature. The latter compounds with the exclusion of purine are characterized, however, by entropies of dimerization which range from nearly twice to almost three times as large (in absolute value) as that found for caffeine. In particular, the entropy of dimerization amounts to −13 eu for purine,[3] −14.6 eu for 7-methylaminopurine, and −22.4 eu for both 6-dimethylaminopurine and 6(methylamine)-9-methylpurine[2] in water at 25 °C.

For these purine derivatives van der Waals interactions between stacked molecules would thus be only one of the factors governing a rather complicated mechanism of association in which water molecules are also heavily involved (but in a manner poorly understood as yet). In this context caffeine would represent a relatively simple case.

(B) *Interaction of Caffeine with Ethidium Bromide and with Urea.* The cationic dye ethidium bromide (EB) has received considerable attention because of the strong, selective interaction it can establish with DNA. Thermodynamic and spectroscopic aspects of EB dimerization in water[18] and of the binding of EB by synthetic polyelectrolytes[18] and by DNA[19] in dilute aqueous solution have recently been studied in this laboratory. Concerning the behavior of EB in water, it is useful to recall that (1) EB is rather reluctant to dimerize (K = 41 M^{-1} at 25 °C) in comparison to most common dyes, (2) the EB absorption spectrum is red-shifted upon dimerization, an infrequent phenomenon for dye aggregation, and (3) the EB dimerization enthalpy (ΔH = −7.6 kcal/mol) differs by no more than about 15% from the average value of −6.5 kcal/mol calculated on the basis of enthalpy of dimerization data for other different dyes.[18]

Pursuant to our interest in a quantitative description of the capability of caffeine to form 1:1 complexes with aromatic compounds in water, it was considered worthwhile to begin with EB, a well-characterized and interesting case itself.

Investigating the spectral properties of EB in aqueous caffeine solutions we find that the dye spectrum is hypochromic and red-shifted with respect to that of the free monomeric dye in water (λ_{max} 480 nm; ϵ_{480} 5270). For example, in 0.1 M caffeine the spectrum of EB (1.8×10^{-4} M) exhibits a maximum absorption at 510 nm with an apparent molar extinction coefficient of ϵ_{510} 4380. The hypochromic effect and red shift are qualitatively similar to those found for EB dimerization as well as for EB binding by polycarboxylates and by DNA.[18] Assuming that a 1:1 complex is formed between caffeine and EB, an equilibrium constant K_{EB} = 126 M^{-1} has been calculated at 25 °C on the basis of series of spectral measurements for different EB/caffeine molar concentration ratios,[20] using the extrapolated value of ϵ_{480} 4050 for the EB–caffeine 1:1 complex. In these experiments self-dimerization of caffeine has been neglected, since its concentration was always below 10^{-2} M.

Calorimetric measurements, carried out as explained in the Experimental Section, have yielded for the enthalpy of EB–caffeine complexation the value ΔH_{EB} = −5.4 ± 0.1 kcal/mol of EB bound at 25 °C (Table II). This figure is just the numerical average of the enthalpies of self-dimerization of caffeine and of EB. The total entropy of complexation then results, ΔS_{EB} = −8.6 eu, corresponding to the cratic contribution well within estimated uncertainties in the K_{EB} and ΔH_{EB} values. Energetically favorable π-electron cloud overlap between EB and caffeine would then he the major source of stability for their 1:1 (stacked) complex in aqueous solution. A similar explanation was afforded for the strong complexation of the dye acriding orange with sarcosine anhydride in dilute aqueous solution once the possible relevance of hydrophobic interactions was ruled out.[8]

TABLE II: Heats of Mixing Aqueous Caffeine (caf) with Aqueous Ethidium Bromide (EB)[a] at 25 °C

$M_{caf} \times 10^3$	Q, cal/s[b]	ΔH, kcal/mol
52.96	-28.8×10^{-6}	−5.41
38.62	-21.0×10^{-6}	−5.28
23.19	-18.3×10^{-6}	−5.42
12.54	-15.2×10^{-6}	−5.49
1.97	-4.6×10^{-6}	−5.34

ΔH°_{EB} = −5.4 ± 0.1 kcal/mol

[a] $M_{EB} = 4.84 \times 10^{-4}$ M. [b] Flow rate 9.58×10^{-6} l./s.

Finally, it may be worth reporting that we have also found by means of measurements of the heat of solution of caffeine (2–6 × 10^{-3} M final molarity) in aqueous urea (0.2–5 M) that such calorimetric data are consistent with the formation of a caffeine–urea 1:1 adduct in solution. The heat of solution data do, in fact, obey the simple equation $\Delta H_{exc}/M = K\Delta H_{urea} - K\Delta H_{exc}$, which follows immediately from the mass law, and where ΔH_{exc} is the "excess" heat of solution of caffeine in a urea solution of molarity M. The best fit parameters are K = 0.50 ± 0.05 M^{-1} and ΔH_{urea} = −3.60 ± 0.10 kcal/mol. Lacking conclusive spectroscopic evidence, interpretation of these data is still open to question, as caffeine and urea might associate either by hydrogen bridges or by a sort of stacking mechanism.[21] More work is being carried out with urea and urea derivatives to elucidate this point.

Acknowledgment. This work has been sponsored by the Italian Consiglio Nazionale delle Richerche, Rome.

References and Notes

(1) (a) P. O. P. Ts'o and S. I. Chan, *J. Am. Chem. Soc.*, **85**, 1289 (1963); (b) P. O. P. Ts'o, I. S. Malvin, and A. C. Olson, *ibid.*, **86**, 4176 (1964).
(2) R. Bretz, A. Lusting, and G. Schwarz, *Biophys. Chem.*, **1**, 237 (1974).
(3) S. J. Gill, M. Downing, and G. F. Sheats, *Biochemistry*, **6**, 272 (1967).
(4) M. G. Marenchic and J. M. Sturtevant, *J. Phys. Chem.*, **77**, 544 (1973).
(5) T. Higuchi and D. A. Zuck, *J. Am. Pharm. Assoc.*, **42**, 132, 138 (1953).
(6) E. Shefter, *J. Pharm. Sci.*, **57**, 1163 (1968).
(7) F. Quadrifoglio, V. Crescenzi, A. Cesàro, and F. Delben, *J. Phys. Chem.*, **75**, 3633 (1971).
(8) V. Crescenzi, A. Cesàro, and E. Russo, *Int. J. Peptide Protein Res.*, **5**, 427 (1973).
(9) N. H. Ishler, T. P. Finucane, and E. Borber, *Anal. Chem.*, **20**, 1162 (1940).
(10) F. J. C. Rossotti and H. Rossotti, "The Determination of Stability Constant", McGraw-Hill, New York, N.Y., 1961, p 190.
(11) "Handbook of Chemistry and Physics", 47th ed, The Chemical Rubber Co., Cleveland, Ohio, 1966.
(12) F. Quadrifoglio and V. Crescenzi, *Biophys. Chem.*, **2**, 64 (1974).
(13) D. D. Kasarda, *Biochim. Biophys. Acta*, **217**, 535 (1970).
(14) P. R. Stoesser and S. J. Gill, *J. Phys. Chem.*, **71**, 564 (1967).
(15) D. J. Sutor, *Acta Crystallogr.*, **11**, 453 (1958).
(16) D. Guttman and T. Higuchi, *J. Am. Pharm. Assoc.*, **46**, 4 (1957).
(17) J. N. Kikkert, G. R. Kelly, and T. Kurucsev, *Biopolymers*, **12**, 1459 (1973).
(18) V. Crescenzi and F. Quadrifoglio, *Eur. Polym. J.*, **10**, 329 (1974).
(19) F. Quadrifoglio, V. Crescenzi, and V. Giancotti, *Biophys. Chem.*, **1**, 319 (1974).
(20) R. W. Ramette, E. A. Dratz, and P. W. Kelly, *J. Phys. Chem.*, **66**, 527 (1962).
(21) W. P. Jenks, "Catalysis in Chemistry and Enzymology", McGraw-Hill, New York, N.Y., 1969, p 461.

(22) J. H. Stern, J. A. Devore, S. L. Hansen, and O. Yaruz, *J. Phys. Chem.*, **78**, 1923 (1974).
(23) The values of Φ and $d\Phi/dm$ used in eq 2 and 3 have been extrapolated from the Φ data at 29.8 and 35 °C. The estimated errors for this procedure are reported.
(24) Recently a value of 3.60 ± 0.06 kcal/mol has been reported for the heat of solution of caffeine in water.[22] This value was reported to be independent of concentration up to 0.01 m.[22] These findings are not in agreement with evidence reported in the present paper as well as with previous data given by Gill et al.[3]

COMMUNICATIONS TO THE EDITOR

Electrometric Study on the Chloride Ion Inclusion into the Poly(α,L-glutamic Acid)–Acridine Orange Complex

Sir: Neutral salts such as potassium chloride are known to affect the absorption spectra, optical rotatory properties, and kinetic aspects of the poly(α,L-glutamic acid) (PLGA)–acridine orange (AO) complex.[1-3] Sato et al. interpreted these phenomena by the assumption that (i) the chloride ion (Cl^-) associates with the AO dimer as follows:[1,4,5]

$$2AO^+ + Cl^- \rightleftharpoons (AO)_2Cl^+ \qquad (1)$$

and then (ii) this $(AO)_2Cl^+$ is bound to the ionized carboxyl groups of PLGA. On the other hand, Schwarz assumed that the AO dimer is present as a divalent cation.[2,6,7]

If AO^+ associates with Cl^- according to (1), the activity of Cl^- would decrease. Thus the validity of their mechanisms could be clearly elucidated from measuring the Cl^- activity in the present system.[8,9] This communication reports the results of emf measurements of the Cl^- activity in the PLGA–AO system.

Acridine orange was used as the hydrochloride salt (AO·HCl). PLGA was used as the sodium salt. The following electrochemical cell was used:

$$HgCl_2(s)/Hg|satd\ KCl\|AO{\cdot}HCl(aq) + PLGA(aq)|Ag/AgCl$$

The emf was measured with a Radiometer pH meter 4d. All solutions were kept at 298 ± 0.5 K. The pH value was adjusted at pH 4.53 ± 0.03 by 5 mM[10] acetic acid–sodium acetate buffer.

In Figure 1 the emf values are plotted against the logarithm of the total amounts of Cl^- added as AO·HCl. It should be noted that the emf values linearly decrease with log[AO·HCl] at all concentrations between 1×10^{-5} and 5×10^{-3} M.[10] In this concentration region the dimer formation of AO takes place markedly.[5,6] From these data, it is concluded that both AO^+ and $(AO)_2^{2+}$ negligibly associate with Cl^-. This conclusion agrees with what was obtained by Padday on other dyes.[8,9]

Figure 2 exhibits the emf values of the following systems: (a) NaCl in water (pH 4.53), (b) PLGA–NaCl in water (pH 4.53), (c) PLGA–AO·HCl in water (pH 4.53), where in system c the glutamyl residue to dye ratio (R/D) was kept constant at R/D = 10. The measurements were performed in the order of a, b, and c. In the presence of the PLGA, the emf values shift down appreciably below [AO·HCl] = 10^{-4} M. Washing the Ag–AgCl electrode with water a whole day after the measurements for the PLGA–NaCl system caused

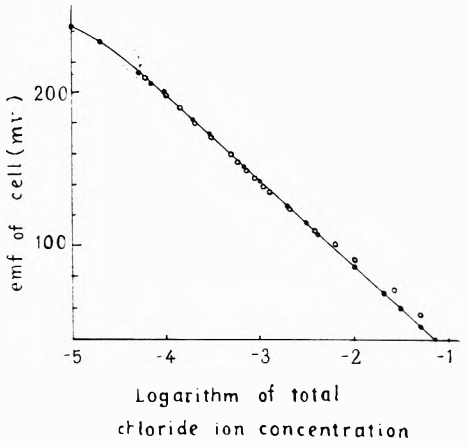

Figure 1. Reversible emf of the cell as a function of the logarithm of the total chloride concentration added as AO·HCl or NaCl: (●) NaCl only; (○) AO·HCl.

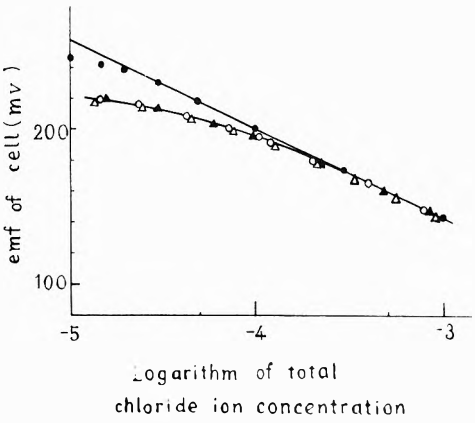

Figure 2. Reversible emf of the cell as a function of the logarithm of the total chloride concentration added as AO·HCl or NaCl: (●) (a) NaCl only; (▲) NaCl immediately after measuring PLGA–NaCl; (○) (b) PLGA–NaCl at pH 4.53; (△) (c) PLGA–AO–HCl at pH 4.53; R/D = 10.

the emf value for system a to recover to the initial value. Thus this shift may be due to the adsorption of PLGA on the Ag–AgCl electrode. The emf values for the PLGA–AO·HCl system coincide with those for the PLGA–NaCl system. The results exactly show that there is no substantial difference in the Cl^- activity between the two systems. Considering that in system b no Cl^- will be included into PLGA which has large negative charges at pH 4.53, it is reasonable to conclude that no significant inclusion of Cl^- takes place in the PLGA·AO complex. This conclusion is supported also by the spectroscopic, the kinetic, and the conductivity measurements.[11]

References and Notes

(1) Y. Sato, M. Hatano, and M. Yoneyama, *Bull. Chem. Soc. Jpn.*, **46**, 1980 (1973).
(2) G. Schwarz and W. Balthaser, *Eur. J. Biochem.*, **12**, 461 (1970).
(3) G. G. Hammes and C. D. Hubbard, *J. Phys. Chem.*, **70**, 1615 (1966).
(4) G. R. Haugen and E. R. Hardwick, *J. Phys. Chem.*, **67**, 2169 (1963).
(5) M. E. Lamm and D. M. Neville, Jr., *J. Phys. Chem.*, **69**, 3872 (1965).
(6) B. H. Robinson, A. Loffler, and G. Schwarz, *J. Chem. Soc., Faraday Trans. 1*, **69**, 56 (1973).
(7) R. E. Ballard and C. H. Park, *J. Chem. Soc. A*, 1340 (1970).
(8) J. F. Padday, *J. Phys. Chem.*, **71**, 3488 (1967).
(9) J. F. Padday, *J. Phys. Chem.*, **72**, 1259 (1968).
(10) 1 M ≡ 1 mol dm^{-3}.
(11) F. Watanabe, to be submitted for publication.

Department of Chemistry
Faculty of Science
Hokkaido University
Sapporo 060 Japan

Fumiyuki Watanabe

Received September 29, 1975

Journal of Chemical and Engineering Data

JANUARY 1976, Vol. 21, No. 1

TABLE OF CONTENTS

CONTENTS

■ Supplementary material for this paper is available separately by direct order (please consult the masthead page). It will also appear following the paper in the microfilm edition of this journal.

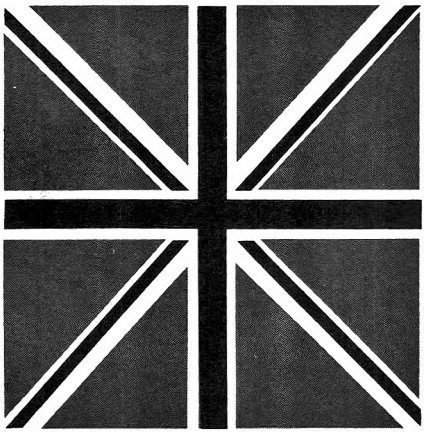

ANNOUNCING
The American Chemical Society is now distributing **SPECIALIST PERIODICAL REPORTS** published by The Chemical Society

The highly-praised **SPECIALIST PERIODICAL REPORTS** are now available for the first time through the American Chemical Society.

This outstanding series provides critical and comprehensive coverage of the latest progress in major areas of chemical research. Each field is examined in depth by foremost authorities on the subject, making each volume an essential resource for the specialist chemist as well as for the newcomer seeking an introduction to the state of the art.

Titles are published annually, and in some cases, biennially. All books postpaid in U.S. and Canada, plus 40 cents elsewhere.

Titles from the series currently available:

Aliphatic Chemistry, Senior Reporter: Prof. W. Parker, Vol 2, 534 pp., 1974 (1972 literature), Cloth bound, $30.25.

The Alkaloids, Senior Reporter: Dr. J. E. Saxton, Vol. 3, 337 pp., 1973, (July 1971-June 1972 literature), Cloth bound $23.50

Amino-acids, Peptides, and Proteins, Senior Reporter: Dr. R. C. Sheppard, Vol. 5, 515 pp., 1974, (1972 literature), Cloth bound $22.00.

Aromatic and Heteroaromatic Chemistry, Senior Reporters: Dr. C. W. Bird & Dr. G. W. H. Cheeseman, Vol. 1, 445 pp., 1973, (Jan. 1971-May 1972 literature), Cloth bound $30.00.

Biosynthesis, Senior Reporter: Prof. T. A. Geissman, Vol. 2, 308 pp., 1973, (1972 literature), Cloth bound $22.00.

Carbohydrate Chemistry, Senior Reporter: Prof. J. S. Brimacombe, Vol. 6, 620 pp., 1973, (1972 literature), Cloth bound $22.00.

Chemical Thermodynamics, Senior Reporter: Prof. M. L. McGlashan, Vol. 1, 362 pp., 1973, (recent literature to Dec. 1971), Cloth bound $22.00.

Colloid Science, Senior Reporter: Prof. D. H. Everett, Vol. 1, 264 pp., 1973, (1970-1971 literature), Cloth bound $18.00.

Dielectric and Related Molecular Processes, Senior Reporter: Prof. Mansel Davies, Vol. 1, 394 pp., 1972, (five years up to Sept. 1971), Cloth bound $22.00.

Electrochemistry, Senior Reporter: Prof. H. R. Thirsk, Vol. 4, 349 pp., 1974, (April 1972-March 1973 literature coverage), Cloth bound $24.75.

Electron Spin Resonance, Senior Reporter: Prof. R. O. C. Norman, Vol. 1, 273 pp., 1973, (Jan. 1971-May 1972 literature), Cloth bound $19.25.

Electronic Structure and Magnetism of Inorganic Compounds, Senior Reporter: Dr. P. Day, Vol. 2, 372 pp., 1973, (Jan. 1971-March 1972 literature), Cloth bound $22.00.

Fluorocarbon and Related Chemistry, Senior Reporters: Dr. R. E. Banks & Dr. M. G. Barlow, Vol. 2, 307 pp., 1974 (1971-1972 literature), Cloth bound, $44.00.

Foreign Compound Metabolism in Mammals, Senior Reporter: Dr. D. E. Hathway, Vol. 2, 513 pp., 1972, (1970-1971 literature), Cloth bound $30.00.

Inorganic Chemistry of the Main Group Elements, Senior Reporter: Prof. C. C. Addison FRS, Vol. 1, 444 pp., 1973, (July 1971-Sept. 1972 literature), Cloth bound $24.75.

Inorganic Chemistry of the Transition Elements, Senior Reporter: Dr. B. F. G. Johnson, Vol. 2, 501 pp., 1973, (Oct. 1971-Sept. 1972 literature), Cloth bound $26.25.

Inorganic Reaction Mechanisms, Senior Reporter: Dr. J. Burgess, Vol. 2, 393 pp., 1972, (Aug. 1970-Dec. 1971 literature), Cloth bound $22.00.

Mass Spectrometry, Senior Reporter: Dr. D. H. Williams, Vol. 2, 356 pp., 1973, (July 1970-June 1972 literature), Cloth bound $22.00.

Molecular Spectroscopy, Senior Reporters: Prof. D. A. Long, Prof. D. J. Millen & Dr. R. F. Barrow, Vol. 1, 622 pp., 1973, (recent literature to Jan. 1972), Cloth bound $33.00.

Molecular Structure by Diffraction Methods, Senior Reporters: Prof. G. A. Sim & Dr. L. E. Sutton, Vol. 1, 824 pp., 1973, (Jan. 1971-Mar. 1972 literature), Cloth bound $41.50.

Nuclear Magnetic Resonance, Senior Reporter: Dr. R. K. Harris, Vol. 2, 406 pp., 1973, (July 1971-May 1972 literature), Cloth bound $24.75.

Organic Compounds of Sulphur, Selenium, and Tellurium, Senior Reporter: Dr. D. H. Reid, Vol. 2, 827 pp., 1973, (April 1970-March 1972 literature), Cloth bound $41.50.

Organometallic Chemistry, Senior Reporters: Prof. E. W. Abel & Prof. F. G. A. Stone, Vol. 2, 612 pp., 1973, (1972 literature), Cloth bound $35.75.

Organophosphorus Chemistry, Senior Reporter: Prof. S. Trippett, Vol. 5, 313 pp., 1974 (July 1972-June 1973 literature), Cloth bound, $27.50.

Photochemistry, Senior Reporter: Prof. D. Bryce-Smith, Vol. 5, 1974 (July 1972-June 1973 literature), Cloth bound, $55.00.

Radiochemistry, Senior Reporter: Dr. G. W. A. Newton, Vol. 1, 131 pp., 1972, (July 1969-Aug. 1971 literature), Cloth bound $12.50.

Spectroscopic Properties of Inorganic and Organometallic Compounds, Senior Reporter: Prof. N. N. Greenwood, Vol. 6, 663 pp., 1973, (1972 literature), Cloth bound $30.00.

Statistical Mechanics, Senior Reporter: Dr. K. Singer, Vol. 1, 256 pp., 1973, (literature up to July 1972), Cloth bound $18.00.

Surface and Defect Properties of Solids, Senior Reporters: Prof. M. W. Roberts & Prof. J. M. Thomas, Vol. 2, 277 pp., 1973, (May 1971-April 1972 literature), Cloth bound $20.75.

Terpenoids and Steroids, Senior Reporter: Dr. K. H. Overton, Vol. 3, 527 pp., 1973, (Sept. 1971-Aug. 1972 literature), Cloth bound $33.00.

Earlier volumes in some titles available on request.

Order from:
Special Issues Sales
American Chemical Society
115 Sixteenth St., N.W.
Washington, D.C. 20036